

JYU DISSERTATIONS 768

Romain Chevigny

Out-Of-Equilibrium and In-Equilibrium Amino Acid-Based Supramolecular Gels

Transient Self-Assembly and Hybrid Materials



UNIVERSITY OF JYVÄSKYLÄ
FACULTY OF MATHEMATICS
AND SCIENCE

JYU DISSERTATIONS 768

Romain Chevigny

**Out-Of-Equilibrium and
In-Equilibrium Amino
Acid-Based Supramolecular Gels
Transient Self-Assembly and Hybrid Materials**

Esitetään Jyväskylän yliopiston matemaattis-luonnontieteellisen tiedekunnan suostumuksella
julkisesti tarkastettavaksi yliopiston Ylistönrinteen salissa FYS1
huhtikuun 29. päivänä 2024 kello 12.

Academic dissertation to be publicly discussed, by permission of
the Faculty of Mathematics and Science of the University of Jyväskylä,
in Ylistönrinne, auditorium FYS1, on April 29, 2024 at 12 o'clock noon.



JYVÄSKYLÄN YLIOPISTO
UNIVERSITY OF JYVÄSKYLÄ

JYVÄSKYLÄ 2024

Editors

Maija Nissinen

Department of Chemistry, University of Jyväskylä

Ville Korkiakangas

Open Science Centre, University of Jyväskylä

Copyright © 2024, by author and University of Jyväskylä

ISBN 978-952-86-0107-4 (PDF)

URN:ISBN:978-952-86-0107-4

ISSN 2489-9003

Permanent link to this publication: <http://urn.fi/URN:ISBN:978-952-86-0107-4>

ABSTRACT

Chevigny, Romain

Out-of-equilibrium and in-equilibrium amino acid-based supramolecular gels:

Transient self-assembly and hybrid materials.

Jyväskylä: University of Jyväskylä, 2024, 79 p.

(JYU Dissertations

ISSN 2489-9003; 768)

ISBN 978-952-86-0107-4 (PDF)

This thesis describes two supramolecular gel systems with different self-assembly processes. The first system is the out-of-equilibrium solvent-induced transient self-assembly of peptide gels. The design, synthesis and characterisation of diprotected short peptide precursors and their gelation trials are described. A deeper focus is placed on the successful gels to decipher the set of reactions regulating the transient assembly. When triggering the reaction by sulfuric acid as an accelerator, two acid-accelerated processes happen simultaneously, but with different kinetics: the primary solvent hydrolysis *in situ* generates a secondary solvent responsible for the interconversion of two acid-activated gelators and the progressive dissolution of the self-assembled network. An inversely proportional correlation is observed between the lifetime (dynamic character) of the gels and their mechanical properties. The lifetime and the mechanical properties are tunable by changing the gelation conditions (*e.g.* precursor structure and concentration and accelerator concentration).

The second system consists of the in-equilibrium self-assembly of *N*-(9-Fluorenylmethoxycarbonyl) phenylalanine (Fmoc-Phe) gelator in a water-based buffer solution triggered by temperature change. Graphene oxide (GO) flakes were incorporated into the gel structure, and the supramolecular interactions between the gelator and GO were studied. Infrared spectroscopy and electron microscopy highlighted that the presence of GO did not affect the 1D and 2D aggregation of Fmoc-Phe. However, a significant difference in the mechanical properties was observed as the hybrid gel was more elastic with GO within the structure. Finally, the bactericidal properties of the neat and hybrid gels towards gram-negative *Escherichia Coli* bacteria were evaluated. The presence of GO increased its antimicrobial activity compared to the neat material.

This work provides fundamental understanding of simultaneous acid-accelerated processes that, coupled with two antagonistic solvents, regulate a transient self-assembly cycle. Also, it supports and enriches the existing literature on hybrid antimicrobial gels by exploiting the synergy between organic gelators and carbon materials.

Keywords: supramolecular gels, in-equilibrium self-assembly, out-of-equilibrium self-assembly, transient materials, peptide gels, hybrid antimicrobial materials, solvent-induced self-assembly.

ABSTRAKTI

Chevigny, Romain

Epätasapainotilassa ja tasapainotilassa olevat aminohappopohjaiset supramolekulaariset geelit: transientti itsejärjestäytyminen ja hybridimateriaalit.

Jyväskylä: Jyväskylän yliopisto, 2024, 79 s.

(JYU Dissertations

ISSN 2489-9003; 768)

ISBN 978-952-86-0107-4 (PDF)

Tämä opinnäytetyö käsittelee kahta erilaista itsejärjestäytyvää, supramolekulaarista geelijärjestelmää. Ensimmäinen järjestelmä on liuotinvälitteinen, tasapainotilasta poikkeava, hetkellisesti itsejärjestäytyvä peptidigeeli. Rikkihappolisäyso-gelaattorien esiastetta sisältävään liuokseen käynnistää kaksi eri reaktiokinetiikan hallitsemaa reaktiota: primäärisen liuottimen *in situ* -hydrolyysi tuottaa sekundäärisen liuottimen, joka aiheuttaa happoaktivaation kautta suojatusta dipeptidistä syntyneiden kahden gelaattorin interkonversion. Samanaikaisesti itsejärjestäytynyt geeliverkosto liukenee vaiheittain. Syntyneiden geelien elinikä ja niiden mekaaniset ominaisuudet olivat kääntäen verrannollisia ja geelien dynaamisia ja mekaanisia ominaisuuksia voitiin säätää muuttamalla geelilytymisolosuhteita (esim. gelaattorin esiasteen rakenne ja konsentraatio sekä hapon konsentraatio).

Toinen järjestelmä koostuu lämpötilamuutoksella aiheutetusta Fmoc-suojatun fenyylialaniinigelaattorin (Fmoc-Phe) tasapainotilaisesta itsejärjestäytymisestä puskuriliuoksessa. Geeliin lisättiin grafeenioksidihiuksia (GO), ja gelaattorin ja GO:n välisiä supramolekulaarisia vuorovaikutuksia tutkittiin infrapunaspektroskopialla ja elektronimikroskopialla. GO:n läsnäolo materiaalissa ei vaikuttanut Fmoc-Phe:n 1D- ja 2D-järjestäytymiseen. Mekaanisissa ominaisuuksissa havaittiin merkittävä ero: kun GO:n määrä materiaalissa lisääntyi, hybridigeelin joustavuus kasvoi. GO lisäsi materiaalin antimikrobista aktiivisuutta gram-negatiivista *Escherichia Coli* -bakteeria vastaan.

Työ tuotti uutta tietoa epätasapainotilaisista, hetkellisistä geeleistä, joiden itsejärjestäytymiskykyä voidaan säädellä kahden vastakkaisesti toimivan liuottimen ja happoaktivaattorin avulla. Lisäksi saatiin uutta tietoa antimikrobisista hybridigeeleistä hyödyntämällä orgaanisen gelaattorin ja hiilimateriaalin välistä synergiaa.

Avainsanat: supramolekulaariset geelit, epätasapainotilan itsejärjestäytyminen, tasapainotilan itsejärjestäytyminen, hetkelliset materiaalit, peptidigeelit, antimikrobiset hybridimateriaalit, liuotinvälitteinen itsejärjestäytyminen.

Author

Romain Chevigny
Department of Chemistry
Nanoscience Center
University of Jyväskylä
P.O. Box 35
FI-40014 Jyväskylä, Finland
romain.r.chevigny@jyu.fi
ORCID: 0000-0002-5463-9745

Supervisors

Professor Maija Nissinen
Department of Chemistry
Nanoscience Center
University of Jyväskylä
P.O. Box 35
FI-40014 Jyväskylä, Finland

Professor Mika Pettersson
Department of Chemistry
Nanoscience Center
University of Jyväskylä
P.O. Box 35
FI-40014 Jyväskylä, Finland

Reviewers

Professor Luisa de Cola
Department of Pharmaceutical Sciences
University of Milan
Italy

Doctor Loïc Stefan
Macromolecular Chemistry-Physics Laboratory
University of Lorraine, Nancy
France

Opponent

Professor Christoph A. Schalley
Institute of Chemistry and Biochemistry
Free University of Berlin
Germany

PREFACE

The story of my journey in Jyväskylä began in the fall of 2020 when I started my six-month master's internship in the Nanoscience Center after a positive email from my future supervisor stating that she had an available position for me in the group. Then I felt comfortable here and stayed. I met amazing friends and colleagues who gave me the feeling of belonging somewhere outside my home country and made these years of work at JYU possible.

My deepest gratitude goes to my supervisor, Professor Maija Nissinen, for taking me in my early career and providing me with a rich environment to develop professionally. I always found her door open when needing advice on all aspects of the PhD life, whether research, teaching or administration. I am also deeply grateful to my second supervisor, Professor Mika Pettersson, for all the scientific insights I received from him throughout this journey. I was lucky to have supportive supervisors with a good combination of expertise in organic and supramolecular chemistry and spectroscopy so that I always had the chance to receive the best I needed, when needed.

I also owe a lot to the people I met over the years in JYU for all the scientific discussions we had in the corridors of NSC. I want to thank Stratos, Johanna, Henna and Elsa for the joyful time in the synthesis lab and during lunch time, and Dimitri and Aku for making our office feel warm and lively. I also want to thank staff members Eero, Pasi and Tatu for their advice and expertise on spectroscopic measurements and Andreas for his help with electronic microscopy. So much of my work could not have been done without the help and guidance I received. Finally, I thank everyone whose names are not stated here for making JYU such a pleasant environment to work in.

I would like to thank Professor Luisa de Cola and Doctor Loïc Stefan for dedicating their time to reviewing this thesis. I also thank Professor Christoph Schalley for being my opponent and travelling such a long distance to discuss my work with me. Last but not least, I had the chance to meet an amazing collaborator, Professor Jennifer Hiscock, who gave me vital advice and who believed in my research abilities.

Of course, my friends and family back home had a huge impact on my mental health by helping me relax and forget work while I spent time at home in France. They always supported me loudly or silently, even though none of them had a chemistry or science background. They believed in what I was doing with my life and always showed interest in my work, for real or by politeness. My deepest gratitude and love go to my partner Lou, who dropped her life in France and crossed Europe just to support me in Finland for several years. I could not have done anything without her by my side. From this, the best thing that ever happened to me is our daughter Chiara, born here in Jyväskylä, who brought me so much happiness and love beyond what I ever imagined.

Jyväskylä, 06.01.2024
Romain Chevigny

LIST OF INCLUDED PUBLICATIONS

- I** Romain Chevigny, Johanna Schirmer, Carmen C. Piras, Andreas Johansson, Elina Kalenius, David K. Smith, Mika Pettersson, Efstratios D. Sitsanidis and Maija Nissinen, Triggering a transient organo-gelation system in a chemically active solvent, *Chem. Commun.*, **2021**, 57, 10375-10378.
- II** Romain Chevigny, Efstratios D. Sitsanidis, Johanna Schirmer, Eero Hulkko, Pasi Myllyperkiö, Maija Nissinen, and Mika Pettersson, Nanoscale probing of the supramolecular assembly in a two-component gel by near-field infrared spectroscopy, *Chem. Eur. J.*, **2023**, e202300155.
- III** Romain Chevigny, Henna Rahkola, Efstratios D. Sitsanidis, Elsa Korhonen, Jennifer R. Hiscock, Mika Pettersson and Maija Nissinen, Solvent-Induced Transient Self-Assembly of Peptide Gels: Gelator-Solvent Reactions and Material Properties Correlation, *Chem. Mater.*, **2024**, 36, 407-416.
- IV** Efstratios D. Sitsanidis, Lara A. L. Dutra, Johanna Schirmer, Romain Chevigny, Manu Lahtinen, Andreas Johansson, Carmen C. Piras, David K. Smith, Marja Tiirola, Mika Pettersson and Maija Nissinen, Probing the gelation synergies and anti-*Escherichia coli* activity of Fmoc-phenylalanine/graphene oxide hybrid hydrogel, *ACS Omega*, **2023**, 8, 10225-10234.

Author's contribution

The author performed the syntheses of the peptide precursors and gelator molecules, and conducted all characterisations and analysis using NMR, IR, and UV spectroscopies, as well as rheology and phase transition temperature experiments in publications **I** and **III**. In publication **II**, the author carried out the AFM imaging, nano-FTIR measurements, and data analysis. The author performed the sample preparation and fluorescence imaging analysis for the antimicrobial screening in publication **IV**. The author wrote the original manuscript drafts of publications **I**, **II** and **III**, and reviewed the manuscript of publication **IV**.

Other related publications by the author:

- V Johanna Schirmer, Romain Chevigny, Aleksei V. Emelianov, Eero Hulkko, Andreas Johansson, Pasi Myllyperkiö, Efstratios D. Sitsanidis, Maija Nissinen and Mika Pettersson, Diversity at the nanoscale: Laser-oxidation of single-layer graphene affects Fmoc-phenylalanine surface-mediated self-assembly, *Phys. Chem. Chem. Phys.*, **2023**, 25, 8725-8733.

ABBREVIATIONS

1D, 2D, 3D	One-dimensional, Two-dimensional, Three dimensional
ACN	Acetonitrile
AFM	Atomic force microscopy
ATR	Attenuated total reflectance
Boc	<i>tert</i> -butyloxycarbonyl
CD	Circular dichroism
Cin	Cinnamoyl
CNT	Carbon nanotube
CQD	Carbon quantum dot
<i>d</i> ₆ -DMSO	<i>d</i> ₆ -dimethylsulfoxide
DCM	Dichloromethane
DMF	Dimethylformamide
DMSO	Dimethylsulfoxide
DSA	Dissipative self-assembly
<i>d</i> -DSA	Direct dissipative self-assembly
<i>i</i> -DSA	Indirect dissipative self-assembly
<i>E. coli</i>	<i>Escherichia coli</i>
eq	Equivalent
EtOH	Ethanol
Fmoc	<i>N</i> -(9-Fluorenylmethoxycarbonyl)
Fmoc-Phe	<i>N</i> -(9-Fluorenylmethoxycarbonyl)- <i>L</i> -phenylalanine
FTIR	Fourier transform infrared
GdL	Glucono- δ -lactone
GO	Graphene oxide
HIM	Helium ion microscopy
HR-MS	High-resolution mass spectrometry
LMW	Low molecular weight
LVR	Linear viscoelastic region
MeOH	Methanol
MGC	Minimum gelation concentration
MIR	Mid-infrared
Nap	Naphthalene
NMR	Nuclear magnetic resonance
PBS	Phosphate buffer saline
Phe-Phe	<i>L</i> -phenylalanyl- <i>L</i> -phenylalanine
Pyr	Pyrene
QCL	Quantum cascade laser
R.T.	Room temperature
SANS	Small angle neutron scattering
SEM	Scanning electron microscopy
SSG	Self-supporting gel
sSNOM	Scattering scanning near-field optical microscope

TBTU	2-(1H-Benzotriazole-1-yl)-1,1,3,3-tetramethylammonium tetrafluoroborate
<i>t</i> Bu	<i>tert</i> -butyl
<i>t</i> BuOAc	<i>tert</i> -butyl acetate
<i>t</i> BuOH	<i>tert</i> -butanol
TEM	Transmission electron microscopy
T _{gel-sol}	Phase transition temperature
UV-vis	Ultraviolet-visible

CONTENTS

ABSTRACT

ABSTRAKTI

PREFACE

LIST OF INCLUDED PUBLICATIONS

ABBREVIATIONS

CONTENTS

1	INTRODUCTION	13
1.1	Gels and their classification.....	13
1.2	Gelation triggers	14
1.3	Self-assembly and non-covalent interactions in gels.....	17
1.4	Carbon-loaded hybrid gel systems	19
1.5	Out-of-equilibrium transient self-assembly.....	21
1.5.1	Dissipative (dynamic) self-assembly (DSA).....	21
1.5.2	Chemical and alternative fuelling for DSA systems.....	23
1.5.3	Applications of transient materials	26
2	CHARACTERISATION OF SUPRAMOLECULAR GELS.....	29
2.1	Standard characterisation methods.....	29
2.1.1	Nuclear magnetic resonance spectroscopy and high-resolution mass spectrometry	29
2.1.2	Optical spectroscopy.....	30
2.1.3	Electron and scanning probe microscopies	31
2.1.4	Rheology.....	31
2.2	Nanoscale spectroscopic characterisation.....	32
3	RESULTS AND DISCUSSION	35
3.1	Liquid-phase peptide synthesis ^{I,III}	35
3.1.1	Synthesis of protected di- and tripeptides.....	35
3.1.2	Deprotection of di- and tripeptides.....	35
3.2	Molecular scale characterisation and interconversion cycle	37
3.2.1	Gelation protocols and outcome ^{I,III,IV}	37
3.2.2	Precursor structure and accelerator effect on gelator/gel formation and self-abolishment ^{I,III}	39
3.2.3	Introducing solvent-induced self-assembly ^{III}	44
3.3	Higher-order organisation.....	45
3.3.1	Morphological assessment ^{III,IV}	45
3.3.2	Bulk infrared characterisation ^{III,IV}	47
3.3.3	Nanoscale infrared characterisation ^{II}	50
3.3.4	Ultraviolet-visible and fluorescence spectroscopies ^{III,IV}	56
3.4	Macroscopic properties of the gels ^{I,III,IV}	58
3.5	Antimicrobial properties of amino acid-based gels ^{IV}	64

4	CONCLUSIONS.....	68
	REFERENCES.....	70
	ORIGINAL PAPERS	

1 INTRODUCTION

1.1 Gels and their classification

Gels are an important and extensively studied sub-category of soft materials used in numerous applications. These materials mainly consist of solvent (typically over 99 wt%) encapsulated within the three-dimensional (3D) network formed by crosslinked polymers or the self-assembly of small molecules (~ 1 wt%), referred to as gelators.^[1-3] The structure is maintained by surface tension and capillary forces between the entrapped solvent and the assembled network, therefore yielding self-supporting gels (SSGs).^[4-6] The different combinations of solvents and gelators offer a broad range of materials suitable for different applications, such as biomedical, cosmetic and food industry.

Gels are classified depending on the nature of the encapsulated solvent or the interactions between gelators leading to their formation (Figure 1). Materials formed using water (or water-based solutions) as a solvent phase constitute the heavily studied class of hydrogels, whereas organic solvents are used in organogels.^[7-10] The breadth of applications for hydrogels is continuously expanding, but most of them are found in the biomedical field. Due to the intrinsic biocompatibility of water and bio-inspired hydrogelator design, the variety of systems is ultimately limitless, with applications such as tissue engineering, drug delivery, cell culturing, active molecule carriers and anion sensing.^[11-13] Similarly, organogels with biocompatible solvents such as mineral and vegetable oils are widely used in cosmetics, drug delivery, food processing and 3D printing.^[5,14-16]

The term xerogel refers to gels whose solvent phase has been dried, leading to the collapse of the assembled structure. Xerogels differ from aerogels in which the encapsulated phase is gas. In this case, the network does not collapse and the material can keep its 3D structure.

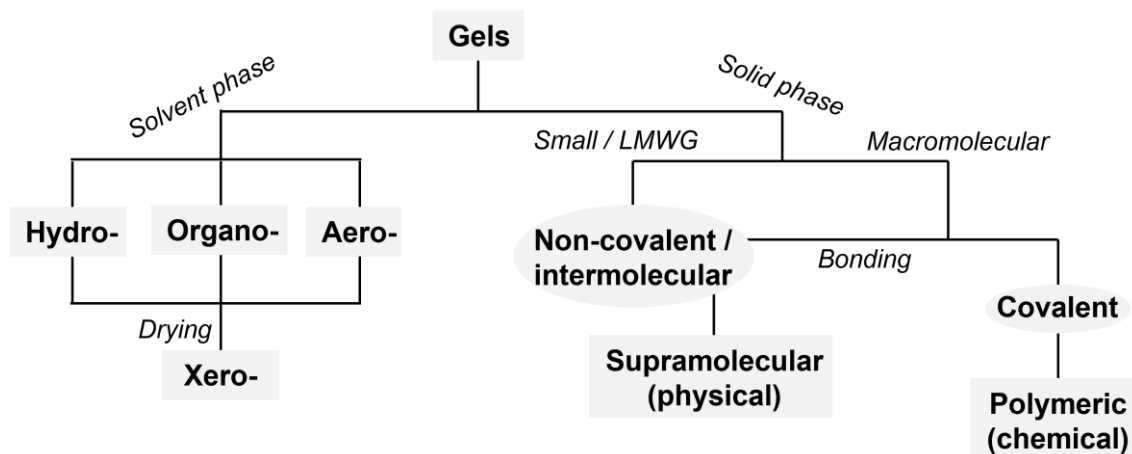


Figure 1. Classification of gels depending on the solvent phase and the type of molecular bonding.

Low molecular weight (LMW) gels are an important and heavily studied class of gels that arise from the self-assembly of small molecules. Among the smallest, amino acid, nucleopeptide, and other peptide-based gelators offer biocompatibility and versatility due to the high degree of structural modification possibilities to suit different needs.^[17-20] The development of synthetic LMW gelators has further widened the possibilities of gelator design.^[21-23]

Under specific conditions (*i.e.* concentration, pH, and temperature), low molecular weight gelators interact non-covalently to form one-dimensional (1D) structures. Non-covalent interactions, such as hydrogen bonding, π - π stacking, electrostatic and Van der Waals interactions are responsible for the molecular aggregation, in addition to hydrophobic and hydrophilic interactions.^[24-26] Hence, gels formed by non-covalent interactions are referred to as supramolecular (or physical) gels. On the other hand, gels can also be obtained by permanent cross-linking of the gelators through covalent bonds assisted by cross-linker molecules. These materials are referred to as polymeric (or chemical) gels. Although polymeric gels consist of permanent covalent bonds, supramolecular polymer gels are reported in the literature. They refer to polymeric fibres interacting non-covalently to form the 3D network.^[27-29] The inherent property of supramolecular gels is the reversibility of the self-assembly triggered by an external input of energy (*i.e.* heating), which reverses the process and triggers the gel-to-sol transition.^[2] The projects summarized in this thesis revolve around amino acid-based supramolecular gels. Therefore, a stronger emphasis will be placed on LMW gels.

1.2 Gelation triggers

Gelation is a sensitive process which is not yet fully understood. Only experiments and trials will tell whether a molecule will form a gel or not due to all the factors affecting gelation. Although previous studies have proposed

models to predict the gelation ability of compounds, it is not possible to explain why some form a gel and some do not.^[2,30-31] Triggering the gelation process can be achieved using a wide range of methods (Figure 2) affecting different chemical and physical properties of the molecules.

For instance, the gelation of LMW amino acid-based gelators having a free carboxylic acid at the C-terminus (α -carbonyl) is often triggered by adjusting the pH (pH switch method).^[32-34] Typically, the gelator is suspended in solution (water-based or organic solvents for hydrogels and organogels, respectively) at room temperature (R.T.) followed by a rise of pH with the addition of a base (most often NaOH) up to pH 9-11. The α -carbonyl of the gelator is then deprotonated due to the low pKa value of the α -carbonyls,^[35] which enhances the solubility. Subsequently, the pH is decreased using an acid (typically HCl), which gradually re-protonates the α -carbonyl until the gel forms through hydrophobic aggregation.

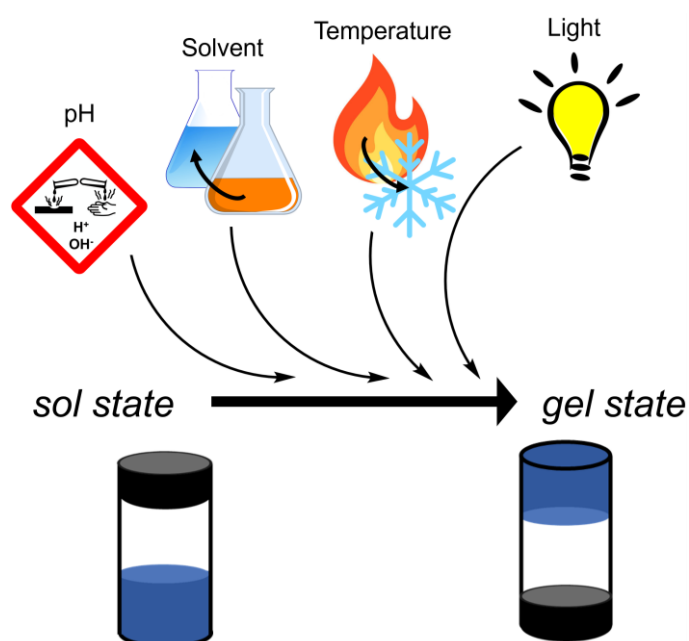


Figure 2. Schematic depiction of the different ways to trigger gelation (*i.e.* sol-to-gel transition)

The $pK_a < 3$ of the α -carbonyl for all 20 natural amino acids would suggest that no self-assembly is observed at pH above the pK_a . However, the self-assembly of peptides has been achieved at higher and neutral pH values due to hydrophobic/hydrophilic interactions regulating self-assembly, inducing shifts of the pK_a upon self-assembly^[33,36] As manual lowering of the pH leads to non-uniform and heterogeneous materials, several methods have been developed to prepare homogeneous gels. One of them is the *in situ* pH mediation using, for instance, glucono- δ -lactone (GdL).^[37,38] This sugar-based cyclic ester self-hydrolyses to gluconic acid in a water environment. Upon self-hydrolysis, a fast pH decrease within the first 60 minutes is observed, which then starts to equilibrate and reach a stable pH value around 300 minutes. The slope of the pH

decrease depended on the gelator's chemical structure, while the final pH value at equilibrium after 300 minutes is quantitatively similar regardless of the peptide backbone.^[37] Another method to homogeneously reduce the pH is using a chemical reaction-triggered pH reduction.^[39] Potassium persulfate ($K_2S_2O_8$) is added into the gelator solution, followed by heating at 50 °C for several hours and cooling down to R.T. The decomposition of $K_2S_2O_8$ in water gradually decreases the pH *in situ* to form homogeneous hydrogels.

In addition to the pH switch, solvent mediation (solvent switch) is a widely used trigger for peptide gelation.^[3,40,41] Gelation is induced by the change in solvent quality and polarity. In this method, a high amount of gelator is dissolved in a low amount of organic solvent (most commonly dimethyl sulfoxide (DMSO)), followed by the addition of an aqueous solution.^[42] Gelation is then observed after allowing the mixture to rest for some time. Studies also showed that the final DMSO/H₂O volume ratio directly affects the gel properties.^[42,43] Another study showed that gel materials can be obtained by solvent switch method using hexafluoroisopropanol (HFIP), ethanol or acetone.^[1,44] These materials were stable over a range of pH and temperature. In addition to deionised water, water-based solutions such as phosphate buffer saline (PBS), minimum essential medium (MEM) and cell culture media can also be used to trigger gelation by solvent mediation. Systematic studies have shown that the choice of water-based solvent directly affects the rheological (mechanical) properties of the formed materials.^[45] The final pH must be controlled to form materials with a suitable pH for biomedical applications.

Alternatively, direct energy input to the system can trigger gelation upon energy dissipation. The energy can be, for instance, increased temperature or sonication. Typically, gelators are suspended in the solvent and heated to a certain temperature for a certain time. The hot mixture is then left to cool down undisturbed to R.T. for gelation. The properties of the gels can be changed by modifying the temperature, equilibration time, and cooling rate.^[21,46-48] Ultraviolet (UV) light has also been reported as a useful trigger for both gelation and the gel-to-sol transition.^[49-51] For instance, a cinnamoyl (Cin) *N*-protected phenylalanine gelator has been reported to show gel-to-sol and gel-to-sol-to-gel transitions upon irradiation with UV light due to the reversible *cis-trans* isomerisation of Cin-Phe. Cin-Phe forms a hydrogel by the pH switch trigger, which turns into a solution upon 254 nm UV light irradiation. The gel phase is recovered by subsequent irradiation with visible light. The light beam is intrinsically easily tunable in intensity and shape which gives rise to selective gelation and multi-domain systems.^[52-54]

Enzymatic reactions have also been reported to trigger gelation, with self-assembly occurring upon deprotection of a functional group by a suitable enzyme.^[50,55,56] For instance, the phosphono group ($-PO_3H_2$) protected tyrosine unit can be deprotected to tyrosine by phosphatase enzyme. This change in molecular structure affects the balance of the hydrophobic and hydrophilic character of the gelator, leading to gelation. This type of gelation has been applied to, for example, compounds containing phenylalanine or lysine units.^[50,56,57]

Another enzymatic reaction leading to gelation is using the urease enzyme. In this case, the fine control of the conditions offered by the catalytic reaction in terms of final pH (depending on the introduced urea) and hydrolysis rate (depending on the concentration of urease enzyme) allows for the tuning of the material properties.^[58,59]

1.3 Self-assembly and non-covalent interactions in gels

The self-assembly of small molecules is a complex process involving several factors or parameters which can be tuned to achieve gelation. The first criterion to consider in assessing whether gelation is possible under specific conditions is the minimum gelation concentration (MGC). This parameter reflects the concentration threshold below which the amount and strength of the interactions are insufficient to support the formation of SSGs.^[60-64] Concentration screening is used to investigate the gelation ability of a specific gelator under specific conditions. Consequently, the vial inversion method (evaluating the lack of free gravitational flow) and rheology are common techniques to confirm gelation. Vial inversion does not require a rheometer or an actual measurement, but the method verifies only that the material is self-supporting and lacks free-flowing solvent, while rheology gives a more detailed mechanical analysis on the material's viscoelastic behaviour and if it can be referred to as a gel. Therefore, vial inversion should always be backed up by rheological measurements to properly assess gelation.

Amino acid-based gelators with 1 – 5 amino acid motifs are widely used short peptide gelators. Their small size offers wide possibilities for interactions and folding during self-assembly,^[65] and synthetic organic chemistry allows for endless functionalisation and modification possibilities (amino acid sequence, length, protective groups and hydrophobicity/hydrophilicity) and consequently tunable materials for specific applications. The main driving forces of the self-assembly of small molecules are weak, low energy, non-covalent interactions such as hydrogen bonding and π - π stacking, along with electrostatic and van der Waals forces.^{[20,66-68],I,II} In addition, solute-solvent interactions involving changes in hydrophobicity and hydrophilicity of the gelator in the solvent environment are also important. Solvent switch and pH switch triggers are both examples of these interactions. Specifically, peptide-based gelators bear carbonyl groups, C-terminus carboxylic acid and N-terminus amine groups, which are prone to strong hydrogen bonding interactions. This is further expanded, for instance, to urea and nucleobase-modified gelators bearing additional hydrogen bonding donor and acceptor groups.^[69-72] Due to the intense π - π stacking interactions coupled with a high hydrophobic character, aromatic amino acids, such as phenylalanine, tryptophan and tyrosine, are often included in the peptide sequence when designing peptide-derivative gelators.^[21,73] Additionally, the peptide sequence can be modified to include hydrophilic sites using charged side-chained amino acids (*e.g.* lysine and glutamic acid). Amino acids exhibiting

hydrophobic side chains, such as valine or leucine, have also been reported to impact on the gelation ability of peptide gelators. In fact, hydrocarbon side chains with sp^3 hybridised carbons are mobile and, therefore, able to rotate and fold, favouring or hindering the self-assembly process.^[24,73-76]

A common method to increase the gelation ability of amino acid-based gelators is increasing their hydrophobicity by modifying their structure at each side of the sequence.^[77] For this, a plethora of protecting groups (almost exclusively aromatic) can be covalently attached to the *N*-terminus, increasing the hydrophobic and amphiphilic character of the molecule by suppressing the terminal amine group. On the other hand, the *C*-terminus carboxylic acid is, in most cases, unaltered, leaving the hydrophilic and strongest hydrogen bonding donor site available. The main protective groups in peptide gelators are, non-exhaustively, fluorenylmethyloxycarbonyl (Fmoc), naphthalene (Nap), Cin (see section 1.2) and pyrene (Pyr). The addition of aromatic terminal groups can allow for the gelation of otherwise non-gelling molecules by increasing π - π interactions and conformational restrictions. Depending on the chosen group, biological and optical properties can be added to the gelator.

Metallogels is another sub-class of supramolecular gels. These materials are formed by coordination interactions between ligands (organic molecules) and a metal ion centre, leading to a 3D supramolecular network. Most commonly the metals are from the d block of the periodic table, such as zinc, iron, copper, nickel and cobalt, or even from the f block, such as europium.^[70,78,79] Studies have shown that the modification of the ligands led to differences in the materials' mechanical properties. Altering the redox state of the metal ion and the coordination complex, changes the colour and fluorescence properties of the materials. Some metallogels are also reported to be thermochromic and thermoresponsive, that is, their supramolecular structures are modified under different temperature conditions.^[7,80]

The aggregation of small molecules into a complex entangled 3D network is a multistep process occurring across multiple length scales.^[2,42] Under specific temperature, pH, etc conditions, gelator molecules primarily in suspension in an isotropic solution (Figure 3, left) begin to aggregate into a 1D chain through non-covalent interactions (Figure 3, middle). This phenomenon, referred to as self-assembly, occurs spontaneously as a thermodynamically-driven process if the assembly has a negative free Gibbs energy.^[81] Similarly, the free Gibbs energy for the dissolution of the assembly is positive, meaning that the molecules prefer to minimise the hydrophobic and hydrophilic interactions. It has been reported that by correlation with rheological data the higher the free Gibbs energy, the stronger the gel is.^[82] The 1D aggregates (primary structure) further self-assemble along with folding and twisting, generating the secondary structure. The most reported secondary structures for short peptide-based supramolecular gels containing aromatic groups either in the peptide sequence or in the terminal protective group are the parallel and anti-parallel β -sheet motifs. Longer peptide sequence or higher-ordered structures can allow for the folding into α -helices.^[74,83-87] Further entanglement of the formed fibrils leads to a highly entangled 3D

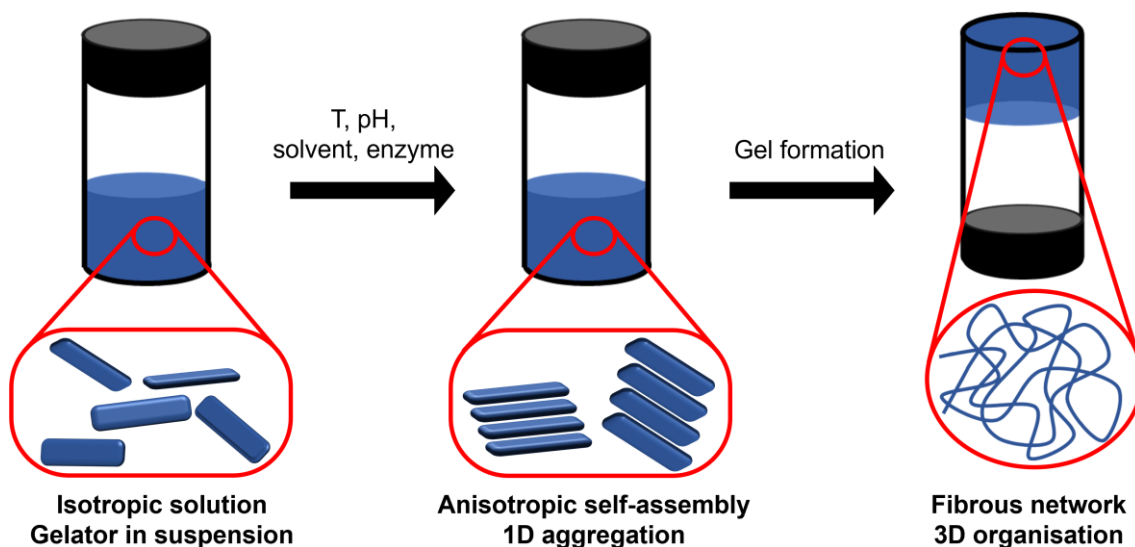


Figure 3. Self-assembly and molecular interactions across multiple length scales. Development of supramolecular interactions after external trigger leading to gelation.

network of coiled, branched fibres entrapping the solvent by capillary forces (Figure 3, right).

1.4 Carbon-loaded hybrid gel systems

The past decade has witnessed a drastic increase in the development and preparation of carbon-loaded or carbon-based soft materials.^[88] The incorporation of such rigid materials within the gel matrices has led to soft materials with enhanced mechanical properties and tunable morphologies. For example, it was observed that the stiffness of polymer gels increased with the amount of introduced GO sheets until the lubrication effect of the sheets countered this effect.^[89] In addition, carbon nanostructures introduce electrical and thermal conductivity along with porous structures, allowing for further functionalisation of the hybrid materials. Some carbon-based nanomaterials (carbon nanotubes (CNT), carbon quantum dots (CQD) and graphene-derivative sheets such as graphene oxide (GO)) show inherent biocompatibility and a low cytotoxicity along with antibacterial activity. Therefore, combining soft materials and carbon nanomaterials in hybrid soft materials will widen the range of biomedical applications, such as drug delivery, tissue engineering and wound healing.

GO is the most common type of graphene material used in gel matrices due to the improved solubility to water-based solutions by the presence of hydroxyl, epoxy and carboxylic acid groups. In comparison, pristine graphene is highly water insoluble, and difficult to homogeneously suspend in a water-based solution with a tendency to precipitate and agglomerate without external stimuli

to minimise the surface tension.^[90] The incorporation of GO into a suspension of Pyrene-protected phenylalanine-based tripeptide significantly lowered the MGC of the resulting hybrid gel compared to the unloaded peptide gel. Presumably, this is due to π - π stacking interactions between the GO sheets and the Pyr protecting group.^[91] π - π interactions between the protective groups and the GO sheets were observed by fluorescence measurements of organogels and hydrogels formed by Pyr protected sugar gelator in the presence of GO flakes upon heating/cooling-coupled sonication trigger method.^[92] Light-responsive hybrid polymeric gels were formed with an aqueous GO suspension through light-induced polymerisation of *N*-isopropylacrylamide. The light-responsive behaviour of these gels (*i.e.* gel-to-sol transition upon laser exposition) is reversible using near-infrared light. This behaviour has potential applications as biomaterials for drug delivery with controllable delivery rate and “on/off” response.^[93] Biocompatible polyvinyl alcohol-based polymeric hydrogels loaded with GO were also used for wound treatment.^[94] The electrical conductivity and the mechanical properties of the material were comparable to that of the skin tissue. GO within the matrix demonstrated growth inhibition of *Staphylococcus aureus* (gram-positive bacteria) and cytocompatibility towards fibroblast cells. Also, the presence of GO in chitosan hydrogels showed great injectability and self-healing properties, and the amount of GO loaded into the polymeric matrix allowed the tuning of the mechanical properties of the gels. *In vivo* experiments showed the promising use of this material for wound healing.^[95]

Another representative of graphitic materials is CNTs, which exhibit high electrical conductivity. When incorporated into the gel matrix, CNTs offer enhanced conductivity and optical properties (fluorescence) and improve mechanical properties, such as rigidity, stiffness, elasticity, thermal stability and self-healing ability of the material.^[96-99] CNT-based polymeric and supramolecular hydrogels have been used to develop antibacterial materials towards various gram-negative and gram-positive bacteria, where the presence of CNTs in the matrix increased the bactericidal activity synergistically.^[100-101] CNT-loaded hybrid hydrogels have also been reported for the transdermal drug delivery of large molecules without using syringes/needles as electrically responsive gels exhibited tunable release through electro-permeation of the skin.^[102-103]

Another interesting feature of carbon materials is their optical properties in terms of fluorescence and interaction with light. CQDs produce reactive oxygen species, which cause oxidative stress upon irradiation of visible/near infrared light and further antimicrobial activity in hybrid materials.^[104,105] Light responsive CQD-loaded hydrogels released anticancer drugs from the network due to the gel-to-sol transition upon NIR light irradiation. Meantime, during irradiation, the creation of reactive oxygen species by the CQDs shows antimicrobial activity towards gram-positive (*Staphylococcus aureus*) and gram-negative (*Vibrio cholerae*) bacteria.^[106] CQD-loaded polymeric hydrogels can also be used for photodynamic therapy and bacteriostasis. Some materials showed

sensitivity to wound pH levels under UV and visible light in addition to bacterial growth inhibition.^[107]

1.5 Out-of-equilibrium transient self-assembly

1.5.1 Dissipative (dynamic) self-assembly (DSA)

For the previous supramolecular gel systems, the self-assembly is thermodynamically driven. This means that initially in the non-assembled state the gelator molecules are high in the energy landscape. An input of energy (*i.e.* triggers, section 1.2) allows the gelators to overcome the energy barrier and to fall into the global minimum free energy state of the energy landscape. Thus, the self-assembly is thermodynamically favoured and in-equilibrium (Figure 4a). In in-equilibrium self-assembly, molecules can further exchange between the higher (dissolved non-assembled state) and lower energy state (self-assembled state) with equal kinetic rates. Therefore, the exchange of matter and energy is null.^[108]

However, in nature, most assemblies exist out-of-equilibrium under the constant exchange of energy and matter with their surrounding environment to sustain the transient state.^[109-111] These systems exhibit useful and unique properties, such as stimuli-responsiveness, self-healing and controllable lifetime. In this case, the non-assembling molecules (*i.e.* precursor molecules) residing in a lower energy state are converted to active molecular building blocks by an input of energy (Figure 4b). Although activation pushes them to a higher energy, the assembled state of these building blocks is in a lower energy state. Thus, self-assembly is energetically favoured. The transient assembly is sustained by the constant consumption of energy. If the energy source is finite in the system (closed systems), the energy is dissipated, reversing the process and converting the active molecules back to the non-assembling precursor state. In out-of-equilibrium assembly, the different reaction kinetics should be taken into account. This means that the formation rate of the activated molecules (*i.e.* consumption of energy) and, consequently, the rate of self-assembly should be higher than the energy dissipation rate (*i.e.* deactivation reaction regenerating the precursors).^[112-115] Once the energy source is consumed, the non-equilibrium assembly collapses with the recovery of the precursors. Theoretically, if the energy source is infinite (open systems), the self-assembly can reach a steady state with the coexistence of the assembled and non-assembled states of the molecules.

In dissipative self-assembly (DSA) systems, the precursor building blocks are activated through an irreversible reaction. This means that the entity taking part in the activation reaction (*i.e.* fuel) is irreversibly transformed to a non-reactive species released into the medium (*i.e.* waste), with the reaction rate R_1 (Figure 4c). To be considered DSA, the system must consist of two antagonist reactions with competing kinetics. In this case, the second reaction requires another entity that will convert them back to the precursor state upon reaction with the activated gelators.

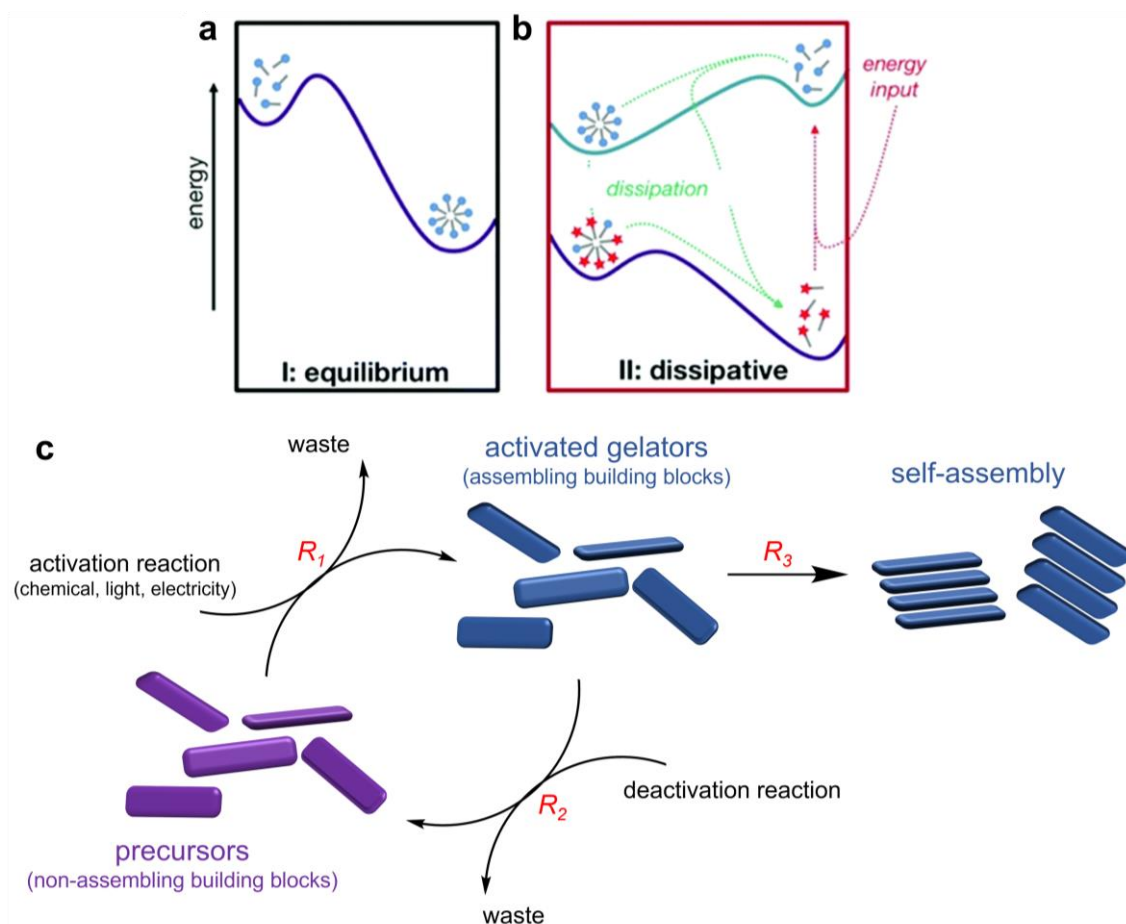


Figure 4. Schematic representation of the energy landscapes for a) in-equilibrium and b) dissipative self-assembly. Reproduced from ref. 113 with permission from the Royal Society of Chemistry. c) Schematic depiction of a dissipative self-assembly cycle. A fuel converts the precursor molecules to activated gelators (activation reaction). The formed building blocks can further self-assemble into higher-order architectures. The deactivation reaction restores the precursor state, which induces the collapse of the assemblies.

The rate of this reaction is denoted R_2 . For the assembled structure to exist and be observed, the rate R_1 and R_3 (rate of self-assembly) need to be higher than R_2 so that the presence of activated gelator lingers long enough to encounter others, resulting in self-assembly. If the rate R_2 is higher than R_1 and R_3 , freshly activated gelators will convert back to non-assembling species before self-assembling. The coupling of the self-assembly with both competing reactions is necessary for the formation of DSA systems.^[108,116-119]

DSA systems can be further sub-categorised into direct (*d*-DSA) and indirect (*i*-DSA). *d*-DSA refers to the direct consumption of the energy source (fuel), activating the precursors. In *i*-DSA systems, the fuel does not react directly with the precursor, but at first, an intermediate reaction transforms the fuel into a reactive species that will subsequently induce chemical or morphological changes to the precursor, thus activating it and leading to self-assembly. For instance, irradiation on 2-[(E)-2-(2-Hydroxy-phenyl)-vinyl]-1,3,3-trimethyl-3H-indolium (light-sensitive hydroxyl containing organic compound) will induce

the ring closure and ether formation that releases a proton in the medium.^[120] The change in pH will then protonate the precursors and convert them into less hydrophilic molecules which will then self-assemble. Removal of the light source reverses the process and triggers the collapse of the assemblies. Side reaction products were also reported to induce the transient, out-of-equilibrium self-assembly in water.^[121] The presence of yeast in the medium, along with a sugar (here sucrose), released carbon dioxide (CO₂) upon biological conversion. The chemical equilibrium between CO₂ and bicarbonate releases a proton, which protonates the negatively charged species, leading to the supramolecular assembly and the formation of a fibrous network. However, CO₂ slowly escapes from the aqueous phase, pushing the equilibrium towards its formation. This means that the protons were scavenged from the gelators, leading to the collapse of the network.

1.5.2 Chemical and alternative fuelling for DSA systems

In DSA systems, the term “fuel” is employed for the activation reaction, which rely on the consumption of irreversibly transformed form of energy, which transforms the precursor state to the active gelator state. When this energy is a chemical compound, which reacts with the precursor, the system is called chemically-fuelled self-assembly.^[122-125] Typically, a finite amount of fuel added in the system reacts spontaneously with the precursor, triggering the self-assembly of the activated gelators. Intrinsically, systems based on chemical-fuelling generate side-product wastes whose concentration progressively increases, saturating the environment. Although these products are often undesired, it is not possible to eliminate them in closed systems.

A Fmoc-protected tripeptide containing alanine and aspartic acid has both carboxylic acids of the terminal aspartic acid protonated in water at a pH above its pKa. Upon the addition of 1-Ethyl-3-(3-dimethylaminopropyl)carbodiimide (EDC) as a fuel, the cyclic anhydride is formed. The disappearance of the charges in the compound increases its hydrophobicity inducing self-assembly (Figure 5a).^[110,124] Upon consumption by the precursor, EDC fuel is converted to the waste (EDU) released into the system. The resulting transient hydrogel exhibited self-healing properties observed using confocal fluorescence microscopy with complete healing over 30 min. However, the accumulation of waste within the material hindered its self-healing ability.^[116]

In other examples, deprotonated carboxylic acid containing precursors dissolved in a basic water environment were activated by the addition of methyl containing reactants, such as iodomethane^[112] or dimethyl sulphate^[114] (Figure 5b and c). The activation reaction (esterification) led to the aggregation of the activated gelators and subsequent fibre network formation, along with the release of iodide and methyl sulphate into the medium. On the other hand, the deactivation reaction (ester hydrolysis) rejected methanol. The fibre formation and dynamic properties of the materials were affected by the increasing presence of side products waste, which hindered the fibre formation.

The obtention of transient assemblies using chemical fuels was also reported by dynamic peptide bond formation.^[126,127] The enzyme-catalysed bond formation between a modified phenylalanine and aspartame formed the assembling dipeptide and led to self-assembly. The activated gelator was reverted back to the amino acid precursor by the same enzyme causing disassembly. It was also found that the constant generation of waste in the medium decreased the efficacy of the activation reaction with a decreasing percentage of its formation over the assembly/disassembly cycles.

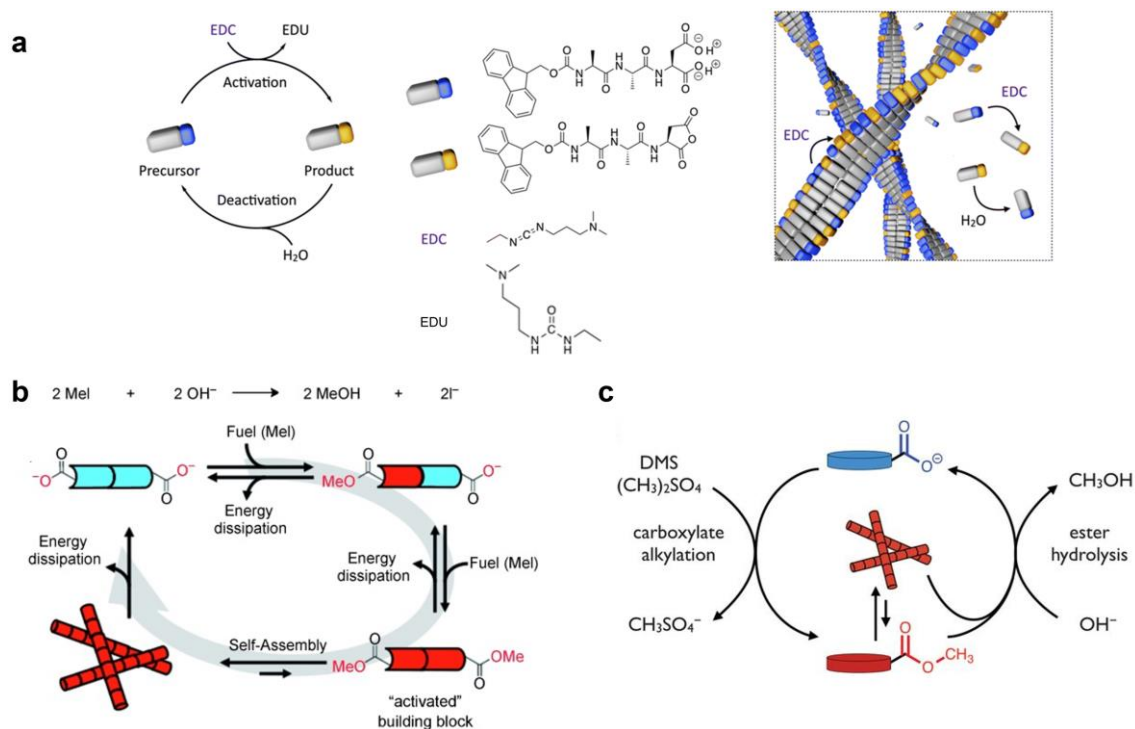


Figure 5. Example of chemically-fueled self-assembly. a) Activation of the precursor from negatively charged carboxylic acid to neutral anhydride by consumption of EDC and release of EDU. The activated gelators self-assemble driven by hydrophobic interactions. Reproduced from ref. 121 under CC-BY 3.0 license. b) Methylation of the negatively charged carboxylic acid precursor by the consumption of iodomethane and release of iodide. Reproduced from ref. 117 with permission from John Wiley and Sons. c) Similar precursor activation using dimethyl sulfate and release of methyl sulfate ion. Reproduced from ref. 119 with permission from the American Association for the Advancement of Science.

Light-fueled DSA materials were developed to counter the waste generation issue intrinsic to chemically-fuelled systems.^[113,120,128,129] The use of photons to induce a change in the chemical structure of precursors is a cleaner method that prevents chemical reactions from happening, therefore eliminating undesired side-products. Another interesting property of light-fuelled materials is the high degree of spatial control, which can be obtained by shaping the light beam or using optical masks to cover a specific sample area, thus selectively triggering gelation. For instance, the *trans*-isomer of an azodibenzoic acid containing long hydrophobic alkyl chains had a favourable self-assembly into

linear sheets or tapes under visible light. However, when exposed to UV light for about 2 h, the photoisomerization induces a conformational change to the *cis*-isomer. In this case, cyclic supramolecular structures form that further elongate to rod-like shapes. The light-induced assembled system maintained its transient conformation for about 2h at R.T. before reverting to the *trans*- state by thermal relaxation.^[130] Another study reported the use of a photo-switchable gelator containing an open 6-membered ring (Figure 6a). The open ring closed upon UV irradiation, forming a gel exhibiting a different fibrous network and higher thermal stability. By the use of photomasks, spatial control over gelation with distinct gel and sol domains was achieved (Figure 6b).^[131] These properties can be exploited to form smart optical materials with controllable lifetime and spatial organisation.

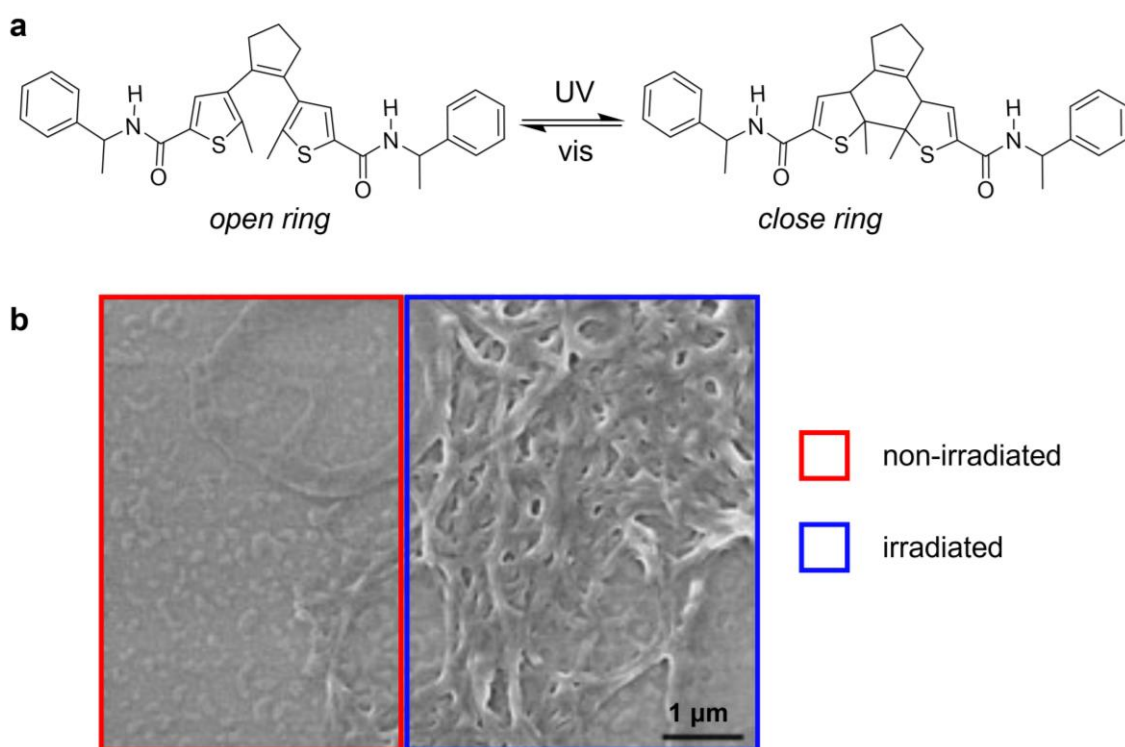


Figure 6. Example of light fueled self-assembly. a) The gelator molecule showing the open ring (left) and its UV-induced closed ring counterpart (right). The absence of UV light reverts the activated gelator to its precursor state. b) SEM images of the gel with selective light irradiation using photomasks showing the UV light-induced fibrous network formation (blue) and the absence of supramolecular structures (red). Reproduced from ref. 136 with permission from John Wiley and Sons.

Recently, an electrically-fueled DSA system was reported.^[132] In this system, the transfer of an electron to the electrode caused the oxidation of a biocompatible iron complex, which then acted as a fuel by converting the monomer precursors to the activated dimer form. The dimers self-assembled into fibres growing from the electrode surface towards the solution. The presence of dithiothreitol in the solution deactivated the gelators, thus breaking the assemblies. In this system, no waste is produced in the activation reaction, but only in the deactivation reaction.

1.5.3 Applications of transient materials

In contrast to equilibrium materials, out-of-equilibrium materials can self-heal from physical damage. This is due to the constant generation of available gelators for self-assembly through activation and deactivation reactions.^[133,134] Controlling the rates of these reactions allows for temporal control over the assemblies and, consequently, the material. Such materials are used for applications that are required to sustain the assembled form for a certain timeframe before self-abolishing. Controlling and tuning this timeframe to suit different needs and purposes has been the main focus of the studies.^[135] One ideal use for self-abolishing materials is self-erasing inks.^[136] For this, the material should display a change in colour or turbidity between the non-assembled and assembled states. An example of UV-light driven self-erasing inks is based on gold or silver nanoparticles functionalised with alkyl chains terminated by azobenzene in the *trans*- conformation. Upon irradiation, the non-thermodynamically favoured *cis*-isomer conformation forms, causing the aggregation of the nanoparticles and inducing a change in the colour of the solution from red to blue or yellow to blue. After the introduction and fixation of the precursor solution in a polymer gel, the use of photomasks or UV-light pen allowed for the spatial control of the aggregation, and patterns could be drawn on the surface of the gel (Figure 7a) The assemblies decayed after removing the light source, and the messages or drawings disappeared from the gel. The lifetime of the ink could be tuned within a wide range of time.

Chemically-fueled assemblies are also used as temporary ink systems. A solution of Fmoc-protected aspartic acid precursor was embedded into a polymer gel and, upon addition of EDC fuelling agent, the formation of the anhydride led to self-assembly because of reduced solubility due to the removal of the negative charges.^[137] A change in the turbidity from a clear precursor solution to a blur material accompanied the assembly enabling selective patterning by controlling the location where the fuel was applied (Figure 7b). Upon depletion of the fuel, the clear solution was recovered, and the markings disappeared. The lifetime of the ink could be controlled by varying the amount of fuel. The material also displayed reusability by the addition of a new batch of fuel on the gel.

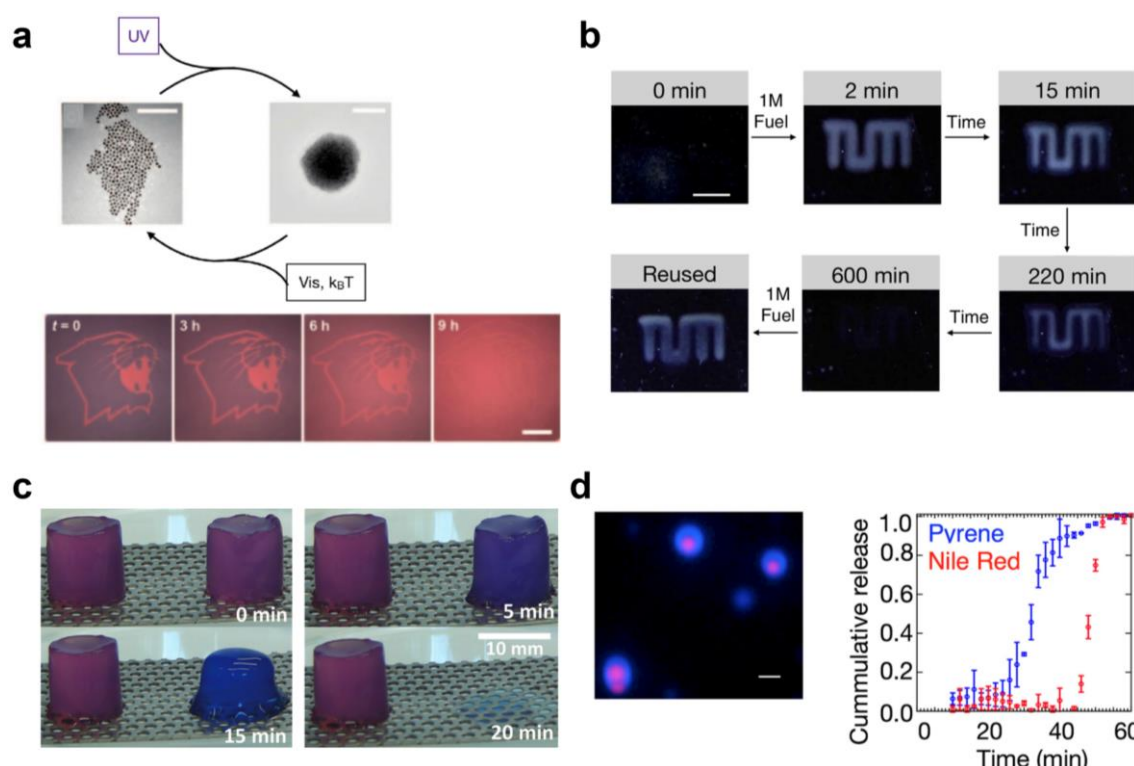


Figure 7. Examples of out-of-equilibrium materials used as self-erasing inks or temporary delivery devices. a) UV-light induced aggregation of functionalized nanoparticles, inducing a color change that reverts after a few hours. Reproduced from ref. 142 with permission from John Wiley and Sons. b) Chemically-fueled transient assembly displaying a change in turbidity that vanishes over time. Reproduced from ref. 143 under CC-BY 4.0 license. c) Comparison between in-equilibrium stable gel (left) and self-abolishing gel (right) for the release of a dye after a pre-determined time. Reproduced from ref. 147 with permission from John Wiley and Sons. d) Localization of a red dye (in the core) and a blue dye (in the outer shell) depending on the time of incorporation in the material (left) that shows sequential release upon degradation from the outside to the inside (right). Reproduced from ref. 143 under CC-BY 4.0 license.

Another application for materials with a definite lifetime is the controlled delivery of targeted compounds. In equilibrium materials, the release rate is generally relatively constant over time from the beginning to the total release of the compound.^[13,138-140] However, out-of-equilibrium materials can show a burst release at the end of their assembled state, which can be programmed or pre-determined.^[123,141] For instance, the self-abolishing hydrogel consisting of Fmoc-Leu-Gly (leucine-glycine motifs) was formed using citric acid as a fuelling agent and urea/urease as a deactivator. The acidic pH induced by the release of the proton from citric acid protonated the terminal carboxylic acid of the peptide, thus increasing its hydrophobicity and leading to gelation. Simultaneously, the release of ammonia from the decomposition of urea by the urease slowly raised the pH back to basic conditions. Depending on the amount of urease, the self-abolishing timeframe was tunable. The incorporation of a drug into both stable (Figure 7c, left side gel) and transient (Figure 7c, right side gel) hydrogel matrix led to drug delivery materials with distinct release regimes. The control of the

deactivator in the gel gave temporal control over the occurrence of the burst release.^[141]

The Fmoc-glutamic acid (Fmoc-Glu) colloids were also reported as delivery carriers, although with a slightly different mechanism. Fmoc-Glu self-assembled by hydrophobic interactions into spherical colloids upon formation of its cyclic anhydride counterpart by reaction with EDC. Due to the low stability of the anhydride in water, hydrolysis reverted the gelator back to the precursor state within a timeframe determined by the amount of fuel. The addition of dyes into the system at different time points during the assembly led to the spatial location of the dyes within the colloidal assembly. For instance, a red dye added at the beginning along with the fuel located within the core, whereas a blue dye added later during the assembly process located on the outer shell (Figure 7d, left).^[137] The collapse of the supramolecular structure initiated from the outer shell, thus leading to the sequential release of the dyes in a controllable manner (Figure 7d, right). In addition, tuning the lifetime of the assembly allowed the release at predetermined times.

Self-immolative materials also spark interest in delivery platforms due to the on/off assembly response to external stimuli. A recent study showed that upon activation of the precursor by a fuel, the activated gelators assemble into micelle droplets and collapse after depletion of the fuel. However, adding an excess of precursor later in the materials' lifetime induced a fast disassembly.^[123] This specificity was used for selective induction of a burst release. A linear release was observed until the addition of the immolative trigger, which caused an immediate and abrupt increase in the release rate of the encapsulated molecule.

2 CHARACTERISATION OF SUPRAMOLECULAR GELS

2.1 Standard characterisation methods

2.1.1 Nuclear magnetic resonance spectroscopy and high-resolution mass spectrometry

Supramolecular gel materials can be characterised at different length scales by various techniques, some of which give information on multiple length scales in the same measurement (Figure 8). The final applications of a material are strongly dependent on its properties. Therefore, a thorough assessment of their structure and properties using a combination of several techniques is required. As supramolecular gels form through the self-assembly of small organic molecules, spectroscopic methods are of great importance to unravel the processes leading to gelation. Nuclear magnetic resonance (NMR) spectroscopy is a powerful tool for studying the intermolecular interactions (1D aggregation) between the gelators by following the shift of a specific proton signal,^[10,72,142] in addition to their chemical identity.^[125,127] In in-equilibrium gel systems, the gelators remain chemically stable, meaning chemical reactions do not alter their structures. Therefore, liquid-state NMR spectroscopy (1D and 2D) allows the study of the development of intermolecular interactions between specific functional groups of the gelators, such as hydrogen bonding. During gelation, the free rotation of the molecules is significantly hindered by intermolecular interactions, leading to the broadening and disappearance of the signals. Solid-state NMR spectroscopy, on the other hand, allows to study the assemblies that have a solid-like behaviour. In the case of out-of-equilibrium gel systems, cascade or coupled chemical reactions transform the precursors into activated gelators and *vice versa*. At the same time, the fuel and brake are converted to waste products. Liquid-state NMR spectroscopy is, in this case, an important method for deciphering the chemical

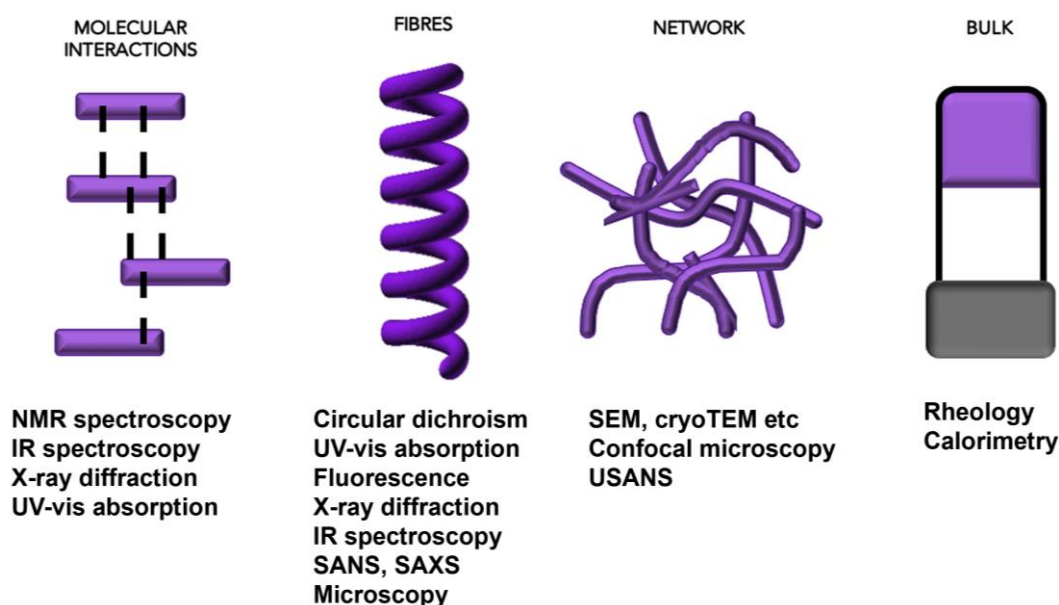


Figure 8. Characterisation techniques commonly used in the community for the investigation of self-assembly at each length scale. Reproduced from ref. 2 under CC-BY license.

transformations and the identity of the entities responsible for gelation. The results can be complemented with high-resolution mass spectrometry (HR-MS). If the compound in the NMR spectrum is also observed in the HR-MS spectrum, it ensures the accuracy of the findings.

2.1.2 Optical spectroscopy

Fourier transform infrared (FTIR), ultraviolet-visible (UV-vis) and fluorescence spectroscopies allow to probe the intermolecular interactions between the self-assembled gelator molecules at the bulk state, giving important information on the molecular-level organisation in primary and secondary organisation (Figure 8). Depending on the technique, *i.e.*, the wavelength of the light used, different length scales can be probed, thus providing a thorough understanding of the molecular packing in 1D and 2D. More specifically, monitoring the shift or disappearance of a vibrational band in the IR spectrum of a gel suggests that the corresponding functional group is involved in self-assembly.^[13,143] Bands arising at the amide I region (1700 cm^{-1} to 1600 cm^{-1}) correspond to secondary structures such as α -helices or β -sheets.^[9,144] Similarly, the self-assembly of aromatic peptide-based gels can be assessed by observing the behaviour of the $\pi \rightarrow \pi^*$ transition band in the UV-vis spectrum of a gel. Upon π - π stacking, overlapping π -orbitals will alter the shape and/or position of this electronic transition band. For instance, bathochromic (redshift, longer wavelength) or hypsochromic (blueshift, shorter wavelength) shifts indicate J- or H-type aggregates of the gelators, respectively.^[145,146] Additionally, the loss of vibronic structure (or fine structure) and increase/decrease of the intensity indicate π - π stacking interactions. Similarly to UV-vis spectroscopy, fluorescence spectroscopy probes

the aggregation process of monomers and allows to study the molecular packing by observing the shift of the emission peak or quenching of the fluorescence signal.^[80,147] The higher-order architectures can also be probed by circular dichroism (CD) and small angle neutron scattering (SANS).

2.1.3 Electron and scanning probe microscopies

Electron microscopies, such as scanning electron microscopy (SEM), transmission electron microscopy (TEM), or analogous cryogenic versions (cryo-SEM and cryo-TEM).^[40,116,148] are routinely used for morphological analysis of 3D networks of gels (Figure 8). Imaging the fibrous network gives important information on its microscopic structure, such as fibre size and porosity, microscopic topology, such as height and width, packing density, and helical pitch. These features can be later controlled and tuned for targeted medical applications, such as materials for 3D cell cultures or drug delivery platforms. As microscopic techniques are based on surface analysis, the drying process is the major point to consider in sample preparation. The network of gels dried at room temperature (R.T.) tends to crumble and structurally rearrange over time as the solvent slowly evaporates.^[149] Therefore, microscopic images obtained on these samples do not reflect the reality of the “wet gel” in its bulk state. However, cryogenic microscopies allow the samples to be cooled to sub-evaporation temperatures, hence freezing the fibrous network in its current organisation.^[150] TEM and SEM have the advantages of being non-destructive techniques and high resolution down to around 10 nm.

Helium ion microscopy (HIM) uses a helium ion beam for the imaging of structures. In contrast to SEM, generating one secondary electron per incident electron, HIM generates 3 – 9 electrons per helium ion interacting with the surface. Thus, it creates a better signal, increases the contrast between the different types of materials, has better spatial resolution and can be used for the imaging of non-conductive samples. In addition, although more scarcely, atomic force microscopy (AFM) in tapping mode is used to investigate the network topology.^[83,151,152] However, a metallic tip scanning over the surface can be destructive on soft samples, such as gel fibres, if the tapping amplitude or the cantilever frequency is too high. Therefore, a slow scan speed is required to avoid destroying the sample. The tip convolution effect is a well-known effect generating artefacts in the x, y plane of AFM measurements, whereas the z -direction is highly accurate.^[153] Electron microscopy is hence preferred for the morphological study of gels over AFM.

2.1.4 Rheology

Rheology is extensively used to probe macroscopic and mechanical properties of soft materials like gels (Figure 8). This technique is widely used and useful to understand and investigate material properties such as phase transition temperature ($T_{\text{gel-sol}}$) and self-healing ability. Amplitude sweep measurements, that is, exposing the material to an increasing shear strain at a constant frequency,

determine two important parameters representative of the material's mechanical behaviour: the storage modulus (or elastic modulus G' , representing the solid-like behaviour) and the loss modulus (or viscous modulus G'' , expressing the liquid-like behaviour). Gelation is assessed only if G' is greater than G'' , meaning that the gel behaves as a viscoelastic solid. Subsequently, frequency sweep measurements, that is, exposing the material to an increasing angular frequency at a constant shear strain, are carried out within the linear viscoelastic region to determine the stiffness of the gels represented by the G' value.^[115,154,155,156] Gels used as scaffolds in a biomedical context for cell culturing need to exhibit a stiffness quantitatively similar to the cells. Therefore, rheological experiments are of great importance in this field. In addition, reformation cycles or self-healing properties can be investigated after mechanical/thermal breaking using this technique.

2.2 Nanoscale spectroscopic characterisation

Scattering scanning near-field optical microscope (sSNOM) is an emerging technique that has drawn a lot of attention in various fields of material science, chemistry and biology.^[157,158] This technique essentially combines the morphological study of AFM with the absorptive properties of organic molecules towards the IR light. Unlike far-field IR spectroscopy, probing the sample at the bulk scale, sSNOM allows for IR measurements at the nanoscale. The IR incident light is focused at the apex of the oscillating AFM tip, and upon reaching the sample's surface, a highly concentrated electric near-field is generated. An interferometer then records the scattered light, which contains the absorptive properties of the probed material with a spatial resolution down to the size of the tip apex (~ 20 nm).^[159-162] IR spectra obtained from near-field and far-field measurements can be interpreted similarly, although slight shifts of the IR peaks can be observed depending on the probing depth (related to the demodulation order or harmonics) and the topology of the sample.^[163]

Importantly, sSNOM can work in nano-imaging and nano-spectroscopy modes. In nano-imaging mode, quantum cascade lasers (QCLs) irradiate a single wavelength (chosen by the operator) onto the sample during the AFM scan. The scattered light contains both the optical amplitude and phase corresponding to the reflectivity (amplitude s_n signal) and the absorption (phase φ_n signal) of the sample, respectively, with n the demodulation order (Figure 9a). Therefore, the interpretation of the phase signal yields the relative absorption of the sample at a specific wavelength, compared to the background, for each pixel of the AFM scan. It is important to note that the higher the demodulation order, the higher the contribution from the sample and the lower the background contribution. However, the lower the collected signal is, the higher the demodulation order. Therefore, based on the experiments, the typical order used is $n = 3$.

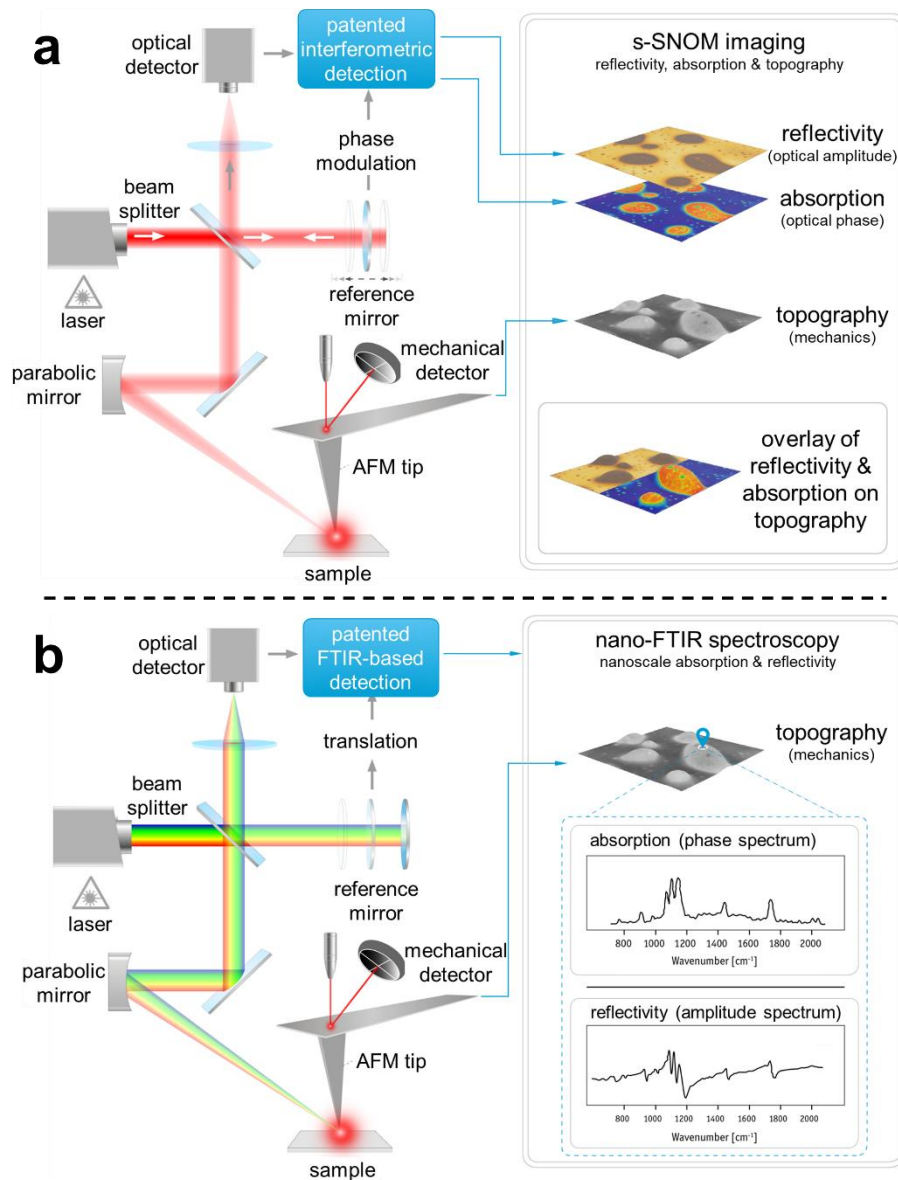


Figure 9. Instrument setup in sSNOM experiments operated in a) nano-imaging mode and b) nano-spectroscopy mode. The laser input was QCLs in nano-imaging and a broadband femtosecond laser source in nano-spectroscopy. Reproduced from Neaspec, attocube systems AG (<https://www.attocube.com/en/business-sectors/nanoscale-analytics>)

In nano-spectroscopy (or nano-FTIR) mode, a broadband femtosecond laser illuminates the tip, and the scattered light is recorded by an asymmetric Michelson interferometer. As for nano-imaging, the interferogram contains the near-field phase φ_n and amplitude s_n . The plot of φ_n corresponds to the nano-FTIR spectrum of the sample (Figure 9b). Due to the mechanical drift of the stage, a new topography image is recorded between each nano-FTIR spectrum acquisition to ensure the correct location of the tip on the fibres.

This technique is a powerful tool to probe the secondary organisation and intermolecular interactions at the nanoscale, therefore highlighting the heterogeneity depending on the morphological features of a gel network. For

example, surface analyses of polymeric thin films have been performed to study the chemical composition and structural defects.^[164-167] The intracellular structure of plant cell walls along with the monitoring of cell development have been investigated,^[168-171] as well as structural changes in viruses^[172,173] and detection of amyloid- β proteins (responsible for Alzheimer's disease) in individual neurons.^[174] sSNOM has also been used to elucidate the structural arrangement of protein fibrils.^[175,176]

3 RESULTS AND DISCUSSION

3.1 Liquid-phase peptide synthesis ^{I,III}

3.1.1 Synthesis of protected di- and tripeptides

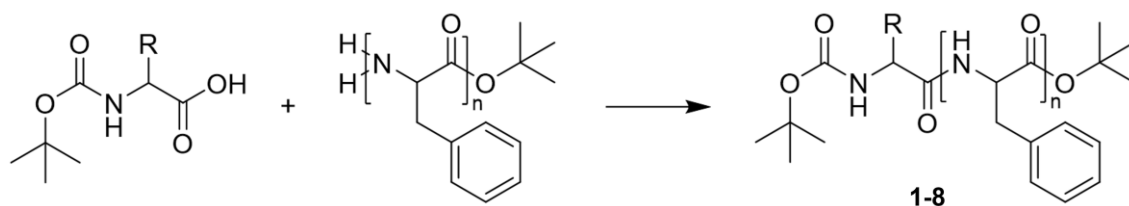
The diprotected dipeptide precursors **1** and **3-8** and tripeptide **2** were synthesised by forming an amide bond using TBTU, a widely used coupling agent in peptide synthesis, between the desired protected amino acids in the liquid phase (Figure 10). Compound **1** containing L-phenylalanine-L-phenylalanine (diphenylalanine or Phe-Phe) core served as a reference for developing the other precursors **2** and **3**. Their hydrophobic and/or aromatic characters were modified to induce changes in the material structures and properties and, in addition, to generalise the gelation mechanism to a variety of phenylalanine-based peptides **2-8** (Table 1). For the diprotected tripeptide precursor **2**, two additional steps were required. The first step was the deprotection of the Boc- group at the *N*-terminus of precursor **1**. The second step was forming an amide bond to attach another amino acid unit to the deprotected *N*-terminus. Additional details can be found in the supplementary information document of publication **III**.

Fmoc-Phe (**9**) used in hybrid gelation studies was commercially available and used without further purification (Figure 12b).

3.1.2 Deprotection of di- and tripeptides

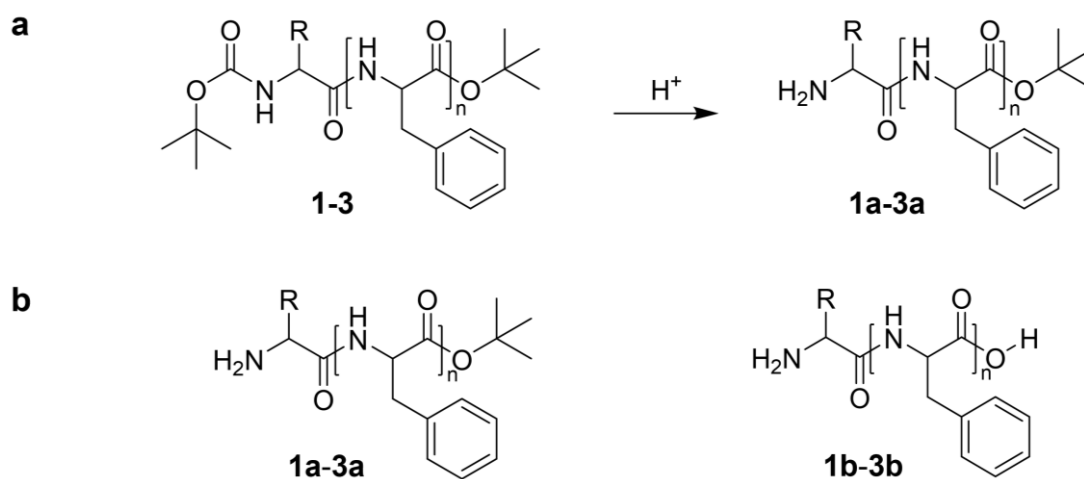
The monoprotected gelators **1a-3a** were obtained by selective deprotection of the Boc- group in the presence of the *t*Bu ester group in an acidic environment (pH 1) using sulphuric acid (Figure 11). The fully deprotected gelators **1b-3b** were commercially available and used without further purification. The structures of the previously reported compounds **1-3**, **5-7**, **1a** and **3a** were verified by ¹H NMR spectroscopy and HR-MS. Novel compounds **4**, **8** and **2b** were characterised with

a full set of 1D and 2D NMR spectroscopy (^1H , ^{13}C , dept-135, HSQC and HMBC), HR-MS and melting points.



Compounds	R			Yield (%)
n = 1	CH ₂ Ph	Phe	1	60
	CH ₂ CH(CH ₃) ₂	Leu	3	63
	CHCH ₃ CH ₂ CH ₃	Ile	4	54
	CH(CH ₃) ₂	Val	5	60
	CH ₃	Ala	6	54
	CH ₂	Gly	7	66
	CH ₂ PhOH	Tyr	8	63
	n = 2	CH ₂ Ph	Phe	2

Figure 10. Synthesis route and yields for preparing the dipeptide precursors **1** and **3-8** ($n = 1$) and the tripeptide precursor **2** ($n = 2$).



Gelators	R		Yield (%)	Gel	
n = 1	CH ₂ Ph	Phe	1a / 1b	95	I IV
	CH ₂ CH(CH ₃) ₂	Leu	3a / 3b	78	III
n = 2	CH ₂ Ph	Phe	2a / 2b	90	II

Figure 11. a) Synthesis route for the preparation of the activated gelators **1a-3a**. b) Structures of gelators **1a-3a** and the *in situ* formed gelators **1b-3b**.

3.2 Molecular scale characterisation and interconversion cycle

3.2.1 Gelation protocols and outcome ^{I,III,IV}

Precursor molecules **1-3** were solubilised (or suspended depending on their solubility) in *t*BuOAc at a concentration ranging from 25 mM to 100 mM and sonicated to ensure the homogeneity of the mixture (Table 1). The accelerator (concentrated H₂SO₄, 1.0 equivalent (eq)) was added, and the vials were left undisturbed for at least 12 h for gelation. The non-flowing character of the materials was assessed by the vial inversion method (Figure 12a), and gelation (*i.e.* the viscoelastic behaviour) was verified by rheological measurements (section 3.4).

Table 1. Gelation concentration screening of precursors **1-8** in *t*BuOAc solvent (1 mL) at R.T. *o* indicates the formation of SSGs and *x* the solution and/or the precipitation of the precursors.

Molarity (mM)	Precursor							
	1	2	3	4	5	6	7	8
100	o	o	o	x	x	x	x	x
50	o	o	o	x	x	x	x	x
25	o	o	o	x	x	x	x	x

o: SSG

x: solution or precipitation

Precursors **1** (Boc-Phe-Phe-*Ot*Bu), **2** (Boc-Phe-Phe-Phe-*Ot*Bu) and **3** (Boc-Leu-Phe-*Ot*Bu) led to self-supporting gels (SSGs) **I**, **II** and **III**, respectively. Free-flowing solutions and precipitates were observed for precursors **4-7** and **8**. The multicomponent gel **IV** was obtained by using **2** and **3** with a 1:1 ratio. The leucine motif in **3** has been reported to be, along with phenylalanine, an effective gelling amino acid, explaining why precursor **3** led to SSG.^[73,177] Precursors **4-7** containing shorter aliphatic side chains did not form SSGs, presumably due to steric effects, meaning that no favourable Gibbs free energy conditions for the gel formation. Although tyrosine-containing peptides have been reported as gelators,^[65] other reports that its presence hinders gelation.^[21] In our case, precursor **8** containing tyrosine residue precipitated after the addition of the accelerator in the medium. An additional hydroxyl group of tyrosine compared to phenylalanine may prevent gelation due to electrostatic repulsions.

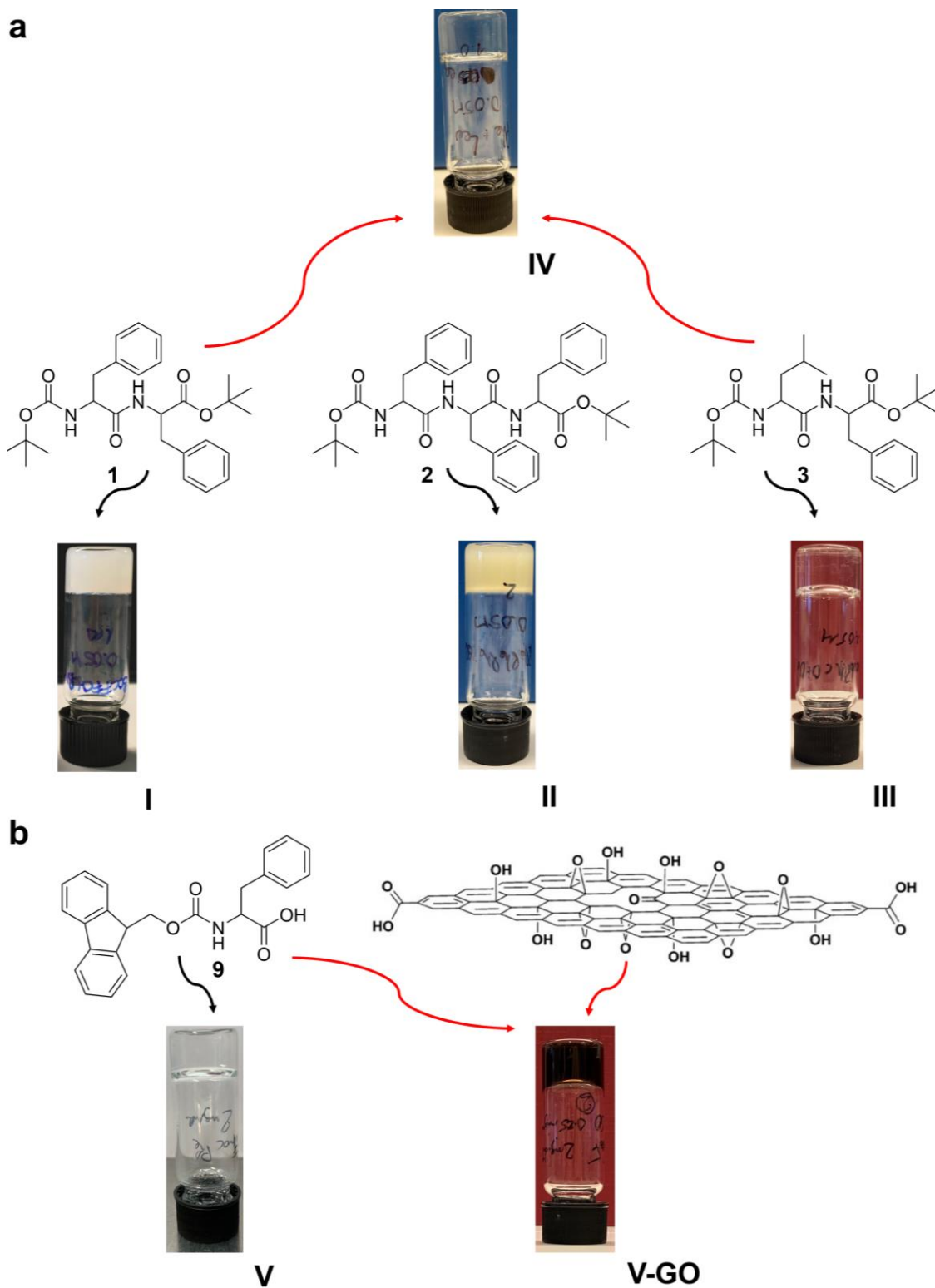


Figure 12. a) The chemical structures of the precursors corresponding to gels I-IV and vial inversion of SSGs verifying the lack of free-flowing solution. b) The chemical structures of Fmoc-Phe and GO sheet and vial inversion of SSGs V and V-GO verifying the lack of free-flowing solution.

The gelation of Fmoc-Phe was performed in a phosphate buffer saline (PBS) solution. The gelator was suspended at a concentration ranging from 1 to 6 mg/mL and sonicated until a fine suspension was obtained (Table 2). The vials were heated at 80 °C for 30 min and left undisturbed to cool down at R.T. for 12 h, yielding transparent gels (Figure 12b). Gelation was first assessed by the vial inversion method and verified by rheological measurements (section 3.4). Graphene oxide (GO) was incorporated in the gels before heating at concentrations 0.25–1 mg/mL using 2 mg/mL and 6 mg/mL of Fmoc-Phe resulting in homogeneous gels (Table 2 and Figure 12b).

Table 2. Gelation concentration screening of Fmoc-Phe gel **V** and Fmoc-Phe/GO gel **V-GO** in PBS solution (1 mL) at R.T. *o* indicates the formation of SSGs and *x* the solution.

Fmoc-Phe (mg/mL)	GO (mg/mL)	Outcome
1	0	x
2	0	o
2	0.25	o
2	0.5	o
2	1	o
6	0	o
6	0.25	o
6	1	o

o: SSG

x: solution

3.2.2 Precursor structure and accelerator effect on gelator/gel formation and self-abolishment ^{LIII}

An important point in triggering the formation of supramolecular gels by pH-switch or heating/cooling is that these methods trigger the self-assembly of small molecules without altering their structures, that is, no chemical reaction happens for self-assembly to occur. In our case, gelation is triggered by the addition of an acid accelerator in the medium, which causes chemical modifications affecting the precursor structure.

NMR spectra of the R.T. or freeze-dried xerogel **I** (one day after gelation) were measured in *d*₆-dimethylsulfoxide (*d*₆-DMSO) and compared with synthesised reference compounds (Figure 13). In the gel state, the absence of the Boc protective group (at 1.28 ppm in the spectrum of precursor **1**) and the broad peak at 8.06 ppm corresponding to the protonated terminal amine indicate the deprotection of precursor **1** to compound **1a**. Two amide NH peaks are present at 8.89 ppm and 8.83 ppm, and the NH₃⁺, Ar, CH, and CH₂ peaks have double integrals compared to **1a**, whereas the *t*Bu peak at 1.31 ppm does not. Therefore, the presence of compounds **1a** (*t*Bu protected, Figure 11) and **1b** (fully deprotected, Figure 11) are observed in the gel state. Thus, in this system, gelation is induced by the formation of two gelators, as confirmed by HR-MS measurements.

In addition, a broad peak at 4.38 ppm corresponding to the OH group of *tert*-butanol (*t*BuOH) is present in the gel spectrum. This secondary solvent

originates from the *in situ* hydrolysis of the primary solvent, *t*BuOAc, by the acid accelerator in the medium. Control experiments to monitor the hydrolysis reaction of *t*BuOAc showed an increasing amount of *t*BuOH over time.

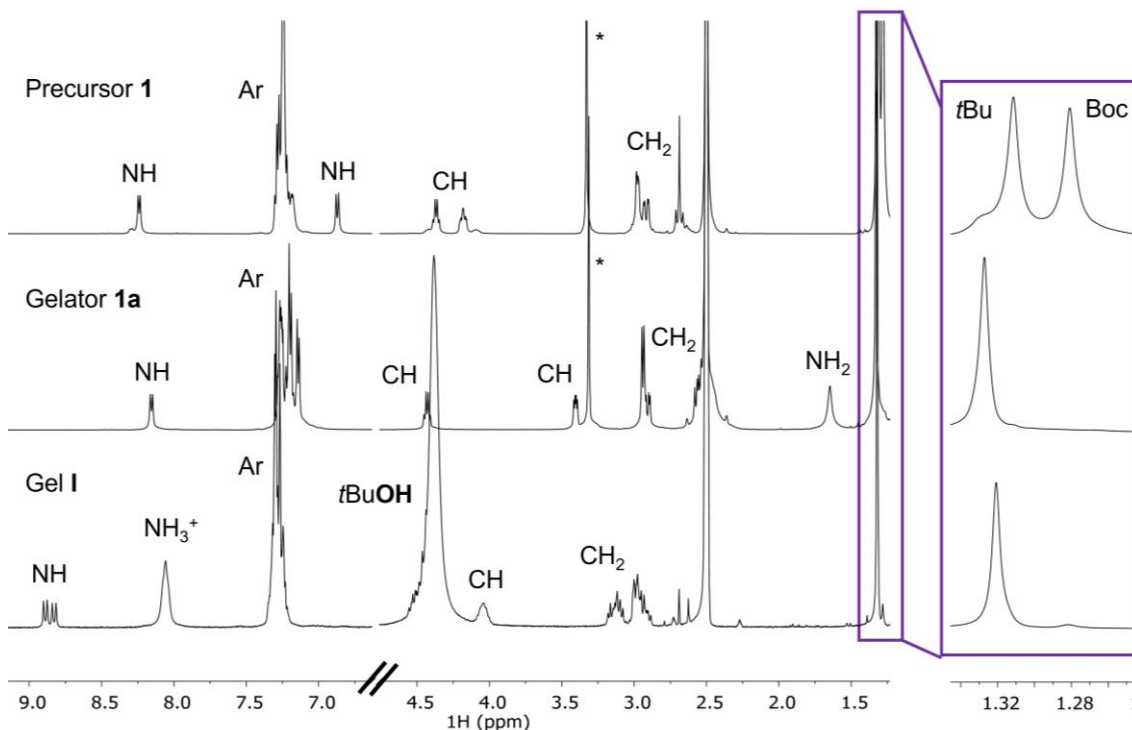


Figure 13. ^1H NMR (500 MHz, d_6 -DMSO) spectra of precursor **1**, gelator **1a** and gel **I**, with a scale break from 5 to 6.5 ppm. Inset is the magnification of the protective group region.

The collapse of the material was observed after 4 days. Therefore, the gel is self-abolishing due to the intrinsically occurring gel-to-sol transition without any external stimuli/trigger. To further understand the mechanism inducing the collapse of the gel, time decay assessment was performed by recording the ^1H NMR spectra of gel **I** at different time points throughout the gel's lifetime (Figure 14, black spectra). Both amide protons are present at 8.92 ppm (**1a**) and 8.85 ppm (**1b**) throughout the material's lifetime, although at different ratios (Figure 14, red rectangle). The random ratio evolution over three experiment batches suggests that the evolution of the ratio is not responsible for the material's collapse.

The hypothesis is that the secondary solvent *t*BuOH, which is always formed and present in the gels, is responsible for the solubilisation of the network. To verify this assumption, a set of solvents of increasing polarity - *t*BuOH, ethanol (EtOH), methanol (MeOH) and water - were added on top of the gel to monitor their dissolution. The dissolution rate of the gels was proportional to the polarity of the solvent: dissolution in 1 mL of water took 5 min, methanol 15-20 min, ethanol EtOH \sim 1 h and *t*BuOH \sim 1 day. When gelators **1a** and **1b** were suspended in *t*BuOH, only **1a** was soluble. This suggests that the *in situ* formation of *t*BuOH slowly and progressively solubilises gelator **1a** from the fibrous network until the complete decay of the material.

During swelling experiments, in which gels are treated with the gel's solvent once a day to monitor their swelling capacity and elastic behaviour, gel I remained in the gel state throughout the 20 days of the experiment. In addition, solvent-treated gels were kept undisturbed for up to a year. This observation is in contradiction with the self-abolishing behaviour discussed above. Therefore, to understand this change in behaviour, ^1H NMR spectra were recorded on swollen gels at 20 days, 6 months and 12 months (Figure 14, blue spectra). After swelling, one of the amide signals and the *t*BuOH signal vanished, and the water signal (3.57 ppm at day 20 and 3.30 ppm at months 6 and 12) appeared. The *t*Bu signal at 1.31 ppm remained constant in all spectra. These results suggest that *via* repeated solvent treatment, both the acid accelerator and *t*BuOH were removed from the gel media. Hence, without *t*BuOH, the integrity of the fibrous network remained unaffected, and the gels remained stable for a longer period. Additionally, the disappearance of one amide signal and the remaining *t*Bu signal suggest that the constant addition of *t*BuOAc into the medium forced the equilibrium towards the production of the *t*Bu-protected gelator **1a**. HR-MS measurements confirmed this observation. Therefore, the out-of-equilibrium self-assembly of the gels shifted towards a thermodynamically stable state.

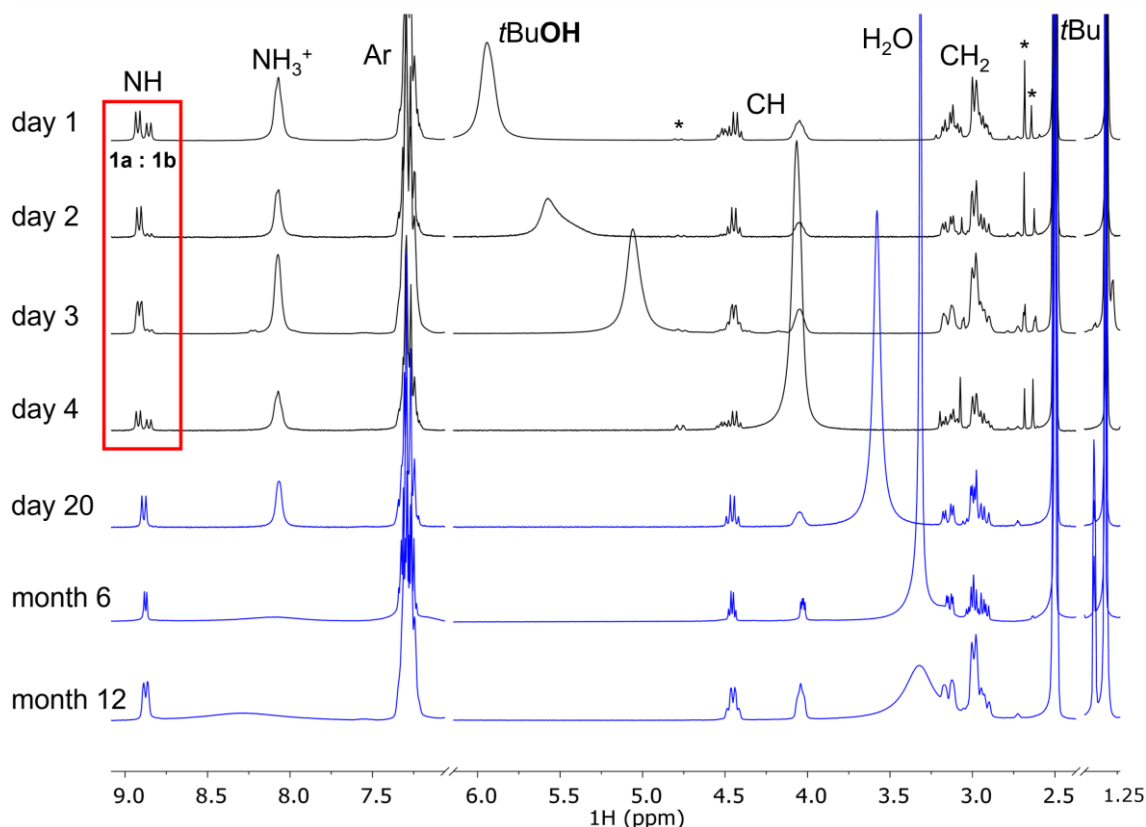


Figure 14. ^1H NMR (300 MHz, d_6 -DMSO) spectra of gel I over four days (black curves, red rectangle highlights the evolution of the ratio of the NH amide protons), at day 20, 6 months and 12 months (blue curves).

Under identical gelation conditions (*t*BuOAc solvent, 50 mM, accelerator 1.0 eq), precursors **2** and **3** led to SSGs **II** and **III**, respectively. The multicomponent gel **IV** was obtained by using **2** and **3** with a 1:1 ratio. The ¹H NMR spectra were recorded on the dried gels (one day after gelation) to investigate whether the change in the precursor structure affects the gelator and gel formation (Figure 15).

Two amide signals are observed at 8.83 – 8.76 ppm for dipeptide-based gel **III**, corresponding to gelators **3a** and **3b** (Figure 15 red insert). For tripeptide-based gel **II**, two sets of two amide groups are observed between 8.73 – 8.52 ppm, along with two smaller amide signals at 8.33 ppm and 8.22 ppm (hollow circles). These negligible signals (about 10 % of the primary amide signals) belong to the rotamer of **2** in *d*₆-DMSO, not observed at higher temperatures or when measured in *d*-chloroform (CDCl₃). In gel **III**, the disappearance of the Boc signal is observed (blue insert), proving the deprotection of the precursor, similarly to gel **I**. Interestingly, the spectrum of gel **IV** is the mere superimposition of the spectra of gels **I** and **III**, with a negligible shift of the two *t*Bu signals. Three amide signals are observed at 8.89 – 8.76 ppm, for which the middle signal accounts for two protons (red insert). HR-MS measurements supported NMR spectroscopy results for chemical identity investigation.

Control gelation using the mono-protected compounds **1a–3a** as precursors yielded SSG with identical reaction equilibria. This shows that the irreversible Boc-deprotection is not the crucial factor, whereas the *t*Bu protective group at the C-terminus is. Therefore, in conclusion, the reaction mechanism leading to the formation of the gelators and, consequently, the gel and the secondary solvent *t*BuOH, is similar regardless of the peptide backbone of the gelator.

Although identical in the equilibria responsible for their formations, gels **I–IV** exhibit different lifetimes: 4 days (**I**), 8 days (**II**), 10 days (**IV**) and 20 days (**III**). The solubility of the different gelators in *t*BuOH and the mechanical properties of the gel (stiffness and elasticity, discussed in section 3.4) are potential explanations for this behaviour.

¹H NMR spectra were obtained from gels **I–IV** at half of their respective lifetime. Expected gelators were observed in their respective gel systems, although at a different ratio. This suggests that the interconversion between the gelators continues throughout the gels' lifetime. NMR spectra obtained after the gel-to-sol transition also showed the expected gelators. Therefore, the gelator interconversion is not responsible for the decay of the gels, which supports the previous hypothesis of the role of the secondary solvent *t*BuOH.

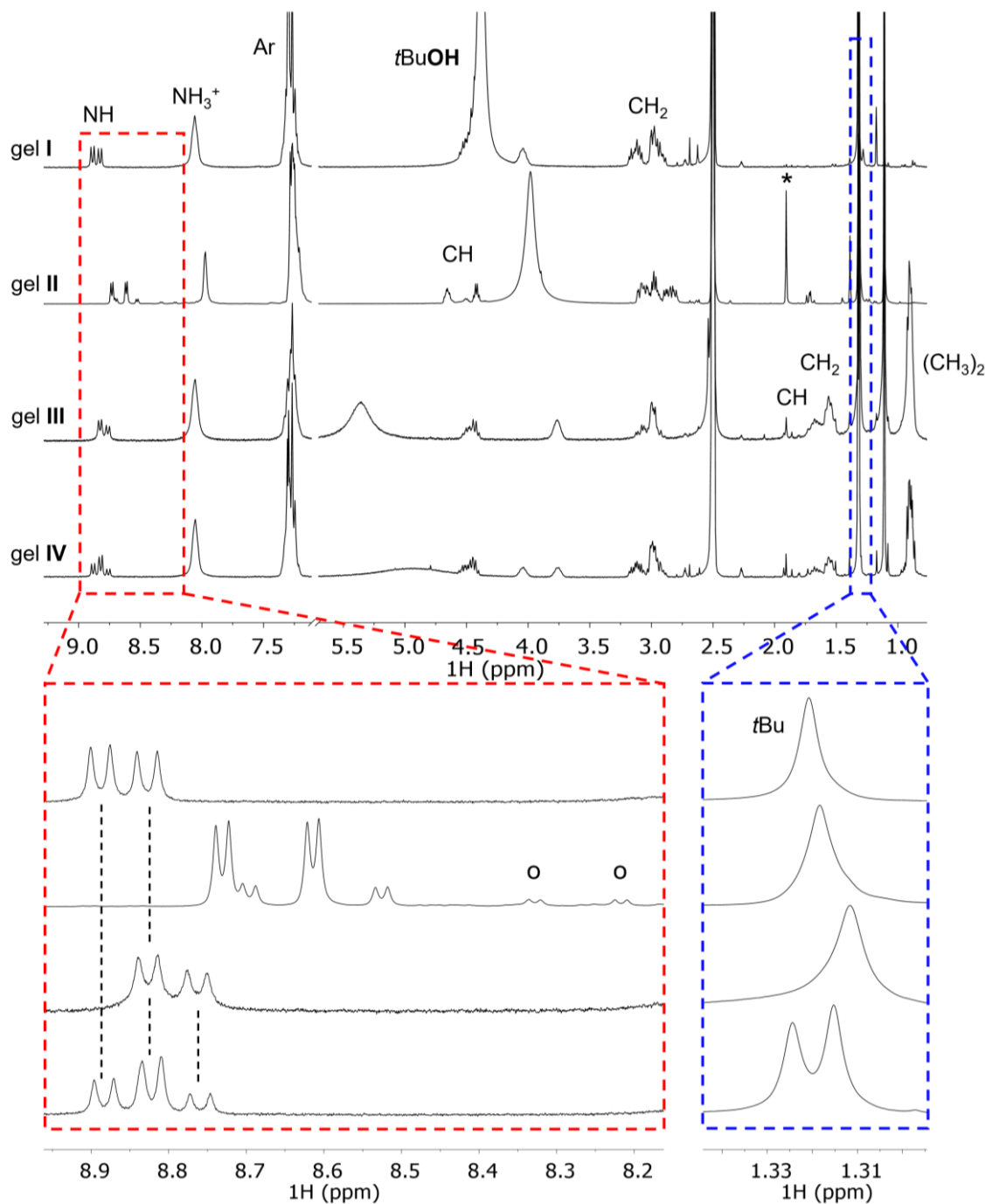


Figure 15. ^1H NMR (300 MHz, d_6 -DMSO) spectra of gels **I-IV** with a magnification of the amide spectral region (red inset) and the *t*Bu protective group spectral region (blue inset). Circles represent the rotamer present in gel **II**.

In addition to gels formed using 1.0 eq of acid accelerator, the amount of acid was changed to 0.5 eq to investigate whether it affects the above-mentioned equilibria. All gel systems **I-IV** formed within the same timescale as with 1.0 eq (~ 12 h). ^1H NMR spectra showed additional multiplet signals (NH, CH_2 , CH and *t*Bu) close to those measured using 1.0 eq, corresponding to the precursor molecules. For gels **I-III**, three compounds were observed in the gel state (precursor + activated gelators), whereas in gel **IV**, four compounds were

observed (two precursors + activated gelators). Precursors were also observed by HR-MS measurements.

The results suggest that although a lower amount of accelerator leaves unreacted precursors in the medium, a sufficient amount of activated gelators is produced for gelation. More importantly, although the mechanisms of gelator formation are identical, the lifetimes of the gels were significantly different. Regardless of the precursor, the gels did not exhibit a gel-to-sol transition, that is, the gels lost their transient character. These materials are, therefore, not self-abolishing but stable in time (up to more than a year). Since a lower amount of accelerator was used, a lower amount of *t*BuOH formed during the solvent hydrolysis. Therefore, this amount was insufficient to induce the collapse of the gels.

Similarly, 1.5 eq of accelerator was used to induce gelation. Interestingly, gels I-IV exhibited a faster gel-to-sol transition of around 1 – 3 days. Therefore, the amount of accelerator introduced in the system dictates the formation rate of *t*BuOH and, consequently, the self-abolishment character of the material.

3.2.3 Introducing solvent-induced self-assembly ^{III}

In our systems, the gels do not follow the same pathway observed for DSA systems, although they exhibit transient behaviours.^{III} Once the acid accelerator activates the precursors, the back-conversion is not observed during the gels' lifetime or after decay (Figure 16, left side). Instead, time-dependant NMR spectroscopy measurements indicate a continuous interconversion of the gelators until the gel-to-sol transition.

In contrast to DSA systems, where fuels are usually separate entities added into the system, the reactive species here is the gelation solvent. The addition of accelerator triggers the cascade reactions beginning with the irreversible Boc-deprotection of the peptide precursor, yielding at first the mono-protected gelator **a**, which is then *t*Bu-deprotected towards the fully deprotected gelator **b**. Simultaneously, the primary solvent is hydrolysed *in situ* by the accelerator to form the secondary solvent *t*BuOH, actively participating in the chemical interchange between the gelators (Figure 16, right side). The progressive formation of *t*BuOH is also responsible for the abolishment of the material, as it solubilises the gelators over time. In this system, similarly to DSA, the kinetics of the activation reaction is higher than the deactivation reaction, *i.e.* the gelator solubilisation. Self-assembly is therefore favoured and observable. In addition, temporal control over the lifetime is achieved by modifying the amount of accelerator in the system, thus altering the competition of the reaction rates.

Strictly, this self-assembly cannot be considered as DSA, due to the absence of energy dissipation recovering the precursor state. However, the presence of two competing reaction kinetics, *e.g.* gelator formation rate and secondary solvent formation rate, highlights some similarities. To some extent, the solvent-induced self-assembly also finds similarities with *i*-DSA, in which the fuel is indirectly responsible for the activation of the precursor, that is, an intermediate reaction occur. Here, formation of the secondary solvent, by the accelerator,

responsible for the interconversion of the gelators thus leading to self-assembly, is also responsible for the solubilisation of the assembly thus leading to the collapse of the material.

Gelation was attempted in dichloromethane (DCM), which lacks a *t*Bu group. Then, no gel formation was observed. ¹H NMR spectra analysis revealed the complete deprotection of the precursor with the sole presence of gelator **b** in the system, confirming that a similar protective group is required for the interconversion cycle and subsequent gelation, as both gelators are required. Therefore, transient gels can be obtained from various short peptide precursors, regardless of the peptide backbone (provided that the interactions between amino acid units favour self-assembly), bearing a protective group at the C-terminus identical to that of the solvent, here *tert*-butyl.

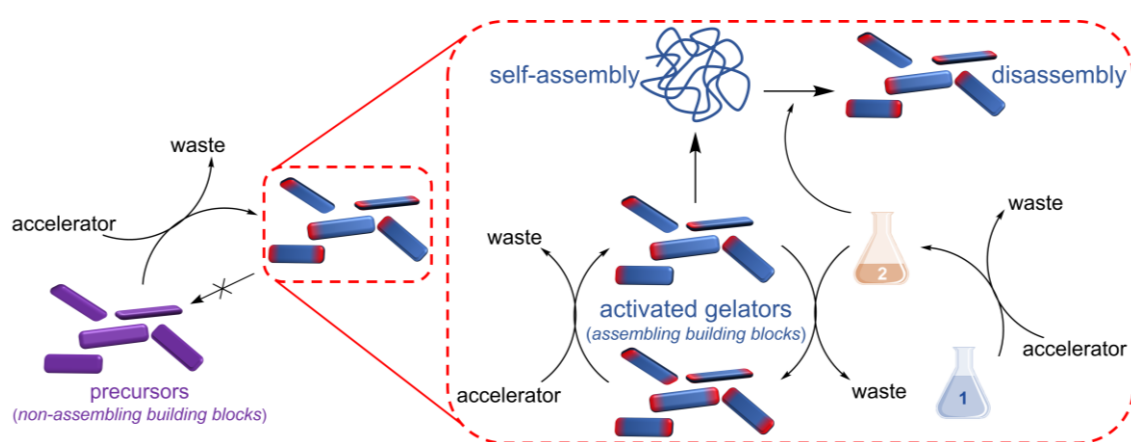


Figure 16. Schematic depiction of the solvent-induced transient self-assembly. Red inset shows the gelator interconversion and the secondary solvent production responsible for the self-abolishment.

3.3 Higher-order organisation

3.3.1 Morphological assessment^{III,IV}

The morphology of the fibrous network of gels **I-IV** (one day after gelation) was investigated using SEM to study the effect of the precursor's chemical structure on the network (Figure 17a-d). To minimise potential structural rearrangement of the network during drying at R.T.,^[149,150] the samples were freeze-dried before imaging. For gel **I** (Figure 17a), single fibres appeared curved and branched, ultimately entangling into a densely packed fibrous network. This verifies the high stiffness measured by rheology (section 3.4). Although exhibiting a similar shape, the fibres of gel **III** appear more spread than that of gel **I**, which correlates to the lower stiffness (Figure 17c) and also helical features are observed (red arrows). For multicomponent gel **IV**, bigger bundles of straight and entangled fibres are observed (Figure 17d). Interestingly, the fibrous network has a different

shape than its individual components, suggesting a new structure and the co-assembly of the different gelators.^[152,178] The SEM images of gel **II** show individual fibres branching out of a potential nucleation point smaller compared to that of gels **I**, **III** and **IV** (Figure 17b).

HIM and TEM have been employed to study the morphology of the network of *N*-(9-fluorenylmethoxycarbonyl)-L-phenylalanine (Fmoc-Phe **9**) hydrogel **V** (one day after gelation). The network shows thin and long entangled fibres, regardless of the technique, with a coiled coil pattern (Figure 17e). Interestingly, HIM images show similar shapes for the hybrid gel **V-GO**'s fibres, suggesting that GO flakes do not affect the self-assembly of Fmoc-Phe. However, fibres appear to grow from the GO flakes (dark grey islands pointed by white arrows) and circle around the flakes. This implies that GO flakes are potential nucleation sites for Fmoc-Phe fibres and that the secondary and tertiary organisation of the fibres interact non-covalently with the flakes.

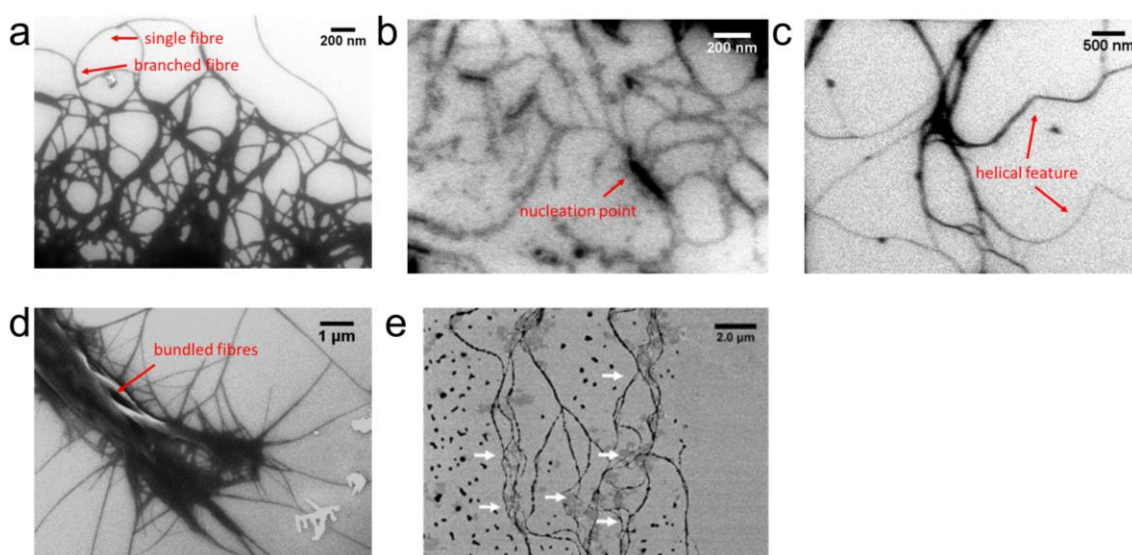


Figure 17. Microscopy images obtained by SEM of gels **I** (a), **II** (b), **III** (c) and **IV** (d) and HIM of gel **V-GO** (e). Reproduced from ref **III** and **IV** under CC-BY 4.0 license. SEM and HIM images were recorded on carbon-coated copper grids.

AFM has been employed to study the network topology of gels **I-IV** (Figure 18a-d, one day after gelation). Gels measured by electronic microscopies and AFM show similar behaviour, although both techniques generate different measurement artefacts. The tip convolution effect, or spatial broadening during AFM scans, affects the measured sample width, thus altering the size of the objects.^[153] As supramolecular gel fibres are assumed to be most commonly spherical, the height values are discussed here, as they are absolute values normalised to a background and not subjected to stretching artefacts. The fibres of gel **I** (Figure 18a) appear straight and densely packed, as in the SEM images, with an average height of 20–30 nm. In gel **III**, the fibres are slightly smaller, although similar in shape, and have an average height of 10–20 nm (Figure 18c). The average height of 5–10 nm and the curvier, more entangled appearance of

the fibres of gel **IV** indicate that the fibrous network of the multicomponent system has a different shape and dimension than that of gels **I** and **III** (Figure 18d) supporting the observation made based on SEM about the formation of a new structure by the co-assembly of the gelators. For gel **II**, the average height of the fibres is 3–7 nm, and curved fibres entangle into wider bundles (Figure 18b). In gel **V**, the average height of single fibres is 2–3 nm.

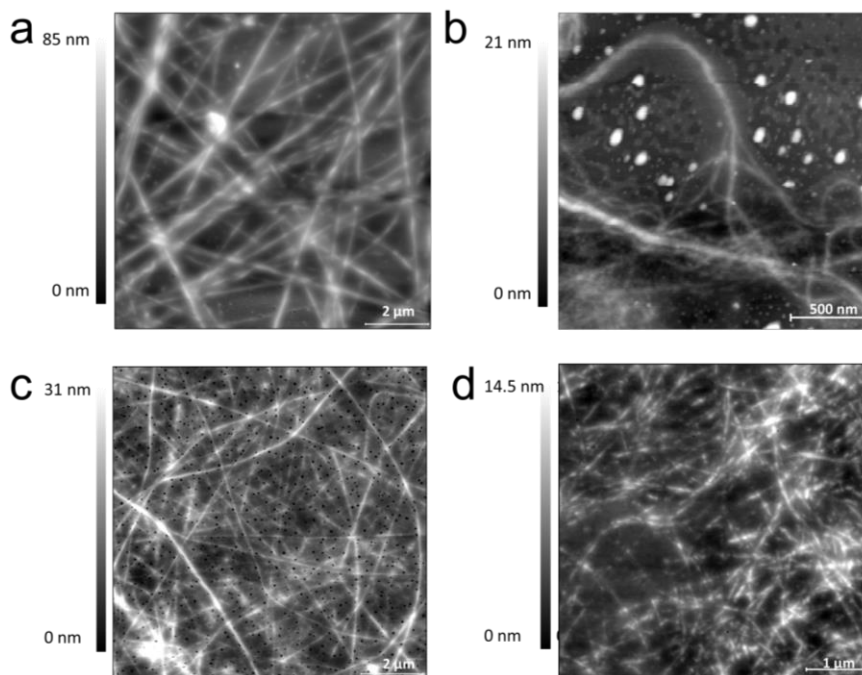


Figure 18. AFM images recorded on gels **I** (a), **II** (b), **III** (c) and **IV** (d). AFM images were recorded on silicon substrates.

3.3.2 Bulk infrared characterisation ^{III,IV}

The far-field FTIR experiments were performed in ATR mode, where incident IR radiation from underneath the sample passes through a diamond crystal and strikes the sample with a specific angle. The incident radiation is reflected multiple times within the sample before reaching the detector. Each time the IR radiation interacts with the sample, the evanescent wave travelling through the sample is absorbed by the IR active groups present in the sample, and the outgoing light contains its absorptive properties. This technique probes the sample at the microscale with a penetration depth of a couple of micrometres, depending on its refractive index and the incident light angle. Thus, the recorded spectrum indicates the absorptive properties of the sample at a micrometre length scale (or bulk scale).

IR spectra were recorded in transmittance on xerogels **I-IV** (50 mM), **V** (2 mg/mL), and **V-GO** (2 and 0.25 mg/mL) from 4000 to 400 cm^{-1} in attenuated total reflectance (ATR) mode (Figure 19) one day after gelation. The region 3500 – 3200 cm^{-1} corresponds to the N-H stretching vibrations of the primary terminal amine and amide groups of gels **I-IV** (Figure 19a). A common N-H stretching

vibration band is centred between 3328 and 3320 cm^{-1} for gels **I**, **III**, and **IV**, and slightly shifted to 3349 cm^{-1} for gel **II**. Compared to the bands of the gelator (Table 3), the bands in the gel state are merged and shifted to lower wavenumbers. This is also observed in the spectra of gels **V** and **V-GO**, in which the N-H stretching band is shifted down from 3316 cm^{-1} to 3313 cm^{-1} after gelation (Figure 19d, purple and orange). These results indicate the participation of the N-H groups in supramolecular interactions, in this case hydrogen bonding.

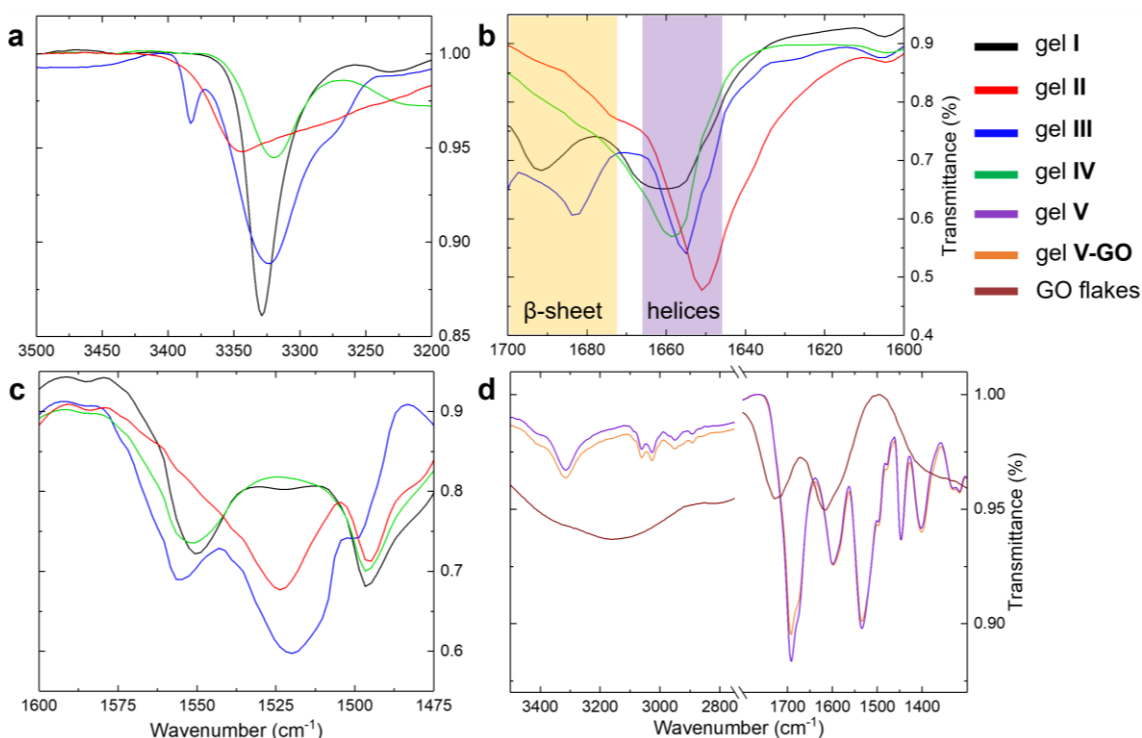


Figure 19. ATR-FTIR transmittance spectra of xerogels **I-IV** in the range a) 3500 – 3200 cm^{-1} , b) Amide I: 1700 – 1600 cm^{-1} and c) 1600 – 1475 cm^{-1} . ATR-FTIR transmittance spectra of xerogels **V** and **V-GO** and GO flakes in the range d) 3500 – 1300 cm^{-1} .

Additionally, the amide I region (1700–1600 cm^{-1}) provides important information on the higher-order architectures of the supramolecular assemblies, such as the secondary structure of the fibres.^[6,75,83,179] A band corresponding to a β -sheet structure at 1691 cm^{-1} ^[180] is present in the spectrum of gel **I** along with a band at 1660 cm^{-1} ^[181,182] assigned to a helical-shaped motif (Figure 19b, black). Due to the length of the peptide sequence which does not support the formation of an α -helix, the helical shape possibly arises from higher helical architectures of the assembly. Although the literature reports mainly a β -sheet structure for Phe-Phe-based gel systems,^[183,184,185] this observation might reflect the presence of a second gelator in the system. Similarly, the spectrum of gel **III** exhibits both β -sheet and helical-like bands at 1682 cm^{-1} and 1655 cm^{-1} , respectively (Figure 19b, blue).

Table 3. C=C stretching and N-H stretching wavenumber peaks (cm⁻¹) of the gelators (neat powders) and gel samples.

Gel system	C=C phenyl ring stretching vibration			N-H stretching vibration		
	Gelator a	Gelator b	Gel	Gelator a	Gelator b	Gel
Gel I	1495	1496	1493	3392, 3346, 3288	3249, 3171	3328
Gel II	1495	1495	1494	3370, 3266	3375, 3363	3349
Gel III	1497	1496	1495	3364, 3319	3392, 3340	3323
Gel IV	1495, 1497	1496, 1496	1495	3392, 3364, 3346, 3319, 3288	3392, 3340, 3249, 3171	3320
	C=C Fmoc ring stretching vibration					
	Gelator		Gel	Gelator		Gel
Gel V	759, 738		755, 733	3316		3313
Gel V-GO			755, 733			3313

To investigate the effect of drying on the secondary structure, IR spectra were recorded on non-dried (“wet”) gels, which showed similar bands, although shifted by ~4 cm⁻¹. However, the spectrum of gel II shows solely a band at 1651 cm⁻¹ attributed to a helical assembly (Figure 19b, red), despite literature reporting β -sheet features for Phe-Phe-Phe-based gels.^[186,187] The presence of two gelators is again possibly the reason for this observation. In the spectra of gel V and V-GO, two bands at 1691 cm⁻¹ and 1674 cm⁻¹, assigned to β -sheet structure, consistent with the literature (Figure 19d),^[13,188,189] indicate that the presence of GO does not affect the secondary structure of the Fmoc-Phe fibres, even if present during nucleation and growth.

Optical spectroscopies (*e.g.* IR and UV-vis) are powerful tools to investigate the mode of assembly (co-assembly or self-sorting) of a multicomponent system.^[144,178] In the case of self-sorting, the spectrum of the multicomponent system is the superimposition of its individual components’ spectra, whereas a different spectrum would be observed in the case of co-assembly.^[152] A band at 1658 cm⁻¹ corresponding to a helical assembly is present in the spectrum of gel IV, but no indication of the β -sheet band, unlike the spectra of its individual components, is observed. Therefore, this suggests the formation of the network by co-assembling gelators.

The spectra of gels I-IV in the range 1600 – 1475 cm⁻¹ (Figure 19c) contain the amide II region (1600 – 1500 cm⁻¹), which indicates C-N stretching and N-H bending of the amide bond. The interpretation of this spectral region is more complicated than that of the amide I. However, the observed redshifts of the bands in the gels’ spectra corroborate the hydrogen bonding interactions upon gelation. The same observation can be made for the amide II region of gels V and V-GO (Figure 19d). For gels I-IV, all spectra show a band at 1495-1493 cm⁻¹ assigned to the C=C stretching of the phenyl rings of the phenylalanine motifs. These bands are redshifted 1 – 3 cm⁻¹ from the bands in the individual gelators’ spectra (Table 3), indicating that the phenyl rings π - π stack during self-assembly. The stretching of the aromatic ring of the Fmoc group is shifted to lower

wavenumbers (from 759 cm⁻¹ and 738 cm⁻¹,^[67] to 755 cm⁻¹ and 733 cm⁻¹) in both gels **V** and **V-GO**, indicating the π -overlap during molecular aggregation. The spectra of gels **V** and **V-GO** are qualitatively and quantitatively similar. This shows that the presence of GO in the medium during self-assembly does not affect the molecular packing and the final fibrous network.^{IV}

3.3.3 Nanoscale infrared characterisation II

sSNOM is a near-field IR technique that allows for recording the absorptive properties of an organic sample towards the IR light with a lateral resolution approximately equivalent to that of the AFM tip, that is, ~ 20 nm (nanoscale).^[190,191,192] It should be noted that subtle shifts in the wavenumber of infrared peaks in the near-field can be observed compared to the far-field.^[163] To the best of our knowledge, the structural investigation of supramolecular gel fibres has not been mentioned before the studies carried out by our group (publications **II** and **V**).^{II,V}

The far-field ATR-FTIR spectrum of the bulk gel **I** was chosen as a reference (Figure 20). The amide I region (1700 – 1600 cm⁻¹) shows characteristic bands at 1691 cm⁻¹ and 1660 cm⁻¹ corresponding to β -sheet and helical arrangements, respectively (red dashed lines). Additionally, the bands corresponding to C=C stretching of the aromatic rings (P_1^{ref} , 1493 cm⁻¹), N-H stretching in the amide II region (P_2^{ref} , 1550 cm⁻¹), the C=O stretching of the *tert*-butyl ester carbonyl of **1a** (P_3^{ref} , 1712 cm⁻¹) and the C=O stretching of the carboxylic acid carbonyl of **1b** (P_4^{ref} , 1732 cm⁻¹) are of interest (represented by the green dashed lines) when studying the non-covalent interactions driving the gel formation at the nanoscale. These will also highlight the heterogeneity of the interactions within the network that cannot be assessed by far-field IR spectroscopy.

Three spatial locations were studied to elucidate secondary structures and intermolecular interactions at different topological features within the fibrous network: single fibres and fibres in parallel and perpendicular arrangement. Figure 21a shows the location for the nano-FTIR spectrum recording on a single fibre (red circle) along with the location of the background (reference) spectrum (orange dot). The four bands of interest (P_1 : 1488 cm⁻¹, P_2 : 1557 cm⁻¹, P_3 : 1720 cm⁻¹ and P_4 : 1754 cm⁻¹; Table 4) are present in the spectra (Figure 21b). The downshift of P_1 , P_3 and P_4 compared to the reference peak position in the gelators' powder spectra suggests that the phenyl rings undergo π - π stacking while the C-terminal carbonyl groups are H-bonded. The downshifts of the peak position of the ester carbonyl (~ 10 cm⁻¹) and the carboxylic acid carbonyl (~ 26 cm⁻¹) are not of the same magnitude. The difference is presumably due to the greater hydrogen bond tendency of free carboxylic acids and the steric hindrance caused by the bulky *tert*-butyl group.^[193]

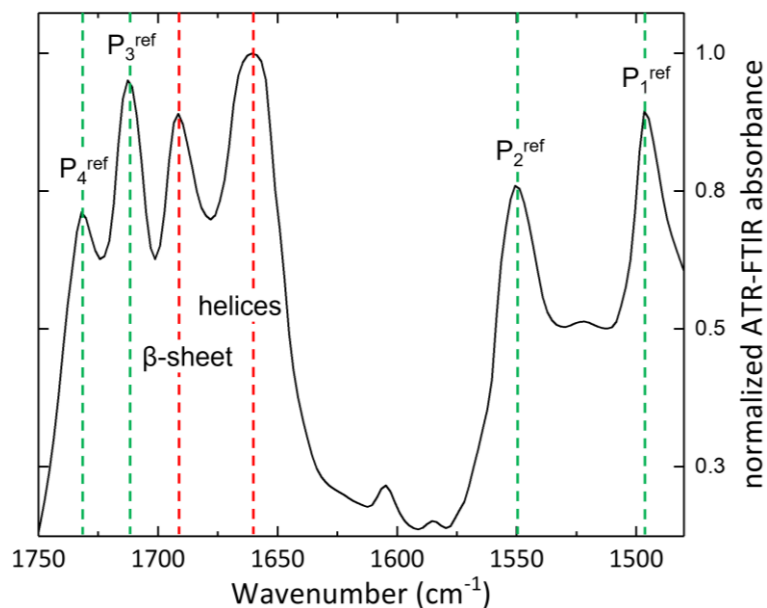


Figure 20. ATR-FTIR spectrum of gel **I** from 1475 to 1750 cm^{-1} in absorbance mode. Green dashed lines refer to the vibrational bands of interest $P_{1\text{ref}}$, $P_{2\text{ref}}$, $P_{3\text{ref}}$, and $P_{4\text{ref}}$, and red dashed lines to the amide I region.

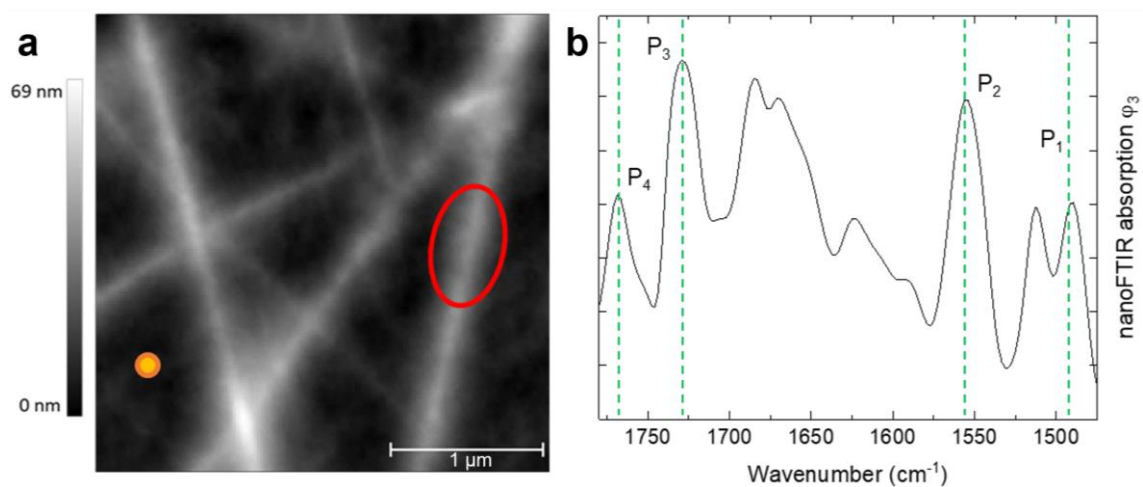


Figure 21. a) Topological (height-sensor) image of single fibres on a gold surface. The red circle indicates the position of the recorded nano-FTIR spectrum and the orange spot indicates the position of the recorded reference spectrum. b) nano-FTIR spectrum of a single fibre. Adapted from ref. **II** under CC-BY 4.0 license.

Although the supramolecular interactions responsible for the formation of a 1D fibre are similar at the nano- (near-field measurement) and bulk scale (far-field measurement), the magnitude is different. For instance, the observed shifts of the carbonyl groups P₃ and P₄ in a single fibre are lower than the bulk gel, suggesting that the hydrogen bonding interactions are weaker. This can be an effect of the far-field measurements, averaging a high number of entities and topographical conformations, whereas near-field measurements solely probe the interactions responsible for the formation of a single fibre.

Table 4. Peak position for P₁, P₂, P₃ and P₄ (cm⁻¹) in the nano-FTIR spectrum of single, parallel, and crossed fibres. Reference position in ATR-FTIR spectra of the synthesized gelators **1a** and **1b** and the bulk gel.

	Single fibre	Parallel fibre	Crossing fibre	Gelator 1a	Gelator 1b	Bulk gel
P ₁	1488	1496	1489	1496	1497	1493
P ₂	1557	1546	1556	/	1550	1550
P ₃	1727	1720	1729	1732	/	1712
P ₄	1754	1743	1761	/	1780	1731

Investigation of higher-order organisations within the fibrous network highlighted a different trend. The strength of the intermolecular interactions and the participation of the functional groups in fibre formation are affected by the spatial orientation (*e.g.* entanglement) of the 1D fibres. For instance, fibres in a parallel arrangement interacting along the longitudinal fibre axis exhibit differences in the IR spectra compared to single fibres. The topology image (Figure 22a) shows the selected fibres and the point where the nano-FTIR spectrum was recorded (red circle). Based on the extracted 3D profile, the distance between the height maxima of the fibres is approximately 20 - 30 nm (Figure 22b). Since the lateral resolution of the measurement is equal to the size of the tip apex (~20 nm), the spectroscopic recording at this position will give information on the interactions holding the fibres in contact (Figure 22c). The observed peak position in the nano-FTIR spectrum (Figure 22d) for P₁ (C=C aromatic stretching) at 1496 cm⁻¹ compared to the reference peak position (Table 4) suggests that the involvement of π - π stacking is negligible. On the contrary, the downshift of the H-bonded groups (P₂ (1546 cm⁻¹), P₃ (1720 cm⁻¹) and P₄ (1743 cm⁻¹)) is greater than for the single fibre. This indicates that, at this specific point, the hydrogen bonding interactions maintaining the structure are stronger than for the formation of a single 1D fibre.

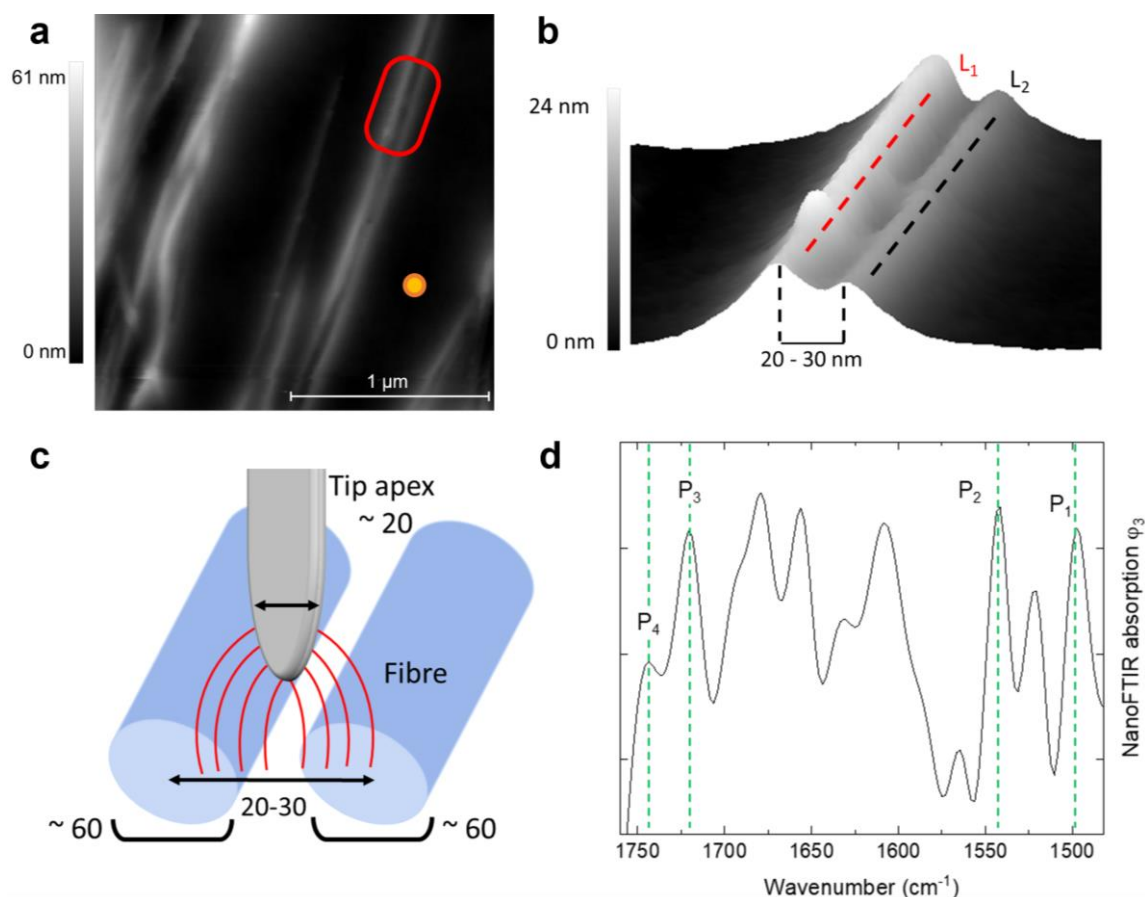


Figure 22. a) Topological (height-sensor) image of two parallel fibres on a gold surface. The red circle indicates the position of the recorded nano-FTIR spectrum and the orange spot the position of the recorded reference spectrum. b) 3D topography view of the fibres in contact with the distance between the height maxima of fibre 1 (red) and fibre 2 (black). c) Depiction of the nano-FTIR measurement probing the contact point of the fibres. d) nano-FTIR spectrum of parallel fibres. Adapted from ref. **II** under CC-BY 4.0 license.

Another interesting feature of the network is the point at which two fibres cross (Figure 23a). The 3D topological view shows that both fibres fuse at the crossing point (Figure 23b). As the height of the fibres is approximately 20 – 30 nm, the lateral resolution of the instrument (~20 nm) allows to probe the supramolecular interactions responsible for maintaining such structure (Figure 23c). Among the four bands of interest, P₁ is observed at 1489 cm⁻¹, thus showing a significant downshift similar to that measured for the single fibres (Figure 23d). The ester (P₃ at 1729 cm⁻¹) and the carboxylic acid (P₄ at 1761 cm⁻¹) carbonyls exhibit the lowest downshift among the three spatial locations. These results suggest that to maintain the perpendicular arrangement, π-π staking interactions prevail, whereas hydrogen bonding interactions are minor.

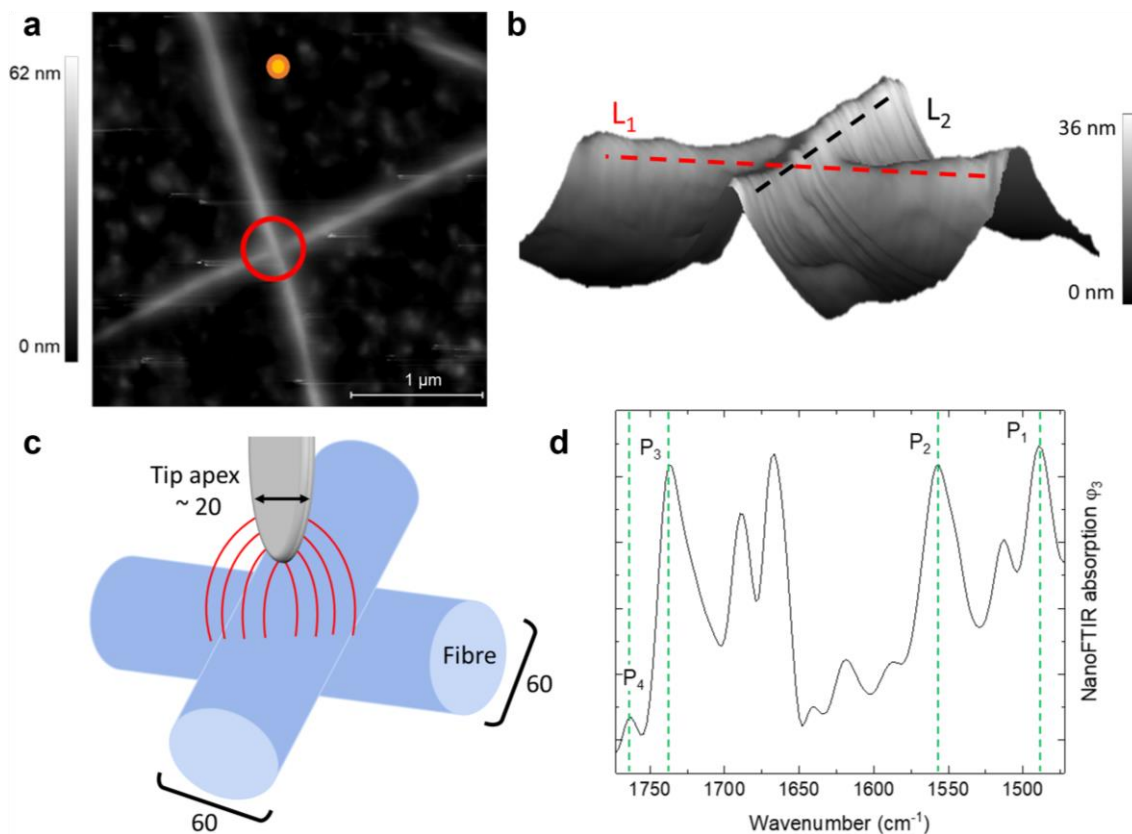


Figure 23. a) Topological (height-sensor) image of two crossing fibres on a gold surface. The red circle indicates the position of the recorded nano-FTIR spectrum and the orange spot the position of the recorded reference spectrum. b) 3D topography view of the fibres in perpendicular contact. c) Depiction of the nano-FTIR measurement probing the contact point of the fused fibres. d) nano-FTIR spectrum of perpendicular fibres. Adapted from ref. **II** under CC-BY 4.0 license.

The topological features of the network affect not only the intermolecular interactions between gelators but also the higher-order molecular organisation, such as the secondary structures. To assess these changes, a more detailed analysis of the amide I region was performed. In the spectrum of a single fibre (Figure 24a), four bands are observed upon deconvolution of the amide I region. For the deconvolution process, the number of individual bands was determined using the minima of the second derivative. Three bands correspond to parallel and anti-parallel β -sheet structures (1627 cm^{-1} , 1669 cm^{-1} and 1690 cm^{-1}), while the fourth band corresponds to helical structures (1652 cm^{-1}). Subsequent fitting of the peak area assuming Gaussian shapes gave the distribution of 10 % helices and 90 % β -sheets. Similar spectral analyses were carried out for parallel fibres (Figure 24b: 20 % helices and 80 % β -sheets) and crossing fibres (Figure 24c: 4 % helices and 96 % β -sheets). The results (Table 5) suggest that the network topology also affects the higher-order organisation within the fibres, and the gel is structurally heterogeneous. It should be noted that the peak position of the secondary structures is quantitatively similar between the locations, only the relative composition after band fitting is different.

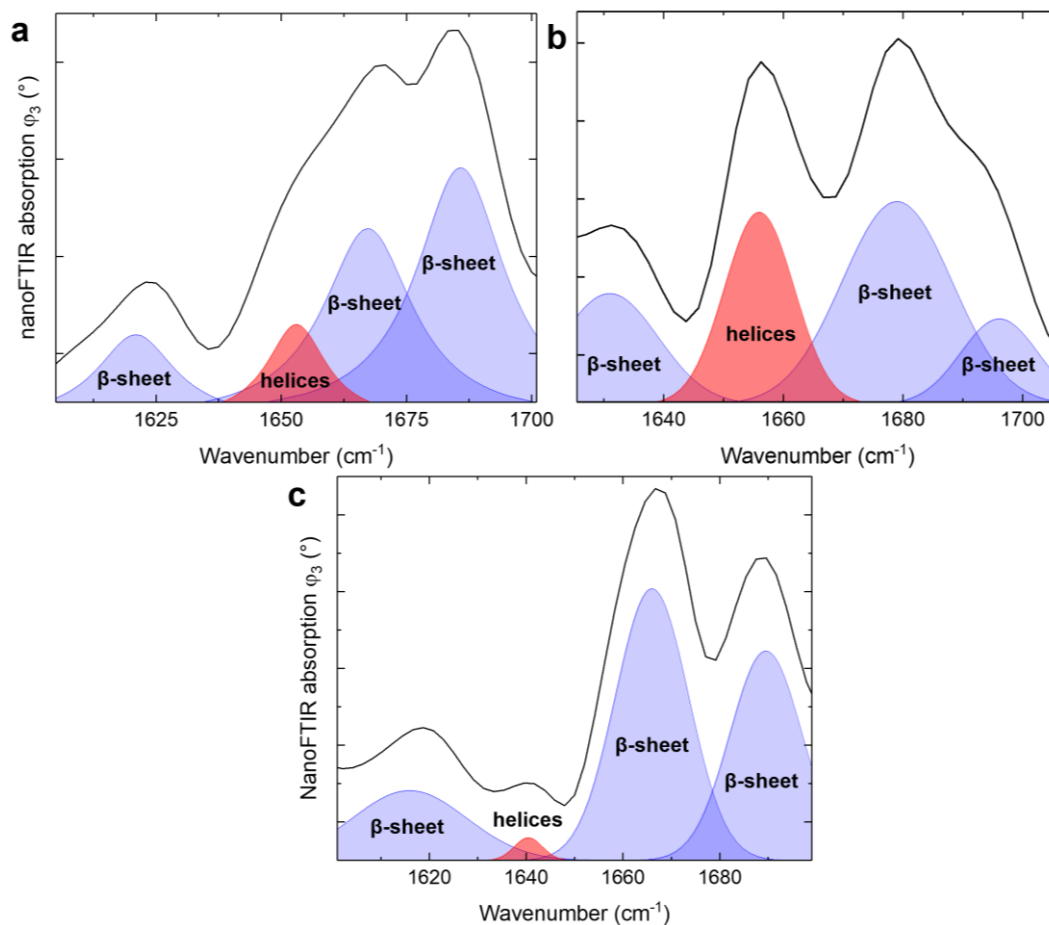


Figure 24. Magnification of the amide I region of the spectra of a) single fibre, b) parallel fibres and c) crossing fibres. Deconvolution of the amide I band highlighting the characteristic bands for the secondary structures β -sheet (blue) and helices (red). Adapted from ref. **II** under CC-BY 4.0 license.

Table 5. Peak positions (cm^{-1}) and composition (%) of the secondary structure at three spatial locations of the fibrous network.

	Single fibre		Parallel fibres		Crossing fibres	
β -sheet	1627		1626		1627	
β -sheet	1669	90 %	1679	80 %	1670	96 %
anti- β -sheet	1690		1691		1690	
helical	1652	10 %	1653	20 %	1651	4 %

Near-field measurements allowed us to study in detail the effect of the topology on the intermolecular interactions responsible for self-assembly. We found that the material is structurally heterogeneous, concerning both the supramolecular forces between gelators and the higher-order structures. Currently, only the sSNOM can probe the infrared properties of organic materials at the nanoscale, although drying artefacts can be observed due to the nature of the AFM measurements. Further studies can be carried out using liquid state or “wet” gels and probing the infrared properties through a membrane, as reported for biological samples.^[194]

3.3.4 Ultraviolet-visible and fluorescence spectroscopies ^{III,IV}

UV-vis spectroscopy also enables the study of supramolecular interactions in gels.^[47] Specifically, the phenyl ring of the phenylalanine moiety gives a characteristic absorption signal in the UV range corresponding to the $\pi \rightarrow \pi^*$ transition of the aromatic ring.^[195,196] Following the shift of this band upon gelation indicates the type of aggregates (H (blueshift) or J (redshift) type) present in the material.^[197] The UV-vis spectra of precursors **1** – **3** in acetonitrile (ACN) at a concentration of 50 mM showed the characteristic vibronic structure of phenylalanine with the absorption peak (λ_{\max}) centred at 258 nm (Figure 25a, dashed lines). To investigate the effect of the solvent (solvatochromism, *i.e.* the shift of the absorption maxima depending on the solvent)^[198] and concentration, the UV spectra were also recorded in *t*BuOAc at 5 mM (Figure 25a, dotted lines) and 50 mM (Figure 25a, solid lines), but no significant shift of the λ_{\max} was observed. Gelation induced a slight redshift of the λ_{\max} to 259 nm for gels **I** and **III** and 260 nm for gel **II** (Figure 25b, solid lines). The shift is minor (1–2 nm) compared to naphthalene and anthracene residues due to the weakly absorbing character of phenylalanine.^[199] However, the redshift indicates the formation of J type aggregates upon π -overlap. Measurements were performed on gels one day after gelation.

The partial loss of vibronic structure is observed for gels **I** (black) and **II** (red) attributed to charge transfer over molecular aggregation,^[145,200,201] but not for gels **III** (blue) and **IV** (green), presumably due to a weaker transition (one phenylalanine moiety). Additionally, an increase in the absorption intensity for gel **I** and **II** is observed upon gelation, in contrast to previous gel studies reporting a decrease in intensity upon aggregation.^[145,146,202] Background normalised spectra, due to the scattering of the opaque gels, still show an increase in intensity. This could partially be due to the aggregation-induced enhanced emission phenomenon, which also relates to the absorption.^[203-205] The absorption intensity of gel **IV** is in between that of its individual component's gel. The $n \rightarrow \pi^*$ transitions, attributed to C=O groups and N-H amide groups, observed at longer wavelengths are also redshifted, suggesting hydrogen bond interactions. The shift is proportional to the precursor's aromatic character (**3** < **1** < **2**).

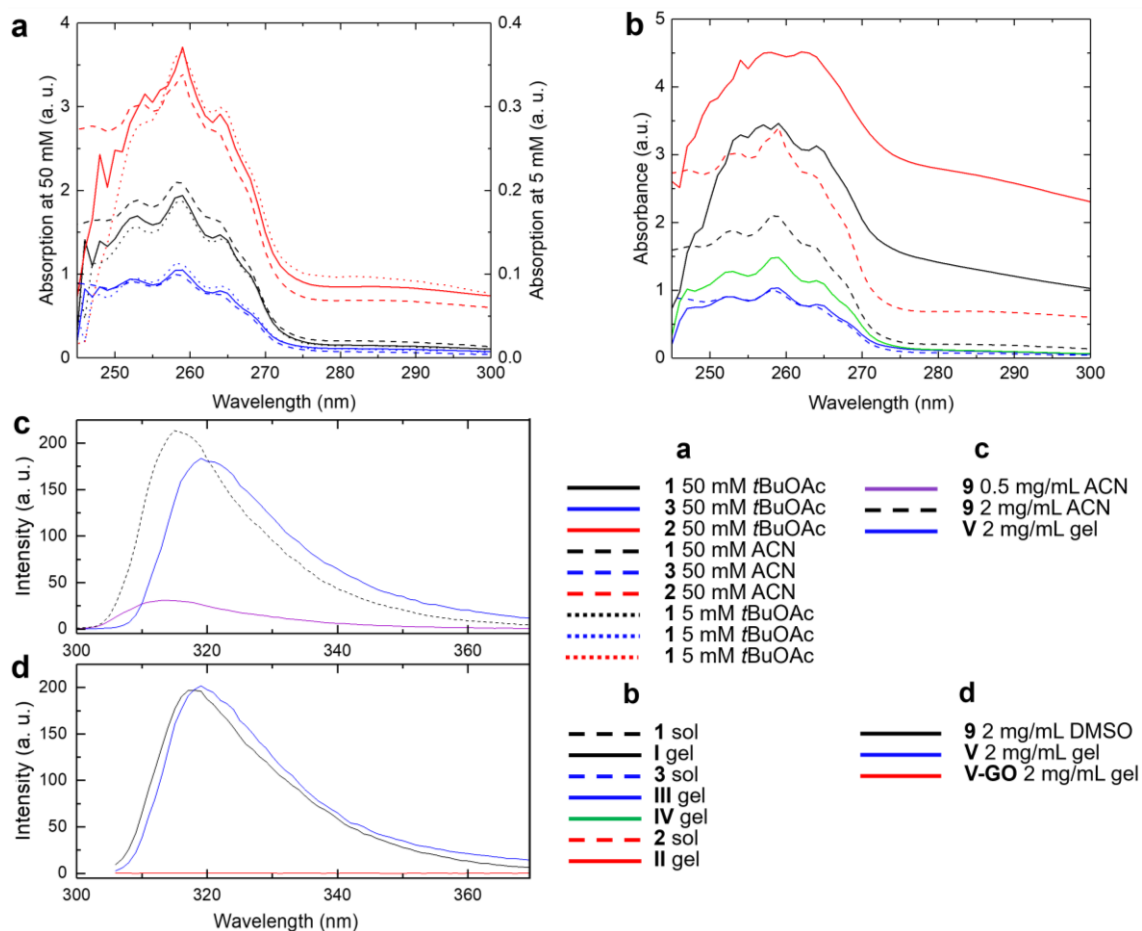


Figure 25. UV-vis absorption spectra of a) precursors **1-3** in solution; b) the corresponding gels **I-IV** (green) at 50 mM. Fluorescence emission spectra of c) gelator **9** in solution and gel **V**; d) **9** in solution, gel **V** and hybrid gel **V-GO**. The excitation wavelength was 289 nm for c) and 296 nm for d).

The fluorescence properties of gels **I - IV** were not investigated due to the high emission intensity saturating the detector. The high concentration required for gel formation (50 mM or ~20 - 30 mg/mL) was unsuitable for such experiments. However, the fluorescence spectra of gel **V**, requiring a lower amount of gelator (2 mg/mL), were recorded one day after gelation. Due to the insolubility of Fmoc-Phe **9** in PBS solution at R.T., it was first dissolved in ACN (Figure 25c, purple line) at a low concentration of 0.5 mg/mL to record the emission spectrum of the monomer species free of intermolecular interactions. The spectrum shows the emission band centred at 313 nm corresponding to the fluorenyl moiety (Fmoc). Upon increasing concentration to that of the gel (2 mg/mL, Figure 25c black dashed line), the emission band was slightly redshifted to 315 nm, suggesting that intermolecular interactions already take place in the solution state at the given concentration. The spectrum recorded in the gel state (gel **V**) shows an emission band at 319 nm (Figure 25c, blue line), suggesting that the Fmoc protective group is involved in π - π stacking interactions upon gelation.^[33,206-208]

Similar measurements were performed with gelator **9** dissolved in DMSO at a concentration of 2 mg/mL (Figure 25d, black line). The emission band is observed at 318 nm, while the emission band in the gel state was at 319 nm. The redshift of the fluorescence emission of the gelator in two solvents verifies the solvent polarity dependency of fluorescence measurements.^[209] For the measurements to reflect the redshift of the fluorescence emission upon π -overlap as closely as possible, the gelator should be dissolved in the same solvent as that of the gel. Unfortunately, Fmoc-Phe is insoluble in PBS at R.T. The spectra could be recorded from the heated solution (80 °C) before gelation, but the gelators might already be activated, and a higher temperature could lead to changes in the fluorescence properties.^[210] The fluorescence emission of gel **V-GO** is not observed (Figure 25d, red line). This suggests that supramolecular interactions causes quenching of the fluorescence due to the energy transfer between the Fmoc group of the excited molecules to GO, or the intense black colour of gel **V-GO** traps the emitted light and prevents its detection.

3.4 Macroscopic properties of the gels ^{I,III,IV}

The mechanical properties of gels **I-IV**, **V** and **V-GO** were investigated by rheology on gels one day after gelation. Different parameters, such as gelator concentration and acid equivalent, were assessed for the transient materials **I-IV** to determine their impact on the macroscopic scale (bulk state). Gelation is verified when the G' value is higher than the G'' value.^[78,211]

Amplitude sweep measurements were performed on gels **I-IV** at R.T. by varying the shear strain γ in the 0.01 – 100 % range at a constant frequency of 1 Hz (Figure 26). For all four systems, the G' curve (black square lines) was higher than the G'' curve (red circle line), verifying the viscoelastic nature of the materials, that is, gels. The point at which G' and G'' cross (γ_{cross}) corresponds to the rupture of the material and its transition from a viscoelastic solid to a viscous liquid. This specific point also informs about the elastic properties, and for these systems, it increases in order: $\gamma_{\text{cross}}^{\text{I}}$ (1.5 %, Figure 26a) < $\gamma_{\text{cross}}^{\text{III}}$ (3 %, Figure 26c) < $\gamma_{\text{cross}}^{\text{IV}}$ (3.5 %, Figure 26d) < $\gamma_{\text{cross}}^{\text{II}}$ (over 100 %), Table 6. The observed trend suggests that the elasticity of the material increases with decreasing number of aromatic units in the precursors from gel **I** (Phe-Phe core in **1**) to gel **III** (Leu-Phe core in **3**). Gel **IV** shows a higher γ_{cross} implying that the synergy between the gelators **1a/b** and **3a/b** improves the elasticity of the dual-component material. The γ_{cross} for gel **II** can be extrapolated above 100 % shear strain (as also reported for highly elastic gels^[212]), showing the highest elasticity of all gels. However, this result is against the trend observed for **I**, **III** and **IV**. The additional phenylalanine motif in precursor **2** (Phe-Phe-Phe core), providing a higher hydrophobicity and more available sites for π - π stacking, seems to give a more stable molecular aggregation. Therefore, the difference in the fibrillar arrangement within the material is potentially the reason for the higher elasticity.

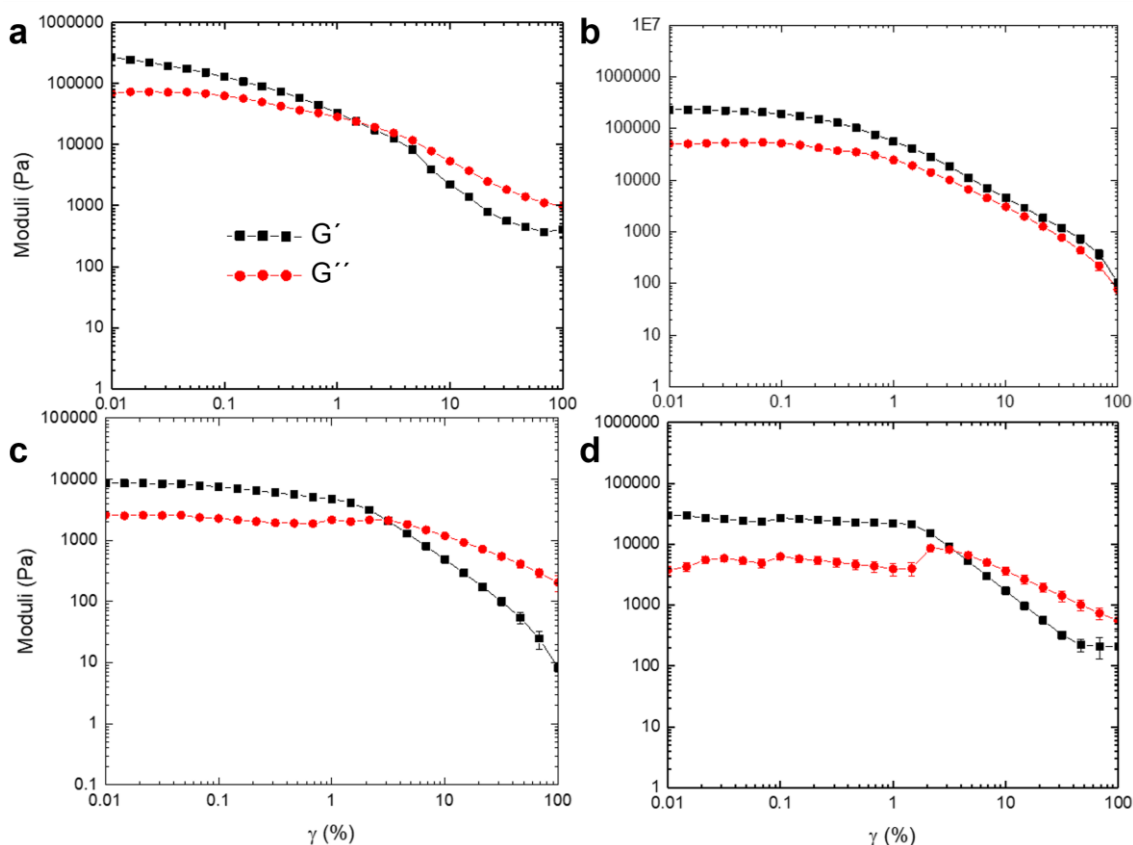


Figure 26. Rheology amplitude sweeps measurements of a) gel I, b) gel II, c) gel III and d) gel IV at a concentration of 50 mM and 1 eq of acid. Measurements were triplicates and averaged. Errors bars calculated by standard deviation.

Similar amplitude sweep measurements were performed on gels I-IV, at a concentration of 50 mM but with a lower amount of acid accelerator (0.5 eq instead of 1 eq). All gels verified the viscoelastic behaviour, exhibiting a G' value higher than a G'' value. Interestingly, gels I, III and IV are more elastic than their 1.0 eq counterparts (1.3 – 3-fold increase, Table 6), while the γ_{cross} of gel II is over 100 % shear strain, similarly to its 1.0 eq counterpart. This suggests that the presence of precursor and/or a lower amount of gelator within the gels lead to increased elasticity. The effect of the precursor concentration was also investigated for gels III and IV. The comparison of the γ_{cross} values for gel III shows a decreasing elasticity with an increasing concentration: $\gamma_{\text{cross}}^{25\text{mM}}$ (6.5 %) > $\gamma_{\text{cross}}^{50\text{mM}}$ (3 %) > $\gamma_{\text{cross}}^{100\text{mM}}$ (2 %). A similar trend is observed for gel IV where $\gamma_{\text{cross}}^{50\text{mM}}$ (3.5 %) > $\gamma_{\text{cross}}^{100\text{mM}}$ (1.2 %). The difference in elasticity based on the precursor concentration seems equivalent between each system (~ 2-fold) and is quantitatively similar to that based on the accelerator equivalent (1.3–3-fold). Therefore, the elastic behaviour of the materials can be tuned with the same magnitude by varying the equivalent of accelerator to trigger gelation and the concentration of initial precursor.

Table 6. Stiffness G' (kPa) and elasticity γ_{cross} (%) of gels **I-IV** at different precursor concentrations and accelerator amounts.

Gel	[M]	G' (kPa)		γ_{cross} (%)	
		0.5 eq	1.0 eq	0.5 eq	1.0 eq
Gel I	0.05 M	180	420	4.2	1.5
Gel II	0.05 M	147	320	No crossing points	
Gel III	0.025 M	n.m. ^[a]	10	n.m.	6.5
	0.05 M	11	6.5	9	3
	0.1 M	n.m.	330	n.m.	2
Gel IV	0.05 M	52	20	4.5	3.5
	0.1 M	n.m.	155	n.m.	1.2

[a] not measured

The stiffness of gels **I-IV** was investigated by frequency sweep measurements at a constant concentration of 50 mM. The G' value of gel **I** was 420 kPa (Figure 27a, black line) and 320 kPa for gel **II** (Figure 27a, red line). These stiffness values are in the range of the bladder and gut tissue.^[213,214] In contrast to the elastic properties, the stiffness of the materials remains qualitatively similar regardless of the additional aromatic unit in the precursor's structure. However, for gel **III** (Figure 27a, blue line), the low stiffness value of 6.5 kPa (in the range of the lung and liver tissue.^[213,214]) correlates with a lower number of aromatic rings and a higher elasticity compared to gel **I**. Although the lower G' value of gel **III** can also be attributed to a lower number of hydrophilic hydrocarbons, the stiffness decrease is much higher (60-fold) than reported in the literature (2 - 10-fold depending on the side chain length)^[6,215] The multicomponent gel **IV** exhibits a G' value of 20 kPa which is in between that of its individual component's gels although closer to that of gel **III** (Figure 27a, green line). This also supports the conclusion that a new network has formed by co-assembly of the gelators.^[178,216]

Frequency sweep measurements were also performed on gels **III** and **IV** at different precursor concentrations with a constant equivalent of the accelerator of 1.0 eq (Table 6). A negligible increase of the G' value between gel **III** at 50 mM (6.5 kPa, Figure 27b, blue dashed line) and 25 mM (10 kPa, Figure 27b, blue solid line) is observed. However, the stiffness of gel **III** at 100 mM is higher by approximately 30-fold (330 kPa, Figure 27b, blue dotted line). A similar trend is observed for gel **IV**, whose G' value increased by approximately 8-fold from the 50 mM gel (20 kPa, Figure 27b, green solid line) to that at 100 mM (155 kPa, Figure 27b, green dotted line).

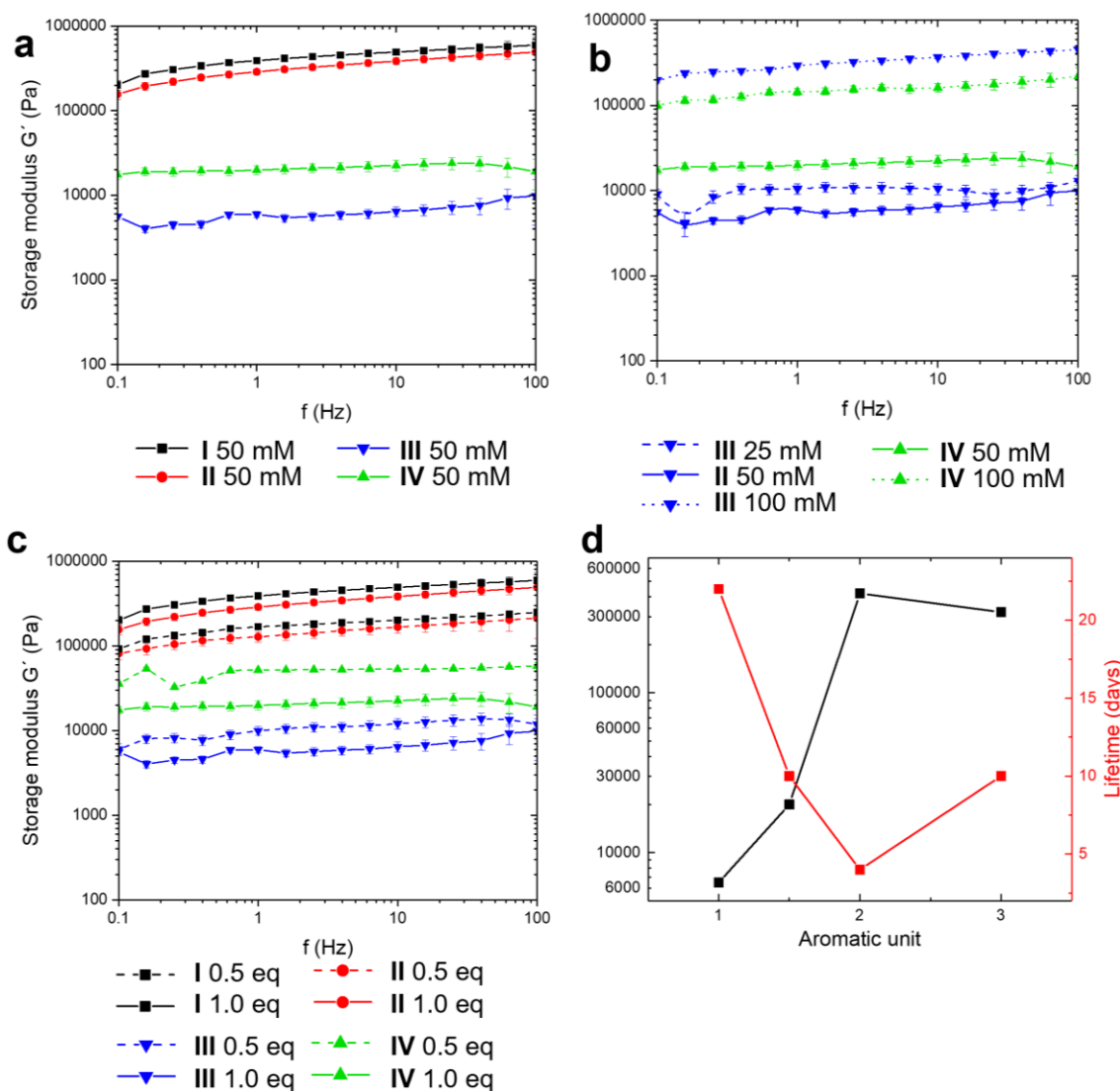


Figure 27. Frequency sweep measurements of a) gels **I-IV** formed with 1.0 eq of accelerator under a constant shear strain γ , b) gel system **III** and **IV** at different concentrations with 1.0 eq of accelerator, c) gels **I-IV** at 50 mM with different amount of accelerator. d) Plot of the elastic moduli (black) against the lifetime (red) of gels **I-IV** in function of the number of aromatic units in the precursor. Error bars are calculated by standard deviation. Reproduced from ref **III** under CC-BY 4.0 license.

The effect of the accelerator amount was investigated for gels **I-IV** formed with either 0.5 eq or 1.0 eq at a constant concentration of precursors of 50 mM. Gels **I** (Figure 27c, black lines) and **II** (Figure 27c, red lines) showed an approximately 2-fold decrease in stiffness from 1.0 eq to 0.5 eq conditions, whereas gels **III** (Figure 27c, blue lines) and **IV** (Figure 27c, green lines) showed an increase in stiffness of the same magnitude. The mechanical properties of these materials seem more sensitive to a difference in precursor concentration than the acid accelerator used to trigger gelation. It should be noted that varying both parameters yields materials with a broad range of mechanical properties, which could be useful for designing materials for applications requiring fine control of

the stiffness, such as tissue engineering and cell culturing, in which living tissues and cells are sensitive to the mechanical properties of their environment.

Figure 27d shows the evolution of the G' (black line, left y-axis) and the lifetime (red line, right y-axis) of the gels in function of the number of aromatic units in the precursors' structure. The evolution of the lifetime is inversely proportional to the material's stiffness. Therefore, stiffer materials have a shorter lifetime and *vice versa*. The solubility of the different gelators in the secondary solvent *t*BuOH can explain this finding. Indeed, solubility controls showed that the ester-protected gelators **a** are soluble in *t*BuOH while the free carboxylic acid gelators **b** are not. The mechanical properties of the materials also play a role in the self-abolishment, presumably due to the stiffness to withstand the progressively dissolved network before the gel-to-sol transition.

Fmoc-Phe hydrogel **V** and Fmoc-Phe/GO hybrid hydrogel **V-GO** were investigated to study the effect of GO on the mechanical properties of the material. The effect of the gelator concentration in gel **V** was investigated by frequency sweep measurements (Figure 28a). The G' value increased from 160 Pa (neuron or brain tissue stiffness)^[213,214] to 3 600 Pa (~ 20-fold, fat or soft tissue stiffness)^[213,214] upon increasing the concentration of Fmoc-Phe **9** from 2 mg/mL (Figure 28a, black) to 6 mg/mL (Figure 28a, orange), respectively. In addition, five gels were prepared with different concentrations of GO in the range of 0 – 1 mg/mL, while the gelator concentration was kept constant at 2 mg/mL (Figure 28b and 28c). Although random, the evolution of the G' value appears negligible for the GO concentration from 0 mg/mL to 0.75 mg/mL (160 Pa to 210 Pa). However, at the highest concentration of GO (1 mg/mL), the increase in stiffness is greater (370 Pa, ~2-fold), although a previous study reports a 7-fold increase upon addition of GO in the gel.^[91] The evolution of γ_{cross} values and G' values in function of the GO concentration in the hybrid gels are not linear but follow a similar trend, that is, an increase of the stiffness is observed along with the increase in the materials' elasticity, and *vice versa*.

The phase transition temperature ($T_{\text{gel-sol}}$) is a measure of the temperature at which the materials undergo the gel-to-sol transition and refers to the thermal stability. $T_{\text{gel-sol}}$ was measured by gradually heating the gel samples (one day after gelation) with a 5 °C step. After reaching the equilibrium state (10 min), the vial inversion method verified the non-free-flowing character of the materials. The $T_{\text{gel-sol}}$ correspond here to the transition to the complete free-flowing solution state and increases in order gel **III** (40 °C) < gel **I** (45 °C) < gel **II** (55 °C). Therefore, the transition temperature is proportional to the number of aromatic units in the structure (Table 7). In contrast to the rheological data, the $T_{\text{gel-sol}}$ of gel **IV** was 35 °C, lower than that of its individual components' gels. The difference between the 3D network related to the $T_{\text{gel-sol}}$ and the π - π stacking interactions related to the gel stiffness is possibly the reason for the difference in behaviour.^[199]

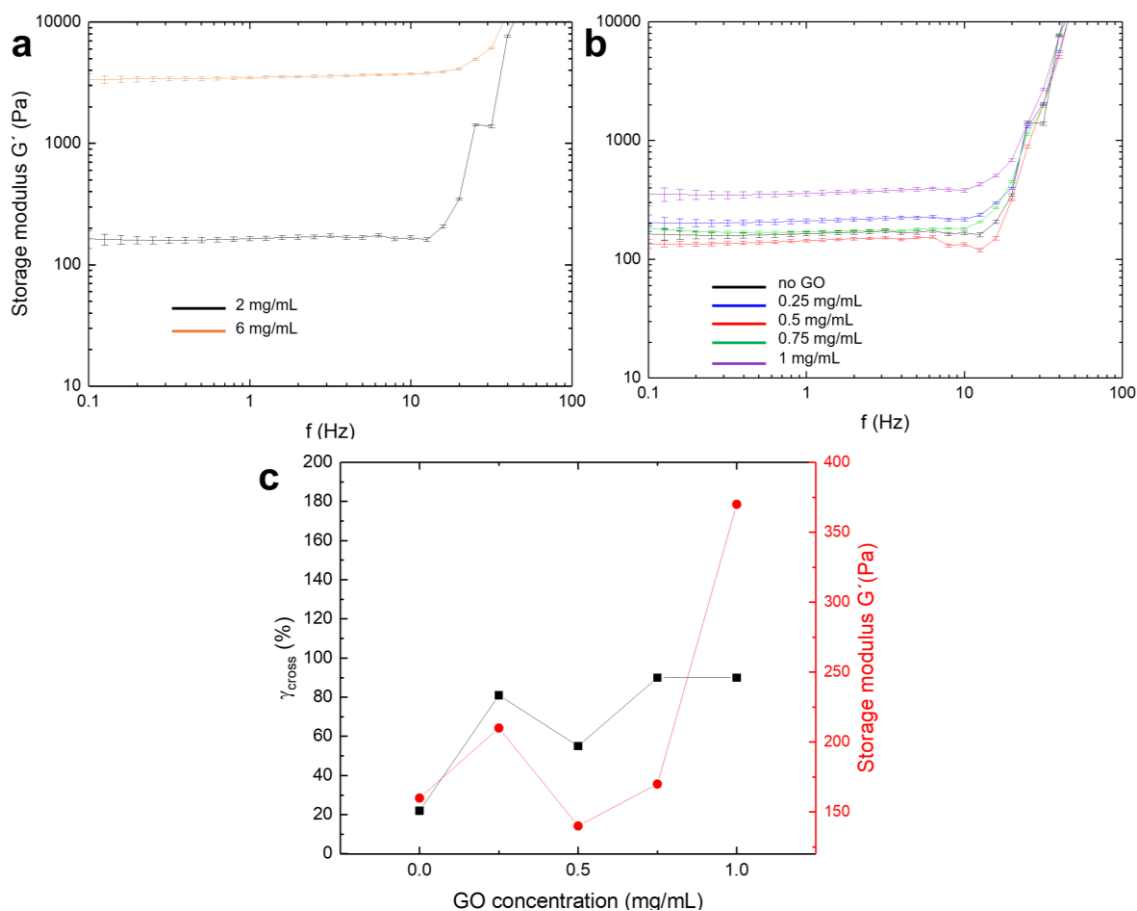


Figure 28. Frequency sweep measurements of a) Fmoc-Phe gel V at 2 mg/mL and 6 mg/mL and b) Fmoc-Phe hybrid gel V-GO with a constant concentration of Fmoc-Phe (2 mg/mL) and a varying concentration of GO. c) Comparison of the elasticity (γ_{cross} values) from the amplitude sweep measurements (left black axis) and the stiffness (G' values) from the frequency sweep measurements (right red axis) of samples shown in b) in function of the GO concentration.

In addition, the precursor concentration affects the $T_{\text{gel-sol}}$, as it increased proportionally to the concentration (10 °C increase from 25 mM to 100 mM, Table 7), similarly to the stiffness. This suggests that the materials' mechanical properties and thermal stability are concentration-dependent.

Table 7. Phase transition temperatures (°C) of gels I, II, III and IV and their dependency on the gel concentration.

$T_{\text{gel-sol}}$ (°C)	Gel concentration		
	25 mM	50 mM	100 mM
Gel I	45	50	55
Gel II	55	65	65
Gel III	40	45	50
Gel IV	35	40	45

The $T_{\text{gel-sol}}$ of gels **V** and **V-GO** was investigated to study the effect of the gelator and GO concentrations on thermal stability. As for the rheological studies, the gelator concentration was increased from 2 mg/mL to 6 mg/mL, while the GO concentration was increased from 0 to 1 mg/mL with a step of 0.25 mg/mL for each gelator concentration value (Table 8). At 2 mg/mL for gel **V**, the $T_{\text{gel-sol}}$ was 35 °C and increased proportionally with the GO concentration until 50 °C (**V-GO**). Therefore, the presence of GO within the network increases the heat resistance of the hybrid material, while mechanical properties are not significantly altered. This is in line with spectroscopic and rheological results, where the presence of GO did not alter the secondary structure, intermolecular interactions and mechanical properties. For material applications used in the human body, the $T_{\text{gel-sol}}$ should be higher than the body temperature (~ 37 °C). Therefore, gel **V** would not be suitable as the body temperature would trigger the gel-to-sol transition but gels with a GO concentration of 0.75 mg/mL or higher would be suitable. However, when the gelator concentration is increased to 6 mg/mL, the $T_{\text{gel-sol}}$ of gel **V** is 60 °C, remaining constant upon increasing the concentration of GO. Thus, at this high concentration of gelator, the presence of GO does not alter the thermal stability of the materials and all **V-GO** gels at this gelator concentration would be suitable for applications used in the human body.

Table 8. Phase transition temperature (°C) of gels **V** and **V-GO** and their dependency on the gelator and GO concentration.

Gels V/V-GO	Concentration of Fmoc-Phe and <i>GO</i> (mg/mL)									
	2					6				
	0	0.25	0.5	0.75	1	0	0.25	0.5	0.75	1
$T_{\text{gel-sol}}$ (°C)	35	40	45	50	50	60	60	60	60	60

3.5 Antimicrobial properties of amino acid-based gels ^{IV}

Supramolecular amino acid-based hydrogels have been extensively studied for their potential antimicrobial/antiviral biomedical applications, which can be tuned modifying the gelation conditions, gelator structure and the presence of additives.^[32,217-222] Recent studies showed that antibacterial properties could be further optimised and tuned by addition of metal (*e.g.* gold and silver), drugs, carbon dots, carbon nanotubes and other graphene-based materials within the 3D encapsulated solvent.^[88]

The antibacterial properties of gels **V** and **V-GO**, along with a suspension of GO in PBS solvent, were investigated against gram-negative *Escherichia coli* (*E. coli*) bacteria. The *in vitro* bacterial growth was assessed by measuring the optical density of the bacterial cultures in the different materials at a wavelength of 600 nm (OD_{600} , Figure 29) over 40 h of incubation in relation to the control. The materials were evaluated at five concentrations (Table 9) prepared by serial dilutions from D1 (highest concentration, lowest dilution factor) to D5 (lowest

Table 9. Dilution factors and final concentrations of the individual components tested against *E.coli*. The concentration of hybrid gel is obtained by addition of the individual components' concentration.

Gel components	Dilution factors				
	D1	D2	D3	D4	D5
Fmoc-Phe (mg/mL)	1.0	0.50	0.25	0.13	0.63
GO ($\mu\text{g/mL}$)	125	62.50	31.25	15.63	7.81

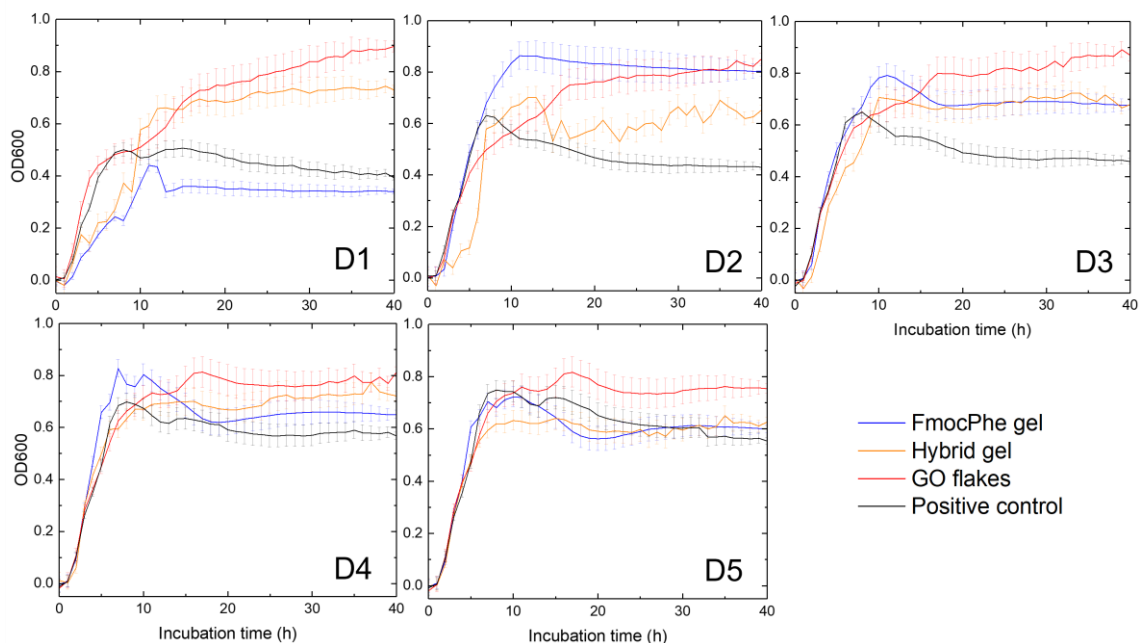


Figure 29. Optical density measurements of the bacterial cultures in gel V (blue), gel V-GO (orange) and a suspension of GO in PBS (red) at different dilution factors D1-D5 of the materials recorded at 600 nm over 40 h. The black curves correspond to the positive control. Error bars were calculated by standard deviation. Adapted from ref. IV under CC-BY 4.0 license.

concentration, highest dilution factor), with D1 showing a dilution factor of 2 compared to gel V and V-GO (2 mg/mL of Fmoc-Phe and 0.25 mg/mL of GO).

Gel V at D1 shows slight antibacterial properties since the OD₆₀₀ values remain below that of the positive control (in which only the bacteria are present in the culture medium) for 40 hours. However, from D2 and below, the decrease in concentration results in the loss of bactericidal properties after 10 h of incubation, as the OD₆₀₀ readings indicate a higher population of bacteria than in the control culture. This suggests that within this timeframe the concentration limit at which Fmoc-Phe and GO hinder bacterial growth is 1.0 mg/mL and 62.50 $\mu\text{g/mL}$, respectively. The high bacterial population observed for all dilution factors in the samples containing hybrid gel V-GO and GO suspension suggests that the GO sheets offer a scaffold for bacterial growth (*i.e.* surfaces to attach on and proliferate).

The data from the OD₆₀₀ measurements (Figure 29, D1) were extracted and plotted individually to study the antibacterial effect of the materials at the highest concentration in detail. Three time points (5 h, 10 h and 20 h of incubation time, Figure 30a) were assessed, and each cell viability value was normalised to the control (100 % cell viability, only bacteria in the broth, no other disturbances). Within the first 5 h, gel **V** showed bactericidal properties since only 44 % of the bacteria were left alive in the culture. Similarly, bacteria in contact with hybrid gel **V-GO** showed only 56 % cell viability. The population in the GO suspension was higher than that of the control, supporting the hypothesis of GO acting as a scaffold for bacterial growth. This result is a discrepancy compared to the literature reporting the antibacterial activity of graphene-based materials, in which GO was found to have a high bactericidal activity against *E. coli*.^[223] Indeed, in our case and for all incubation time and dilution, GO was found to promote bacterial growth. After 10 h of incubation at D1, the bacteria population in the GO sample remained quantitatively similar. For both gels **V** and **V-GO**, the bacteria population in the culture increased, suggesting that the growth inhibition properties of the materials decreased. Finally, the bacterial population remained constant after 20 h of incubation in contact with gel **V**, whereas the presence of GO in hybrid gel **V-GO** presumably favoured the growth of *E. coli*.

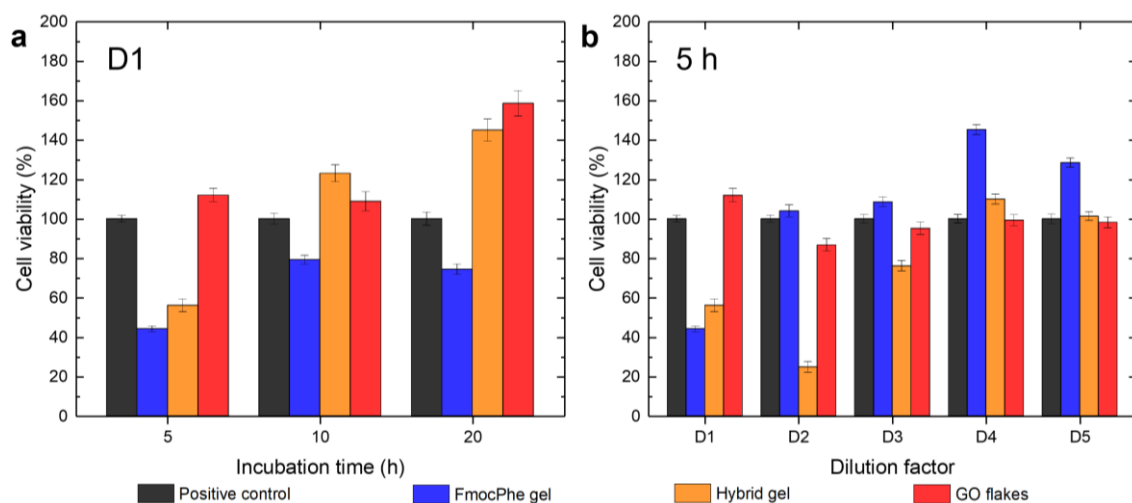


Figure 30. Cell viability (%) obtained by OD₆₀₀ measurements a) at 5 h, 10h and 20 h at D1 dilution factor. b) 5 serial dilutions at 5 h of incubation. All values for each time point were normalized to the control value of the same time point for clarity and comparison. Adapted from ref. **IV** under CC-BY 4.0 license.

Similarly, the data for all materials were extracted and plotted for the serial dilution factors D1-D5 after 5 h of incubation time (Figure 30b). Hybrid gel **V-GO** displayed bactericidal activity for the three lowest dilution factors, D1-D3 (the cell viability is lower than that of the control). The dilution D2 shows the lowest bacterial population among the three, indicating that this concentration is optimal. Gel **V** loses its bactericidal activity from D2 and below, whereas the GO suspension shows qualitatively similar bacterial growth to the control regardless of the dilution factor. The overall results suggest that the D1 dilution factor

(highest concentration) is the most optimal for bacterial growth inhibition for at least the first 5 h. Lower materials concentrations result in the loss of antibacterial properties.

Live/dead staining assay was performed on D1 dilution samples after 5 h of incubation to detect damaged or intact cell membranes visually. A green fluorescent dye (Syto9) was used to stain live and dead bacteria, while a red fluorescent dye (PI) was used to stain bacteria with damaged cell membranes selectively. Fluorescence microscopy was used to qualitatively image the bacteria cultures in contact with each material sample and the control without numerical/statistical analysis (Figure 31). The results agree with the optical density measurements and show mainly live bacteria (mostly green coloured bacteria) in the control culture. Bacteria in the GO suspension are mainly alive and agglomerated, supporting the hypothesis that GO creates a scaffold for bacteria to attach to. Bacteria in contact with the hybrid gel V-GO are mainly dead, although more are alive than in the culture in contact with gel V, corroborating the numerical results obtained by OD₆₀₀ measurements. In this study, Fmoc-Phe gel shows low antibacterial activity towards gram-negative *E. coli*. In the literature, Fmoc-amino acid gels have been reported to exhibit antibacterial activity towards gram-positive bacteria.^[219,224]

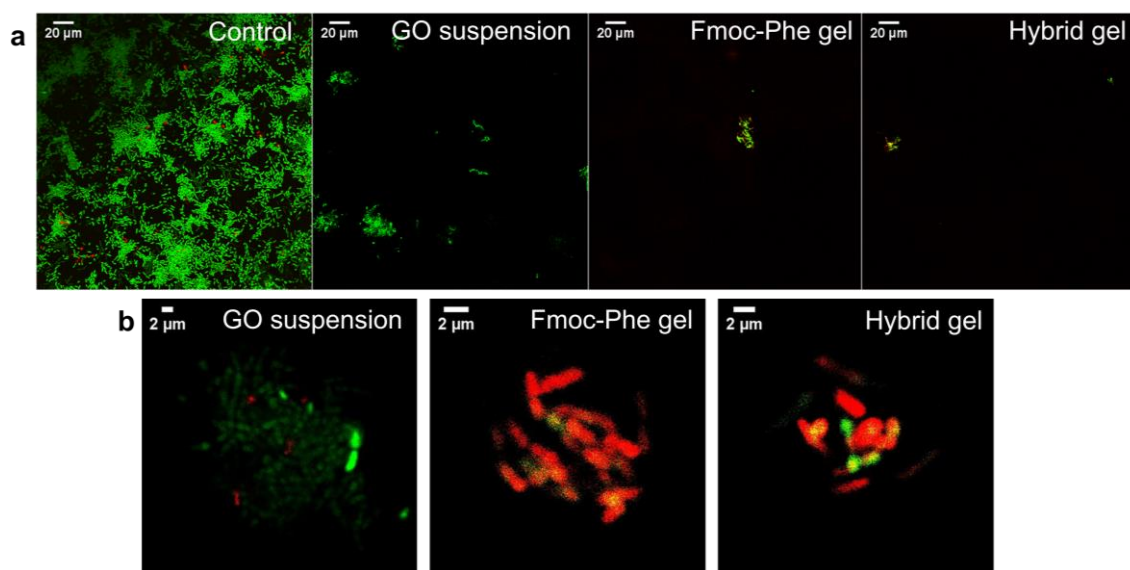


Figure 31. a) Fluorescence spectroscopy images of the live/dead bacteria assay after 5 h of incubation at D1 dilution factor of GO suspension, gel V and gel V-GO. b) is a magnification for clarity. Green fluorescence indicates bacteria with intact and damaged cell membranes, while red fluorescence indicates bacteria with broken membranes (dead bacteria). Reproduced from ref. IV under CC-BY 4.0 license.

4 CONCLUSIONS

Supramolecular gelation is a complex phenomenon that requires a “try and see” approach. Due to the large number of parameters influencing this process, it is rather difficult to predict whether a molecule will gel in a solvent. Although some studies have demonstrated successful predictions on the gelation of short amino acid-based systems (mono- and dipeptides), it is usually difficult for more complex systems. Systematic studies comparing chemical structures, solvents and gelation conditions give a lot of insights into designing gel systems, for instance which functional groups are more likely to favor self-assembly. This approach becomes even more complex when designing out-of-equilibrium systems, such as DSA, due to the increased number of parameters to consider, such as competing reaction kinetics of fuel consumption and deactivation rate.

In this thesis, a new type of out-of-equilibrium self-assembly was developed. This system, so-called solvent-induced self-assembly, was investigated at multiple length scales, and the gelation parameters were varied to assess their impact on the resulting materials, both from a dynamic and mechanical properties point of view. Within the initial set of eight peptide precursors, three formed gels under the specified conditions. Two of these precursors consisted of phenylalanine (di- or tripeptide) and one leucine, along with phenylalanine (dipeptide). The lack of gel formation for other precursors was suggested to be because of the high freedom of σ -bond rotation (aliphatic side chains shorter than leucine) and electrostatic repulsion (tyrosine).

Molecular scale characterisation indicated that the proposed mechanism of gel formation, *i.e.* precursor deprotection causing *in situ* formation of two activated gelators and their chemical interconversion over time, and the formation of the secondary solvent responsible for the materials’ abolishment, was similar for all gel systems. The difference in the dynamic nature, represented by the lifetime of the materials (*i.e.* spontaneous gel-to-sol transition or self-abolishment), varied depending on the chemical structure of the precursor. This was suggested to be a consequence of the different solubility of the gelators in primary and secondary solvents. In addition, precursor concentration and accelerator amount affected the dynamic nature of the materials, the latter by

modifying the rate and amount of secondary solvent formation. Varying the gelation conditions not only affected the lifetime of the gels, but also their macroscopic properties (e.g. stiffness and elasticity). A direct correlation between the dynamic and mechanical properties was observed, that is, softer gels have a higher lifetime and *vice versa*.

This work highlighted the development of transient materials whose properties can be finely tuned by varying gelation conditions. A wide range of lifetime and stiffness can be obtained simply by changing the precursor structure and concentration, and the amount of accelerator. However, further work must be done to investigate the different kinetics regulating the assembly and disassembly processes. Additionally, future applications such as temporary ink writing with spatial control of the assembly on a surface or a switch to water-based solvents using an external *t*Bu group supplier to sustain the transient character of the materials can be envisioned. The intrinsic biocompatibility of peptide hydrogels would allow such solvent-induced self-assembled systems to be used for drug delivery exhibiting a controllable burst release, for instance. This work also highlighted the use of sSNOM for the nanoscale analysis of the supramolecular assembly. It enabled the study of secondary organizations and non-covalent interactions leading to gelation, depending on the topology of the network, with a spatial resolution of ~ 20 nm, highlighting the heterogeneity of the assembly.

On the other hand, the gelation properties of nanocarbon-loaded amino acid-based hydrogels and the influence of GO on the self-assembly process were investigated. The presence of GO within the network does not disrupt the self-assembly and the fibre formation during gelation, but electron microscopy showed that the fibres seem to entangle around the GO flakes on higher-order organizations. Infrared spectroscopy revealed that the 1D aggregation of the gelators in the neat and hybrid gels are identical, suggesting that GO does not interfere with the molecular aggregation. Similarly, the 2D structures (β -sheets in our case) are identical between both gels, supporting the previous findings. The stiffness of Fmoc-Phe gels is in the range of the brain tissue stiffness, allowing them to be potentially used for brain tissue regeneration. The presence of GO in the system, studied at different concentrations, negligibly modified the stiffness of the hybrid materials but had more impact on the elastic behavior. The hybrid materials have a higher microbicidal activity than the neat hydrogel, and they display it at lower concentrations, even though GO alone promotes bacterial growth by offering additional surfaces as scaffolds for bacterial attachment. This highlights the synergy between organic gels and carbon materials as additives, supporting the literature on carbon-based hybrid materials for biomedical applications.

Overall, this thesis brings fundamental studies on the development of a new self-assembly process that can be employed for materials requiring a transient behavior and tunable properties, along with enriching the pool of synergistic hybrid antimicrobial materials.

REFERENCES

- [1] A. Mahler, M. Reches, M. Rechter, S. Cohen, E. Gazit, *Adv. Mater.* **2006**, *18*, 1365–1370.
- [2] E. R. Draper, D. J. Adams, *Chem* **2017**, *3*, 390–410.
- [3] Y. Wang, Q. Geng, Y. Zhang, L. Adler-Abramovich, X. Fan, D. Mei, E. Gazit, K. Tao, *J. Colloid Interface Sci.* **2023**, *636*, 113–133.
- [4] P. Dastidar, *Gels* **2019**, *5*, 15.
- [5] C. L. Esposito, P. Kirilov, V. G. Roullin, *J. Controlled Release* **2018**, *271*, 1–20.
- [6] K. Azyat, D. Makeiff, B. Smith, M. Wiebe, S. Launspach, A. Wagner, M. Kulka, N. Godbert, *Gels* **2022**, *9*, 5.
- [7] N. M. Sangeetha, U. Maitra, *Chem. Soc. Rev.* **2005**, *34*, 821.
- [8] D. Tripathy, A. S. Gadtya, S. Moharana, *Polym-Plast. Tech. Mat.* **2023**, *62*, 306–326.
- [9] M. Suzuki, S. Owa, M. Kimura, A. Kurose, H. Shirai, K. Hanabusa, *Tetrahedron Lett.* **2005**, *46*, 303–306.
- [10] L. A. Estroff, A. D. Hamilton, *Chem. Rev.* **2004**, *104*, 1201–1218.
- [11] S. Correa, A. K. Grosskopf, H. Lopez Hernandez, D. Chan, A. C. Yu, L. M. Stapleton, E. A. Appel, *Chem. Rev.* **2021**, *121*, 11385–11457.
- [12] H. Cao, L. Duan, Y. Zhang, J. Cao, K. Zhang, *Signal Transduct. Target. Ther.* **2021**, *6*, 426.
- [13] R. Choe, S. Il Yun, *E-Polymers* **2020**, *20*, 458–468.
- [14] R. M. Martinez, C. Rosado, M. V. R. Velasco, S. C. S. Lannes, A. R. Baby, *Int. J. Cosmet. Sci.* **2019**, *41*, 109–117.
- [15] L. Zeng, X. Lin, P. Li, F. Q. Liu, H. Guo, W. H. Li, *Prog. Org. Coat.* **2021**, *159*, 106417.
- [16] A. Vintiloiu, J. C. Leroux, *J. Controlled Release* **2007**, *125*, 179–192.
- [17] D. M. Raymond, B. L. Abraham, T. Fujita, M. J. Watrous, E. S. Toriki, T. Takano, B. L. Nilsson, *ACS Appl. Bio Mater.* **2019**, *2*, 2116–2124.
- [18] M. K. Pradhan, D. Gupta, K. R. Namdev, Anjali, C. Miglani, A. Pal, A. Srivastava, *Nanoscale* **2022**, *14*, 15079–15090.
- [19] P. Ravarino, N. Di Domenico, M. Barbalinardo, D. Faccio, G. Falini, D. Giuri, C. Tomasini, *Gels* **2022**, *8*, 98.
- [20] T. Giraud, P. Hoschtettler, G. Pickaert, M.-C. Averlant-Petit, L. Stefan, *Nanoscale* **2022**, *14*, 4908–4921.
- [21] T. Das, M. Häring, D. Haldar, D. Díaz Díaz, *Biomater. Sci.* **2018**, *6*, 38–59.
- [22] J. T. Van Herpt, M. C. A. Stuart, W. R. Browne, B. L. Feringa, *Chem. Eur. J.* **2014**, *20*, 3077–3083.
- [23] S. Kiran, P. Dwivedi, R. Khatik, S. Hameed, M. Dwivedi, F. Huang, R. X. Xu, *Chem. Commun.* **2019**, *56*, 285–288.
- [24] M. Maity, U. Maitra, *Eur. J. Org. Chem.* **2017**, *2017*, 1713–1720.
- [25] G. Charalambidis, E. Georgilis, M. K. Panda, C. E. Anson, A. K. Powell, S. Doyle, D. Moss, T. Jochum, P. N. Horton, S. J. Coles, M. Linares, D.

- Beljonne, J.-V. Naubron, J. Conradt, H. Kalt, A. Mitraki, A. G. Coutsolelos, T. S. Balaban, *Nat. Commun.* **2016**, *7*, 12657.
- [26] J.-H. Park, M.-H. Kim, M.-L. Seo, J.-H. Lee, J.-H. Jung, *Polymers* **2022**, *14*, 400.
- [27] L. Yang, X. Tan, Z. Wang, X. Zhang, *Chem. Rev.* **2015**, *115*, 7196–7239.
- [28] H. Yao, Q. Zhou, Y. Zhang, Y. Hu, X. Kan, Y. Chen, G. Gong, Q. Zhang, T. Wei, Q. Lin, *Chin. Chem. Lett.* **2019**, 4–7.
- [29] A. Sharko, D. Livitz, S. De Piccoli, K. J. M. Bishop, T. M. Hermans, *Chem. Rev.* **2022**, *122*, 11759–11777.
- [30] J. K. Gupta, D. J. Adams, N. G. Berry, *Chem. Sci.* **2016**, *7*, 4713–4719.
- [31] P. W. J. M. Frederix, G. G. Scott, Y. M. Abul-Haija, D. Kalafatovic, C. G. Pappas, N. Javid, N. T. Hunt, R. V. Ulijn, T. Tuttle, *Nat. Chem.* **2015**, *7*, 30–37.
- [32] R. Sharma, A. Lallhall, S. Puri, N. Wangoo, *ACS Appl. Bio Mater.* **2023**, *6*, 494–506.
- [33] V. Jayawarna, M. Ali, T. A. Jowitt, A. F. Miller, A. Saiani, J. E. Gough, R. V. Ulijn, *Adv. Mater.* **2006**, *18*, 611–614.
- [34] E. Quigley, J. Johnson, W. Liyanage, B. L. Nilsson, *Soft Matter* **2020**, *16*, 10158–10168.
- [35] D. R. Lide, *CRC Handbook of Chemistry and Physics*, CRC Press, Boca Raton, FL, **2005**.
- [36] C. Tang, A. M. Smith, R. F. Collins, R. V. Ulijn, A. Saiani, *Langmuir* **2009**, *25*, 9447–9453.
- [37] D. J. Adams, M. F. Butler, W. J. Frith, M. Kirkland, L. Mullen, P. Sanderson, *Soft Matter* **2009**, *5*, 1856–1862.
- [38] A. Rajbhandary, B. L. Nilsson, *Biopolymers* **2017**, *108*, DOI 10.1002/bip.22994.
- [39] B. Ding, Y. Li, M. Qin, Y. Ding, Y. Cao, W. Wang, *Soft Matter* **2013**, *9*, 4672–4680.
- [40] A. Rajbhandary, W. W. Brennessel, B. L. Nilsson, *Cryst. Growth Des.* **2018**, *18*, 623–632.
- [41] S. Awhida, E. R. Draper, T. O. McDonald, D. J. Adams, *J. Colloid Interface Sci.* **2015**, *455*, 24–31.
- [42] J. Raeburn, A. Zamith Cardoso, D. J. Adams, *Chem. Soc. Rev.* **2013**, *42*, 5143.
- [43] N. A. Dudukovic, C. F. Zukoski, *Soft Matter* **2014**, *10*, 7849–7856.
- [44] J. Raeburn, C. Mendoza-Cuenca, B. N. Cattoz, M. A. Little, A. E. Terry, A. Zamith Cardoso, P. C. Griffiths, D. J. Adams, *Soft Matter* **2015**, *11*, 927–935.
- [45] J. Raeburn, G. Pont, L. Chen, Y. Cesbron, R. Lévy, D. J. Adams, *Soft Matter* **2012**, *8*, 1168–1174.
- [46] H. Wang, Z. Yang, D. J. Adams, *Mater. Today* **2012**, *15*, 500–507.
- [47] G. Yu, X. Yan, C. Han, F. Huang, *Chem. Soc. Rev.* **2013**, *42*, 6697–6722.
- [48] L. S. Birchall, S. Roy, V. Jayawarna, M. Hughes, E. Irvine, G. T. Okorogheye, N. Saudi, E. de Santis, T. Tuttle, A. A. Edwards, R. V. Ulijn, *Chem. Sci.* **2011**, *2*, 1349–1355.

- [49] Michal E. Roth-Konforti, Michela Comune, Michal Halperin-Sternfeld, Irena Grigoriants, Doron Shabat, Lihi Adler-Abramovich, *Macromol. Rapid Commun.* **2018**, 1800588.
- [50] X. Li, Y. Gao, Y. Kuang, B. Xu, *Chem. Commun.* **2010**, 46, 5364.
- [51] J. Shi, Y. Gao, Z. Yang, B. Xu, *Beilstein J. Org. Chem.* **2011**, 7, 167–172.
- [52] J. Raeburn, T. O. Mc Donald, D. J. Adams, *Chem. Commun.* **2012**, 48, 9355–9357.
- [53] D. J. Cornwell, D. K. Smith, *Chem. Commun.* **2020**, 12465.
- [54] E. R. Draper, E. G. B. Eden, T. O. McDonald, D. J. Adams, *Nat. Chem.* **2015**, 7, 848–852.
- [55] Y. M. Abul-Haija, S. Roy, P. W. J. M. Frederix, N. Javid, V. Jayawarna, R. V. Ulijn, *Small* **2014**, 10, 973–979.
- [56] Z. Yang, H. Gu, D. Fu, P. Gao, J. K. Lam, B. Xu, *Adv. Mater.* **2004**, 16, 1440–1444.
- [57] J. R. Fores, A. Bigo-Simon, D. Wagner, M. Payrastre, C. Damestoy, L. Blandin, F. Boulmedais, J. Kelber, M. Schmutz, M. Rabineau, M. Criado-Gonzalez, P. Schaaf, L. Jierry, *Polymers* **2021**, 13, 1793.
- [58] S. Panja, K. Boháčová, B. Dietrich, D. J. Adams, *Nanoscale* **2020**, 12, 12840–12848.
- [59] S. Buzzaccaro, V. Ruzzi, F. Gelain, R. Piazza, *Gels* **2023**, 9, 347.
- [60] B. O. Okesola, D. K. Smith, *Chem. Soc. Rev.* **2016**, 45, 4226–4251.
- [61] L. R. De Mello, V. Carrascosa, E. Rebelato, M. A. Juliano, I. W. Hamley, V. Castelletto, S. V. Vassiliades, W. A. Alves, C. R. Nakaie, E. R. Da Silva, *Langmuir* **2022**, 38, 3434–3445.
- [62] P. Savage, S. Gao, J. Esposto, B. Adhikari, N. Zabik, H. B. Kraatz, S. H. Eichhorn, S. Martic-Milne, *J. Mol. Struct.* **2022**, 1263, 133116.
- [63] R. Parveen, P. Dastidar, *Chem. Eur. J.* **2016**, 22, 9257–9266.
- [64] B. Hu, H. Yan, Y. Sun, X. Chen, Y. Sun, S. Li, Y. Jing, H. Li, *Artif. Cells Nanomed. Biotechnol.* **2020**, 48, 266–275.
- [65] X. Du, J. Zhou, J. Shi, B. Xu, *Chem. Rev.* **2015**, 115, 13165–13307.
- [66] P. Hoschtettler, G. Pickaert, A. Carvalho, M.-C. Averlant-Petit, L. Stefan, *Chem. Mater.* **2023**, 35, 4259–4275.
- [67] A. Croitoriu, L. E. Nita, A. G. Rusu, A. Ghilan, M. Bercea, A. P. Chiriac, *Polymers* **2022**, 14, 3354.
- [68] E. Scarel, O. Bellotto, P. Rozhin, S. Kralj, M. Tortora, A. V. Vargiu, R. De Zorzi, B. Rossi, S. Marchesan, *Soft Matter* **2022**, 18, 2129–2136.
- [69] Q. Yu, D. Li, M. Cai, F. Zhou, W. Liu, *Tribol. Lett.* **2016**, 61, 1–13.
- [70] P. Byrne, G. O. Lloyd, L. Applegarth, K. M. Anderson, N. Clarke, J. W. Steed, *New J. Chem.* **2010**, 34, 2261.
- [71] M. George, G. Tan, V. T. John, R. G. Weiss, *Chem. Eur. J.* **2005**, 11, 3243–3254.
- [72] G. M. Peters, J. T. Davis, *Chem. Soc. Rev.* **2016**, 45, 3188–3206.
- [73] J. D. Tang, C. Mura, K. J. Lampe, *J. Am. Chem. Soc.* **2019**, 141, 4886–4899.
- [74] G. Ghosh, R. Barman, A. Mukherjee, U. Ghosh, S. Ghosh, G. Fernández, *Angew. Chem. Int. Ed.* **2022**, 61, e202113403.

- [75] A. Saiani, A. Mohammed, H. Frielinghaus, R. Collins, N. Hodson, C. M. Kielty, M. J. Sherratt, A. F. Miller, *Soft Matter* **2009**, *5*, 193–202.
- [76] P. C. Lyu, J. C. Sherman, A. Chen, N. R. Kallenbach, *Proc. Natl. Acad. Sci. U.S.A.* **1991**, *88*, 5317–5320.
- [77] I. W. Hamley, *ACS Appl. Bio Mater.* **2023**, *6*, 384–409.
- [78] L. Arnedo-Sánchez, Nonappa, S. Bhowmik, S. Hietala, R. Puttreddy, M. Lahtinen, L. De Cola, K. Rissanen, *Dalton Trans.* **2017**, *46*, 7309–7316.
- [79] O. Kotova, R. Daly, C. M. G. dos Santos, M. Boese, P. E. Kruger, J. J. Boland, T. Gunnlaugsson, *Angew. Chem.* **2012**, *124*, 7320–7324.
- [80] M. Mukherjee, M. K. Dixit, Y. Kumar, A. Kalam, M. Dubey, *Mol. Syst. Des. Eng.* **2022**, *7*, 1422–1433.
- [81] B. A. Grzybowski, C. E. Wilmer, J. Kim, K. P. Browne, K. J. M. Bishop, *Soft Matter* **2009**, *5*, 1110.
- [82] A. R. Meyer, C. R. Bender, D. M. Dos Santos, F. I. Ziembowicz, C. P. Frizzo, M. A. Villetti, J. M. Reichert, N. Zanatta, H. G. Bonaccorso, M. A. P. Martins, *Soft Matter* **2018**, *14*, 6716–6727.
- [83] R. Xing, C. Yuan, S. Li, J. Song, J. Li, X. Yan, *Angew. Chem. Int. Ed.* **2018**, *57*, 1537–1542.
- [84] L. Thomson, D. McDowall, L. Marshall, O. Marshall, H. Ng, W. J. A. Homer, D. Ghosh, W. Liu, A. M. Squires, E. Theodosiou, P. D. Topham, L. C. Serpell, R. J. Poole, A. Seddon, D. J. Adams, *ACS Nano* **2022**, *16*, 20497–20509.
- [85] C. Gila-Vilchez, M. C. Mañas-Torres, Ó. D. García-García, A. Escribano-Huesca, L. Rodríguez-Arco, V. Carriel, I. Rodríguez, M. Alaminos, M. T. Lopez-Lopez, L. Álvarez De Cienfuegos, *ACS Appl. Polym. Mater.* **2023**, *5*, 2154–2165.
- [86] M. Halperin-Sternfeld, A. Pokhojaev, M. Ghosh, D. Rachmiel, R. Kannan, I. Grinberg, M. Asher, M. Aviv, P. X. Ma, I. Binderman, R. Sarig, L. Adler-Abramovich, *J. Clin. Periodontol.* **2023**, *50*, 200–219.
- [87] E. R. Draper, K. L. Morris, M. A. Little, J. Raeburn, C. Colquhoun, E. R. Cross, T. O. McDonald, L. C. Serpell, D. J. Adams, *CrystEngComm* **2015**, *17*, 8047–8057.
- [88] Y. Li, Y. Han, H. Li, X. Niu, D. Zhang, K. Wang, *Small* **2023**, 2304047.
- [89] V. Alzari, D. Nuvoli, S. Scognamillo, M. Piccinini, E. Gioffredi, G. Malucelli, S. Marceddu, M. Sechi, V. Sanna, A. Mariani, *J. Mater. Chem.* **2011**, *21*, 8727.
- [90] S. Nardecchia, D. Carriazo, M. L. Ferrer, M. C. Gutiérrez, F. D. Monte, *Chem. Soc. Rev.* **2013**, *42*, 794–830.
- [91] B. Adhikari, J. Nanda, A. Banerjee, *Chem. Eur. J.* **2011**, *17*, 11488–11496.
- [92] Q.-Y. Cheng, D. Zhou, Y. Gao, Q. Chen, Z. Zhang, B.-H. Han, *Langmuir* **2012**, *28*, 3005–3010.
- [93] C. Zhu, Y. Lu, J. Peng, J. Chen, S. Yu, *Adv. Funct. Mater.* **2012**, *22*, 4017–4022.
- [94] W. Hanif, A. Hardiansyah, A. Randy, L. A. T. W. Asri, *RSC Adv.* **2021**, *11*, 29029–29041.

- [95] W. Feng, Z. Wang, *Carbohydr. Polym.* **2022**, 294, 119824.
- [96] M. Mihajlovic, M. Mihajlovic, P. Y. W. Dankers, R. Masereeuw, R. P. Sijbesma, *Macromol. Biosci.* **2019**, 19, 1800173.
- [97] J.-F. Guillet, Z. Valdez-Nava, M. Golzio, E. Flahaut, *Carbon* **2019**, 146, 542–548.
- [98] S. Roy, A. Banerjee, *RSC Adv.* **2012**, 2, 2105.
- [99] P. Rozhin, S. Adorinni, D. Iglesias, T. Mackiol, S. Kralj, M. Bisetto, M. Abrami, M. Grassi, M. Bevilacqua, P. Fornasiero, S. Marchesan, *Chem. Eur. J.* **2023**, e202301708.
- [100] L. Suo, H. Wu, P. Wang, Z. Xue, J. Gao, J. Shen, *J. Biomed. Mater. Res.* **2023**, 111, 73–84.
- [101] N. A. Mohamed, N. F. Al-Harby, M. S. Almarshed, *Int. J. Biol. Macromol.* **2019**, 132, 416–428.
- [102] J. Guillet, E. Flahaut, M. Golzio, *ChemPhysChem* **2017**, 18, 2715–2723.
- [103] G. Cirillo, M. Curcio, U. G. Spizzirri, O. Vittorio, P. Tucci, N. Picci, F. Iemma, S. Hampel, F. P. Nicoletta, *Eur. Polym. J.* **2017**, 90, 1–12.
- [104] Y. Xiang, C. Mao, X. Liu, Z. Cui, D. Jing, X. Yang, Y. Liang, Z. Li, S. Zhu, Y. Zheng, K. W. K. Yeung, D. Zheng, X. Wang, S. Wu, *Small* **2019**, 15, 1900322.
- [105] S. Kumari, S. Rajit Prasad, D. Mandal, P. Das, *J. Colloid Interface Sci.* **2019**, 553, 228–238.
- [106] S. Panda, B. ChawPattnayak, P. Dash, B. Nayak, S. Mohapatra, *ACS Appl. Polym. Mater.* **2022**, 4, 369–380.
- [107] K. Zheng, Y. Tong, S. Zhang, R. He, L. Xiao, Z. Iqbal, Y. Zhang, J. Gao, L. Zhang, L. Jiang, Y. Li, *Adv. Funct. Mater.* **2021**, 31, 2102599.
- [108] S. A. P. Van Rossum, M. Tena-Solsona, J. H. Van Esch, R. Eelkema, J. Boekhoven, *Chem. Soc. Rev.* **2017**, 46, 5519–5535.
- [109] N. Singh, G. J. M. Formon, S. De Piccoli, T. M. Hermans, *Adv. Mater.* **2020**, 32, 1–6.
- [110] B. A. K. Kriebisch, A. Jussupow, A. M. Bergmann, F. Kohler, H. Dietz, V. R. I. Kaila, J. Boekhoven, *J. Am. Chem. Soc.* **2020**, 142, 20837–20844.
- [111] F. Della Sala, S. Neri, S. Maiti, J. L.-Y. Chen, L. J. Prins, *Curr. Opin. Biotechnol.* **2017**, 46, 27–33.
- [112] J. Boekhoven, A. M. Brizard, K. N. K. Kowlgi, G. J. M. Koper, R. Eelkema, J. H. Van Esch, *Angew. Chem. Int. Ed.* **2010**, 49, 4825–4828.
- [113] S. De, R. Klajn, *Adv. Mater.* **2018**, 30, 1–6.
- [114] J. Boekhoven, W. E. Hendriksen, G. J. M. Koper, R. Eelkema, J. H. Van Esch, *Science* **2015**, 349, 1075–1080.
- [115] S. Bianco, S. Panja, D. J. Adams, *Gels* **2022**.
- [116] J. Rodon-Fores, M. A. Würbser, M. Kretschmer, B. Rieß, A. M. Bergmann, O. Lieleg, J. Boekhoven, *Chem. Sci.* **2022**, 13, 11411.
- [117] N. Singh, B. Lainer, G. J. M. Formon, S. De Piccoli, T. M. Hermans, *J. Am. Chem. Soc.* **2020**, 142, 4083–4087.
- [118] J. Li, C. Yan, H. Wang, E. Lu, Y. Wang, X. Guo, J. Wang, *ACS Appl. Polym. Mater.* **2023**, 5, 1067–1074.

- [119] G. Ragazzon, L. J. Prins, *Nat. Nanotechnol.* **2018**, *13*, 882–889.
- [120] D. Samanta, R. Klajn, *Adv. Opt. Mater.* **2016**, *4*, 1373–1377.
- [121] C. A. Angulo-Pachón, J. F. Miravet, *Chem. Commun.* **2016**, *52*, 5398–5401.
- [122] A. Jain, S. Dhiman, A. Dhayani, P. K. Vemula, S. J. George, *Nat. Commun.* **2019**, *10*, 1–9.
- [123] P. S. Schwarz, L. Tebcharani, J. E. Heger, P. Müller-Buschbaum, J. Boekhoven, *Chem. Sci.* **2021**, *12*, 9969–9976.
- [124] F. Schnitter, A. M. Bergmann, B. Winkeljann, J. Rodon Fores, O. Lieleg, J. Boekhoven, *Nat. Protoc.* **2021**, *16*, 3901–3932.
- [125] N. Singh, A. Lopez-Acosta, G. J. M. Formon, T. M. Hermans, *J. Am. Chem. Soc.* **2022**, *144*, 410–415.
- [126] S. Debnath, S. Roy, R. V. Ulijn, *J. Am. Chem. Soc.* **2013**, *135*, 16789–16792.
- [127] C. G. Pappas, I. R. Sasselli, R. V. Ulijn, *Angew. Chem. Int. Ed.* **2015**, *54*, 8119–8123.
- [128] M. Liu, C. N. Creemer, T. J. Reardon, J. R. Parquette, *Chem. Commun.* **2021**, *57*, 13776–13779.
- [129] M. Weißenfels, J. Gemen, R. Klajn, *Chem* **2021**, *7*, 23–37.
- [130] F. Rakotondradany, M. A. Whitehead, A. Lebuis, H. F. Sleiman, *Chem. Eur. J.* **2003**, *9*, 4771–4780.
- [131] J. J. D. De Jong, P. R. Hania, A. Pugžlys, L. N. Lucas, M. De Loos, R. M. Kellogg, B. L. Feringa, K. Duppen, J. H. Van Esch, *Angew. Chem. Int. Ed.* **2005**, *44*, 2373–2376.
- [132] S. Selmani, E. Schwartz, J. T. Mulvey, H. Wei, A. Grosvirt-Dramen, W. Gibson, A. I. Hochbaum, J. P. Patterson, R. Ragan, Z. Guan, *J. Am. Chem. Soc.* **2022**, *144*, 7844–7851.
- [133] S. Mondal, D. Halder, *New J. Chem.* **2021**, *45*, 4773–4779.
- [134] G. Wang, S. Liu, *ChemSystemsChem* **2020**, *2*, e1900046.
- [135] B. Rieß, J. Boekhoven, *ChemNanoMat* **2018**, *4*, 710–719.
- [136] R. Klajn, P. J. Wesson, K. J. M. Bishop, B. A. Grzybowski, *Angew. Chem. Int. Ed.* **2009**, *48*, 7035–7039.
- [137] M. Tena-Solsona, B. Rieß, R. K. Grötsch, F. C. Löhrer, C. Wanzke, B. Käsdorf, A. R. Bausch, P. Müller-Buschbaum, O. Lieleg, J. Boekhoven, *Nat. Commun.* **2017**, *8*, 15895.
- [138] M. Kurbasic, C. D. Romano, A. M. Garcia, S. Kralj, S. Marchesan, *Gels* **2017**, *3*, 29.
- [139] S. H. Hiew, J. K. Wang, K. Koh, H. Yang, A. Bacha, J. Lin, Y. S. Yip, M. I. G. Vos, L. Chen, R. M. Sobota, N. S. Tan, C. Y. Tay, A. Miserez, *Acta Biomater.* **2021**, *136*, 111–123.
- [140] C. Wanzke, M. Tena-Solsona, B. Rieß, L. Tebcharani, J. Boekhoven, *Mater. Horiz.* **2020**, *7*, 1397–1403.
- [141] T. Heuser, E. Weyandt, A. Walther, *Angew. Chem. Int. Ed.* **2015**, *54*, 13258–13262.
- [142] D. Banik, R. Dutta, P. Banerjee, S. Kundu, N. Sarkar, *J. Phys. Chem. B* **2016**, *120*, 7662–7670.

- [143] E. Parisi, A. M. Garcia, D. Marson, P. Posocco, S. Marchesan, *Gels* **2019**, *5*, 5.
- [144] E. Rosa, C. Diaferia, E. Gianolio, T. Sibillano, E. Gallo, G. Smaldone, M. Stornaiuolo, C. Giannini, G. Morelli, A. Accardo, *Macromol. Biosci.* **2022**, *22*, 2200128.
- [145] S. Ghosh, X.-Q. Li, V. Stepanenko, F. Würthner, *Chem. Eur. J.* **2008**, *14*, 11343–11357.
- [146] W. Wagner, M. Wehner, V. Stepanenko, S. Ogi, F. Würthner, *Angew. Chem.* **2017**, *129*, 16224–16228.
- [147] S. Sivagnanam, K. Das, I. Pan, A. Barik, A. Stewart, B. Maity, P. Das, *ACS Appl. Bio Mater.* **2023**, *6*, 836–847.
- [148] M. C. Mañas-Torres, C. Gila-Vilchez, F. J. Vazquez-Perez, P. Kuzhir, D. Momier, J. C. Scimeca, A. Borderie, M. Goracci, F. Burel-Vandenbos, C. Blanco-Elices, I. A. Rodriguez, M. Alaminos, L. Á. De Cienfuegos, M. T. Lopez-Lopez, *ACS Appl. Mater. Interfaces* **2021**, *13*, 49692–49704.
- [149] D. Adams, *Gels* **2018**, *4*, 32.
- [150] L. L. E. Mears, E. R. Draper, A. M. Castilla, H. Su, Zhuola, B. Dietrich, M. C. Nolan, G. N. Smith, J. Douth, S. Rogers, R. Akhtar, H. Cui, D. J. Adams, *Biomacromolecules* **2017**, *18*, 3531–3540.
- [151] M. Du, P. Zhu, X. Yan, Y. Su, W. Song, J. Li, *Chem. Eur. J.* **2011**, *17*, 4238–4245.
- [152] J. Raeburn, D. J. Adams, *Chem. Commun.* **2015**, *51*, 5170–5180.
- [153] J. Canet-Ferrer, E. Coronado, A. Forment-Aliaga, E. Pinilla-Cienfuegos, *Nanotechnology* **2014**, *25*, 395703.
- [154] R. Kakehashi, N. Tokai, M. Nakagawa, K. Kawasaki, S. Horiuchi, A. Yamamoto, *Gels* **2023**, *9*, 261.
- [155] D. K. Duraisamy, P. D. Sureshbhai, P. Saveri, A. P. Deshpande, G. Shanmugam, *Chem. Commun.* **2022**, *58*, 13377–13380.
- [156] Y. Tominaga, S. Kanemitsu, S. Yamamoto, T. Kimura, Y. Nishida, K. Morita, T. Maruyama, *Colloids Surf. Physicochem. Eng. Asp.* **2023**, *656*, 130416.
- [157] X. Chen, D. Hu, R. Mescall, G. You, D. N. Basov, Q. Dai, M. Liu, *Adv. Mater.* **2019**, *31*, 1804774.
- [158] M. Dendisová, A. Jenišťová, A. Parchaňská-Kokaislová, P. Matějka, V. Prokopec, M. Švecová, *Anal. Chim. Acta* **2018**, *1031*, 1–14.
- [159] L. Mester, A. A. Govyadinov, S. Chen, M. Goikoetxea, R. Hillenbrand, *Nat. Commun.* **2020**, *11*, 1–10.
- [160] M. Meyns, S. Primpke, G. Gerdt, *Anal. Methods* **2019**, *11*, 5195–5202.
- [161] T. Taubner, R. Hillenbrand, F. Keilmann, *Appl. Phys. Lett.* **2004**, *85*, 5064–5066.
- [162] N. Ocelic, A. Huber, R. Hillenbrand, *Appl. Phys. Lett.* **2006**, *89*, 87–90.
- [163] S. Mastel, A. A. Govyadinov, T. V. A. G. De Oliveira, I. Amenabar, R. Hillenbrand, *Appl. Phys. Lett.* **2015**, *106*, 1–6.
- [164] J. Kim, W. Lee, H. Kim, D. Y. Ryu, H. Ahn, B. Chae, *Spectrochim. Acta A Mol. Biomol. Spectrosc.* **2022**, *274*, 121095.

- [165] T. E. Tesema, R. Mcfarland-Porter, E. Zerai, J. Grey, T. G. Habteyes, *J. Phys. Chem. C* **2022**, *126*, 7764–7772.
- [166] C. Westermeier, A. Cernescu, S. Amarie, C. Liewald, F. Keilmann, B. Nickel, *Nat. Commun.* **2014**, *5*, 1–6.
- [167] F. Huth, A. Govyadinov, S. Amarie, W. Nuansing, F. Keilmann, R. Hillenbrand, *Nano Lett.* **2012**, *12*, 3973–3978.
- [168] K. J. Kaltenecker, T. Gölz, E. Bau, F. Keilmann, *Sci. Rep.* **2021**, *11*, 1–12.
- [169] H. Amrania, L. Drummond, R. C. Coombes, S. Shousha, L. Woodley-Barker, K. Weir, W. Hart, I. Carter, C. C. Phillips, *Faraday Discuss.* **2016**, *187*, 539–553.
- [170] K. Kanevche, D. J. Burr, D. J. Nürnberg, P. K. Hass, A. Elsaesser, J. Heberle, *Commun. Biol.* **2021**, *4*, 1–8.
- [171] M. Lucidi, D. E. Tranca, L. Nichele, D. Ünay, G. A. Stanciu, P. Visca, A. M. Holban, R. Hristu, G. Cincotti, S. G. Stanciu, *GigaScience* **2020**, *9*, 1–12.
- [172] M. Brehm, T. Taubner, R. Hillenbrand, F. Keilmann, *Nano Lett.* **2006**, *6*, 1307–1310.
- [173] S. Gamage, M. Howard, H. Makita, B. Cross, G. Hastings, M. Luo, Y. Abate, *PLoS ONE* **2018**, *13*, 1–12.
- [174] R. O. Freitas, A. Cernescu, A. Engdahl, A. Paulus, J. E. Levandoski, I. Martinsson, E. Hebisch, C. Sandt, G. K. Gouras, C. N. Prinz, T. Deierborg, F. Borondics, O. Klementieva, *Cells* **2021**, *10*, 1–15.
- [175] M. Paulite, Z. Fakhraai, I. T. S. Li, N. Gunari, A. E. Tanur, G. C. Walker, *J. Am. Chem. Soc.* **2011**, *133*, 7376–7383.
- [176] S. Paul, A. Jenišťová, F. Vosough, E. Berntsson, C. Mörman, J. Jarvet, A. Gräslund, S. K. T. S. Wärmländer, A. Barth, *Commun. Chem.* **2023**, *6*, 163.
- [177] X. Yu, L. Chen, M. Zhang, T. Yi, *Chem. Soc. Rev.* **2014**, *43*, 5346.
- [178] E. R. Draper, D. J. Adams, *Chem. Soc. Rev.* **2018**, *47*, 3395–3405.
- [179] S. Cai, B. R. Singh, *Biophys. Chem.* **1999**, *80*, 7–20.
- [180] A. Barth, C. Zscherp, *Q. Rev. Biophys.* **2002**, *35*, 369–430.
- [181] A. Barth, *Biochim. Biophys. Acta Bioenerg.* **2007**, *1767*, 1073–1101.
- [182] M. Reches, E. Gazit, *Isr. J. Chem.* **2005**, *45*, 363–371.
- [183] X. Yan, P. Zhu, J. Li, *Chem. Soc. Rev.* **2010**, *39*, 1877–1890.
- [184] X. Yan, Y. Cui, Q. He, K. Wang, J. Li, *Chem. Mater.* **2008**, *20*, 1522–1526.
- [185] N. Chauhan, Y. Singh, *ACS Biomater. Sci. Eng.* **2020**, *6*, 5507–5518.
- [186] S. Basak, N. Nandi, S. Paul, I. W. Hamley, A. Banerjee, *Chem. Commun.* **2017**, *53*, 5910–5913.
- [187] K. Ariga, J. I. Kikuchi, M. Naito, N. Yamada, *Polym. Adv. Technol.* **2000**, *11*, 856–864.
- [188] V. Singh, K. Snigdha, C. Singh, N. Sinha, A. K. Thakur, *Soft Matter* **2015**, *11*, 5353–5364.
- [189] C. Diaferia, E. Rosa, G. Morelli, A. Accardo, *Pharmaceuticals* **2022**, *15*, 1048.
- [190] L. Mester, A. A. Govyadinov, R. Hillenbrand, *Nanophotonics* **2022**, *11*, 377–390.
- [191] I. Amenabar, S. Poly, M. Goikoetxea, W. Nuansing, P. Lasch, R. Hillenbrand, *Nat. Commun.* **2017**, *8*, 14402.

- [192] R. Krutokhvostov, A. A. Govyadinov, J. M. Stiegler, F. Huth, A. Chuvilin, P. S. Carney, R. Hillenbrand, *Opt. Express* **2012**, *20*, 593.
- [193] K. B. Beć, Y. Futami, M. J. Wójcik, T. Nakajima, Y. Ozaki, *J. Phys. Chem. A* **2016**, *120*, 6170–6183.
- [194] K. J. Kaltenecker, *Sci. Rep.* **2021**.
- [195] C. Hazra, T. Samanta, V. Mahalingam, *J. Mater. Chem. C* **2014**, *2*, 10157–10163.
- [196] E. Martín-Tornero, F. J. Sierra-Tadeo, I. Durán-Merás, A. Espinosa-Mansilla, *J. Fluoresc.* **2019**, *29*, 1445–1455.
- [197] N. J. Hestand, F. C. Spano, *Chem. Rev.* **2018**, *118*, 7069–7163.
- [198] T. G. Mayerhöfer, J. Popp, *ChemPhysChem* **2020**, *21*, 1218–1223.
- [199] P. Bairi, B. Roy, P. Routh, K. Sen, A. K. Nandi, *Soft Matter* **2012**, *8*, 7436.
- [200] I. Hisaki, H. Shigemitsu, Y. Sakamoto, Y. Hasegawa, Y. Okajima, K. Nakano, N. Tohnai, M. Miyata, *Angew. Chem. Int. Ed.* **2009**, *48*, 5465–5469.
- [201] P. J. Pacheco-Liñán, C. Martín, C. Alonso-Moreno, A. Juan, D. Hermida-Merino, A. Garzón-Ruíz, J. Albaladejo, M. Van Der Auweraer, B. Cohen, I. Bravo, *Chem. Commun.* **2020**, *56*, 4102–4105.
- [202] T. Ishi-i, K. Murakami, Y. Imai, S. Mataka, *J. Org. Chem.* **2006**, *71*, 5752–5760.
- [203] A. Dawn, T. Shiraki, S. Haraguchi, H. Sato, K. Sada, S. Shinkai, *Chem. Eur. J.* **2010**, *16*, 3676–3689.
- [204] Y. Hong, J. W. Y. Lam, B. Z. Tang, *Chem. Commun.* **2009**, 4332.
- [205] B.-K. An, D.-S. Lee, J.-S. Lee, Y.-S. Park, H.-S. Song, S. Y. Park, *J. Am. Chem. Soc.* **2004**, *126*, 10232–10233.
- [206] C. Lai, W. Guo, X. Tang, M. Pei, *Chin. J. Chem.* **2012**, *30*, 507–511.
- [207] C. Tang, R. V. Ulijn, A. Saiani, *Langmuir* **2011**, *27*, 14438–14449.
- [208] T. Sonallya, L. Sruthi, A. P. Deshpande, G. Shanmugam, *J. Mol. Liq.* **2021**, *342*, 116945.
- [209] L. V, P. P, V. A, *Madridge J. Anal. Sci. Instrum.* **2017**, *2*, 21–24.
- [210] A. Vyšniauskas, M. Qurashi, N. Gallop, M. Balaz, H. L. Anderson, M. K. Kuimova, *Chem. Sci.* **2015**, *6*, 5773–5778.
- [211] A. Aufderhorst-Roberts, W. J. Frith, M. Kirkland, A. M. Donald, *Langmuir* **2014**, *30*, 4483–4492.
- [212] Å. Öhrlund, *J. Cosmet. Dermatol. Sci. Appl.* **2018**, *08*, 47–54.
- [213] A. M. Handorf, Y. Zhou, M. A. Halanski, W. J. Li, *Organogenesis* **2015**, *11*, 1–15.
- [214] C. F. Guimarães, L. Gasperini, A. P. Marques, R. L. Reis, *Nat. Rev. Mater.* **2020**, *5*, 351–370.
- [215] T. Komiyama, Y. Harada, T. Hase, S. Mori, S. Kimura, M. Yokoya, M. Yamanaka, *Chem. Asian J.* **2021**, *16*, 1750–1755.
- [216] L. E. Buerkle, S. J. Rowan, *Chem. Soc. Rev.* **2012**, *41*, 6089.
- [217] S. Misra, S. Mukherjee, A. Ghosh, P. Singh, S. Mondal, D. Ray, G. Bhattacharya, D. Ganguly, A. Ghosh, V. K. Aswal, A. K. Mahapatra, B. Satpati, J. Nanda, *Chem. Eur. J.* **2021**, *27*, 16744–16753.

- [218] M. E. Afami, I. E. Karim, I. About, S. M. Coulter, G. Laverty, F. T. Lundy, *Materials* **2021**, *14*, DOI 10.3390/ma14092237.
- [219] I. Irwansyah, Y. Q. Li, W. Shi, D. Qi, W. R. Leow, M. B. Y. Tang, S. Li, X. Chen, *Adv. Mater.* **2015**, *27*, 648–654.
- [220] V. Prakash, Y. Christian, A. S. Redkar, A. Roy, R. Anandalakshmi, V. Ramakrishnan, *Soft Matter* **2022**, *18*, 6360–6371.
- [221] W. Li, X. Hu, J. Chen, Z. Wei, C. Song, R. Huang, *J. Mater. Sci. Mater. Med.* **2020**, *31*, DOI 10.1007/s10856-020-06410-9.
- [222] A. Y. Gahane, P. Ranjan, V. Singh, R. K. Sharma, N. Sinha, M. Sharma, R. Chaudhry, A. K. Thakur, *Soft Matter* **2018**, *14*, 2234–2244.
- [223] S. Liu, T. H. Zeng, M. Hofmann, E. Burcombe, J. Wei, R. Jiang, J. Kong, Y. Chen, *ACS Nano* **2011**, *5*, 6971–6980.
- [224] Y.-Y. Xie, Y.-W. Zhang, X.-T. Qin, L.-P. Liu, F. Wahid, C. Zhong, S.-R. Jia, *Colloids Surf. B* **2020**, *193*, 111099.



ORIGINAL PAPERS

I

TRIGGERING A TRANSIENT ORGANO-GELATION SYSTEM IN A CHEMICALLY ACTIVE SOLVENT

by

Romain Chevigny, Johanna Schirmer, Carmen C. Piras, Andreas Johansson, Elina Kalenius, David K. Smith, Mika Pettersson, Efstratios D. Sitsanidis, and Maija Nissinen

Chemical Communication, 2021, 57, 10375-10378

<https://doi.org/10.1039/D1CC04021A>

Link to SI material:

<https://pubs.rsc.org/en/content/articlelanding/2021/cc/d1cc04021a>

Reproduced with permission by Royal Society of Chemistry.



Triggering a transient organo-gelation system in a chemically active solvent†

Cite this: *Chem. Commun.*, 2021, 57, 10375

Received 24th July 2021,
Accepted 14th September 2021

DOI: 10.1039/d1cc04021a

rsc.li/chemcomm

Romain Chevigny,[†] Johanna Schirmer,[‡] Carmen C. Piras,^b Andreas Johansson,[†] Elina Kalenius,[†] David K. Smith,^b Mika Pettersson,^a Efstratios D. Sitsanidis^{†*} and Maija Nissinen^{†*}

A transient organo-gelation system with spatiotemporal dynamic properties is described. Here, the solvent actively controls a complex set of equilibria that underpin the dynamic assembly event. The observed metastability is due to the *in situ* formation of a secondary solvent, acting as an antagonist against the primary solvent of the organogel.

In nature, energy dissipating biomolecular assemblies form transiently under the constant exchange of energy and matter with the environment. However, many artificial assembled systems lack the complexity of their natural counterparts as the assembly event occurs at thermodynamic equilibrium. There is increasingly intense interest in metastable gelation systems that assemble in a dynamic, kinetically controlled way, for example, in response to the presence of fuel and then disassemble when the fuel is depleted.^{1–3} Van Esch *et al.*, for example, used an alkylating agent as fuel to generate a low molecular weight gelator (LMWG) ester, while the process was reversed by ambient hydrolysis.⁴ A number of reports built on this demonstrating that hydrogels can exist in non-equilibrium states using various fuels.^{5–8}

Transient materials do not only depend on cyclic fuelled dissipative systems. In the seminal work of Heuser *et al.*,⁹ the catalytic temporal control of a pH-responsive dipeptide consists of an alternative approach towards transient peptide gels. The self-assembly of LMWGs is a dynamic process, strongly dependent on their structural features and the nature of the gelation trigger, either physical or chemical.^{10,11} For example, photo-responsive gelators have been reported to assemble towards

out-of-equilibrium systems,^{12,13} deprotection of a Boc group has been used to convert organogelators to hydrogels,¹⁴ simple deprotection reactions can yield gels *in situ*,¹⁵ and enzyme-mediated chemical changes can trigger self-assembly.^{16–18} Catalysis plays an intimate role in controlling non-equilibrium fuelled systems in both assembly/disassembly pathways. A case as such describes gelation in which the fuel derives catalytically from a “pre-fuel”.¹⁹ Additionally, catalysis has been reported to trigger an interplay between pH and oxidation, leading to the transient assembly of dendritic peptide monomers.²⁰ Among amino acid based gelators, phenylalanine derivatives are efficient LMWGs, yielding self-supporting gels.^{21,22} Working on a multistep synthesis towards a set of phenylalanine based organogelators, we serendipitously noticed the *in situ* gelation of dipeptide *N*-*tert*-butyloxycarbonyl (Boc)-*L*-phenylalanyl-*L*-phenylalanine *tert*-butyl ester (Boc-Phe-Phe-*Or*Bu **1**), triggered by the selective deprotection of the Boc group in the presence of the *tert*-butyl group (Fig. 1 and Fig. S1, ESI†).

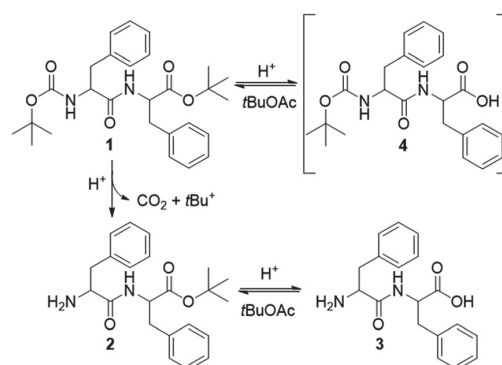


Fig. 1 Selective deprotection of the Boc-group in the presence of the *tert*-butyl group under acidic conditions. Gelation is induced by the chemical equilibrium between products **2** and **3**.

^a Department of Chemistry, Nanoscience Center, University of Jyväskylä, P.O. Box 35, FI-40014 JYU, Finland. E-mail: maija.nissinen@jyu.fi

^b Department of Chemistry, University of York, Heslington, York, YO10 5DD, UK

^c Department of Physics, Nanoscience Center, University of Jyväskylä, P.O. Box 35, FI-40014 JYU, Finland

† Electronic supplementary information (ESI) available: Materials and methods, synthetic protocols, NMR, FT-IR and HR-MS spectra, gelation trials, swelling and rheology plots. See DOI: 10.1039/d1cc04021a

‡ These authors contributed equally.



Communication

Herein, we focus on deciphering the gelation mechanism and understanding how the dynamic nature of the reaction equilibrium affects the stability of the obtained organogel. In many cases, the solvent in gelation systems plays a relatively passive role in simply supporting the assembly event. In this system, however, it plays an active and chemically intimate role in controlling the equilibria that underpin the dynamic assembly process.

The deprotection reaction is based on the protocol of Lin *et al.*²³ The precursor gelator **1** is suspended in *tert*-butyl acetate (*t*BuOAc) at a concentration of 0.5 M. When adding 1.5 equivalents of sulfuric acid to the reaction mixture, dipeptide **1** is selectively deprotected at the carbamate group to give the ester Phe–Phe–*Ot*Bu **2** (Fig. 1 and S2, ESI[†]) in 95% yield. According to Lin *et al.*,²³ the driving force of the reaction is the formation and release of carbon dioxide formed by the irreversible cleavage of the Boc group. Their studies showed that the *C*-terminal ester is also deprotected to give the mono-carbamate protected dipeptide Boc–Phe–Phe **4**. This process is rapid and reversible as *t*BuOAc regenerates the tertiary cation (*t*Bu⁺), therefore reforming the ester group of **1**. In this way, the solvent plays an intimate role in the reaction cycle. However, our studies showed that gelation is achieved when adding less sulfuric acid (1.0 equivalent) while keeping the concentration of **1** constant (0.5 M). In this sense, sulfuric acid can be considered an “accelerator” for the gelation process.

To identify the minimum gelation concentration (MGC) of precursor **1** (0.05 M; Table S1, ESI[†]), we performed a series of concentration screening trials. Gelation, assessed by the vial inversion method, occurred within 12 h upon addition of the acid at room temperature. In addition, we measured the gel-to-sol phase transition temperature ($T_{\text{gel-sol}}$) by controlled heating of the gels. Irrespective of their concentration, all samples appeared stable up to 45–50 °C. Heating at 55 °C resulted in the collapse of the gels to a solution. However, they reformed upon cooling, verifying the thermoreversible nature of the gel (Fig. S3, ESI[†]).

The organogel has a lifespan of four days, after which it turns into a solution. Under acidic conditions, the deprotection of **1** could occur to a full extent towards *L*-phenylalanyl-*L*-phenylalanine (Phe–Phe) **3** before *t*BuOAc regenerates ester **2**. Therefore, gelation must be triggered either by Phe–Phe **3**, the mono-protected ester **2** or both potential gelators **2** and **3**. The slow decay of the organogel within four days could suggest possible changes in the chemical equilibrium between dipeptide counterparts **2** and **3**. Therefore, to identify the gelling agents and investigate the gelation mechanism with respect to the reaction equilibrium, we performed nuclear magnetic resonance (NMR) studies on the dried gel (xerogel I-dried xerogel dissolved in deuterated d_6 -DMSO) of a freshly prepared organogel.

Both ¹³C and ¹H NMR spectra of xerogel I confirmed the presence of the mono-protected **2** and fully deprotected **3** dipeptides, in approximately 1:0.9 ratio (Fig. 2 and Fig. S5, S6, ESI[†]). The two doublets at ~9.0 ppm are attributed to the two NH groups of the peptide bonds. Integration of the

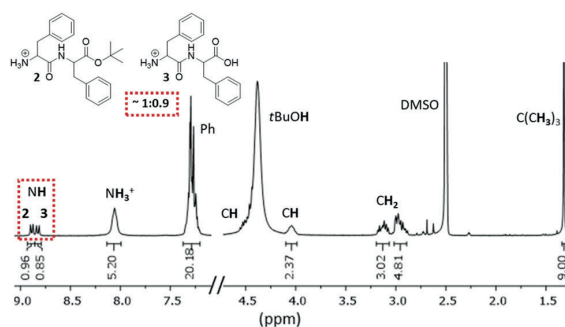


Fig. 2 ¹H NMR (300 MHz, d_6 -DMSO) spectrum of xerogel I. Gelation is induced by products **2** and **3**.

remaining signals shows twice the number of H atoms, except for the *tert*-butyl group. The broad band at 4.4 ppm is due to the hydroxyl group of *tert*-butyl alcohol (*t*BuOH), a side product of the ester **2** deprotection. The broad peak at ~8 ppm corresponds to the protonated *N*-terminus of compounds **2** and **3** under acidic conditions. The presence of both compounds in the xerogel was also confirmed by high-resolution mass spectroscopy (HR-MS, Fig. S10, ESI[†]).

To assess potential changes in the ratio of compounds **2** and **3** and their impact on the gel's lifetime, we recorded the NMR spectra of dissolved dried xerogels, prepared at different time points, ranging from the formation of the gel (day 1) until the transition to the solution phase (day 4). Although both compounds **2** and **3** were present in the system, their ratio appeared to change randomly over 4 days (Fig. 3). Interestingly, the dynamic interconversion between dipeptides **2** and **3** does not seem to be responsible for the collapse of the gel but rather the formation of *t*BuOH over time.

Indeed, when we added *t*BuOH on the surface of freshly prepared organogels, they collapsed within 48 h, in contrast to the untreated material. Additional control experiments with water showed that the gel collapses almost immediately upon

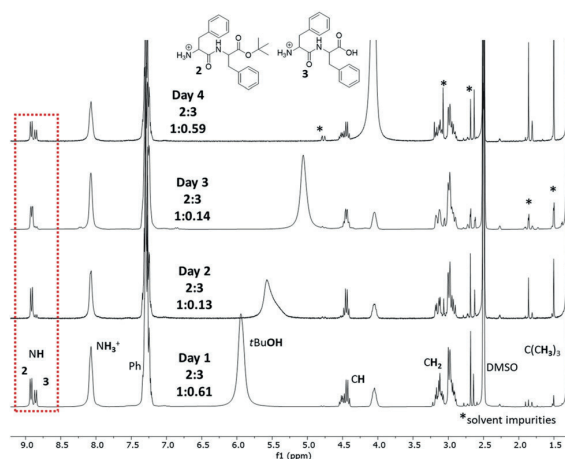


Fig. 3 ¹H NMR (300 MHz, d_6 -DMSO) spectra of xerogels over 4 days.



addition. The water in the system originates from the acid solution and solvents. However, its amount is insufficient to break the gel structure as the untreated organogel collapses after 4 days. Upon addition of the acid, part of the formed *tert* butyl cation ($t\text{Bu}^+$) re-esterifies Boc-Phe-Phe **4** towards Boc-Phe-Phe-*Ot*Bu **1** (Fig. 1) in a rapid process, as per the given mechanism. Based on the control experiments and the obtained NMR spectra, we, therefore, suggest that the formation of *t*BuOH at a slower pace is responsible for the re-esterification of Phe-Phe **3** to the mono-protected ester Phe-Phe-*Ot*Bu **2**.

To clarify the observed random evolution of compounds **2** and **3** over time and their contribution to gel formation, we tested whether components **2** and **3** could form alone a self-supporting gel in *t*BuOAc. In the absence of sulfuric acid, ester **2** did not gel, indicating that compound **2** cannot form gels independently. However, when 1.0 equivalent of the acid was added, compound **3** formed *in situ*, leading to a mixture of **2** and **3** at a 0.9 : 1 ratio that once again yielded a self-supporting organogel. NMR analysis of the corresponding xerogel (**II**) showed qualitative spectra similar to xerogel (**I**) (Fig. S5 and S6, ESI†). In contrast, Phe-Phe **3** did not gel in *t*BuOAc even after the addition of the acid. Thus, to induce gelation under the given conditions, the presence of both compounds **2** and **3** is required.

Gelation is dynamically driven by the presence of acid in the system. The organogel appears to be thermodynamically *meta*-stable since supramolecular forces between derivatives **2** and **3** develop relatively rapidly (12 h), leading to gelation. The observed interconversion between gelators **2** and **3** does not affect the stability of the gel. In contrast, the formation of *t*BuOH, which occurs more slowly over four days, converts the gel to a solution, as it seems to act antagonistically against *t*BuOAc (Fig. 4). Therefore, the presence of *t*BuOAc, which reverses the conversion of **2** into **3**, the process that otherwise

forms *t*BuOH, effectively acts as a brake on the process. In principle, the balance between the “accelerating” sulfuric acid and the “braking” *t*BuOAc will dictate the gel’s metastability. This means that the degradation time could be controlled, for example, by changing the acid concentration. Indeed, when only 0.5 equivalents of acid were used, the lifetime of the gels extended beyond 4 weeks (Table S2, ESI†). Such an approach might be beneficial for applications that require the formation and controlled degradation of soft materials at a given time.^{24–27}

According to the literature, diphenylalanine-based nanostructures adopt β -sheet conformations when assembled, as per the reported positions of the amide I bands.^{28–30} Here, the xerogel shows a peak at 1661 cm^{-1} suggesting the potential formation of 3_{10} -helices³¹ rather than a parallel or antiparallel β -sheet secondary structure.

In addition, we performed swelling studies on the organogel in *t*BuOAc to assess its stability. Two gel specimens at concentrations of 0.05 M (MGC) and 0.1 M were used. The calculated swelling degree (SD-%) of each sample against time revealed that swelling is concentration-dependent (Fig. S4, ESI†). At the MGC (0.05 M), swelling reached a plateau after sixteen days, whereas at a higher concentration (0.1 M), no swelling was observed, even after ten days of continuous measurements. The swollen material absorbed solvent up to 6% of its initial weight, demonstrating a high degree of elasticity. Rheology studies at the MGC before swelling revealed a storage modulus (G') of 10890 Pa and a loss modulus (G'') of 2474 Pa, respectively (Fig. S12, ESI†).

Although the standard organogel has a lifespan of four days, both materials remained intact for twenty days during the swelling studies. Seven months later, the swollen gel was still stable. The lifespan expansion suggests that the solvent treatment affected the consistency and potentially the materials’ supramolecular network. Therefore, we recorded the NMR spectra of the swollen gel (Fig. S8 and S9, ESI†) to assess potential changes in its consistency. In contrast to the initial organogel, only ester **2** was detected. It seems likely that adding extra solvent and the material’s swelling helps prevent the deprotection of compound **2** towards **3**. Indeed, removing excess solvent from the gel’s surface during each measurement will also decrease the acid concentration, effectively removing some of the “accelerator” from the system. Meanwhile, *t*BuOAc forms the tertiary cation in excess and regenerates ester **2**, acting as a “brake”. We reason that these processes combine to extend the lifetime of the metastable gel. Interestingly, when the mixture of **2** and **3** is treated with *t*BuOAc in this way, compound **2** can maintain the gel behaviour, whereas, on its own, it cannot establish a gel. This indicates, as is often seen for metastable gels that the assembly pathway plays an important role in controlling the material’s performance.³²

Notably, during the swelling studies, the conditions changed since sulfuric acid concentration was now present at less than 1.0 equivalent. To relate the results of swelling studies with potential alterations of the gel’s network, we performed scanning electron microscopy (SEM) imaging of the gel samples

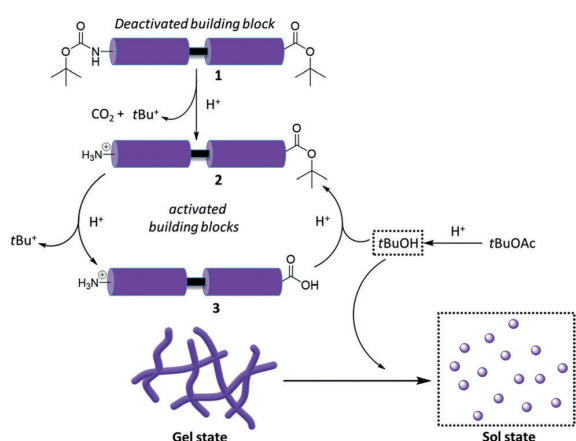


Fig. 4 Transient assembly: precursor **1** is activated by acid “accelerator” towards gelators **2** and **3**. The solvent (*t*BuOAc) acts as a “brake”, reversing the conversion of **2** into **3** and preventing the formation of *t*BuOH, which otherwise causes the gel to decay.



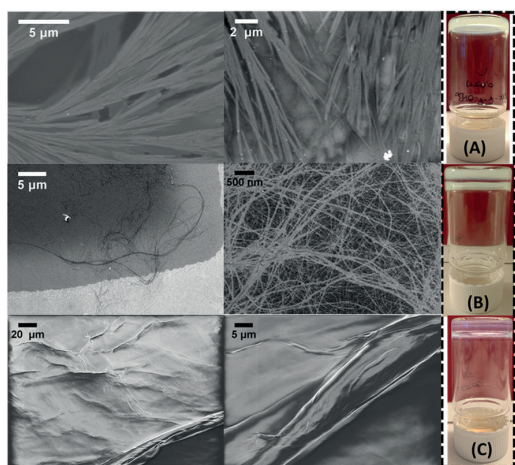


Fig. 5 SEM imaging after (A) 1 day; (B) 20 days; (C) 7 months. Inset depicts the corresponding bulk gels. The double layer (B and C) is a mirror effect due to the camera's angle.

(Fig. 5). Images taken immediately after the gel formation revealed a dense three-dimensional network of branched, entangled, plated ribbons. The swollen material after twenty days of treatment showed elongated, fine fibres in coil-coiled constructions. Seven months later, the network consisted of thicker fibres intertwined into wider bundles. This suggests the slow dynamic evolution of the structure over time.³³

Our studies prove a gelation system, which evolves dynamically over time through a set of coupled reactions, some of which are in equilibrium. Sulfuric acid is the reaction “accelerator”, driving the deprotection reactions of NHBoc and *t*Bu-ester forward. The solvent (*t*BuOAc) acts as a “brake” by effectively reversing the ester deprotection. This prevents the formation of *t*BuOH, which otherwise appears to trigger the gel-to-sol transition. The organogel is thermodynamically *meta*-stable and responds to the presence of the “accelerator” or the “brake”. For example, swelling of the material with additional solvent limits the hydrolysis of the ester and the formation of *t*BuOH, thus, extending its lifespan and altering its supramolecular network. Therefore, sample-handling procedures could introduce, to some extent, tuneability to the micro- and macroscopic properties of gels. This system constitutes a rare example in which the solvent does not only play a passive role in supporting the gelation process but is intimately involved in the chemical equilibria, which underpin the dynamic gelation event itself and helps trigger gel assembly/breakdown.

The authors would like to acknowledge Jane and Aatos Erkko Foundation for supporting the current work.

E. S. and R. C. designed and performed the synthesis, characterization and gelation experiments with J. S. and wrote the original draft, C. C. P. did the rheological measurements and data interpretation with E. S., E. K. did the mass spectrometric studies and analysis, A. J. did the microscopic imaging and visualization, D. S. is responsible for rheological resources, data interpretation and review and editing of the manuscript,

M. P. supervised the work of J. S. and acquired the funding and resources, M. N. supervised the work of R. C., was responsible for project management and review and editing of the manuscript with input from all authors.

Conflicts of interest

There are no conflicts to declare.

Notes and references

- J. Boekhoven, W. E. Hendriksen, G. J. Koper, R. Eelkema and J. H. van Esch, *Science*, 2015, **349**(6252), 1075–1079.
- C. A. Angulo-Pachón and J. F. Miravet, *Chem. Commun.*, 2016, **52**, 5398–5401.
- S. Dhiman and S. J. George, *Bull. Chem. Soc. Jpn.*, 2018, **91**, 687–699.
- J. Boekhoven, A. M. Brizard, K. N. K. Kowli, G. J. M. Koper, R. Eelkema and J. H. van Esch, *Angew. Chem.*, 2010, **122**, 4935–4938.
- G. Ragazzon and L. J. Prins, *Nat. Nanotechnol.*, 2018, **13**, 882–889.
- W. A. Ogdan and Z. Guan, *ChemSystemsChem*, 2020, **2**, e1900030.
- B. Rieß, R. K. Grötsch and J. Boekhoven, *J. Chem.*, 2020, **6**, 552–578.
- F. della Sala, S. Neri, S. Maiti, J. L. Y. Chen and L. J. Prins, *Curr. Opin. Biotechnol.*, 2017, **46**, 27–33.
- T. Heuser, E. Weyandt and A. Walther, *Angew. Chem., Int. Ed.*, 2015, **54**(45), 13258–13262.
- E. R. Draper and D. J. Adams, *Chem*, 2017, **3**, 390–410.
- X. Du, J. Zhou, J. Shi and B. Xu, *Chem. Rev.*, 2015, **115**, 13165–13307.
- T. Muraoka, C. Y. Koh, H. Cui and S. I. Stupp, *Angew. Chem., Int. Ed.*, 2009, **48**, 5946–5949.
- S. Chen, R. Costil, F. K. C. Leung and B. L. Feringa, *Angew. Chem., Int. Ed.*, 2021, **60**, 11604–11627.
- T. Kar, S. K. Mandal and P. K. Das, *Chem. – Eur. J.*, 2011, **17**, 14952–14961.
- G. Aykent, C. Zeytun, A. Marion and S. Özçubukçu, *Sci. Rep.*, 2019, **9**, 1–8.
- S. Toledano, R. J. Williams, V. Jayawarna and R. V. Ulijn, *J. Am. Chem. Soc.*, 2006, **128**, 1070–1071.
- V. Nele, C. E. Schutt, J. P. Wojciechowski, W. Kit-Anan, J. J. Douth, J. P. K. Armstrong and M. M. Stevens, *Adv. Mater.*, 2020, **32**, 1905914.
- S. Panja, K. Boháčová, B. Dietrich and D. J. Adams, *Nanoscale*, 2020, **12**, 12840–12848.
- N. Singh, B. Lainer, G. J. M. Formon, S. De Piccoli and T. M. Hermans, *J. Am. Chem. Soc.*, 2020, **142**(9), 4083–4087.
- D. Spitzer, L. L. Rodrigues, D. Straßburger, M. Mezger and P. Besenius, *Angew. Chem., Int. Ed.*, 2017, **56**(48), 15461–15465.
- T. Das, M. Häring, D. Haldar and D. Díaz Díaz, *Biomater. Sci.*, 2018, **6**, 38–59.
- S. Marchesan, A. V. Vargiu and K. E. Styan, *Molecules*, 2015, **20**, 19775–19788.
- L. S. Lin, T. L. Jr, E. E. De Laszlo, Q. Truong, T. Kamenecka and W. K. Hagmann, *Tetrahedron Lett.*, 2000, **41**, 7013–7016.
- B. Rieß and J. Boekhoven, *ChemNanoMat*, 2018, **4**, 710–719.
- M. Tena-Solsona, B. Rieß, R. K. Grötsch, F. C. Löhrer, C. Wanzke, B. Käs Dorf, A. R. Bausch, P. Müller-Buschbaum, O. Lieleg and J. Boekhoven, *Nat. Commun.*, 2017, **8**, 1–8.
- J. L. Y. Chen, S. Maiti, I. Fortunati, C. Ferrante and L. J. Prins, *Chem. – Eur. J.*, 2017, **23**, 11549–11559.
- T. Heuser, E. Weyandt and A. Walther, *Angew. Chem., Int. Ed.*, 2015, **54**, 13258–13262.
- M. Reches and E. Gazit, *Isr. J. Chem.*, 2005, **45**, 363–371.
- X. Yan, P. Zhu and J. Li, Self-assembly and application of diphenylalanine-based nanostructures, *Chem. Soc. Rev.*, 2010, **39**, 1877–1890.
- R. Huang, R. Su, W. Qi, J. Zhao and Z. He, *Nanotechnology*, 2011, **22**, 245609.
- J. Kong and S. Yu, *Acta Biochim. Biophys. Sin.*, 2007, **39**, 549–559.
- F. Tantakitti, J. Boekhoven, X. Wang, R. V. Kazantsev, T. Yu, J. Li, E. Zhuang, R. Zandi, J. H. Ortony, C. J. Newcomb, L. C. Palmer, G. S. Shekhawat, M. O. La Cruz, G. C. Schatz and S. I. Stupp, *Nat. Mater.*, 2016, **15**, 469–476.
- M. M. Smith and D. K. Smith, *Soft Matter*, 2011, **7**, 4856–4860.





II

NANOSCALE PROBING OF THE SUPRAMOLECULAR ASSEMBLY IN A TWO-COMPONENT GEL BY NEAR-FIELD INFRARED SPECTROSCOPY

by

Romain Chevigny, Efstratios D. Sitsanidis, Johanna Schirmer, Eero Hulkko, Pasi
Myllyperkiö, Maija Nissinen, and Mika Pettersson

Chemistry – A European Journal, 2023, e202300155

<https://doi.org/10.1002/chem.202300155>

Link to SI material: [https://chemistry-
europe.onlinelibrary.wiley.com/doi/full/10.1002/chem.202300155](https://chemistry-europe.onlinelibrary.wiley.com/doi/full/10.1002/chem.202300155)

Reproduced with permission by Wiley.

Nanoscale Probing of the Supramolecular Assembly in a Two-Component Gel by Near-Field Infrared Spectroscopy

Romain Chevigny,^[a] Efstratios D. Sitsanidis,^[a] Johanna Schirmer,^[a] Eero Hulkko,^[a, b] Pasi Myllyperkiö,^[a] Maija Nissinen,^{*[a]} and Mika Pettersson^{*[a]}

Abstract: The design of soft biomaterials requires a deep understanding of molecular self-assembly. Here a nanoscale infrared (IR) spectroscopy study of a two-component supramolecular gel is introduced to assess the system's heterogeneity and supramolecular assembly. In contrast to far-field IR spectroscopy, near-field IR spectroscopy revealed differences in the secondary structures of the gelator molecules and non-covalent interactions at three distinct nano-locations of the gel network. A β -sheet arrangement is

dominant in single and parallel fibres with a small proportion of an α -helix present, while the molecular assembly derives from strong hydrogen bonding. However, at the crossing point of two fibres, only the β -sheet motif is observed, with an intense π - π stacking contribution. Near-field nanospectroscopy can become a powerful tool for the nanoscale distinction of non-covalent interactions, while it is expected to advance the existing spectroscopic assessments of supramolecular gels.

Introduction

Fourier transform infrared (FTIR) spectroscopy is widely used to probe the secondary structure of proteins and elucidate their conformations and folding.^[1–5] Supramolecular gels, especially those consisting of amino acids or small peptides, have gained momentum for the development of soft artificial biomaterials to mimic the extracellular matrix (ECM) for biomedical applications.^[6–11] To date, the secondary and higher-order architectures of the gelator molecules are mainly probed by ultraviolet-visible (UV-vis), circular dichroism (CD) and far-field FTIR spectroscopy techniques.^[12–19] However, these techniques solely probe the intermolecular interactions of the gelator molecules and higher-order molecular assemblies within the gel network at the macroscale (i.e. in bulk systems). Indeed, the far-field ATR-FTIR spectra of supramolecular gels contain the average of the vibrational bands of the gel system. At the macroscale, the study of the amide I (1600 to 1700 cm^{-1}) and

amide II (1500 to 1600 cm^{-1}) regions in peptide-based gels gives valuable information on the secondary structure of the gelator molecules and, consequently, their organization in fibrils and fibres, which form the three-dimensional (3D) gel network.^[17–19]

To decipher the molecular/higher-order assemblies and type of interactions in a supramolecular gel system, overcoming the sub-diffraction limit of light and probing at the nanoscale is crucial. Scattering scanning near-field optical microscopy (sSNOM) is an emerging surface spectroscopy technique that has received increasing interest over the past decade.^[20] This method combines the topological study of atomic force microscopy (AFM) with the absorptive properties of infrared (IR) radiation on organic molecules. The IR incident radiation is focused at the apex of the probing tip into a highly concentrated electric near-field, which interacts with the sample. The interferometric recording of the scattered light provides infrared spectra at a spatial resolution approximately equivalent to that of the tip (20 nm).^[21–28] sSNOM has been used for the analysis of polymeric thin film surfaces,^[24,29–35] imaging of cells,^[36–40] viruses^[41,42] and neurons^[43] and the structural elucidation of protein fibrils.^[44–46]

Although the secondary structure of protein fibrils has been successfully studied by sSNOM, in supramolecular gels the self-assembly of the gelator molecules (e.g. secondary structure) and the type of non-covalent intermolecular interactions (e.g. hydrogen bonding and π - π stacking) responsible for self-assembly have not yet been studied at the nanoscale. To address the nanoscale probing of molecular self-assembly and elucidate higher-order architectures, such as inter-fibrillar interactions, we introduce sSNOM studies of a two-component amino acid-based organogel, which has been recently introduced by our group (Figure 1).^[47] We demonstrate that the high sensitivity of nanoFTIR can distinguish the type of secondary structural features among two structurally similar gelator

[a] R. Chevigny, Dr. E. D. Sitsanidis, J. Schirmer, Dr. E. Hulkko, Dr. P. Myllyperkiö, Prof. M. Nissinen, Prof. M. Pettersson
Department of Chemistry, Nanoscience Center
University of Jyväskylä
P.O. Box Jyväskylä, 35, 40014 JYU (Finland)
E-mail: mika.j.pettersson@jyu.fi
maija.nissinen@jyu.fi

[b] Dr. E. Hulkko
Department of Biological and Environmental Sciences
Nanoscience Center
University of Jyväskylä
P.O. Box Jyväskylä, 35, 40014 JYU (Finland)

 Supporting information for this article is available on the WWW under <https://doi.org/10.1002/chem.202300155>

 © 2023 The Authors. Chemistry - A European Journal published by Wiley-VCH GmbH. This is an open access article under the terms of the Creative Commons Attribution License, which permits use, distribution and reproduction in any medium, provided the original work is properly cited.

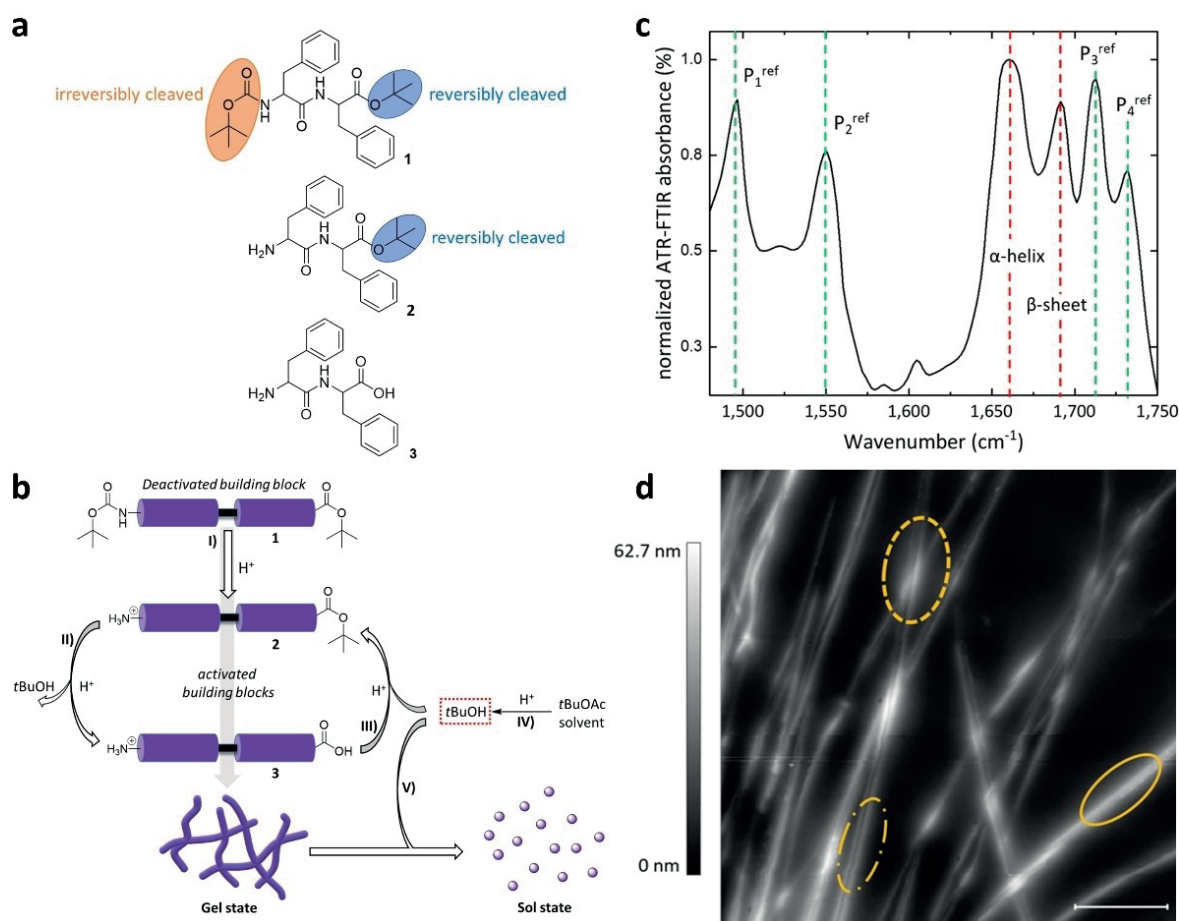


Figure 1. From molecular self-assembly to the macroscopic characteristics of the gel. a) Chemical structures of the protected precursor gelator **1** and activated gelators **2** and **3**. Irreversibly cleaved Boc- group and reversibly cleaved *tert*-butyl groups are highlighted in orange and blue, respectively. b) Schematic depiction of the transient assembly mechanism. I) activation of the precursor gelator **1** into the active molecular building blocks **2** and **3**; II) hydrolysis of **2**; III) esterification of **3**; IV) hydrolysis of *t*BuOAc solvent; V) dissipation of the gel network. c) ATR-FTIR spectrum of the bulk gel system in the range of 1475 to 1750 cm⁻¹ showing the main vibrational bands. Red dashed lines indicate the amide I peaks. The P₁^{ref}, P₂^{ref}, P₃^{ref} and P₄^{ref} peaks (green dashed lines) refer to the vibrations of the functional groups of interest (C=C aromatic stretching, amide II N–H bending, C=O ester stretching and C=O carboxylic acid stretching, respectively). The amide II region shows the N–H bending of the amide group. d) Topography image of the gel's fibres on a gold surface (5 × 5 μm, scale bar 1 μm). Single fibre (plain circle), crossing point of two single fibres (dashed circle) and two parallel fibres (dash-dotted circle).

molecules. We also introduce sSNOM as a valuable tool for investigating the heterogeneity of multicomponent supramolecular gel networks in high spatial resolution and overcoming surface analysis constraints.

Results and Discussion

Model Gel

In our bimolecular gel system, a chemically active solvent (*tert*-butyl acetate, *t*BuOAc) controls a set of coupled reactions that promote the dynamic assembly event.^[47] The two gelator molecules form in situ by the coupled deprotection/protection reactions of the precursor gelator *N*-*tert*-butoxycarbonyl-L-

phenylalanyl-L-phenylalanine-*tert*-butyl ester (Boc-Phe-Phe-O*t*Bu) **1** (Figure 1a). Gelation occurs through the irreversible deprotection of the Boc- group in the presence of the *tert*-butyl group, triggered by the addition of sulphuric acid in the medium, as it forms the activated building block Phe-Phe-O*t*Bu **2** (Figure 1a/b). The *tert*-butyl ester group of **2** is reversibly deprotected to form the free carboxylic acid counterpart Phe-Phe **3**, which reforms to the *tert*-butyl ester **2** through the hydrolysis of the *t*BuOAc solvent. Through hydrolysis, the *t*BuOAc solvent provides the *t*Bu⁺ cation needed to esterify **3** towards **2** and generates the secondary solvent *tert*-butyl alcohol (*t*BuOH), which acts antagonistically against the primary solvent *t*BuOAc. Indeed, unlike the free acid **3**, its *tert*-butylated counterpart **2** is soluble in *t*BuOH, thus leading to the progressive dissolution of the supramolecular network.

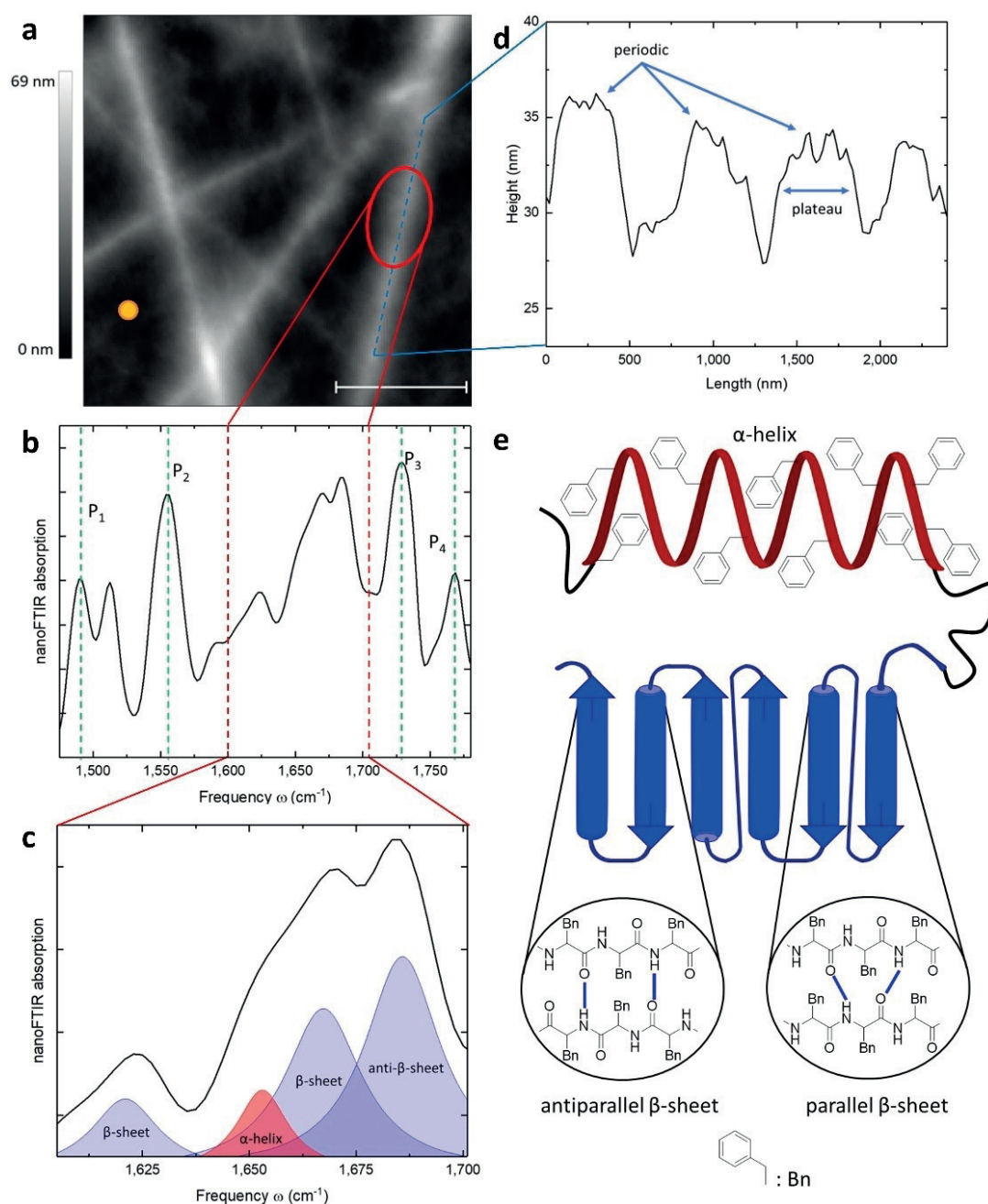


Figure 2. Spectroscopic and structural information of a single fibre. a) Topography image of the formed fibres on a gold surface ($3 \times 3 \mu\text{m}$, scale bar $1 \mu\text{m}$). The orange spot indicates the location of the recorded reference spectrum for b). b) NanoFTIR spectrum of a single fibre recorded at the position marked by the red circle in a). Average of 10 interferograms, 20 ms integration time. A reference spot was taken on the gold surface. P_1 , P_2 , P_3 and P_4 (green dashed lines) correspond to the vibrational bands of the functional groups of interest (C=C aromatic stretching, N-H amide bending, C=O ester stretching and C=O carboxylic acid stretching, respectively). c) NanoFTIR expansion spectrum of the amide I area ($1600\text{--}1700 \text{ cm}^{-1}$) indicated by the red dashed lines in b). Experimental spectrum (black curve) and fitting function for each individual peak. Blue fits refer to β -sheet secondary structures and red fit to an α -helix. d) The height profile of the cross-section taken at the position marked by the blue dashed line in a). The obtained features (periodicity and plateau of height) indicate both β -sheet and α -helical structures.^[52] e) Schematic representation of the secondary structures adopted by the single fibres.

The hydrolysis/esterification cycles between compounds **2** and **3** control the formation of the supramolecular network.

Interestingly, for this dynamic system to initiate the gelation process, both building blocks **2** and **3** are required (Figure S1).

Therefore, the supramolecular network consists of two structurally similar entities differing only at their C-terminus (free carboxylic acid and *tert*-butyl ester), which are intimately linked to one another since neither can support gelation individually.

The far-field ATR-FTIR spectrum of the bulk organogel (Figure 1c and Figure S2) shows the characteristic vibrational bands at 1691 cm⁻¹ and 1660 cm⁻¹, which correspond to β -sheet and α -helical secondary structures, respectively.^[2,4,5] In general, for diphenylalanine-based (Phe-Phe) supramolecular gels, mainly a β -sheet secondary structure (both parallel and anti-parallel) is reported, relating to the strength of π - π stacking and hydrogen bonding interactions.^[11,47–51] Therefore, in our study, the obtained peaks P₁ (1496 cm⁻¹, C=C aromatic), P₂ (1550 cm⁻¹, N–H amide II), P₃ (1712 cm⁻¹, *tert*-butyl ester of **2**) and P₄ (1732 cm⁻¹, carboxylic acid of **3**)^[2,3] and the amide I region are of primary importance to reveal the heterogeneity in molecular organization and how non-covalent interactions drive the network formation at the nanoscale.

Nanoscale Packing Modes and Interactions in a Single Fibre

The 3D gel network consists of single fibres entangled into wider bundles (Figure 1d).^[47,51] Here, we compare the supramolecular interactions, as observed, in a single fibre, along two parallel fibres and at the crossing point of two fibres by near-field spectroscopy, which is an important tool to identify non-covalent interactions responsible for the molecular assembly at the nanoscale. Indeed, in contrast to far-field ATR-FTIR, it enables the selective recording of the nanoscale IR profile of a distinguished higher-order structure, such as a single fibre. Therefore, we recorded the nanoFTIR spectrum at a specific position along an individual fibre (Figure 2a), which showed the four vibrational bands of interest, as already observed in the bulk material (P₁, P₂, P₃ and P₄ marked by the green dashed lines in Figure 2b). It is reasonable to assume that due to intermolecular interactions, the shifts observed for P₃ and P₄ are insufficient to inverse their positions. Therefore, we assign the lower wavenumber peak to P₃ and the higher wavenumber peak to P₄. A summary of the peak positions is presented in Table 1 (Figure S5a and Table S1), along with the reference positions in the spectra of the synthesized gelators (powder materials, Figure S3 and S4) and the bulk gel, measured by far-field ATR-FTIR. Based on the nanoFTIR data, the lower wavenumbers of the P₁ (C=C aromatic), P₃ (C=O ester) and P₄ (C=O carboxylic acid) bands in the single fibre, compared to the synthesized gelators (powder materials), indicate that both functional groups are involved in the assembly event. The results are in accordance with previously reported data for assemblies of the Phe-Phe motif.^[11,48–51]

Although the type of interactions is similar at the nanoscale (single fibre/nanoFTIR) and bulk gel (macroscale/ATR-FTIR), their strength is different, as the wavenumbers for both carbonyl group signals are significantly higher in the single fibre spectrum. This suggests that along an individual fibre, the hydrogen bonding originating from the C-terminal carbonyl groups of **2** and **3** is weaker compared to the bulk material. This

is due to the averaging of the far-field FTIR, which takes all entities and conformations into account. In contrast, at the nanoscale, only the interactions involved in the formation of a single fibre are collected. The downshift of P₄ is much higher than that of P₃, meaning that the carboxylic acid interacts stronger than the ester group. The reason for this is the steric hindrance caused by the bulky *tert*-butyl group and the stronger hydrogen bonding tendency of free carboxylic acids, confirmed by a previously reported study on carboxylic acid complex formation.^[52]

A more detailed study of the amide I region (Figure 2c) revealed a convoluted band which gave rise to four distinct peaks upon deconvolution. The minima of the second derivative within the region of interest were used to determine the number of the individual bands for subsequent fitting (see more in Supporting Information). The peak at 1652 cm⁻¹ is attributed to an α -helical structure (red fitting curve), while the three peaks at 1627 cm⁻¹, 1669 cm⁻¹ and 1690 cm⁻¹ correspond to parallel and antiparallel β -sheet structures (blue fitting curves).^[4,5] In contrast to previous studies on Phe-Phe-based supramolecular materials where mainly a β -sheet structure is reported,^[11,49,50] here the calculated distribution, as obtained by Gaussian fitting (bandwidth, assuming the same intrinsic intensity), is 10% and 90% for α -helical and β -sheet structures, respectively. This highlights the high spatial resolution of nanoFTIR in assessing the structural differences at the nanoscale, compared to the bulk material far-field ATR-FTIR studies at the macroscale.

In addition to spectroscopy recordings, the height profile measurements have also been used to describe the secondary structure of fibres.^[53] We obtained the height profile of a cross-section taken at the same spot as the nanoFTIR spectrum (Figure 2d). The presence of a plateau of height indicates an α -helix, whereas periodic features reveal β -sheet structures. There is some difference in observed height between this measurement and the literature^[53] but it can be explained by the difference in the structure of the reported gelators. Thus, the height pattern provides information on the secondary structure. Both secondary structures are present in the 3D gel network, while the orientation of the side chains dictates whether the molecular arrangement of the gelators is parallel or antiparallel in the β -sheet motif (Figure 2e).

Nanoscale Packing Modes and Interactions of Two Parallel Fibres in Contact

The molecular arrangement giving rise to a single 1D fibre originates from π - π stacking and hydrogen bonding. For higher-order organizations, however, the strength of the interactions and the type of functional groups involved are affected by the spatial orientation and/or entanglement of the 1D fibres within the supramolecular network. For instance, probing the contact point of two parallel fibres along their longitudinal axes (Figure 3a) reveals differences in the peak intensity and position compared to the IR profile of a single fibre. The 3D topography depiction (Figure 3b) of the two-fibre

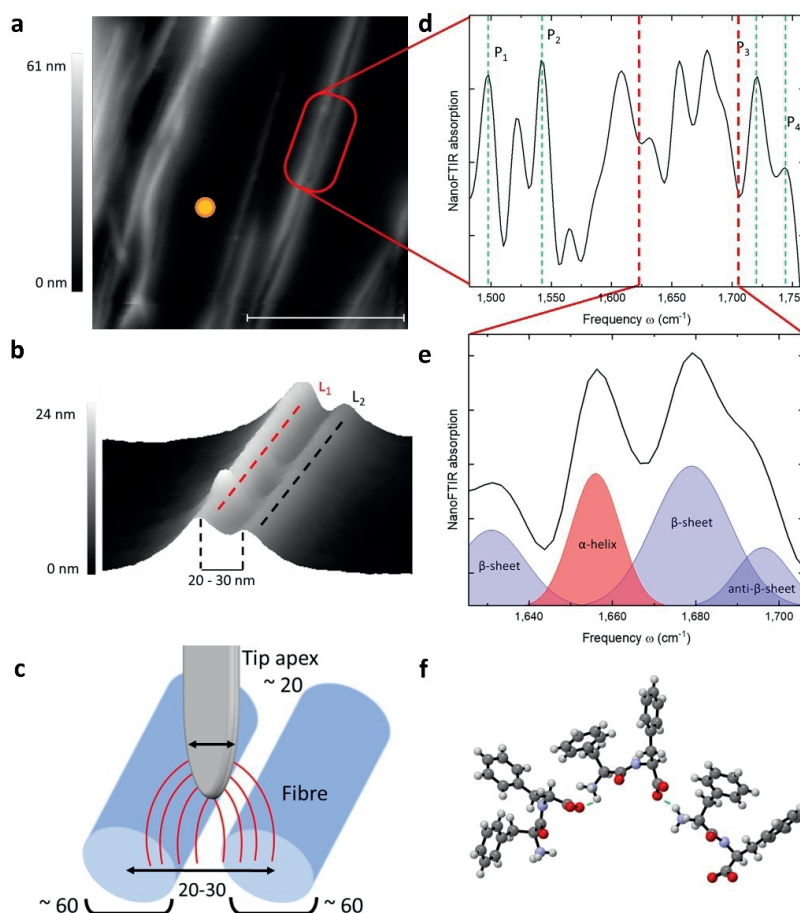


Figure 3. Supramolecular arrangement along two parallel fibres. a) Topography image of two parallel fibres on a gold surface ($2 \times 2 \mu\text{m}$, scale bar $1 \mu\text{m}$). The orange spot indicates the location of the recorded reference spectrum for d). b) 3D magnification of the red rectangle in a), showing two parallel fibres. Vertical dashed lines show the distance between the height maxima. The red (L_1) and black (L_2) dashed lines refer to the cross-section height profile measurement in Figure S6. c) Schematic depiction of the near-field measurement. The probed volume includes the contact point of the two parallel fibres. Numerical values are in nanometres. d) NanoFTIR spectrum of the parallel fibres recorded at the position marked by the red rectangle in a). Average of 10 interferograms, 40 ms integration time. A reference spot was taken on the gold surface. P_1 , P_2 , P_3 and P_4 (green dashed lines) correspond to the vibrational bands of the functional groups of interest (C=C aromatic stretching, N-H amide bending, C=O ester stretching and C=O carboxylic acid stretching, respectively). e) NanoFTIR spectral expansion of the amide I area ($1600\text{--}1700 \text{ cm}^{-1}$) indicated by the red dashed lines in d). Experimental spectrum (black curve) and fitting function for each individual peak. Blue fits refer to β -sheet and the red fit to an α -helical structure. f) Schematic depiction of the hydrogen bonding interactions in the molecular arrangement of two adjacent fibres in contact.^[55]

system depicts the location of the nanoFTIR measurement. The height of the individual fibres is between 20–30 nm as well as the distance between the height maxima of the cross-section. These values correspond to tubular structures with a diameter of 20–30 nm in contact with each other. The lateral dimension is much larger in the image ($\sim 60 \text{ nm}$ for each individual fibre) presumably due to the tip convolution effect arising from the AFM probing tip. The recorded image is, therefore, a convolution of the actual object and the finite size tip.^[54] As the near-field, generated by the oscillation of the tip on the surface, probes at a spatial resolution of $\sim 20 \text{ nm}$, the recording of the nanoFTIR spectrum covers both fibres and their contact point, allowing us to study the spectral differences compared to a single fibre (Figure 3d). The four bands of interest (P_1 , P_2 , P_3 and

P_4 , marked by the green dashed lines) are summarized in Table 1 (see also Figure S5b). The peak corresponding to the aromatic moieties (P_1) is not shifted compared to the ATR-FTIR profile of the gelator molecules **2** and **3** (powder materials). This suggests that the phenyl rings are not involved in stacking interactions along the parallel fibres. However, a small shift of the amide II peak (P_2) is observed, whereas the carbonyl groups P_3 and P_4 show a higher downshift. The results suggest that hydrogen bonding is stronger when two fibres are connected at their longitudinal axes than in a single fibre. As for single fibre, the terminal carbonyl groups (carboxylic acid and ester) show a different shift depending on their steric hindrance and bulkiness.

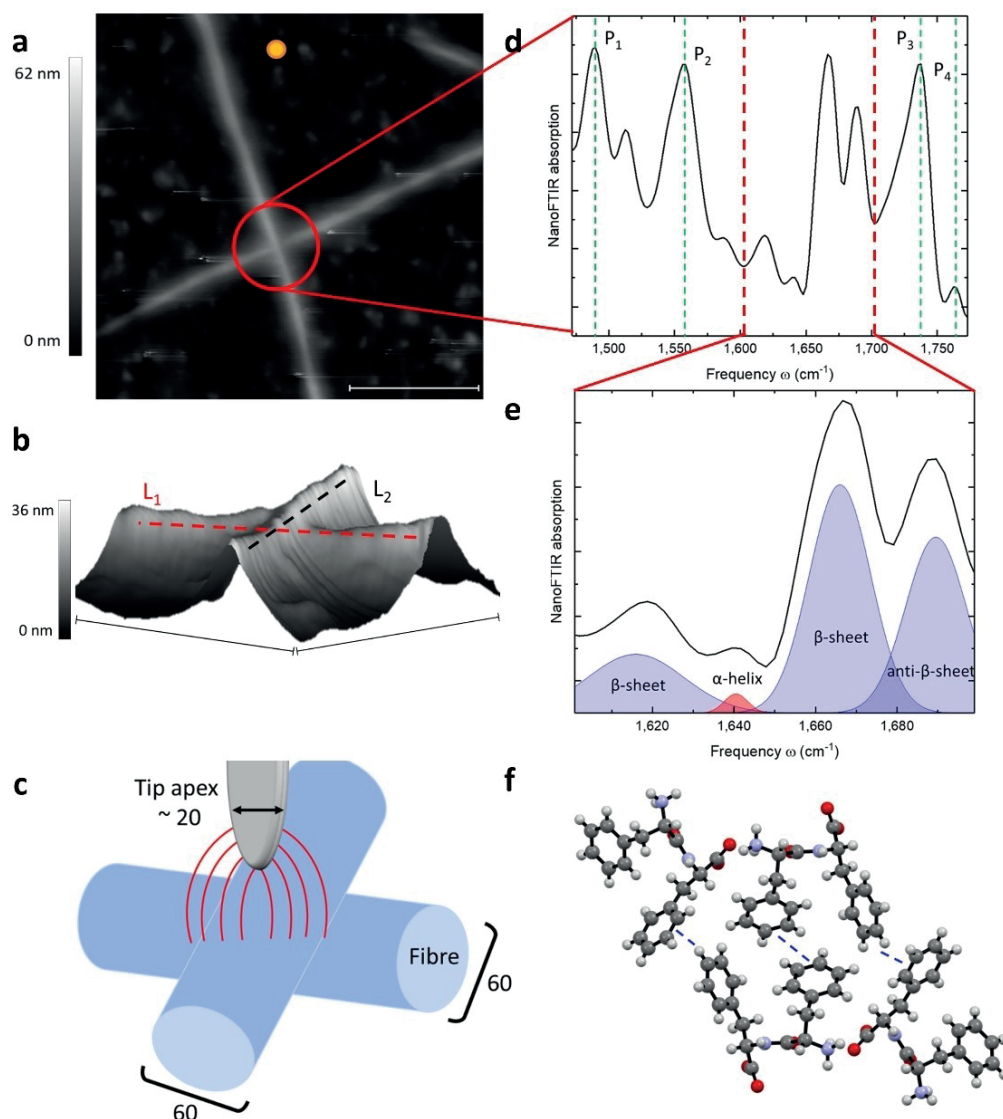


Figure 4. Secondary structure difference at the crossing point of two fibres. a) Topography image of two crossing fibres on a gold surface ($3 \times 3 \mu\text{m}$, scale bar $1 \mu\text{m}$). The orange spot indicates the location of the recorded reference spectrum for (d). b) 3D magnification of the red circle in a), showing the crossing point of two fibres (scale bar 800 nm). Dashed lines L_1 (red) and L_2 (black) refer to the cross-section height profile measurement in Figure S7. c) Schematic depiction of the near-field measurement. Numerical values are in nanometres. d) NanoFTIR spectrum of the crossing point of two fibres (obtained from the position marked by the red circle in a). Average of 10 interferograms, 20 ms integration time. A reference spot was taken on a gold surface. P_1 , P_2 , P_3 and P_4 (green dashed lines) correspond to the vibrational bands of the functional groups of interest (C=C aromatic stretching, N-H amide bending, C=O ester stretching and C=O carboxylic acid stretching, respectively). e) NanoFTIR spectral expansion of the amide I area ($1600\text{--}1700 \text{ cm}^{-1}$) indicated by the red dashed lines in (d). Experimental spectrum (black curve) and fitting function for each individual peak. Blue fits refer to β -sheet and the red fit to an α -helix secondary structure. f) Schematic depiction of the hydrogen bonding and π - π stacking interactions in the molecular arrangement of the two adjacent fibres in perpendicular contact.^[55]

The deconvolution of the amide I region reveals four bands (Figure 3e) with equivalent positions to the single fibre IR profile (1653 cm^{-1} corresponding to an α -helical structure (red fitting curve) and the peaks 1626 cm^{-1} , 1679 cm^{-1} and 1691 cm^{-1} corresponding to parallel and antiparallel β -sheet arrangements (blue fitting curves)). The calculated composition by Gaussian fitting (20% and 80% for α -helix and β -sheet,

respectively) is also qualitatively similar to the single fibre nanoFTIR measurements. Therefore, although the strength of the supramolecular interactions differs with the spatial location of the fibres, the secondary structures are not affected.

A cross-section of each fibre (L_1 (red) and L_2 (black) lines, Figure 3b) was also used to assess the secondary structure. The corresponding height profile (Figure S6) shows the character-

mainly by hydrogen bonding, mainly originating from the carboxylic acid group, since its shift is higher than that of the bulky ester group. In both configurations, the secondary structure is constant, with a significant contribution of β -sheet and a small proportion of α -helix. However, there is a tremendous change at the crossing point of two fibres, where a preference towards π - π stacking with a weaker contribution of hydrogen bonding is observed. The secondary structure is dominated by β -sheet with a negligible proportion of α -helix. Our findings are consistent with the previously reported results on similar supramolecular gels studied as bulk materials by far-field IR and other spectroscopic methods.^[11,48,49,51] However, nanoFTIR spectroscopy gives a deeper insight into the heterogeneity of supramolecular systems and increases our understanding of the molecular assembly modes in relation to the features of the supramolecular network at the nanoscale.

The sSNOM, therefore, proved to be a sensitive and reliable technique to study soft supramolecular materials, as it enables the direct spectroscopic assessment of the molecular building block arrangement while overcoming surface analysis constraints.^[57] Thus, this technique has the potential to become a routine spectroscopic assessment tool and expand the range of techniques to study soft supramolecular gels.

Authors contributions

R.C.: Conceptualization, Investigation, Formal Analysis, Validation, Writing - original draft, review & editing. **E.D.S.:** Conceptualization, Investigation, Writing - review & editing. **J.S.:** Investigation, Writing - review & editing. **E.H.:** Investigation, Resources, Writing - review & editing. **P.M.:** Investigation, Resources. **M.N.:** Supervision. **M.P.:** Supervision, Funding acquisition.

Acknowledgements

The authors would like to acknowledge the Jane and Aatos Erkkö foundation for supporting the current work.

Conflict of Interest

The authors declare no conflict of interest.

Data Availability Statement

The data that support the findings of this study are available from the corresponding author upon reasonable request.

Keywords: IR spectroscopy · near-field · secondary structure · self-assembly · transient gel

[1] S. Cai, B. R. Singh, *Biophys. Chem.* **1999**, *80*, 7–20.

- [2] A. Barth, *Prog. Biophys. Mol. Biol.* **2000**, *74*, 141–173.
 [3] A. Barth, C. Zscherp, *Q. Rev. Biophys.* **2002**, *35*, 369–430.
 [4] A. Barth, *Biochim. Biophys. Acta Bioenerg.* **2007**, *1767*, 1073–1101.
 [5] J. Kong, S. Yu, *Acta Biochim. Biophys. Sin.* **2007**, *39*, 549–559.
 [6] J. D. Tang, C. Mura, K. J. Lampe, *J. Am. Chem. Soc.* **2019**, *141*, 4886–4899.
 [7] W. K. Restu, Y. Nishida, S. Yamamoto, J. Ishii, T. Maruyama, *Langmuir* **2018**, *34*, 8065–8074.
 [8] J. Fraczyk, W. Lipinski, A. Chaberska, J. Wasko, K. Rozniakowski, Z. J. Kaminski, M. Bogun, Z. Draczyński, E. Menaszek, E. Stodolak-Zych, M. Kaminska, B. Kolesinska, *Molecules* **2018**, *23*, 1–19.
 [9] E. González-Díaz, S. Varghese, *Gels* **2016**, *2*, 20.
 [10] G. Fichman, E. Gazit, *Acta Biomater.* **2014**, *10*, 1671–1682.
 [11] X. Yan, P. Zhu, J. Li, *Chem. Soc. Rev.* **2010**, *39*, 1877–1890.
 [12] L. J. White, C. Wark, L. Croucher, E. R. Draper, J. R. Hiscock, *Chem. Commun.* **2020**, *56*, 9557–9560.
 [13] E. D. Sitsanidis, C. C. Piras, B. D. Alexander, G. Siligardi, T. Jávorfí, A. J. Hall, A. A. Edwards, *Chirality* **2018**, *30*, 708–718.
 [14] Z. Shen, Y. Jiang, T. Wang, M. Liu, *J. Am. Chem. Soc.* **2015**, *137*, 16109–16115.
 [15] J. T. van Herpt, M. C. A. Stuart, W. R. Browne, B. L. Feringa, *Chem. Eur. J.* **2014**, *20*, 3077–3083.
 [16] J. Shi, Y. Gao, Z. Yang, B. Xu, *Beilstein J. Org. Chem.* **2011**, *7*, 167–172.
 [17] E. Parisi, A. M. Garcia, D. Marson, P. Posocco, S. Marchesan, *Gels* **2019**, *5*, 5.
 [18] L. Chen, K. Morris, A. Laybourn, D. Elias, M. R. Hicks, A. Rodger, L. Serpell, D. J. Adams, *Langmuir* **2010**, *26*, 5232–5242.
 [19] E. R. Draper, D. J. Adams, *Chem. Soc. Rev.* **2018**, *47*, 3395–3405.
 [20] X. Chen, D. Hu, R. Mescall, G. You, D. N. Basov, Q. Dai, M. Liu, *Adv. Mater.* **2019**, *31*, 1804774.
 [21] S. Mastel, A. A. Govyadinov, T. V. A. G. De Oliveira, I. Amenabar, R. Hillenbrand, *Appl. Phys. Lett.* **2015**, *106*, 1–6.
 [22] F. Huth, A. Govyadinov, S. Amarie, W. Nuansing, F. Keilmann, R. Hillenbrand, *Nano Lett.* **2012**, *12*, 3973–3978.
 [23] L. Mester, A. A. Govyadinov, R. Hillenbrand, *Nat. Photonics* **2022**, *11*, 377–390.
 [24] J. Kim, W. Lee, H. Kim, D. Y. Ryu, H. Ahn, B. Chae, *Spectrochim. Acta A. Mol. Biomol. Spectrosc.* **2022**, *274*, 121095.
 [25] I. Amenabar, S. Poly, M. Goikoetxea, W. Nuansing, P. Lasch, R. Hillenbrand, *Nat. Commun.* **2017**, *8*.
 [26] C. Westermeier, A. Cernescu, S. Amarie, C. Liewald, F. Keilmann, B. Nickel, *Nat. Commun.* **2014**, *5*, 1–6.
 [27] R. Krutokhvostov, A. A. Govyadinov, J. M. Stiegler, F. Huth, A. Chuvilin, P. S. Carney, R. Hillenbrand, *Opt. Express* **2012**, *20*, 593.
 [28] T. Taubner, R. Hillenbrand, F. Keilmann, *Appl. Phys. Lett.* **2004**, *85*, 5064–5066.
 [29] T. E. Tesema, R. McFarland-Porter, E. Zerai, J. Grey, T. G. Habteyes, *J. Phys. Chem. C* **2022**, *126*, 7764–7772.
 [30] N. Mrkyvkova, A. Cernescu, Z. Futera, A. Nebojsa, A. Dubroka, M. Sojkova, M. Hulman, E. Majkova, M. Jergel, P. Siffalovic, F. Schreiber, *J. Phys. Chem. C* **2021**, *125*, 9229–9235.
 [31] A. M. Siddiquee, A. Hour, K. A. Messalea, J. Lin, T. Daeneke, B. Abbey, A. Mechler, S. Kou, *J. Phys. Chem. Lett.* **2020**, *11*, 9476–9484.
 [32] S. Berweger, D. M. Nguyen, E. A. Muller, H. A. Bechtel, T. T. Perkins, M. B. Raschke, *J. Am. Chem. Soc.* **2013**, *135*, 18292–18295.
 [33] M. Meyns, S. Primpke, G. Gerds, *Anal. Methods* **2019**, *11*, 5195–5202.
 [34] L. Mester, A. A. Govyadinov, S. Chen, M. Goikoetxea, R. Hillenbrand, *Nat. Commun.* **2020**, *11*, 1–10.
 [35] M. Goikoetxea, I. Amenabar, S. Chimenti, M. Paulis, J. R. Leiza, R. Hillenbrand, *Macromolecules* **2021**, *54*, 995–1005.
 [36] S. Bhagia, J. Đurković, R. Lagaña, M. Kardošová, F. Kačík, A. Cernescu, P. Schäfer, C. G. Yoo, A. J. Ragauskas, *ACS Sustainable Chem. Eng.* **2022**, *10*, 3016–3026.
 [37] V. M. R. Zancajo, T. Lindtner, M. Eisele, A. J. Huber, R. Elbaum, J. Kneipp, *Anal. Chem.* **2020**, *92*, 13694–13701.
 [38] K. Kanevche, D. J. Burr, D. J. Nürnberg, P. K. Hass, A. Elsaesser, J. Heberle, *Commun. Biol.* **2021**, *4*, 1–8.
 [39] K. J. Kaltenecker, T. Götz, E. Bau, F. Keilmann, *Sci. Rep.* **2021**, *11*, 1–12.
 [40] H. Amrania, L. Drummond, R. C. Coombes, S. Shousha, L. Woodley-Barker, K. Weir, W. Hart, I. Carter, C. C. Phillips, *Faraday Discuss.* **2016**, *187*, 539–553.
 [41] S. Gamage, M. Howard, H. Makita, B. Cross, G. Hastings, M. Luo, Y. Abate, *PLoS One* **2018**, *13*, 1–12.
 [42] M. Brehm, T. Taubner, R. Hillenbrand, F. Keilmann, *Nano Lett.* **2006**, *6*, 1307–1310.

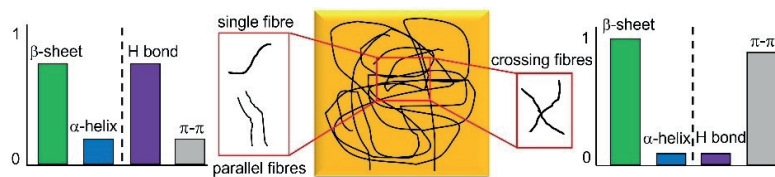
- [43] R. O. Freitas, A. Cernescu, A. Engdahl, A. Paulus, J. E. Levandoski, I. Martinsson, E. Hebisch, C. Sandt, G. K. Gouras, C. N. Prinz, T. Deierborg, F. Borondics, O. Klementieva, *Cells* **2021**, *10*, 1–15.
- [44] I. Amenabar, S. Poly, W. Nuansing, E. H. Hubrich, A. A. Govyadinov, F. Huth, R. Krutokhvostov, L. Zhang, M. Knez, J. Heberle, A. M. Bittner, R. Hillenbrand, *Nat. Commun.* **2013**, *4*, 10.1038/ncomms3890.
- [45] M. Paulite, Z. Fakhraai, I. T. S. Li, N. Gunari, A. E. Tanur, G. C. Walker, *J. Am. Chem. Soc.* **2011**, *133*, 7376–7383.
- [46] M. Dendisová, A. Jenišťová, A. Parchaňská-Kokaislová, P. Matějka, V. Prokopec, M. Švecová, *Anal. Chim. Acta* **2018**, *1031*, 1–14.
- [47] R. Chevigny, J. Schirmer, C. C. Piras, A. Johansson, E. Kalenius, D. K. Smith, M. Pettersson, E. D. Sitsanidis, M. Nissinen, *Chem. Commun.* **2021**, *57*, 10375–10378.
- [48] R. Huang, R. Su, W. Qi, J. Zhao, Z. He, *Nanotechnology* **2011**, *22*, 245609.
- [49] X. Yan, Y. Cui, Q. He, K. Wang, J. Li, *Chem. Mater.* **2008**, *20*, 1522–1526.
- [50] M. Reches, E. Gazit, *Isr. J. Chem.* **2005**, *45*, 363–371.
- [51] S. Marchesan, A. v. Vargiu, K. E. Styan, *Molecules* **2015**, *20*, 19775–19788.
- [52] K. B. Beć, Y. Futami, M. J. Wójcik, T. Nakajima, Y. Ozaki, *J. Phys. Chem. A* **2016**, *120*, 6170–6183.
- [53] R. Xing, C. Yuan, S. Li, J. Song, J. Li, X. Yan, *Angew. Chem. Int. Ed.* **2018**, *57*, 1537–1542; *Angew. Chem.* **2018**, *130*, 1553–1558.
- [54] J. Canet-Ferrer, E. Coronado, A. Forment-Aliaga, E. Pinilla-Cienfuegos, *Nanotechnology* **2014**, *25*, 395703.
- [55] C. H. Görbitz, *Chem. Eur. J.* **2001**, *7*, 5153–5159.
- [56] L. L. E. Mears, E. R. Draper, A. M. Castilla, H. Su, Z. B. Dietrich, M. C. Nolan, G. N. Smith, J. Douth, S. Rogers, R. Akhtar, H. Cui, D. J. Adams, *Biomacromolecules* **2017**, *18*, 3531–3540.
- [57] J. Schirmer, R. Chevigny, A. Emelianov, E. Hulkko, A. Johansson, P. Myllyperkiö, E. D. Sitsanidis, M. Nissinen, M. Pettersson *Phys. Chem. Chem. Phys.* **2023**, *25*, 8725–8733.

Manuscript received: January 17, 2023

Accepted manuscript online: March 15, 2023

Version of record online: ■■■

RESEARCH ARTICLE



Understanding the nanoscale interactions: The determination of the secondary structure of supramolecular gels usually refers to the macroscopic material. It is shown that the

secondary structure and non-covalent interactions driving the self-assembly vary at the nanoscale depending on the configuration of the fibrous network.

R. Chevigny, Dr. E. D. Sitsanidis, J. Schirmer, Dr. E. Hulkko, Dr. P. Myllyperkiö, Prof. M. Nissinen*, Prof. M. Pettersson*

1 – 10

Nanoscale Probing of the Supramolecular Assembly in a Two-Component Gel by Near-Field Infrared Spectroscopy





III

SOLVENT-INDUCED TRANSIENT SELF-ASSEMBLY OF PEPTIDE GELS: GELATOR-SOLVENT REACTIONS AND MATERIAL PROPERTIES CORRELATION

by

Romain Chevigny, Henna Rahkola, Efstratios D. Sitsanidis, Elsa Korhonen, Jennifer
R. Hiscock, Mika Pettersson, and Maija Nissinen

Chemistry of Materials, 2024, 36, 407-416

<https://doi.org/10.1021/acs.chemmater.3c02327>

Link to SI material: <https://pubs.acs.org/doi/10.1021/acs.chemmater.3c02327>

Reproduced with permission by American Chemical Society.

Solvent-Induced Transient Self-Assembly of Peptide Gels: Gelator–Solvent Reactions and Material Properties Correlation

Romain Chevigny, Henna Rahkola, Efstratios D. Sitsanidis, Elsa Korhonen, Jennifer R. Hiscock, Mika Pettersson, and Maija Nissinen*



Cite This: *Chem. Mater.* 2024, 36, 407–416



Read Online

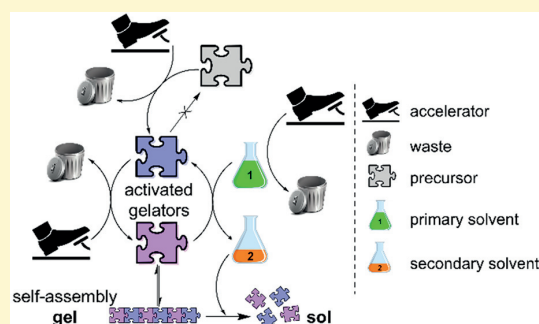
ACCESS |

Metrics & More

Article Recommendations

Supporting Information

ABSTRACT: Herein, we introduce a new methodology for designing transient organogels that offers tunability of the mechanical properties simply by matching the protective groups of the precursor to that of the solvent. We developed solvent-induced transient materials in which the solvent chemically participates in a set of reactions and actively supports the assembly event. The activation of a single precursor by an acid (accelerator) yields the formation of two distinct gelators and induces gelation. The interconversion cycle is supplied by the secondary solvent (originating from hydrolysis of the primary solvent by the accelerator), which then progressively solubilizes the gel network. We show that this gelation method offers a direct correlation between the mechanical and transient properties by modifying the chemical structure of the precursors and the presence of an accelerator in the system. Such a method paves the way for the design of self-abolishing and mechanically tunable materials for targeted purposes. The biocompatibility and versatility of amino acid-based gelators can offer a wide range of biomaterials for applications requiring a controllable and definite lifetime such as drug delivery platforms exhibiting a burst release or self-abolishing cell culture substrates.



INTRODUCTION

Biological supramolecular assemblies, which exist out of equilibrium, are under the constant exchange of energy and matter with their environment to sustain the transient state,^{1–3} in contrast to in-equilibrium biological assemblies. These systems often exhibit interesting properties, such as a triggerable response to external stimuli and self-healing.^{4,5} In contrast to biological assemblies, analogous artificial counterparts form under thermodynamic equilibrium, i.e., the intermolecular interactions, structure, and inner environment are kept stable when no external stimuli/disturbance is applied. In an effort to mimic naturally occurring systems and the unique properties of out-of-equilibrium systems, transient supramolecular materials have gained momentum in the past decades.^{4,6} Transient materials have been envisioned to be used as temporary delivery devices, such as drug delivery platforms^{7–9} and self-abolishing materials.⁴ Therefore, transient organogels can enrich the pool of materials with tunable properties such as finite and controllable release.

Dissipative (or dynamic) self-assembly (DSA) is an extensively studied representative of transient assembly mode, which relies on a reaction cycle,^{10–12} such as that exemplified in Scheme 1. Consumption of energy (i.e., fuel) by a gelator precursor forms the activated building blocks (activation reaction), which subsequently self-assemble.^{13–15} The transient assembled structure exhibits a limited lifetime

governed by depletion of the fuel. Energy dissipation reverses the process, regenerating the non-assembling gelator precursor (deactivation reaction) and inducing the collapse of the network (disassembly). Thus, transient assemblies occur when the rate of energy consumption is higher than that of energy dissipation. Among DSA systems, several types of fuel have been previously reported, including chemical, light, and electrical fueling.^{16–18} Chemically fueled DSA systems intrinsically produce chemical waste during the DSA reaction cycle, that is, side products after activation and/or deactivation reactions, which can be problematic in some applications. Light-fueled DSA systems, which do not release chemical waste into the system, were developed to overcome this problem.¹⁶

Recently, our group introduced the solvent as a new type of chemical agent inducing a transient assembly¹⁹ inspired by DSA. In both dissipative and non-dissipative self-assembly, solvents are encapsulated in the gel network and do not affect the assembly event via chemical reactions. Our “solvent-induced” supramolecular gel (Scheme 1) is a rare case in which

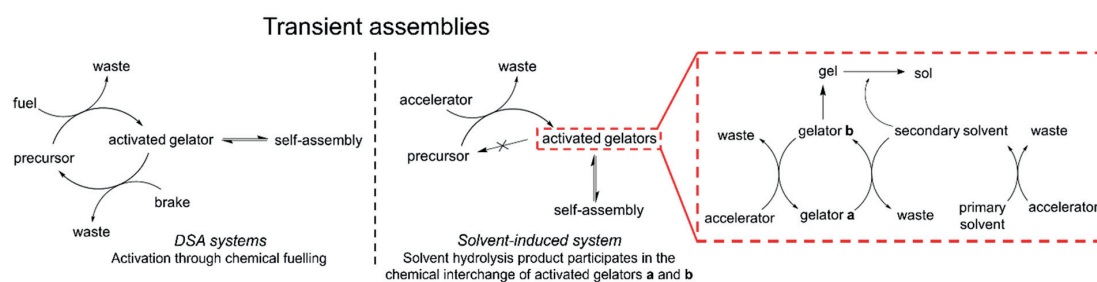
Received: September 12, 2023

Revised: November 21, 2023

Accepted: November 29, 2023

Published: December 15, 2023



Scheme 1. Schematic Description of DSA and Solvent-Induced Self-Assembly Systems^a

^aThe inset represents the set of reactions leading to self-assembly and gel-to-sol transition.

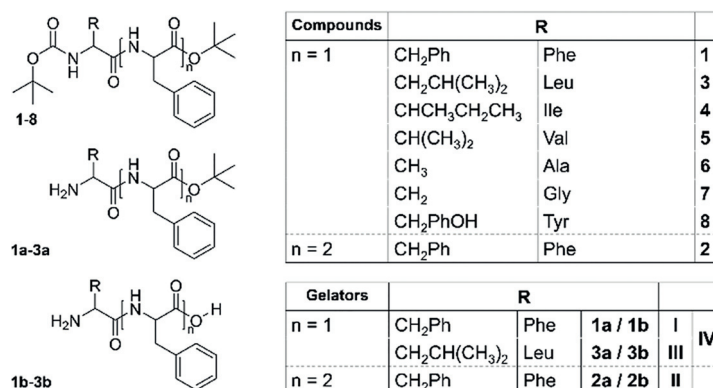


Figure 1. General structures of potential precursors 1–8 (upper table), monoprotected gelators 1a–3a, and deprotected gelators 1b–3b (lower table) as well as the corresponding gel systems I–IV.

the primary solvent, *tert*-butyl acetate (*t*BuOAc), actively controls a set of reactions promoting self-assembly. In contrast to typical DSA, the deprotection of the gelator precursor by an acid accelerator (activation reaction) gives rise to two distinct gelators. The *N*-Boc protective group is irreversibly deprotected, while the *t*Bu ester group at the *C*-terminus is reversibly deprotected. Both gelators interconvert through a cycle of hydrolysis–esterification reactions supplied by the secondary solvent *tert*-butyl alcohol (*t*BuOH), a hydrolysis product of the primary solvent, reintroducing the *tert*-butyl group in the cycle. A key requirement for the proposed mechanism is that the primary solvent and the precursor gelator should have the same protective group, *t*Bu ester, in our case. Interestingly, one of the gelators is soluble in *t*BuOH. Therefore, progressive dissolution of the network is observed over time. This new class of solvent-induced self-assembly is not to be defined as DSA. The transient assembly is induced by two acid-accelerated processes: the primary solvent hydrolysis generating the secondary solvent and the gelators' interconversion. The transient nature of the system relies on the dual role adopted by the solvent, most importantly, the competing kinetics of the secondary solvent formation and the formation/dissolution of the gelators, dictating the assembly/disassembly.

Herein, we deepen and further optimize the solvent-induced transient assembly concept and prove its application to a set of phenylalanine-based peptide precursors bearing the same protective group (*t*Bu) as that of the solvent. We report the transient assembly mechanism and assess the effect of the gelators' chemical structure on the corresponding materials'

properties from the molecular to macroscopic length scale by varying the number of aromatic units (Figure 1). In addition, we decipher the assembly mode and the transitivity character of a multicomponent gel compared to its respective single-component gels. We show that the materials' intrinsic and transitivity properties are tunable, depending on the gelation conditions and gelator structure, thus paving the way toward controllable materials.

EXPERIMENTAL SECTION

Materials. All chemicals were used as supplied without any further purification, unless stated otherwise. (*S*)-Phenylalanine *tert*-butyl ester HCl (Phe-*Ob*Tu) and *N*-(*tert*-butoxycarbonyl)-*L*-tyrosine (Boc-Tyr) were purchased from Carbosynth. *N*-(*tert*-Butoxycarbonyl)-*L*-phenylalanine (Boc-Phe), *N*-(*tert*-butoxycarbonyl)-*L*-valine (Boc-Val), and *N*-(*tert*-butoxycarbonyl)-alanine OH (Boc-Ala) were purchased from TCI. *N*-(*tert*-Butoxycarbonyl)-leucine OH (Boc-Leu), *N*-(*tert*-butoxycarbonyl)-isoleucine OH (Boc-Ile), and *N*-(*tert*-butoxycarbonyl)-glycine OH (Boc-Gly) were purchased from Sigma-Aldrich. 2-(1*H*-Benzotriazole-1-yl)-1,1,3,3-tetramethylammonium tetrafluoroborate (TBTU) and sodium hydrogen carbonate (NaHCO₃) were purchased from Novabiochem and VWR Chemicals, respectively. *tert*-Butyl acetate (*t*BuOAc) was purchased from TCI and sulfuric acid from Fluka.

Methods. NMR Spectroscopy. The spectra of the synthesized compounds and xerogels were recorded on Bruker Advance III HD 300 and 500 MHz spectrometers in *d*₆-DSMO and CDCl₃ solvents. Chemical shifts (δ) are given in parts per million, and the coupling constant (*J*) is given in Hz. The spectra were referenced to the solvent signal (2.5 and 7.26 ppm in ¹H NMR and 39.52 and 77.16 ppm in ¹³C NMR for *d*₆-DSMO and CDCl₃, respectively). ¹³C NMR spectra were

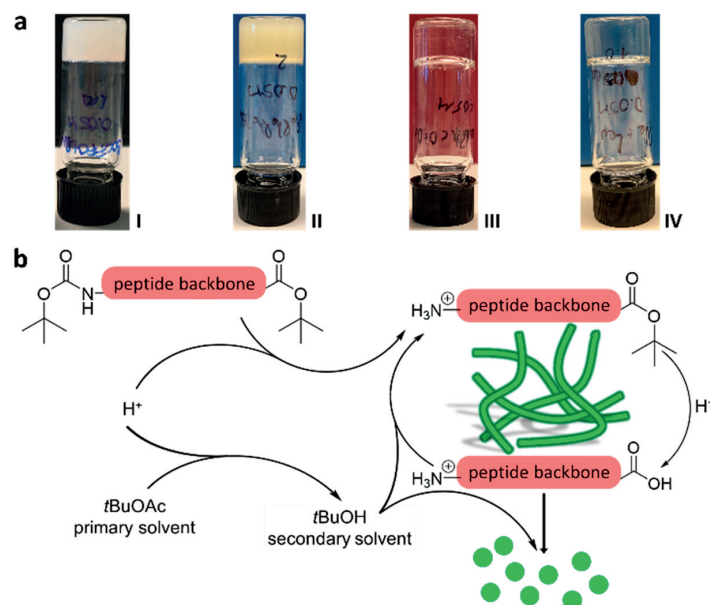


Figure 2. (a) Vial inversion test confirming the lack of flow and thus acting as supporting evidence of material formation for gel systems I, II, III, and IV. Gel IV is the multicomponent gel formed by precursors 1 and 3 with a 1:1 molar ratio. (b) Schematic depiction of the solvent-induced transient assembly.

recorded with a broadband ¹H decoupling. Xerogels were obtained from fresh organogels dried in open air at room temperature (overnight).

FTIR Spectroscopy. The spectra of the synthesized compounds and xerogels were recorded on a Bruker Tensor 27 FT-IR in attenuated total reflectance (ATR) mode. Spectral width: 400–4000 cm⁻¹; number of scans: 124; resolution: 4 cm⁻¹. All spectra were baseline corrected. Xerogels were prepared as mentioned above in the **NMR Spectroscopy** section.

UV–Vis Spectroscopy. The UV–vis spectra of synthesized compounds in ACN and gels were recorded on a PerkinElmer Lambda 850 UV–vis spectrometer (spectral range: 200–500 nm; step: 1 nm; integration time: 0.2 s; slit width: 2 nm). The samples were measured in a 1 mm path length quartz cuvette at room temperature. Gel samples were prepared *in situ* in the quartz cuvettes one day before the measurements.

Rheology. Rheology measurements were performed on an Anton Paar MCR 302 modular compact rheometer with an upper geometry cylinder (cylinder-relative ST10-4V-8.8/97.5). Gel samples (1.0 mL) were prepared in glass vials (Fisherbrand Type III soda lime glass, 14 mm inner diameter) and allowed to rest for one day before measurements for gelation to occur. Frequency sweep measurements were performed within the linear viscoelastic region (LVR) as obtained by amplitude sweep measurements. All measurements were taken in triplicate at room temperature.

SEM Imaging. Microscopy images were obtained on a Zeiss EVO-50XVP microscope. Diluted gels (×10), with the organic solvent used for gelation, were pipetted (1 μL) onto carbon films (400 mesh copper grids) obtained from Agar Scientific and freeze-dried for 1 h before imaging.

RESULTS AND DISCUSSION

Transient Assembly at the Molecular Level. Phenylalanine-derived peptide precursors 1–8 (Figure 1) bearing a phenylalanine unit and varying the second unit by using hydrophobic side-chained amino acids were synthesized (see the **Supporting Information**, Section 1, for synthesis details).

Under identical gelation conditions (*t*BuOAc solvent, 50 mM, 1 equiv of sulfuric acid), four self-supporting gels (SSG) were obtained (Figure 2a). Interestingly, no SSG formed from the precursors bearing tyrosine or an aliphatic side chain shorter than leucine. Although the gelation ability of specific molecules under certain conditions is not fully understood, common trends and hypotheses can be drawn. The presence of phenylalanine (Phe), tyrosine (Tyr), and leucine (Leu) motifs has been reported to play an important role in the self-assembly event. Because of the hydrophobicity, the π – π stacking tendency of Phe and Tyr, and the additional hydrogen-bonding donor site of Tyr, these aromatic amino acids are often present in amino acid-based gelators. Similarly, Leu is widely reported as an efficient amino acid for gelation due to its mobile aliphatic side chain.^{20–22} In our case, the length of the side chain and the electric charge affect the gelation process by electrostatic repulsion and/or steric hindrance²³ which is in line with the existing literature.

The only precursors yielding SSGs (Figure 2a) contain either only phenylalanine or phenylalanine and leucine motifs (Boc-Phe-Phe-*Ot*Bu 1 (gel I), Boc-Phe-Phe-Phe-*Ot*Bu 2 (gel II), and Boc-Leu-Phe-*Ot*Bu 3 (gel III); Figure 1). In addition, the multicomponent gel (gel IV), consisting of precursors 1 and 3 with a 1:1 ratio, was prepared to study whether the mode of assembly is self-sorting (two distinct fibrous networks of each gelator individually) or co-assembly (a single fibrous network consisting of both gelators).²⁴ The comparison of precursors 1, 2, and 3 also gives insight into the effect of the number of aromatic units on the gelation ability and gel properties.

For all systems (I, II, III, and IV), SSGs could be obtained at a concentration down to 25 mM (Tables S2–S5). The phase-transition temperatures (Table S1) show an increase proportional to the number of aromatic units, suggesting that the network stiffens by increasing the aromatic character of the

precursors. Importantly, under similar gelation conditions (50 mM, 1.0 equiv of accelerator), each gel system exhibits a transient character with a different lifetime. Gel I is stable for 4–6 days and gel III for 20–22 days, while multicomponent gel IV collapses after 10 days, showing a lifetime approximately in between that of its individual components. For gel II, the gel-to-sol transition is observed after 8 days.

To assess whether precursors 2 and 3 follow the same transient assembly mechanism as for 1 (Figure 2b), nuclear magnetic resonance (NMR) studies were performed on the xerogels (dried gels) of each system a day after gelation (Figure 3). Gel I shows two amide signals at 8.83 and 8.89 ppm

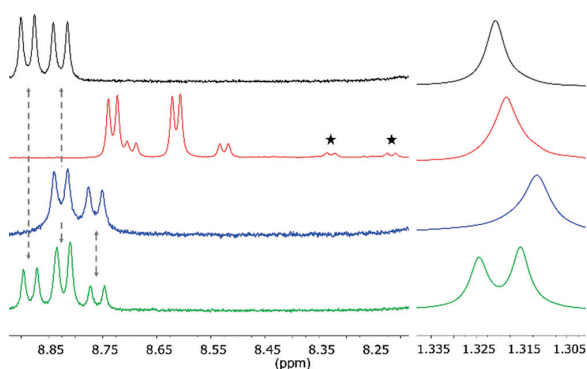


Figure 3. ^1H NMR (300 MHz, d_6 -DMSO) spectra of the dried gel systems I (black), II (red), III (blue), and IV (green) using 1.0 equiv of accelerator. Peaks belonging to the rotamer are marked by a star.

corresponding to gelators 1a and 1b and a singlet at 1.32 ppm attributed to the *t*Bu ester group of 1a (Figure 3, black).¹⁹ Consequently, for gel III (Figure 3, blue), an identical trend is observed with the formation of 3a and 3b. As precursor 2 contains an additional amino acid unit compared to 1 and 3, two amide signals are expected per gelator present in gel II (Figure 3, red). The peaks marked with an asterisk correspond to a rotamer of 2a observed in d_6 -DMSO (Figure S5). Increasing temperature provides additional energy lifting the rotational restriction of the single bond. Therefore, ^1H NMR spectra recorded at 30, 70, and 90 °C show the coalescence of the rotamer peaks (Figure S6). Additionally, the presence of the rotamer was confirmed by recording the spectrum in a different solvent, here, CDCl_3 , in which no additional signals were observed (Figure S3). HR-MS also confirmed the presence of a single molecule.

At the amide region, the spectrum of multicomponent gel IV (Figure 3, green) is the superimposition of its individual component's gel systems (Figure 3, black and blue). As precursors 1 and 3 are present, four gelator molecules are observed in the gel state. Indeed, three amide signals (including the overlapping signal at 8.83 ppm corresponding to two amide groups) and two *t*Bu ester signals are seen. The results are supported by HR-MS measurements confirming four distinct gelators 1a, 1b, 3a, and 3b. In all gels' NMR spectra, a broad peak at around 3–6 ppm corresponds to *t*BuOH, as supported by the control experiment of induced hydrolysis of *t*BuOAc (Figure S26). In addition, NMR spectra were measured on the xerogels of each system at half of their respective lifetimes. All systems follow an identical trend; that is, the expected gelators are present in the corresponding gels, although in a different ratio (Figures S35, S41, and S47).

These results suggest that throughout the lifetime of the gels, the chemical interchange carries on until the materials collapse.

Surprisingly, all systems formed SSGs also when a lower amount of accelerator was used to trigger gelation (0.5 equiv instead of 1.0 equiv). Analysis of the ^1H NMR spectra of these gels revealed that the same reactions occurred, as the spectra are quantitatively similar. However, since half the amount of triggering agent (acid accelerator) was used, the remains of the unreacted precursors were also present in the systems (Figures S29, S33, S39, and S45). Notably, because less accelerator was used to trigger the hydrolysis cycle (required water originates from the aqueous accelerator), a smaller amount of *t*BuOH formed during gelation. Therefore, gels made with 0.5 equiv of accelerator do not show a transient character, unlike those made with 1.0 equiv, and are stable to date. Respectively, the lifetime of the gels formed using 1.5 equiv of accelerator was shorter (Tables S2–S5). A higher concentration of accelerator produces more *t*BuOH in the medium, increasing the collapse rate of the materials from 4–10 days to 1–3 days.

Additionally, the effect of the precursor concentration on the dynamic properties (lifetime) of the materials was investigated (Tables S2–S5). It was found that gels with a high precursor concentration (100 mM) exhibited longer lifetimes than those with a lower concentration (50 mM). This difference is presumably due to the higher amount of gelator to be dissolved and stronger supramolecular interactions maintaining the assembly.

To verify the assumption that the gelation trigger and the subsequent gelation mechanism are related only to the identities of the C-terminus protective group and solvent, an attempt to induce gelation using the same trigger in dichloromethane (DCM) was made with precursors 1 and 3. No gelation was observed; instead, the product precipitated, and the analysis of the ^1H NMR spectrum revealed the complete deprotection of the precursors (Figure S49). In addition, gelation was attempted using Boc-protected molecules 1a–3a as precursors using the same trigger. SSGs formed within the same time, and ^1H NMR spectroscopy verified the presence of both monoprotected and fully deprotected gelators, along with *t*BuOH, in the medium. Therefore, both the solvent and the precursor's C-terminus must bear the same functional group, in this case *t*Bu ester, for the reaction cycle and gelation to occur, regardless of the peptide backbone and/or the presence of a Boc protective group on the N-terminus.

Higher-Order Assembly Determination. To investigate the effect of the gelators' structure on the fibrous network, scanning electron microscopy (SEM) images shown in Figure 4 were recorded on diluted gels. All samples were freeze-dried for 1 h prior to imaging to minimize potential structural rearrangement of the network during drying at room temperature.²⁵ Gel I (Figure 4a) contains densely packed, curved fibers, branching and entangling with one another, which support the high stiffness value measured by rheology (*vide infra*). In contrast, the fibers of gel III (Figure 4c), although similar in shape to gel I, appear less packed, verifying the lower stiffness than gel I. In addition, helical features are present, supporting the peak corresponding to the helical-type assemblies observed in IR measurements (*vide infra*). For multicomponent gel IV (Figure 4d), straightened fibers highly entangled into bigger bundles are observed. The resulting fibrous network exhibits a different shape than its individual components, suggesting that a new structure has formed and

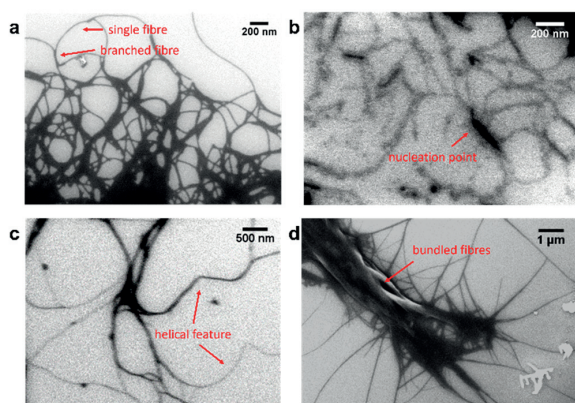


Figure 4. SEM images of (a) gel I, (b) gel II, (c) gel III, and (d) gel IV. The final concentration of all gels was 5 mM after dilution with *t*BuOAc. Samples were pipetted onto a silicon surface and freeze-dried for 1 h prior to imaging.

implying co-assembly of the gelators.²⁶ In gel II, SEM image shows individual curved fibers branching around nucleation points (Figure 4b).

Infrared (IR) spectroscopy was then employed to assess the differences in supramolecular interactions leading to gelation and the structural differences of the gelators. We specifically emphasized on the secondary structures within the amide I region (1700–1600 cm^{-1}). The ATR-FTIR spectra of the xerogels were measured one day after gelation (Figure 5a).

Previously reported diphenylalanine (Phe-Phe)-based supramolecular gels mainly exhibit a β -sheet secondary structure.^{27–31} In our case, for gel I consisting of protected diphenylalanine gelator molecules **1a** and **1b**, a strong band corresponding to a helical-shaped assembly in the higher organization is observed at 1660 cm^{-1} ,³² in addition to the expected β -sheet band at 1691 cm^{-1} (Figure 5a, black).³³ The discrepancy with the literature possibly arises from the presence of two different gelators instead of one. The IR spectrum of gel III (Figure 5a, blue) is qualitatively similar to that of gel I and exhibits both a helical assembly (1655 cm^{-1}) and a β -sheet motif (1682 cm^{-1}). IR spectra recorded on xerogels and non-dried “wet” gels present similar secondary structures with minor shifts (Figures S63b and S65b).

Therefore, the drying conditions do not significantly affect the secondary structures of the gels. Surprisingly, the IR spectrum of gel II only shows a band corresponding to a helical assembly at 1651 cm^{-1} (Figure 5a, red). Although previous literature reports that tripeptide (Phe-Phe-Phe)-based amphiphiles form organogels exhibiting β -sheet structures,³⁴ this is not observed in our case. Similarly to gel I, the discrepancy is possibly due to the presence of a second gelator in the system. Systematic experimental and computational studies report the role and importance of Leu and Phe amino acids in the formation of secondary structures. While Leu is considered a helix former due to the rotational freedom of the γ -branched side chain,³⁵ Phe is reported to favor the formation of β -sheets. However, some reports also highlight the importance of aromatic interactions for helix stabilization³⁶ and that Phe is not necessarily a helix breaker. Additionally, in our systems, the bulky *tert*-butyl group might also disturb the system as a whole and force it to yield divergent arrangements of the building blocks such as helices.

As gel IV is formed by both precursors **1** and **3** with a 1:1 ratio, the IR profile of its xerogel within the amide I region should provide insight into whether self-sorting or co-assembly occurred. If self-sorting occurred, then the mere superimposition of the individual components' spectra would be observed. On the contrary, a different spectrum would be observed in the case of co-assembly. A peak at 1658 cm^{-1} corresponding to a helical-shaped assembly is observed (Figure 5a, green plot), and unlike the gels of its individual components, no β -sheet motif is clearly visible. This suggests that a new structure has formed by the co-assembly of the different gelators.³⁷

In addition to the amide I region, the shifts of specific vibrational bands provide important information on the intermolecular interactions occurring during gelation, i.e., π - π stacking and hydrogen bonding (Table 1). The bands corresponding to the C=C stretching of the phenyl rings appear in the gelators (neat powder) at 1495 cm^{-1} (**1a**), 1496 cm^{-1} (**1b**), 1495 cm^{-1} (**2a**, **2b**), 1497 cm^{-1} (**3a**), and 1496 cm^{-1} (**3b**).³⁸ In the gel phase, these bands shift toward shorter wavenumbers to 1493 cm^{-1} (gel I), 1494 cm^{-1} (gel II), and 1495 cm^{-1} (gel III and IV), which suggests the π - π stacking of the phenyl rings. Although the small shifts of the C=C bands are of the same magnitude as the resolution limit of the instrument, their presence still indicates the involvement of

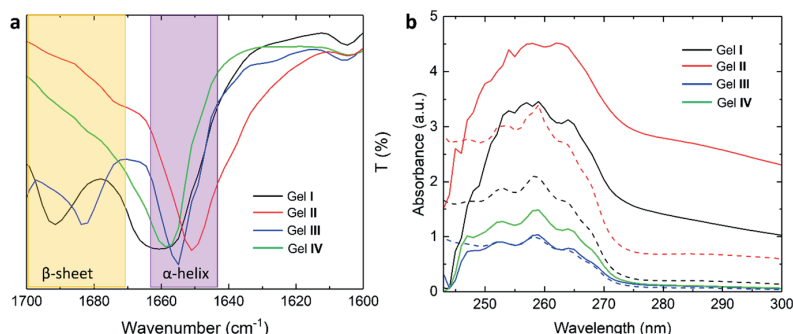


Figure 5. (a) IR spectra of gels I–IV showing the amide I region (1600–1700 cm^{-1}). (b) UV-vis absorption spectra. Dashed curves correspond to the spectra of precursors **1** (black), **2** (red), and **3** (blue) in solution and solid curves to their corresponding gels I, II, III, and IV (green). All measurements were performed on gels one day after gelation. For all samples, in solution and gel state, the concentration was 50 mM. The optical path length was 1 mm.

Table 1. Phenyl Ring C=C Stretching and N-Terminal N-H Stretching Wavenumber Peaks (cm^{-1}) of the Synthesized Gelators (Neat Powders) and Gel Samples

gel system	C=C stretching phenyl rings			N-H stretching terminal amine		
	gelator a	gelator b	gel	gelator a	gelator b	gel
gel I	1495	1496	1493	3392, 3346, 3288	3249, 3171	3328
gel II	1495	1495	1494	3370, 3266	3375, 3363	3349
gel III	1497	1496	1495	3364, 3319	3392, 3340	3323
gel IV	1495, 1497	1496, 1496	1495	3392, 3364, 3346, 3319, 3288	3392, 3340, 3249, 3171	3320

π - π stacking in intermolecular interactions. Additionally, the bands corresponding to the terminal amine are merged and downshifted (gel I: 3328 cm^{-1} ; gel II: 3349 cm^{-1} ; gel III: 3323 cm^{-1} ; gel IV: 3320 cm^{-1}), suggesting hydrogen bonding.

Complementarily to IR, UV-vis spectroscopy provides insights into the molecular packing of the gelators and has been extensively used to elucidate the interactions leading to self-assembly.³⁹ More specifically, information about the π - π stacking of the phenylalanine moiety can be obtained, such as the type of aggregates (H or J), by comparison of the band shift between the spectrum of monomers in solution (interaction free) and the spectrum of the gel (aggregated monomers).⁴⁰ The absorption spectra of the gelators for each system were obtained at the same concentration as those of the gels (50 mM) in acetonitrile to enhance solubility (Figure 5b, dashed curves). Solvatochromism (the shift of the absorption maxima depending on the solvent)⁴¹ and the concentration effect were verified by recording the UV spectra in *t*BuOAc at 50 and 5 mM concentrations.

However, no significant shifts were observed in either case (Figure S50). The center of the absorption band (λ_{max}) at 258 nm for precursors 1–3 corresponds to the $\pi \rightarrow \pi^*$ transition of the phenyl rings. As seen in Figure 5b, the λ_{max} is slightly red-shifted upon gelation to 259 nm for gels I and III and 260 nm for gel II (plain curves). Because of the weakly absorbing

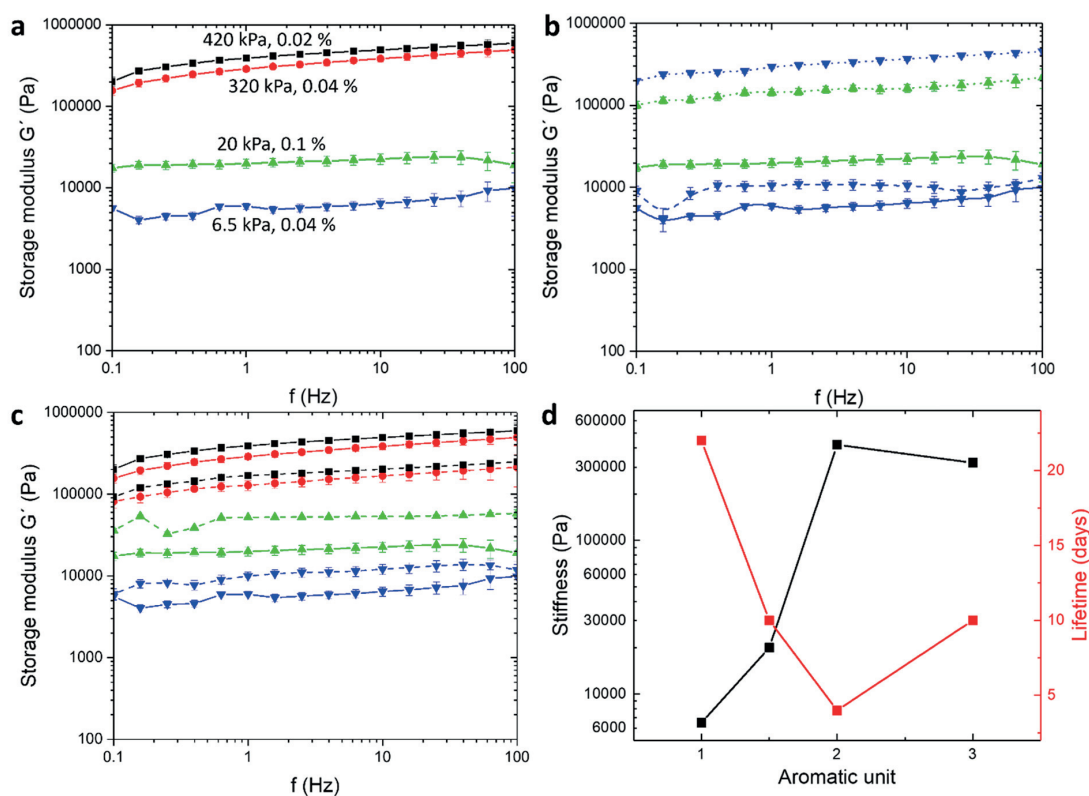


Figure 6. Rheological studies of the gels. (a) Frequency sweep measurements, under a constant shear strain γ (%) of gel I (black, $\gamma = 0.02\%$), gel II (red, $\gamma = 0.04\%$), gel III (blue, $\gamma = 0.04\%$), and gel IV (green, $\gamma = 0.1\%$). The concentration of the gel specimens was 50 mM. (b) Frequency sweep measurements of gel systems III (blue curves) and IV (green curves) at 25 mM (dashes), 50 mM (solid), and 100 mM (dots). Gelation was triggered with 1.0 equiv of H_2SO_4 . (c) Frequency sweep measurements of gel I (black), II (red), III (blue), and IV (green) triggered by 1.0 equiv (solid) and 0.5 equiv (dashes) of H_2SO_4 . All gels were diluted to a concentration of 50 mM. (d) Plot of the elastic moduli (black) against the lifetime (red) of the gels as a function of the number of aromatic units in the precursor. Data markers refer to numerical values from experiments. The point at 1.5 aromatic units corresponds to the average amount of aromatic rings in the system per mole of precursor in gel IV, where the ratio between 1 and 3 is 1:1. Error bars are calculated by standard deviation. Details of the experimental conditions and amplitude sweep measurements are given in the Experimental Section.

character of the phenylalanine residues, compared to, for example, naphthalene and anthracene, the observed shifts are minor (1–2 nm).⁴² However, these results still suggest the π system overlapping in J-aggregate. Additionally, the loss of fine vibronic structure in the spectra of gel I and II is attributed to charge transfer over molecular aggregation.^{43–45} In our case, in contrast to most of the gel aggregation studies reported,^{43,46,47} we observed an absorption intensity increase over gelation, even after normalization due to scattering. This behavior could be explained by the aggregation-induced enhanced emission also related to the absorption profile.^{45,48–50} The red-edge tails observed for gels I and II most probably arise from the scattered light from the aggregates (opaque gels). No broadening is observed for gels III and IV containing just one phenylalanine unit due to its weak $\pi \rightarrow \pi^*$ transition. These results correlate with the rheological profile of the gels; the weaker the π - π interactions, the softer the gels. Interestingly, the intensity of the band of gel IV is observed between those of its individual component's gels. Red-shifts of the weaker, longer wavelength $n \rightarrow \pi^*$ transitions corresponding to the C=O carbonyl and N-H amide groups,⁵¹ respectively, are observed to be significant as the precursors' aromaticity increases ($3 < 1 < 2$). This suggests hydrogen-bonding-type interactions from these groups, consistent with the literature.^{28,52–54}

Macroscopic Properties Assessment. Rheology experiments were performed on the gel systems to assess the correlation between the gelators' structures and the materials' mechanical properties. A material exhibiting a greater storage modulus G' than the loss modulus G'' upon shear strain is considered "solid". At the point this inverts, the material is considered "liquid".^{55,56} For all gel systems, the measured elastic modulus (or storage modulus), G' , is greater than the viscous modulus (or loss modulus), G'' , verifying the viscoelastic nature of the gels. For comparison purposes, Figure 6a presents the oscillatory frequency sweep (FS) experiments performed on gel specimens within the linear viscoelastic region (LVR) one day after gelation at a constant concentration of 50 mM and 1.0 equiv of accelerator. The G' of both gels I (black) and II (red) is 420 and 320 kPa (Table 2), respectively, which is in the range of the bladder and gut

of the lung and liver tissue stiffness.^{57,58} Previous studies show that a difference in the number of hydrophobic aliphatic carbons in the side chains of the gelators also affects the stiffness of the corresponding materials. However, this effect is minor (2–10-fold increase of G' depending on the side chain length) to the observed 60-fold increase when adding three carbons and the aromatic character between leucine and phenylalanine.^{59,60} Despite a lower stiffness, gel III exhibits 2-fold more elastic behavior than gel I (Table 2). The elasticity was assessed by comparison of the G'/G'' cross points of the amplitude sweep measurements. A higher elasticity is indicated by the materials' resistance to shear strain, as the cross point is shifted toward higher shear strain ($\gamma\%$) values. Interestingly, the amplitude sweep measurements of gel II exhibit no crossing points between G' and G'' , although the curves seem to merge at the maximum shear strain γ of 100%, indicating that a crossing point would be observed over this value, as reported earlier for highly elastic gels.⁶¹ The additional phenylalanine motif in precursor 2 provides a higher hydrophobicity and more available sites for π - π stacking than that in precursor 1 (two phenylalanine motifs), giving more stability to the molecular aggregation during gelation. Although more intense π - π stacking yields stiffer materials, the G' values are quantitatively similar for gels I and II, while the elasticity is higher for gel II than for gel I. This suggests that the fiber arrangement (microenvironment) has more impact on the material properties than the molecular interactions. In addition, the G' value of 20 kPa for the multicomponent gel IV (green), although quantitatively closer to gel III than gel I, suggests that a new structure has formed, implying co-assembly of the gelators.²⁴

To further investigate the effect of gelation conditions on the stiffness of the materials, we measured the elastic modulus G' at different concentrations of gel III (monocomponent) and gel IV (multicomponent, Figure 6b). An increase in the precursor concentration yields a stiffer material in both cases (approximately 10–40-fold higher G' value), along with a decrease in the elastic behavior (Table 2).

Similar experiments were performed by changing the amount of accelerator (0.5 or 1.0 equiv) to determine whether the precursor concentration of the precursor or that of the accelerator has a more significant effect on the materials' properties. For all four gel systems, although a quantitatively similar G' value was observed (approximately 3-fold, Figure 6c), the elasticity was found to increase by 1.5–2-fold in gels formed with 0.5 equiv of accelerator. Therefore, we suggest that the mechanical properties of the gels are tunable within a wide range of stiffness by modifying the precursor structure, i.e., the number of aromatic rings, concentration, and the amount of accelerator used to trigger gelation.

The phase-transition temperature ($T_{\text{gel-sol}}$) indicates the thermal stability of the different materials. Gel samples (viscoelastic gel behavior initially confirmed by rheological measurements) were gradually heated by 5 °C increments at 10 min intervals. The vial inversion method was used to verify the gel-to-sol (i.e., the complete transition from self-supporting gel to free-flowing solution) and gel-to-sol-to-gel transitions (Supporting Information, Section 2.4), assuming that after thermal breaking the viscoelastic nature of the gels remains identical with that of the gels initially assessed by oscillatory frequency sweep measurements. The observed $T_{\text{gel-sol}}$ was found to be proportional to the number of aromatic units within the gelator structure (gel III: 40 °C; gel I: 45 °C; and

Table 2. Comparison of the Stiffness (G') and Elasticity (G'/G'' Cross Point) Values of Gels I–IV

	concn (M)	G' (kPa)		G'/G'' cross point (%)	
		0.5 equiv	1.0 equiv	0.5 equiv	1.0 equiv
gel I	0.05	180	420	4.2	1.5
gel II	0.05	147	320	no crossing points	
gel III	0.025	n.m. ^a	10	n.m.	6.5
	0.05	11	6.5	9	3
	0.1	n.m.	330	n.m.	2
gel IV	0.05	52	20	4.5	3.5
	0.1	n.m.	155	n.m.	1.2

^aNot measured.

tissue stiffness.^{57,58} These quantitatively similar values suggest that an additional aromatic moiety (in this case, phenylalanine) does not significantly alter the stiffness of the material.

However, for gel III (blue) bearing an aliphatic leucine unit instead of an aromatic phenylalanine unit, the G' value of 6.5 kPa indicates that lower aromaticity of the gelators yields a softer material (approximately 60-fold), which is in the range

gel II: 55 °C at 50 mM) and to the gel concentration (10 °C increase from 25 to 100 mM, Table S1 and Figure S51). These results suggest that the fibrous network and consequently the bulk material stiffen with the increase in the aromatic character of the gelators. However, the observed temperature for gel IV is lower than that of its individual components, in contrast to the rheological data. This behavior may arise from differences between the fibrous network (related to the $T_{\text{gel-sol}}$) and the π - π interactions (related to the gel stiffness).⁴²

Numerical values of the lifetime (Figure 6d, red y-axis) compared to the mechanical properties (Figure 6d, black y-axis) of the gels, when plotted as a function of the number of aromatic units in the precursor structure, highlight a common trend. The evolution of the stiffness is found to be inversely proportionally to that of the lifetime of the materials, that is, stiff materials have a short lifetime. To ensure the reproducibility of the measurements and the reliability of the results, lifetime monitoring and rheological measurements were performed in triplicate. Systematic studies will be beneficial in the future to corroborate these findings for an extended set of data (gelation conditions, precursors, and acid equivalent). This observation can be assessed based on two factors: the gelators' solubility in the secondary solvent, *t*BuOH, and the material's elasticity. Indeed, control experiments showed that gelators 1a, 2a, and 3a are soluble in *t*BuOH, whereas their deprotected counterparts 1b, 2b, and 3b are insoluble. Therefore, with time, the *in situ* formed *t*BuOH will progressively dissolve the monoprotected gelator 1a, 2a, and 3a until the collapse of the material, as verified and described above. Considering this and the identical reaction cycle for all gel systems depicted in Figure 2b, the mechanical properties of the gels are potential reasons for the different lifetimes. As the fibrous network is progressively dissolved by *t*BuOH, a more elastic material remains self-supporting for a longer period of time before collapsing.

CONCLUSION

We developed solvent-induced transient self-assembly for the formation of a transient gel materials. A diprotected precursor molecule forms *in situ* two gelator building blocks (*N*-deprotected/*C*-protected and *N*-/*C*-deprotected) through activation by an accelerator, while the primary solvent chemically participates in the interconversion cycle between the two activated gelators through the generation of the secondary solvent. Additionally, the secondary solvent progressively solubilizes the fibrous network, leading to the collapse of the material over time. The gelation trigger and subsequent mechanism are related only to the precursor's *C*-terminus protective group and the solvent, therefore offering a wide range of potential gelator candidates for the gelation of peptide-based systems. UV-vis spectroscopic data correlate the strength of the intermolecular interactions to the mechanical properties of the materials. Gels exhibiting greater stiffness showed greater absorption intensity increase and loss of vibronic structure, and *vice versa*, which can further be attributed to the prevalence of the π - π stacking interactions. IR spectroscopy, rheology, thermal stability, and lifetime studies highlighted the co-assembly of the gelators in the multicomponent gel IV. Additionally, the lifetimes of the gels are found to be inversely proportional to their mechanical properties. This work provides important insights into the formation of transient peptide-based supramolecular gels. The biocompatibility and versatility of modified amino acid-based

gelators can be exploited, along with gelation in water-based solutions, to serve targeted medical purposes. The hydrolysis/esterification cycles proposed in this work could be used for developing hydrogels with a wide range of mechanical and transient properties, using, for instance, external *tert*-butylated compounds as a supplier of the *t*Bu group to support the out-of-equilibrium self-assembly. The solvent-induced self-assembly can, therefore, provide interesting alternatives for responsive gelation and self-abolishing materials requiring a definite lifetime, such as delivery systems exhibiting a burst release. Alternatively, the self-abolishing character of these materials could be used for designing temporary ink devices. Thorough dynamic studies on the kinetics of gelator and secondary solvent formation, for instance, by high-pressure liquid chromatography¹⁴ would be beneficial to get insights into the in-depth acid-accelerated processes.

ASSOCIATED CONTENT

Supporting Information

The Supporting Information is available free of charge at <https://pubs.acs.org/doi/10.1021/acs.chemmater.3c02327>.

Materials, synthesis and characterization data of precursors and gels, gelation protocol, ¹H and ¹³C NMR, IR, and UV-vis spectra, rheology amplitude sweep plots, $T_{\text{gel-sol}}$, gelation concentration screening (PDF)

AUTHOR INFORMATION

Corresponding Author

Maija Nissinen – Department of Chemistry, Nanoscience Center, University of Jyväskylä, FI-40014 Jyväskylä, Finland; orcid.org/0000-0001-7560-4632; Email: maija.nissinen@jyu.fi

Authors

Romain Chevigny – Department of Chemistry, Nanoscience Center, University of Jyväskylä, FI-40014 Jyväskylä, Finland; orcid.org/0000-0002-5463-9745

Henna Rahkola – Department of Chemistry, Nanoscience Center, University of Jyväskylä, FI-40014 Jyväskylä, Finland; orcid.org/0009-0006-8667-3944

Efstathios D. Sitsanidis – Department of Chemistry, Nanoscience Center, University of Jyväskylä, FI-40014 Jyväskylä, Finland; orcid.org/0000-0001-5727-1336

Elsa Korhonen – Department of Chemistry, Nanoscience Center, University of Jyväskylä, FI-40014 Jyväskylä, Finland; orcid.org/0009-0002-3208-1864

Jennifer R. Hiscock – School of Physical Sciences, University of Kent, Canterbury, Kent CT2 7NH, U.K.; orcid.org/0000-0002-1406-8802

Mika Pettersson – Department of Chemistry, Nanoscience Center, University of Jyväskylä, FI-40014 Jyväskylä, Finland; orcid.org/0000-0002-6880-2283

Complete contact information is available at: <https://pubs.acs.org/doi/10.1021/acs.chemmater.3c02327>

Notes

The authors declare no competing financial interest.

ACKNOWLEDGMENTS

The authors acknowledge the Jane and Aatos Erkkö Foundation for supporting the current work. J.R.H. thanks

the UKRI Future Leaders Fellowship for funding (MR/T020415/1).

REFERENCES

- (1) Singh, N.; Formon, G. J. M.; De Piccoli, S.; Hermans, T. M. Devising Synthetic Reaction Cycles for Dissipative Nonequilibrium Self-Assembly. *Adv. Mater.* **2020**, *32*, 1–6.
- (2) Van Rossum, S. A. P.; Tena-Solsona, M.; Van Esch, J. H.; Eelkema, R.; Boekhoven, J. Dissipative Out-of-Equilibrium Assembly of Man-Made Supramolecular Materials. *Chem. Soc. Rev.* **2017**, *46*, 5519–5535.
- (3) Ragazzon, G.; Prins, L. J. Energy Consumption in Chemical Fuel-Driven Self-Assembly. *Nat. Nanotechnol.* **2018**, *13*, 882–889.
- (4) Rieß, B.; Boekhoven, J. Applications of Dissipative Supramolecular Materials with a Tunable Lifetime. *ChemNanoMat* **2018**, *4*, 710–719.
- (5) Heuser, T.; Weyandt, E.; Walther, A. Biocatalytic Feedback-Driven Temporal Programming of Self-Regulating Peptide Hydrogels. *Angew. Chem., Int. Ed.* **2015**, *54*, 13258–13262.
- (6) Wang, G.; Liu, S. Strategies to Construct a Chemical-Fuel-Driven Self-Assembly. *ChemSystemsChem* **2020**, *2*, No. e1900046.
- (7) Vintiloiu, A.; Leroux, J. C. Organogels and Their Use in Drug Delivery - A Review. *J. Controlled Release* **2008**, *125*, 179–192.
- (8) Hu, B.; Yan, H.; Sun, Y.; Chen, X.; Sun, Y.; Li, S.; Jing, Y.; Li, H. Organogels Based on Amino Acid Derivatives and Their Optimization for Drug Release Using Response Surface Methodology. *Artificial Cells, Nanomed. Biotechnol.* **2020**, *48*, 266–275.
- (9) Esposito, C. L.; Kirilov, P.; Roullin, V. G. Organogels, Promising Drug Delivery Systems: An Update of State-of-the-Art and Recent Applications. *J. Controlled Release* **2018**, *271*, 1–20.
- (10) Boekhoven, J.; Brizard, A. M.; Kowligi, K. N. K.; Koper, G. J. M.; Eelkema, R.; Van Esch, J. H. Dissipative Self-Assembly of a Molecular Gelator by Using a Chemical Fuel. *Angew. Chem., Int. Ed.* **2010**, *49*, 4825–4828.
- (11) De, S.; Klajn, R. Dissipative Self-Assembly Driven by the Consumption of Chemical Fuels. *Adv. Mater.* **2018**, *30*, 1–6.
- (12) Singh, N.; Lainer, B.; Formon, G. J. M.; De Piccoli, S.; Hermans, T. M. Re-Programming Hydrogel Properties Using a Fuel-Driven Reaction Cycle. *J. Am. Chem. Soc.* **2020**, *142*, 4083–4087.
- (13) Kriebisch, B. A. K.; Jussupow, A.; Bergmann, A. M.; Kohler, F.; Dietz, H.; Kaila, V. R. I.; Boekhoven, J. Reciprocal Coupling in Chemically Fueled Assembly: A Reaction Cycle Regulates Self-Assembly and Vice Versa. *J. Am. Chem. Soc.* **2020**, *142*, 20837–20844.
- (14) Schnitter, F.; Bergmann, A. M.; Winkeljann, B.; Rodon Fores, J.; Lieleg, O.; Boekhoven, J. Synthesis and Characterization of Chemically Fueled Supramolecular Materials Driven by Carbodiimide-Based Fuels. *Nat. Protoc.* **2021**, *16*, 3901–3932.
- (15) Boekhoven, J.; Hendriksen, W. E.; Koper, G. J. M.; Eelkema, R.; Van Esch, J. H. Transient Assembly of Active Materials Fueled by a Chemical Reaction. *Science* **2015**, *349*, 1075–1080.
- (16) Liu, M.; Creemer, C. N.; Reardon, T. J.; Parquette, J. R. Light-Driven Dissipative Self-Assembly of a Peptide Hydrogel. *Chem. Commun.* **2021**, *57*, 13776–13779.
- (17) Deng, J.; Bezold, D.; Jessen, H. J.; Walther, A. Light-Powered, yet Chemically Fueled, Dissipative DNA Systems with Transient Lifecycles. 2019. DOI: [10.26434/chemrxiv.10453769.v1](https://doi.org/10.26434/chemrxiv.10453769.v1).
- (18) Selmani, S.; Schwartz, E.; Mulvey, J. T.; Wei, H.; Grosvirt-Dramen, A.; Gibson, W.; Hochbaum, A. I.; Patterson, J. P.; Ragan, R.; Guan, Z. Electrically Fueled Active Supramolecular Materials. *J. Am. Chem. Soc.* **2022**, *144*, 7844–7851.
- (19) Chevigny, R.; Schirmer, J.; Piras, C. C.; Johansson, A.; Kalenius, E.; Smith, D. K.; Pettersson, M.; Sitsanidis, E. D.; Nissinen, M. Triggering a Transient Organo-Gelation System in a Chemically Active Solvent. *Chem. Commun.* **2021**, *57*, 10375–10378.
- (20) Hamley, I. W. Self-Assembly, Bioactivity, and Nanomaterials Applications of Peptide Conjugates with Bulky Aromatic Terminal Groups. *ACS Appl. Bio Mater.* **2023**, *6*, 384–409.
- (21) Yu, X.; Chen, L.; Zhang, M.; Yi, T. Low-Molecular-Mass Gels Responding to Ultrasound and Mechanical Stress: Towards Self-Healing Materials. *Chem. Soc. Rev.* **2014**, *43*, 5346–5371.
- (22) Maity, M.; Maitra, U. Supramolecular Gels from Conjugates of Bile Acids and Amino Acids and Their Applications. *Eur. J. Org. Chem.* **2017**, *2017*, 1713–1720.
- (23) Tang, J. D.; Mura, C.; Lampe, K. J. Stimuli-Responsive, Pentapeptide, Nanofiber Hydrogel for Tissue Engineering. *J. Am. Chem. Soc.* **2019**, *141*, 4886–4899.
- (24) Draper, E. R.; Adams, D. J. How Should Multicomponent Supramolecular Gels Be Characterised? *Chem. Soc. Rev.* **2018**, *47*, 3395–3405.
- (25) Mears, L. L. E.; Draper, E. R.; Castilla, A. M.; Su, H.; Zhuola; Dietrich, B.; Nolan, M. C.; Smith, G. N.; Douth, J.; Rogers, S.; Akhtar, R.; Cui, H.; Adams, D. J. Drying Affects the Fiber Network in Low Molecular Weight Hydrogels. *Biomacromolecules* **2017**, *18*, 3531–3540.
- (26) Raeburn, J.; Adams, D. J. Multicomponent Low Molecular Weight Gelators. *Chem. Commun.* **2015**, *51*, 5170–5180.
- (27) Chevigny, R.; Sitsanidis, E. D.; Schirmer, J.; Hulkko, E.; Myllyperkiö, P.; Nissinen, M.; Pettersson, M. Nanoscale Probing of the Supramolecular Assembly in a Two-Component Gel by Near-Field Infrared Spectroscopy. *Chem.—Eur. J.* **2023**, *29*, No. e202300155.
- (28) Huang, R.; Su, R.; Qi, W.; Zhao, J.; He, Z. Hierarchical, Interface-Induced Self-Assembly of Diphenylalanine: Formation of Peptide Nanofibers and Microvesicles. *Nanotechnology* **2011**, *22*, No. 245609.
- (29) Yan, X.; Zhu, P.; Li, J. Self-Assembly and Application of Diphenylalanine-Based Nanostructures. *Chem. Soc. Rev.* **2010**, *39*, 1877–1890.
- (30) Marchesan, S.; Vargiu, A. V.; Styan, K. E. The Phe-Phe Motif for Peptide Self-Assembly in Nanomedicine. *Molecules* **2015**, *20*, 19775–19788.
- (31) Yan, X.; Cui, Y.; He, Q.; Wang, K.; Li, J. Organogels Based on Self-Assembly of Diphenylalanine Peptide and Their Application to Immobilize Quantum Dots. *Chem. Mater.* **2008**, *20*, 1522–1526.
- (32) Barth, A. Infrared Spectroscopy of Proteins. *Biochimic. Biophys. Acta Bioenerg.* **2007**, *1767*, 1073–1101.
- (33) Barth, A.; Zscherp, C. What Vibrations Tell Us about Proteins. *Q. Rev. Biophys.* **2002**, *35*, 369–430.
- (34) Ariga, K.; Kikuchi, J. I.; Naito, M.; Yamada, N. FT-IR, TEM, and AFM Studies of Supramolecular Architecture Formed by Tripeptide-Containing Monoalkyl Amphiphiles. *Polym. Adv. Technol.* **2000**, *11*, 856–864.
- (35) Lyu, P. C.; Sherman, J. C.; Chen, A.; Kallenbach, N. R. Alpha-Helix Stabilization by Natural and Unnatural Amino Acids with Alkyl Side Chains. *Proc. Natl. Acad. Sci. U. S. A.* **1991**, *88*, 5317–5320.
- (36) Butterfield, S. M.; Patel, P. R.; Waters, M. L. Contribution of Aromatic Interactions to α -Helix Stability. *J. Am. Chem. Soc.* **2002**, *124*, 9751–9755.
- (37) Abul-Haija, Y. M.; Roy, S.; Frederix, P. W. J. M.; Javid, N.; Jayawarna, V.; Ulijn, R. V. Biocatalytically Triggered Co-Assembly of Two-Component Core/Shell Nanofibers. *Small* **2014**, *10*, 973–979.
- (38) Barth, A. The Infrared Absorption of Amino Acid Side Chains. *Prog. Biophys. Mol. Biol.* **2000**, *74*, 141–173.
- (39) Yu, G.; Yan, X.; Han, C.; Huang, F. Characterization of Supramolecular Gels. *Chem. Soc. Rev.* **2013**, *42*, 6697–6722.
- (40) Hestand, N. J.; Spano, F. C. Expanded Theory of H- and J-Molecular Aggregates: The Effects of Vibronic Coupling and Inter-molecular Charge Transfer. *Chem. Rev.* **2018**, *118*, 7069–7163.
- (41) Mayerhöfer, T. G.; Popp, J. Beyond Beer's Law: Revisiting the Lorentz-Lorenz Equation. *ChemPhysChem* **2020**, *21*, 1218–1223.
- (42) Bairi, P.; Roy, B.; Routh, P.; Sen, K.; Nandi, A. K. Self-Sustaining, Fluorescent and Semi-Conducting Co-Assembled Organogel of Fmoc Protected Phenylalanine with Aromatic Amines. *Soft Matter* **2012**, *8*, 7436–7445.
- (43) Ghosh, S.; Li, X.-Q.; Stepanenko, V.; Würthner, F. Control of H- and J-Type π Stacking by Peripheral Alkyl Chains and Self-Sorting

Phenomena in Perylene Bisimide Homo- and Heteroaggregates. *Chem.—Eur. J.* **2008**, *14*, 11343–11357.

(44) Hisaki, I.; Shigemitsu, H.; Sakamoto, Y.; Hasegawa, Y.; Okajima, Y.; Nakano, K.; Tohnai, N.; Miyata, M. Octadecahydrodibenzo[12]Annulene-Based Organogels: Two Methyl Ester Groups Prevent Crystallization and Promote Gelation. *Angew. Chem., Int. Ed.* **2009**, *48*, 5465–5469.

(45) Pacheco-Liñán, P. J.; Martín, C.; Alonso-Moreno, C.; Juan, A.; Hermida-Merino, D.; Garzón-Ruiz, A.; Albaladejo, J.; Van Der Auweraer, M.; Cohen, B.; Bravo, I. The Role of Water and Influence of Hydrogen Bonding on the Self-Assembly Aggregation Induced Emission of an Anthracene-Guanidine-Derivative. *Chem. Commun.* **2020**, *56*, 4102–4105.

(46) Ishi-i, T.; Murakami, K.; Imai, Y.; Mataka, S. Self-Assembled Fluorescent Hexaazatriphenylenes That Act as a Light-Harvesting Antenna. *J. Org. Chem.* **2006**, *71*, 5752–5760.

(47) Wagner, W.; Wehner, M.; Stepanenko, V.; Ogi, S.; Würthner, F. Living Supramolecular Polymerization of a Perylene Bisimide Dye into Fluorescent J-Aggregates. *Angew. Chem., Int. Ed.* **2017**, *129*, 16224–16228.

(48) Dawn, A.; Shiraki, T.; Haraguchi, S.; Sato, H.; Sada, K.; Shinkai, S. Transcription of Chirality in the Organogel Systems Dictates the Enantiodifferentiating Photodimerization of Substituted Anthracene. *Chem.—Eur. J.* **2010**, *16*, 3676–3689.

(49) Hong, Y.; Lam, J. W. Y.; Tang, B. Z. Aggregation-Induced Emission: Phenomenon, Mechanism and Applications. *Chem. Commun.* **2009**, *29*, 4332–4353.

(50) An, B.-K.; Lee, D.-S.; Lee, J.-S.; Park, Y.-S.; Song, H.-S.; Park, S. Y. Strongly Fluorescent Organogel System Comprising Fibrillar Self-Assembly of a Trifluoromethyl-Based Cyanostilbene Derivative. *J. Am. Chem. Soc.* **2004**, *126*, 10232–10233.

(51) Skrabania, K.; Miasnikova, A.; Bivigou-Koumba, A. M.; Zehm, D.; Laschewsky, A. Examining the UV-Vis Absorption of RAFT Chain Transfer Agents and Their Use for Polymer Analysis. *Polym. Chem.* **2011**, *2*, 2074–2083.

(52) Ravarino, P.; Di Domenico, N.; Barbalinardo, M.; Faccio, D.; Falini, G.; Giuri, D.; Tomasini, C. Fluorine Effect in the Gelation Ability of Low Molecular Weight Gelators. *Gels* **2022**, *8*, 98.

(53) Li, W.; Hu, X.; Chen, J.; Wei, Z.; Song, C.; Huang, R. N-(9-Fluorenylmethoxycarbonyl)-L-Phenylalanine/Nano-Hydroxyapatite Hybrid Supramolecular Hydrogels as Drug Delivery Vehicles with Antibacterial Property and Cytocompatibility. *J. Mater. Sci.: Mater. Med.* **2020**, *31*, 73.

(54) Das, T.; Häring, M.; Haldar, D.; Díaz Díaz, D. Phenylalanine and Derivatives as Versatile Low-Molecular-Weight Gelators: Design, Structure and Tailored Function. *Biomater. Sci.* **2018**, *6*, 38–59.

(55) Aufderhorst-Roberts, A.; Frith, W. J.; Kirkland, M.; Donald, A. M. Micro rheology and Microstructure of Fmoc-Derivative Hydrogels. *Langmuir* **2014**, *30*, 4483–4492.

(56) Arnedo-Sánchez, L.; Nonappa; Bhowmik, S.; Hietala, S.; Puttreddy, R.; Lahtinen, M.; De Cola, L.; Rissanen, K. Rapid Self-Healing and Anion Selectivity in Metallo-supramolecular Gels Assisted by Fluorine-Fluorine Interactions. *Dalton Trans.* **2017**, *46*, 7309–7316.

(57) Guimaraes, C. F.; Gasperini, L.; Marques, A. P.; Reis, R. L. The Stiffness of Living Tissues and Its Implications for Tissue Engineering. *Nat. Rev. Mater.* **2020**, *5*, 351–370.

(58) Handorf, A. M.; Zhou, Y.; Halanski, M. A.; Li, W. J. Tissue Stiffness Dictates Development, Homeostasis, and Disease Progression. *Organogenesis* **2015**, *11*, 1–15.

(59) Azyat, K.; Makeiff, D.; Smith, B.; Wiebe, M.; Launspach, S.; Wagner, A.; Kulka, M.; Godbert, N. The Effect of Branched Alkyl Chain Length on the Properties of Supramolecular Organogels from Mono-N-Alkylated Primary Oxalamides. *Gels* **2023**, *9*, 5.

(60) Komiyama, T.; Harada, Y.; Hase, T.; Mori, S.; Kimura, S.; Yokoya, M.; Yamanaka, M. Effect of Alkyl Chain Length of N-Alkyl-N'-(2-benzylphenyl)Ureas on Gelation. *Chem.—Asian J.* **2021**, *16*, 1750–1755.

(61) Öhrlund, Å. Evaluation of Rheometry Amplitude Sweep Cross-Over Point as an Index of Flexibility for HA Fillers. *J. Cosmetics. Dermatological Sciences and Applications* **2018**, *8*, 47–54.



IV

PROBING THE GELATION SYNERGIES AND ANTI- ESCHERICHIA COLI ACTIVITY OF FMOC- PHENYLALANINE/GRAPHENE OXIDE HYBRID HYDROGEL

by

Efstratios D. Sitsanidis, Lara A. L. Dutra, Johanna Schirmer, Romain Chevigny,
Manu Lahtinen, Andreas Johansson, Carmen C. Piras, David K. Smith, Marja Tiirola,
Mika Pettersson, and Maija Nissinen

ACS Omega, 2023, 8, 10225-10234

<https://doi.org/10.1021/acsomega.2c07700>

Link to SI material: <https://pubs.acs.org/doi/full/10.1021/acsomega.2c07700>

Reproduced with permission by American Chemical Society

Probing the Gelation Synergies and Anti-*Escherichia coli* Activity of Fmoc-Phenylalanine/Graphene Oxide Hybrid Hydrogel

Efstratios D. Sitsanidis, Lara A. L. Dutra, Johanna Schirmer, Romain Chevigny, Manu Lahtinen, Andreas Johansson, Carmen C. Piras, David K. Smith, Marja Tirola, Mika Pettersson, and Maija Nissinen*



Cite This: *ACS Omega* 2023, 8, 10225–10234



Read Online

ACCESS |



Metrics & More

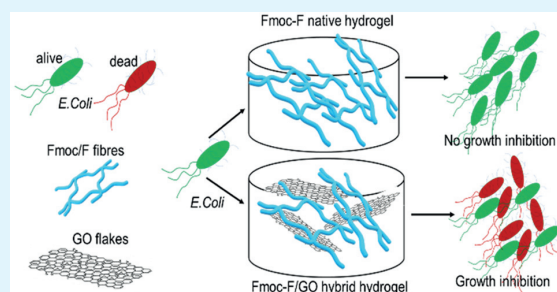


Article Recommendations



Supporting Information

ABSTRACT: The *N*-fluorenyl-9-methoxycarbonyl (Fmoc)-protected amino acids have shown high antimicrobial application potential, among which the phenylalanine derivative (Fmoc-F) is the most well-known representative. However, the activity spectrum of Fmoc-F is restricted to Gram-positive bacteria only. The demand for efficient antimicrobial materials expanded research into graphene and its derivatives, although the reported results are somewhat controversial. Herein, we combined graphene oxide (GO) flakes with Fmoc-F amino acid to form Fmoc-F/GO hybrid hydrogel for the first time. We studied the synergistic effect of each component on gelation and assessed the material's bactericidal activity on Gram-negative *Escherichia coli* (*E. coli*). GO flakes do not affect Fmoc-F self-assembly per se but modulate the elasticity of the gel and speed up its formation. The hybrid hydrogel affects *E. coli* survival, initially causing abrupt bacterial death followed by the recovery of the surviving ones due to the inoculum effect (IE). The combination of graphene with amino acids is a step forward in developing antimicrobial gels due to their easy preparation, chemical modification, graphene functionalization, cost-effectiveness, and physicochemical/biological synergy of each component.



INTRODUCTION

Microbial infections pose a significant threat to human health and are one of the major concerns in public healthcare.¹ Despite the advances in drug development, limitations associated with the treatment of pathogens include antimicrobial resistance (AMR) toward existing medication and the appearance of new diseases.² Currently, new approaches in antimicrobial therapeutics³ and materials are constantly introduced, such as polymers, ceramics, nanoparticles, biomacromolecules, small organic molecules, and hydrogels.^{4–7}

Hydrogels have gained momentum for the treatment and prevention of microbial infections due to their physicochemical and viscoelastic properties, cost-effectiveness, ease of preparation, and manufacturing upscale. In addition, they have high water content and combine low toxicity (high biocompatibility toward mammalian cells) with antimicrobial activity. Their activity can be either inherent or, for example, caused by incorporating antimicrobial agents within the gel matrix, which can increase their spectrum of activity.^{8,9} Recently, several amino acid and peptide-based supramolecular gels have been introduced, of which the *N*-fluorenylmethoxycarbonyl (Fmoc)-protected analogues have shown high application potential.^{10–13}

In particular, the phenylalanine derivative (Fmoc-F) has exhibited antibacterial activity against Gram-positive bacteria, both in the solution and gel state, via a mechanism disrupting the bacterial membrane/wall.^{14,15} Additionally, Fmoc-F inhibits the formation of biofilms and eradicates the already formed ones over surfaces due to its surfactant properties.¹⁶ Despite its efficacy over Gram-positive bacteria, its biocidal effect on Gram-negative bacteria is limited due to its inability to cross the bacterial membrane of Gram-negative microbes. Therefore, to increase the antibacterial spectrum of the amino acid, several Fmoc-F hybrid gels have been fabricated, exploiting the synergistic effect of incorporated antimicrobial agents, for example, aztreonam (AZT) antibiotic,¹⁷ silver ions,¹⁸ berberine chloride,¹⁹ and salicylic acid.²⁰

The research for efficient antimicrobial materials has expanded into carbon nanomaterials, such as graphite (Gt), graphite oxide (GtO), graphene oxide (GO), reduced graphene oxide (rGO), carbon nanotubes (CN), and full-

Received: December 2, 2022

Accepted: February 24, 2023

Published: March 8, 2023



erenes.^{21,22} GO forms stable colloids in water and can be easily chemically modified. Therefore, its antimicrobial activity has been extensively studied against Gram-positive/negative pathogens.^{23,24} Graphene-based materials display antibacterial action as they disrupt the cell membrane and induce oxidative stress by producing reactive oxygen species (ROS). However, the reported results are somewhat controversial since their activity is influenced by several factors, such as their size, morphology, purity, concentration, and type of functionalization.^{25,26}

Since GO flakes have been reported to show antibacterial activity against Gram-negative *Escherichia coli* (*E. coli*),²¹ their incorporation within the Fmoc-F gel network could expand the antibacterial spectrum of the amino acid against *E. coli*.¹⁴ In this study, we combined GO flakes with commercially available Fmoc-F amino acid for the first time to produce Fmoc-F/GO hybrid hydrogel. We investigated the synergistic effect of each component on the gelation process spectroscopically and assessed the macro-/microscopic properties of the hybrid material (Fmoc-F/GO) in relation to the native Fmoc-F hydrogel. In addition, we investigated the antimicrobial activity of the formed gel and its components against Gram-negative *E. coli*.

MATERIALS AND METHODS

Materials. *N*-Fluorenyl-9-methoxycarbonyl-L-phenylalanine (Fmoc-F) was purchased from Sigma-Aldrich, GO water dispersion (0.4 wt %) from Graphenea, and rGO powder (98–99%) from Wholesale Graphene. All reagents were used as supplied.

Preparation of Hydrogels. *Fmoc-F Native Hydrogel.* A suspension of Fmoc-F (2.0 mg/mL) in phosphate buffer solution (PBS, 50 mM, pH 7.4) was sonicated for 2 min and heated at 80 °C for 30 min. The obtained transparent solution was then left to cool down at room temperature for 12 h, giving a self-supporting hydrogel as verified by vial inversion.

Fmoc-F/GO Hybrid Hydrogel. GO flakes were formed by drying GO water dispersion (0.4 wt %) under a vacuum for 2 days. The obtained flakes were suspended in PBS solution (50 mM, pH 7.4) at several concentrations (0.2, 0.5, 0.75, 1.0 mg/mL) by sonication (15 min) before the addition of Fmoc-F (2.0 mg/mL). The resulting Fmoc-F/GO suspension was sonicated (2 min) and heated at 80 °C (30 min). Gelation occurred at room temperature after 12 h and was assessed by the vial inversion method. The GO flakes remained equally distributed through the final gel.

Instrumentation. *Fluorescence Spectroscopy.* Emission spectra were recorded on the Varian Cary Eclipse fluorescence spectrophotometer. Gel samples were formed *in situ* in a quartz cuvette with a path length of 1 cm. The excitation wavelength was 296 nm. Both excitation and emission slit widths were 5 nm.

Fourier Transform Infrared (FT-IR) Spectroscopy. IR spectra were measured on Bruker Tensor 27 FT-IR spectrometer in Attenuated Total Reflection (ATR) mode. (Spectral width: 400–4000 cm⁻¹; absorption mode; step: 2 cm⁻¹; the number of scans: 124). All spectra were baseline corrected.

Raman Spectroscopy. Raman spectra were recorded on Bruker Optics SENTERRA R200-785 Raman microscope (Laser 785 nm). Gels were dried under a vacuum for 2 days and placed on a microscope glass slide before measurement.

Microscopy. Helium ion microscopy (HIM) images were captured on the Zeiss Orion Nanofab microscope and transmission electron microscopy (TEM) images on the JEOL JEM-1400HC microscope. Atomic force microscopy (AFM) imaging was performed on a Bruker Dimension Icon atomic force microscope using PeakForce tapping mode. ScanAsyst-Air probes from Bruker were used during imaging with the peak force set to 2.0 nN. All AFM images were processed with NanoScope Analysis 1.9 software. To prepare xerogel samples for microscopy imaging, carbon films (400 mesh copper grids, Agar Scientific) were dipped into the gels and allowed to dry in the open air overnight.

Rheology. Oscillation rheology was performed on the Malvern Kinexus Pro+ rheometer, fitted with an 8 mm parallel plate upper geometry. All gel samples (1.0 mL volume) were prepared in homemade glass chambers and transferred onto the lower geometry of the instrument as intact gel pellets. Amplitude sweep measurements were performed at an angular frequency of 1.0 Hz, using shear strain ($\gamma\%$) within the range of 0.05–100% at 25 °C. Frequency sweep measurements were performed in triplicate within the linear viscoelastic region (LVR) where the elastic (G') and loss (G'') moduli are independent of the strain amplitude. Each measurement was performed using a shear strain ($\gamma\%$) of 0.25%, at a range of 0.1 to 100 rad/s at 25 °C.

Thermogravimetric Analysis (TGA). Thermogravimetric analysis was performed on PerkinElmer STA 6000 simultaneous thermogravimetric and differential scanning calorimetric analyzer (TG/DSC). Each sample was placed in an open platinum crucible and heated under air atmosphere (flow rate of 40 mL/min) with a heating rate of 10 °C/min at a temperature range of 20–600 °C. The temperature calibration of the analyzer was based on the melting points of indium (156.60 °C) and zinc (419.5 °C). The weight balance was calibrated at room temperature with a standard weight of 50.0 mg. The used sample weights were 6.0–7.0 mg.

Powder X-ray Diffraction (PXRD). Powder X-ray diffraction measurements were performed on a PANalytical X'Pert PRO MPD diffractometer in Bragg–Brentano geometry using Johansson monochromator generated Cu K α 1 radiation ($\lambda = 1.5406$ Å; 45 kV, 40 mA). Each lightly hand-ground powder sample was prepared on a silicon-made “zero-background” inducing holder using petroleum jelly as an adhesive. Diffraction patterns were recorded from a spinning sample by a position-sensitive X'Celerator detector using continuous scanning mode in a 2θ range of 4–70° with a step size of 0.017° and a counting time of 200 s/step. Diffraction data were analyzed using Malvern Panalytical HighScore Plus (v. 4.8).²⁷ The unit cell parameters of neat Fmoc-F powder at RT were determined by the Pawley method²⁸ using the corresponding single crystal structure parameters (CSD database²⁹ entry OGIXOT³⁰) as the basis of least-squares refinement. Variable parameters were as follows: zero-offset, polynomial background, sample displacement, unit cell, and peak profile parameters. Refined unit cell parameters were used for monitoring the structural properties of Fmoc-F and Fmoc-F/GO hybrid xerogels.

Antimicrobial Screening. The antimicrobial activity of Fmoc-F/GO hybrid hydrogel against Gram-negative *E. coli* (strain DSM 882) was assessed by evaluating the bacterial growth/culture density over time (optical density-OD₆₀₀). Two-fold serial dilutions of the Fmoc-F/GO hybrid gel and its corresponding components (Fmoc-F native gel, GO suspen-

sion and PBS) were prepared in Luria–Bertani (LB) broth. Fresh *E. coli* culture, in the exponential growth phase, was used to prepare the bacterial inoculum to a final density of 1.5×10^6 CFU/mL in testing samples. The gel samples, prepared at a range of concentrations (Table 1), were pipetted in a

Table 1. Concentration of Fmoc-F/GO Hybrid Hydrogel Samples for OD₆₀₀ Screening

gel components	D1	D2	D3	D4	D5
Fmoc-F (mg/mL) ^a	1.0	0.5	0.25	0.125	0.0625
GO (μ g/mL) ^a	125	62.5	31.25	15.625	7.8125

^aGiven concentrations of each component of the Fmoc-F/GO hybrid hydrogels prepared by serial dilutions (D1–D5).

honeycomb 96-well plate (200 μ L/well) and incubated in a Bioscreen C spectrophotometer (37 $^{\circ}$ C, continuous shaking with low amplitude and normal speed, OD₆₀₀ readings at 10 min intervals for 24 h). The OD₆₀₀ background values were obtained by subtraction of the negative control values. The OD₆₀₀ background values of the hybrid gel and each component were obtained from samples prepared without bacterial inoculum. The control growth curve for each dilution (with growth medium) was based on the bacterial growth in the presence of the basic growth medium.

Gel samples were prepared based on the given gelation protocol and sterilized under UV light for 1 h. Fluorescence microscopy imaging of the bacteria was performed using a Leica TCS SP8 Falcon microscope. The bacterial cell viability was assessed after 5 h of incubation. *E. coli* were stained by a mixture of SYTO 9 (33.4 μ M working solution) and propidium iodide (PI, 400 μ M working solution) stains. The obtained images were processed by Fiji2 (ImageJ2) software.

RESULTS AND DISCUSSION

Gel Fabrication and Morphological Features. The gelation efficacy of the Fmoc-F/GO hybrid system was assessed by a series of concentration screening trials. The critical gelation concentration (CGC) of the protected amino acid (Fmoc-F) for both gels, native and hybrid, was found to be 2.0 mg/mL (Tables S1, S2). For the hybrid material, the gelation outcome depended only on the amino acid concentration, irrespective of the added amount of GO flakes (Table S2). The gel-to-sol phase transition temperature ($T_{\text{gel-sol}}$) was measured by controlled heating of the gels. The $T_{\text{gel-sol}}$ of the hybrid hydrogel increased only by increasing the amino acid concentration, while the incorporation of GO flakes at different concentrations showed negligible effects (Tables S3, S4). The $T_{\text{gel-sol}}$ study verified the thermoreversible nature (gel-to-sol-to-gel) of the hybrid gel system since all test samples reformed upon cooling within 12 h.

Under the given gelation conditions, the suspension of Fmoc-F/GO yielded a homogeneous self-supporting hydrogel, i.e., no phase separation or precipitation of the GO flakes was observed (Figure 1). However, heating the suspension at a higher temperature and for a longer time (95 $^{\circ}$ C, 1 h) led to the precipitation of GO (Figure S1). When rGO powder was incorporated into the amino acid solution, nonhomogeneous gels formed under the standard gelation conditions (heating at 80 $^{\circ}$ C for 30 min). Indeed, rGO precipitated in all trials at all used concentrations (0.25–1.0 mg/mL, Figure S2). The increased aggregation of GO at a higher temperature may be attributed to various processes such as enhanced collision

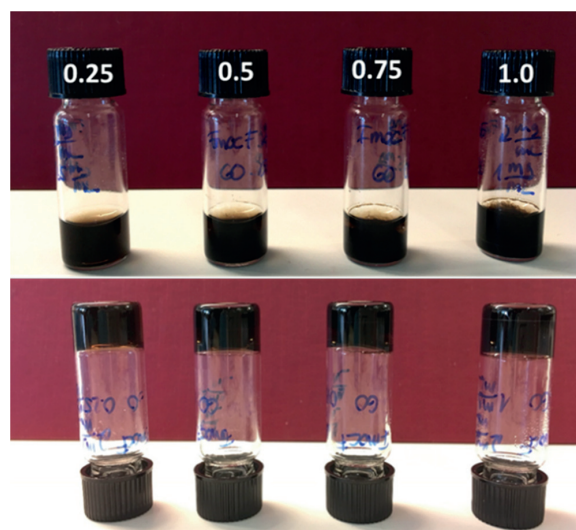


Figure 1. Gelation screening of the Fmoc-F/GO hybrid system at a range of GO concentrations (0.25–1.0 mg/mL). Homogeneous self-supporting gels were formed regardless of the amount of GO. The concentration of Fmoc-F was kept constant (2.0 mg/mL).

frequency, cation dehydration, and reduced electrostatic repulsion, as reported by Gao et al.³¹ in their aggregation kinetics studies of GO in mono- and divalent aqueous solutions.

The morphology of the hybrid gel network was investigated by HIM, TEM, and AFM. The formed Fmoc-F fibers were similar in shape, width, and length among the native and hybrid materials (Figures 2, S3), suggesting that the presence of GO flakes did not affect the self-assembly of the amino acid. Therefore, the molecular packing of the Fmoc-F building blocks seems to follow a specific hierarchy, initially forming one-dimensional polymeric molecular chains, which lead to

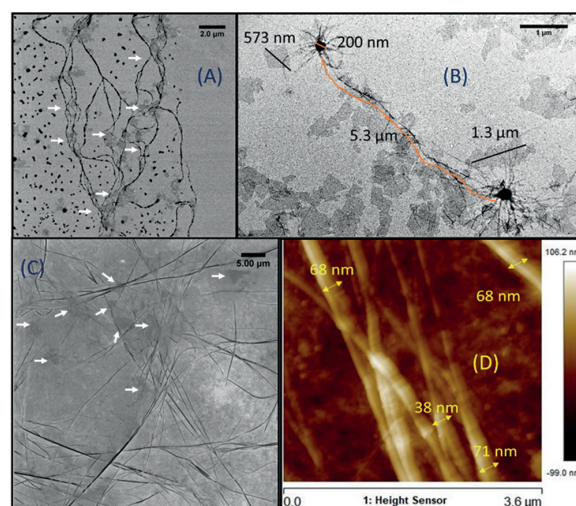


Figure 2. Microscopy images of the Fmoc-F/GO hybrid hydrogel. (A, C) HIM images; (B) TEM image; (D) AFM image with given dimensions of the fibers. The concentrations of Fmoc-F and GO were 2.0 and 0.25 mg/mL, respectively.

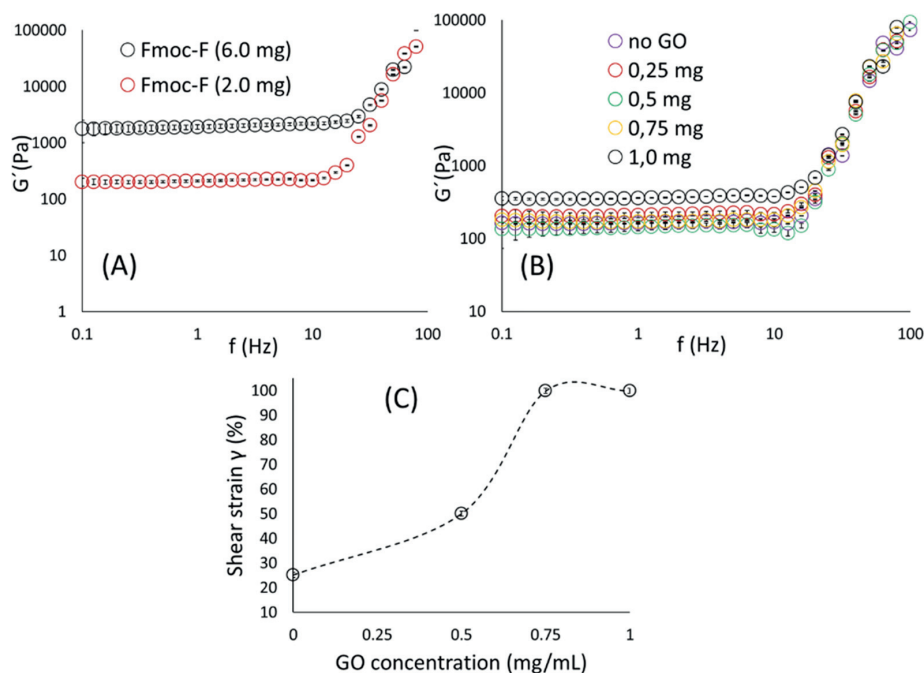


Figure 3. Rheology studies of the hybrid hydrogel. (A) The effect of Fmoc-F concentration on the stiffness (G') of the material. The concentration of GO was kept constant at 0.25 mg/mL. (B) The effect of GO concentration on the stiffness (G') of the material. The concentration of Fmoc-F was kept constant at 2.0 mg/mL. The corresponding G'' values are given in Figure S5A,B. (C) Assessing the elasticity of the hybrid gel: Comparing the G' and G'' cross points of the amplitude sweep measurements in contrast to the amount of added GO. The concentration of Fmoc-F was kept constant at 2.0 mg/mL. Error bars represent standard deviation.

higher architectures that interact with GO, *vide infra*. The three-dimensional network comprises single, branched, and entangled fibers and fine fibers in coiled-coil constructions. Their length varies up to several micrometers, and their width is within the range of ~ 40 – 70 nm (Figure 2D).

The GO flakes, seen as semitransparent sheets in the TEM and HIM micrographs, have various dimensions from nano to micrometers. The flakes are well dispersed in the gel network and encircled by Fmoc-F fibrillar loops (Figures 2A,C, white arrows). Indeed, the fibers are formed on the surface, around the edges and between the GO flakes, showcasing the development of noncovalent interactions between the already-formed fibers and GO. GO flakes do not seem to affect the self-assembly *per se*. However, the size of the flakes needs to be investigated further regarding the nucleation step of Fmoc-F to identify potential connection between the hydrogelation kinetics of the amino acid and the size of GO flakes.

In addition, microscopy imaging revealed spherulitic structures or nucleation points, out of which fibers grow and interpenetrate to adjacent spherulites (Figure 2B). Such structures (microcrystals) have previously been reported in Fmoc-F hydrogels at low pH values, originating from bundles of needle-shaped crystals.³⁰ When spin-cast, the structurally similar diphenylalanine (F–F) dipeptide also grows dendritic structures, which have been interpreted as two-dimensional spherulites.³² For our hybrid Fmoc-F/GO material, the spherulitic pattern does not cover the entire gel network, which mostly consists of branched, entangled fibers. The hydrogel sample was allowed to dry overnight in the open air before imaging, which might have led to the crystallization of Fmoc-F and the formation of the observed spherulites.

Mechanical Properties and Thermogravimetric Analysis.

The viscoelastic properties of the hybrid hydrogel were assessed by oscillatory rheology studies (Figure 3). The frequency sweep measurements were performed on self-supporting gels within the linear viscoelastic region (LVR), in which the storage (G') and loss moduli (G'') are independent of the strain amplitude. For both the native and hybrid hydrogels, the G' had a higher value than the G'' , confirming the materials' viscoelastic nature (gel state) (Figures 3, S4, S5). The stiffness of the hybrid material depends only on the amino acid concentration (Figures 3A, S5A), as the incorporation of GO flakes at different concentrations had a negligible effect on the G' value (Figures 3B, S5B). However, the addition of GO flakes increased the elasticity of the material, as indicated by its resistance to shear strain, since the cross points of the G' and G'' of the amplitude sweep measurements shifted toward higher shear strain ($\gamma\%$) values at higher GO concentrations (Figure 3C). It is of note that the addition of GO resulted in a faster formation of the hybrid material (within 6 h based on the vial inversion method) than the native gel, which required a longer time to fully form (at least 12 h).

The thermogravimetric (TG) data and differential scanning calorimetric (DSC) curves of the neat Fmoc-F powder and the corresponding xerogels (native and hybrid materials) are given in Figure 4 and Table S5. The neat Fmoc-F bulk powder is free of hydrated and nonbound water as the first thermal weight loss can be observed only at 194 °C, indicating the beginning of its thermal decomposition (onset value 218 °C). The primary decomposition occurs steeply between 200 and 350 °C by various degradation and cleavage processes on the

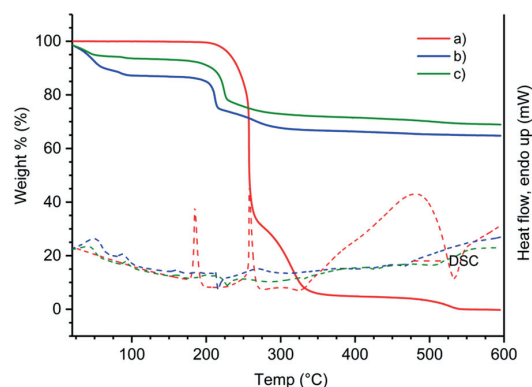


Figure 4. TG curves (solid lines) and DSC curves (dashed lines) of (a) neat Fmoc-F powder, (b) Fmoc-F native xerogel, and (c) Fmoc-F/GO hybrid xerogel, measured under an air atmosphere with a heating rate of 10 °C/min.

carboxylic acid and amide groups and finally at higher temperatures on the aromatic groups, resulting in a carbonaceous residue of ~0.5 wt % at 600 °C.

On the DSC curve, the endothermic melting transition of the neat Fmoc-F powder can be seen at 184.6 °C. The TG curves of both xerogels (native and hybrid) show their first initial weight loss from 22 °C to about 100 °C, indicating the removal of residual water remaining in the xerogels (12.5 and 4.17 wt % on the native gel and hybrid material, respectively). The thermal decomposition of both xerogels initiates at a somewhat lower temperature than that of neat Fmoc-F powder, which may be due to the more porous, less structured, and highly amorphous nature of the xerogels in contrast to the highly crystalline Fmoc-F raw material. Overall, the thermal decomposition processes follow the same path in both xerogels, showing slightly higher residue on the GO-containing xerogel. This is expected due to the thermal stability of the GO sheets.

Molecular Packing. To probe the self-assembly of Fmoc-F in the presence of GO flakes, we compared the Fourier transform infrared (FT-IR) spectra of neat amino acid powder with the native (Fmoc-F) and hybrid (Fmoc-F/GO) xerogels (dried gels) and neat GO flakes (Figure 5). Both xerogels gave identical spectra, however different from neat Fmoc-F powder. Therefore, any interactions between the formed fibers and GO flakes could not be observed. The data confirm the microscopic observations that adding GO to the system did not affect the Fmoc-F self-assembly. In addition, the obtained IR profiles of both xerogels are consistent with previously reported similar systems,^{33,34} meaning that no profound changes occurred during the self-assembly of the amino acid in the hybrid system.

Both xerogels lack the 1720 cm⁻¹ band of the amino acid, which corresponds to the non-hydrogen bonded carbonyl carbamate of the Fmoc group. This shows the involvement of the Fmoc moiety either in H-bond formation or other noncovalent interactions. The amide A and II bands at 3316 and 1537 cm⁻¹, respectively, are shifted in both xerogels, which corroborates the formation of amide–amide H-bonding. A blue shift is also observed for the amide I band (1681 to 1691 cm⁻¹). The C–O/C–N stretching peaks (1254, 1224 cm⁻¹) of neat Fmoc-F merged toward a broader band in both xerogels (~1255 cm⁻¹), while the C–H out of plane band (895 cm⁻¹)

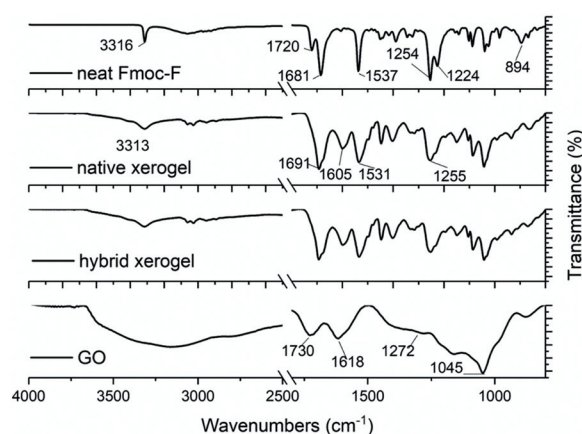


Figure 5. FT-IR spectra of neat Fmoc-F, neat GO, native, and hybrid xerogels. The amino acid concentration in both xerogels was 2.0 mg/mL. GO was added at a concentration of 0.25 mg/mL in the hybrid system. The FT-IR spectra of the phosphate salts Na₂HPO₄·2H₂O and NaH₂PO₄·H₂O used for preparing PBS solution (negative control) are given in Figure S7.

is diminished. Finally, neat GO gave the characteristic peaks of O–H stretching (broad ~3430–2940 cm⁻¹), C=O stretching (1730 cm⁻¹), aromatic C=C and O–H bending (1618 cm⁻¹), epoxy C–O stretching (1272 cm⁻¹), and alkoxy C–O stretching (1045 cm⁻¹), which are not seen in the hybrid xerogel.³⁵

To further explore potential differences in the structure of the materials, we compared the powder X-ray diffraction (PXRD) patterns of the native and hybrid xerogels with the neat bulk powder of Fmoc-F and GO flakes (Figure 6). The Pawley fit (Figure S6) indicates that the crystalline bulk powder, with sharp, distinct diffraction peaks, is phase pure and

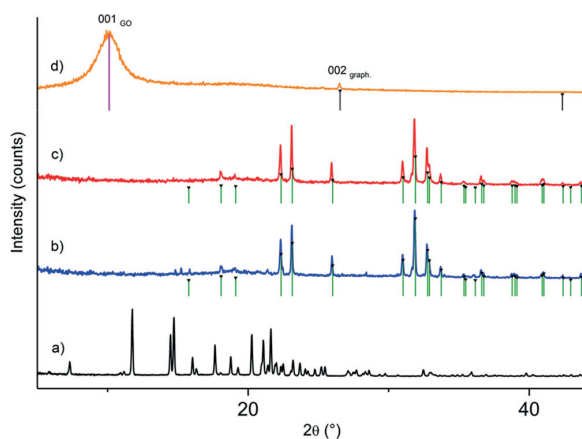


Figure 6. Powder X-ray diffraction patterns of (a) neat Fmoc-F, (b) Fmoc-F native xerogel, (c) Fmoc-F/GO hybrid xerogel, and (d) neat GO. Green vertical markers correspond to characteristic Bragg peak positions of anhydrous Na₂HPO₄, originating from the phosphate buffer solution, which crystallized in both xerogel samples. Black and magenta markers represent graphite and GO phases, respectively. The concentration of Fmoc-F was 2.0 mg/mL in both xerogel samples. GO was added at a concentration of 0.25 mg/mL in the hybrid system.

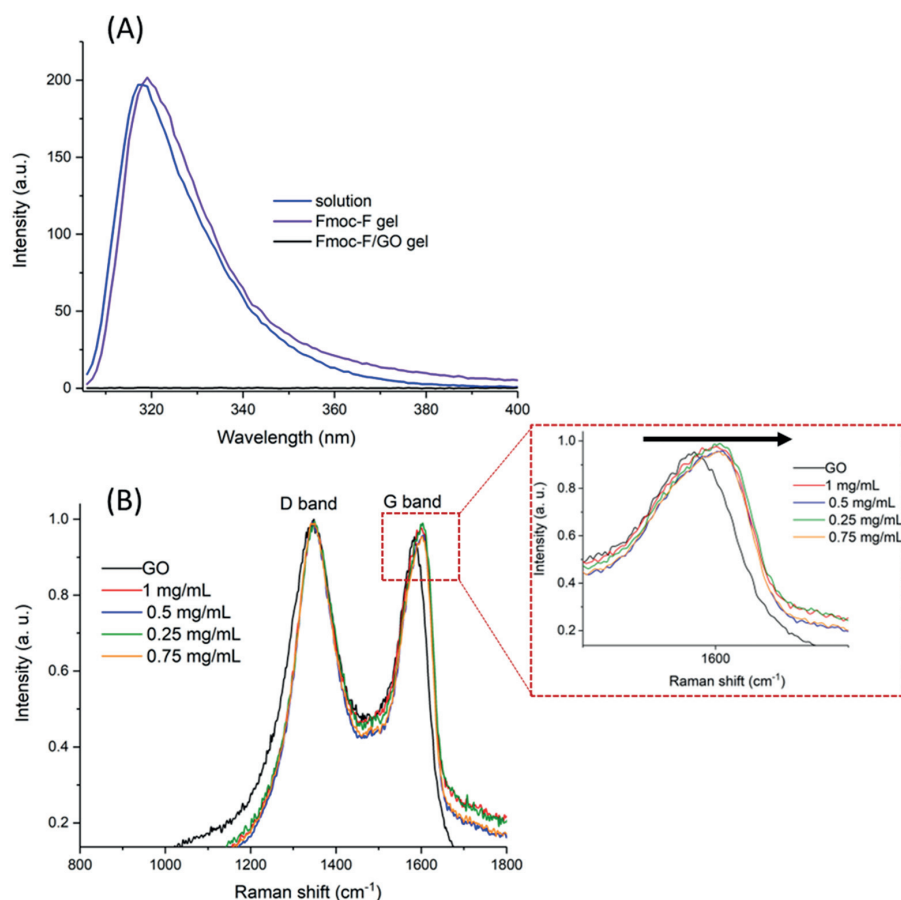


Figure 7. Spectroscopy analysis of the hydrogels. (A) Fluorescence spectra of the Fmoc-F solution in DMSO, native, and hybrid hydrogels. The concentration of Fmoc-F was 2.0 mg/mL and GO 0.25 mg/mL. The corresponding UV–vis spectra are given in Figure S8. (B) Raman spectra of neat GO and the hybrid hydrogel at a range of GO concentrations. The concentration of Fmoc-F was kept constant (2.0 mg/mL). The insert depicts a magnification of the G band plots with an arrow indicating the blue shift by addition of GO.

structurally congruent with the reported single crystal structure since no unindexed peak positions remain in the fit. The crystallographic data and the agreement indices are given in Table S6.

The native Fmoc-F xerogel shows several sharp, distinct diffraction peaks at the angular range of 15–40° 2 θ . However, a search-match phase identification analysis indicated that the obtained peaks do not originate from the Fmoc-F phase. Instead, they are unambiguously characteristic of the anhydrous Na₂HPO₄ phase. The phosphate phase originates from the buffer solution, crystallized during the drying of the hydrogel. Similar peaks have also been reported previously for the Fmoc-F xerogel (gel samples prepared in PBS solution by sonication/heating).³⁴ Here, all gel samples were prepared in PBS solution with sonication/heating-induced gelation, as reported by Thakur et al.,¹⁴ whose materials showed antibacterial properties against Gram-positive bacteria in the solution and gel phases. To avoid strong X-ray diffraction of phosphate salts, gels could be prepared in water, and gelation triggered by the pH switch method. However, we have intentionally followed the gelation protocol of Thakur et al.¹⁴ to prepare materials with known antimicrobial properties. Also, changes in the gelation method and/or the solvent alter self-assembly mode resulting in materials with different properties.

In addition to the phosphate phase peaks, a few very weak peak positions remain unindexed in the pattern, for example, at 14.8°, 15.3°, 19.7°, 20.0°, and 20.7° 2 θ . The peaks may correspond to a small contribution of a different Fmoc-F polymorph or a hydrated form, as suggested by Singh et al.³⁴ Despite the above findings, Fmoc-F in the native xerogel exists in an amorphous form.

The PXRD pattern of neat GO shows that the sample is practically amorphous, as only a few very broad diffraction peaks (humps) can be observed. The strongest broad peak at 10.08° is the characteristic carbon (001) peak for GO sheets, corresponding to a definite *d* spacing of 0.8–0.9 nm, as reported by Marcano et al. and Yasin et al.^{36,37} The GO sample contains also traces of graphite, which is best seen by the characteristic (002) peak at 26.52° 2 θ .

The diffraction pattern of the hybrid xerogel is clearly reminiscent of the native Fmoc-F xerogel pattern. In both patterns, the strongest diffraction peaks can be assigned to the anhydrous Na₂HPO₄ phase. The most significant difference between hybrid and native xerogels is the lack of additional weaker peaks, suggesting that the Fmoc-F fibers have collapsed to a fully amorphous form during the preparation of the hybrid xerogel. This differs, for example, from the previously reported structurally similar Fmoc-glutamic acid/GO gel system, in

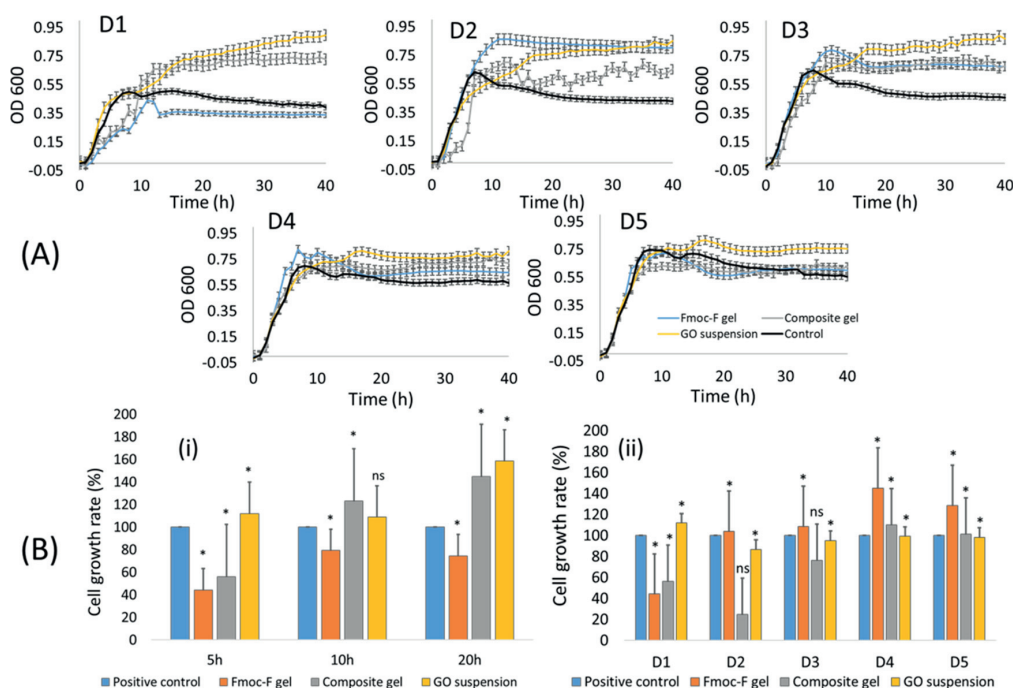


Figure 8. Antibacterial effect of GO flakes and native (Fmoc-F) and hybrid (Fmoc-F/GO) hydrogels against *E. coli*. (A) Optical density measurements of the treated bacterial cultures at five different concentrations over 40 h. (B) The cell viability at different time points of incubation at D1 concentration (i) and after 5 h of incubation at all five concentrations (D1–D5) (ii). * $p < 0.05$; ns, nonsignificant (in relation to the control); statistical analysis was performed with t-Test; $n = 3$. Error bars denote standard deviation.

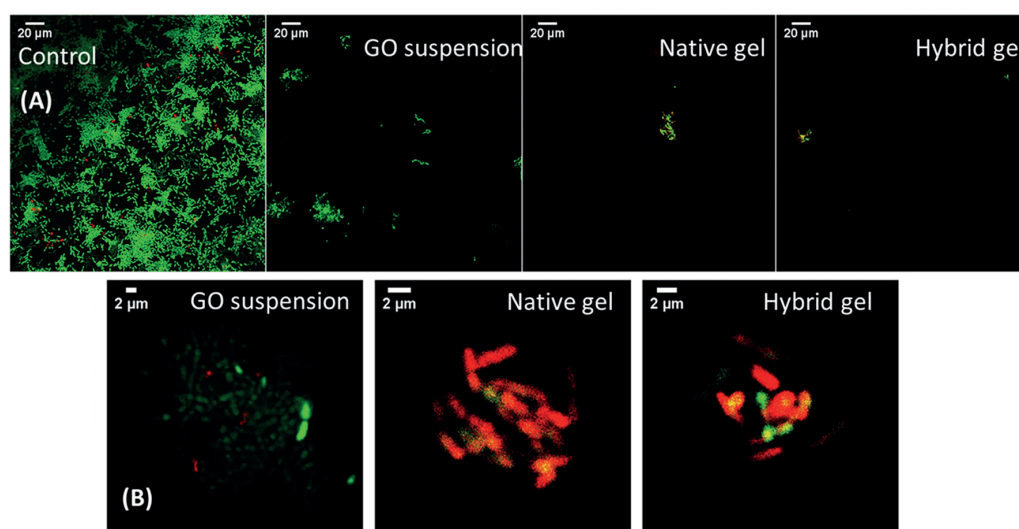


Figure 9. Live/dead staining images of the bacteria after 5 h of incubation at D1 concentration at two different magnifications (A and B). The green fluorescence indicates bacteria with both intact and damaged membrane/wall, and the red fluorescence indicates dead bacteria cells.

which a weak crystalline phase was observed.³⁸ It is also noted that the broad peak of GO and the weaker peak of the graphite phase are missing from the hybrid xerogel PXRD pattern. This suggests that the GO sheets most likely interact with the Fmoc-F fibrous network, which in turn partially causes some delamination of the GO sheets and, thereby, the 10.08° peak is absent.

To explore potential changes in the fluorescent properties of Fmoc-F amino acid at the gel state, we compared the emission spectra of the native and hybrid hydrogels with Fmoc-F at the solution state (Figure 7A). The amino acid shows a strong emission at the solution state, centered at 318 nm on excitation at 296 nm. No significant shifting is observed at the native hydrogel (emission, 319 nm; excitation, 296 nm). However, the fluorescence emission of the hybrid material is quenched,

suggesting either the development of supramolecular interactions between the amino acid (formed Fmoc-F fibers) and GO flakes or just their spatial proximity. To support our findings, we performed Raman spectroscopy studies of the hybrid hydrogel at a range of GO concentrations (Figure 7B). As expected, neat GO showed two fundamental vibrations at ~ 1345 and ~ 1583 cm^{-1} , corresponding to the D and G bands, respectively. The D or disorder-induced band is indicative of lattice defects or appears near the edges of graphene, while the G or graphitic vibrational mode is due to the in-plane motion of the sp^2 hybridized carbon atoms (bond stretching). For all gel samples, irrespective of the amount of added GO, the ID/IG ratio is higher than that of neat GO. In addition, the G band is blue-shifted toward higher values compared to neat GO (~ 1583 to ~ 1600 cm^{-1}). These observations suggest a decrease in the size of the GO basal plane (in-plane sp^2 domains), presumably due to the development of π - π interactions between the Fmoc group of the amino acid and the basal plane of GO flakes.³⁸

Antimicrobial Screening. The antimicrobial activity of neat GO (suspension in PBS) and native (Fmoc-F) and hybrid (Fmoc-F/GO) hydrogels was assessed against Gram-negative *E. coli*. The bacterial growth was evaluated over time, *in vitro*, by measuring the optical density of the treated cultures at a wavelength of 600 nm (OD_{600}). The results were then translated into cell growth rate (%) by considering the cell survival (OD_{600}) of the untreated bacteria (control) as 100%. The samples were evaluated at five different concentrations, prepared by serial dilutions (Table 1, D1–D5) over a period of 40 h (Figure 8). In addition to bacterial growth, the integrity of the bacterial membrane/wall was further assessed by a live/dead staining assay (Figure 9, intact cells are viable cells).

The Fmoc-F native hydrogel, as expected, showed poor bactericidal efficacy, especially after the second dilution (D2). The hybrid hydrogel, however, inhibited *E. coli* growth over three consecutive dilutions (D1–D3), while the GO suspension showed negligible antimicrobial effects at all five concentrations (Figure 8B,ii). Interestingly, the most profound delay in growth population was observed during the first 5 h of incubation for both gel samples, native and hybrid, at the first dilution (Figure 8A, D1). Indeed, the cell growth rate for the native gel was 44% and for the hybrid gel was 56% compared to the control (Figure 8B,i).

After 10 h of incubation, at the first dilution (Figure 8A, D1), only the native hydrogel inhibited bacterial growth, which was kept below that of the control until the end of the measurement (40 h). At the same time point (10 h), the hybrid gel lost its inhibition effect as after that (from 10 to 40 h), the observed cell growth exceeded that of the control (Figure 8A, D1). Further dilutions of the Fmoc-F native gel (D2–D5) did not inhibit/delay the bacterial growth either, resulting in a cell growth increase (Figure 8B, ii). The hybrid hydrogel, instead, led to lower bacterial populations compared to the control for the first three consecutive dilutions (D1–D3). Notably, the inhibition/delay of the bacterial growth for dilutions D1–D3 occurred during the first 5 h of incubation with corresponding cell growth rates of 56%, 25%, and 76% at D1, D2, and D3 dilutions, respectively. After 10 h of incubation, the recorded OD_{600} values exceeded the control values, demonstrating the lack of inhibition effects and bacterial regrowth (Figure 8A, D1, D2, D3).

The data showed that the hydrogels and the GO suspension demonstrate poor antibacterial activity against Gram-negative

E. coli. Although the bacterial growth was delayed for the first 5 h of incubation and a large number of cells died, the remaining ones developed resistance over time and managed to increase their population density compared to the untreated cells. This could be explained by the “inoculum effect” (IE), in which the antimicrobial outcome of a bactericidal depends on the initial population size.³⁹ Several mechanisms related to the IE, such as the “phenotypic heterogeneity” and “bacterial density”, may affect the cell–hydrogel interactions. Therefore, the abrupt bacterial death (in our case within the first 5 h of incubation) is followed by the regrowth of the surviving bacteria, on which the hydrogels do not have an effect due to the IE. In addition, incorporating GO flakes in the gel system may increase the surface area upon which the bacteria can grow. Finally, the extra lipopolysaccharides at the cell wall of Gram-negative *E. coli* could protect them from the Fmoc-F hydrogel, which shows bactericidal effects against Gram-positive bacteria.¹⁰

To further detect the antibacterial efficacy of the samples and evaluate the integrity of the bacterial membrane/wall, we performed a live/dead staining assay, after 5 h of incubation, at the first dilution D1 (Figure 9). The green fluorescent dye (Syto9) stains both live and dead cells, in contrast to the red fluorescent dye (PI), which selectively stains bacteria with destroyed cell walls and membranes. The live/dead imaging data are only qualitative and complement the OD_{600} findings, meaning no statistical analysis was performed about the percentage of dead cells. The imaging data were consistent with the OD_{600} findings. As expected, the untreated bacteria were intact and stained mainly green, while no changes were observed in their morphology. Similarly, those treated with GO suspension were predominantly stained green, with some negligible red fluorescence also present. However, the bacteria treated with both gel samples were mainly stained red, suggesting that most cells were dead.

CONCLUSIONS

In summary, we studied the gelation synergies of Fmoc-F amino acid and GO flakes and assessed the antimicrobial efficacy of the formed hybrid material against Gram-negative *E. coli* for the first time. GO flakes do not affect the self-assembly of Fmoc-F amino acid per se, but the formed fibers interact with the flakes, as we observed by spectroscopy analysis. The incorporation of GO flakes modulates the viscoelastic properties of the hybrid material, which also forms faster than the native gel. The hybrid hydrogel showed poor antimicrobial activity against *E. coli*, likewise the native gel, probably due to the inoculum effect. However, due to its mechanical and physicochemical properties, the Fmoc-F/GO hybrid hydrogel has a high potential for advancing the development of bactericidal soft materials, for example, via the selective immobilization of antibacterial agents on the surface area of GO flakes.

ASSOCIATED CONTENT

Supporting Information

The Supporting Information is available free of charge at <https://pubs.acs.org/doi/10.1021/acsomega.2c07700>.

Concentration screening; gelation and phase transition temperature measurements; helium ion microscopy of native gel; rheological studies; thermogravimetric and differential scanning calorimetry analysis results; powder X-ray diffraction analysis results (PDF)

AUTHOR INFORMATION

Corresponding Author

Maija Nissinen – Department of Chemistry, Nanoscience Center, University of Jyväskylä, FI-40014 Jyväskylä, Finland; orcid.org/0000-0001-7560-4632; Email: maija.nissinen@jyu.fi

Authors

Efstratios D. Sitsanidis – Department of Chemistry, Nanoscience Center, University of Jyväskylä, FI-40014 Jyväskylä, Finland; orcid.org/0000-0001-5727-1336

Lara A. L. Dutra – Department of Biological and Environmental Sciences, Nanoscience Center, University of Jyväskylä, FI-40014 Jyväskylä, Finland

Johanna Schirmer – Department of Chemistry, Nanoscience Center, University of Jyväskylä, FI-40014 Jyväskylä, Finland; orcid.org/0000-0001-9010-3131

Romain Chevigny – Department of Chemistry, Nanoscience Center, University of Jyväskylä, FI-40014 Jyväskylä, Finland; orcid.org/0000-0002-5463-9745

Manu Lahtinen – Department of Chemistry, Nanoscience Center, University of Jyväskylä, FI-40014 Jyväskylä, Finland; orcid.org/0000-0001-5561-3259

Andreas Johansson – Department of Chemistry, Nanoscience Center, University of Jyväskylä, FI-40014 Jyväskylä, Finland; Department of Physics, Nanoscience Center, University of Jyväskylä, FI-40014 Jyväskylä, Finland; orcid.org/0000-0003-0906-6287

Carmen C. Piras – Department of Chemistry, University of York, York YO10 5DD, United Kingdom

David K. Smith – Department of Chemistry, University of York, York YO10 5DD, United Kingdom

Marja Tiitola – Department of Biological and Environmental Sciences, Nanoscience Center, University of Jyväskylä, FI-40014 Jyväskylä, Finland

Mika Pettersson – Department of Chemistry, Nanoscience Center, University of Jyväskylä, FI-40014 Jyväskylä, Finland; orcid.org/0000-0002-6880-2283

Complete contact information is available at: <https://pubs.acs.org/10.1021/acsoomega.2c07700>

Notes

The authors declare no competing financial interest.

ACKNOWLEDGMENTS

The authors would like to acknowledge the Jane and Aatos Erkkö foundation for supporting the current work.

REFERENCES

- (1) Doron, S.; Gorbach, S. L. *Bacterial infections: Overview*. In *International Encyclopedia of Public Health*; Heggenhougen, H. K., Ed.; Academic Press, 2008; pp 273–282.
- (2) Mancuso, G.; Midiri, A.; Gerace, E.; Biondo, C. Bacterial antibiotic resistance: The most critical pathogens. *Pathogens* **2021**, *10* (10), 1310.
- (3) Tse, B. N.; Adalja, A. A.; Houchens, C.; Larsen, J.; Inglesby, T. V.; Hatchett, R. Challenges and opportunities of nontraditional approaches to treating bacterial infections. *Clin. Infect. Dis.* **2017**, *65* (3), 495–500.
- (4) Zhao, X. Antibacterial Bioactive Materials. In *Bioactive Materials in Medicine*; Zhao, X., Courtney, J. M., Qian, H., Ed.; Woodhead Publishing, 2011; chapter 5, pp 97–123.
- (5) Duan, S.; Wu, R.; Xiong, Y. H.; Ren, H. M.; Lei, C.; Zhao, Y. Q.; Zhang, X. Y.; Xu, F. J. Multifunctional antimicrobial materials: From

rational design to biomedical applications. *Prog. Mater. Sci.* **2022**, *125*, 100887.

(6) Mahira, S.; Jain, A.; Khan, W.; Domb, A. J. Antimicrobial Materials—An Overview. In *Antimicrobial Materials for Biomedical Applications*; Domb, A. J., Kunduru, K. R., Farah, S., Ed.; The Royal Society of Chemistry: United Kingdom, 2019; chapter 1, pp 1–37.

(7) Nicolas, M.; Beito, B.; Oliveira, M.; Tudela Martins, M.; Gallas, B.; Salmain, M.; Boujday, S.; Humblot, V. Strategies for antimicrobial peptides immobilization on surfaces to prevent biofilm growth on biomedical devices. *Antibiotics* **2022**, *11* (1), 13.

(8) Yang, K.; Han, Q.; Chen, B.; Zheng, Y.; Zhang, K.; Li, Q.; Wang, J. Antimicrobial hydrogels: promising materials for medical application. *Int. J. Nanomedicine* **2018**, *13*, 2217–2263.

(9) Li, S.; Dong, S.; Xu, W.; Tu, S.; Yan, L.; Zhao, C.; Ding, J.; Chen, X. Antibacterial Hydrogels. *Adv. Sci.* **2018**, *5* (5), 1700527.

(10) Xie, Y. Y.; Zhang, Y. W.; Qin, X. T.; Liu, L. P.; Wahid, F.; Zhong, C.; Jia, S. R. Structure-dependent antibacterial activity of amino acid-based supramolecular hydrogels. *Colloids Surf. B Biointerfaces* **2020**, *193*, 111099.

(11) Wang, H.; Niu, M.; Xue, T.; Ma, L.; Gu, X.; Wei, G.; Li, F.; Wang, C. Development of antibacterial peptides with efficient antibacterial activity, low toxicity, high membrane disruptive activity and a synergistic antibacterial effect. *J. Mater. Chem. B* **2022**, *10*, 1858–1874.

(12) McCloskey, A. P.; Draper, E. R.; Gilmore, B. F.; Lavery, G. Ultrashort self-assembling Fmoc-peptide gels for anti-infective biomaterial applications. *J. Pept. Sci.* **2017**, *23* (2), 131–140.

(13) Rai, A.; Ferrão, R.; Palma, P.; Patricio, T.; Parreira, P.; Anes, E.; Tonda-Turo, C.; Martins, M. C. L.; Alves, N.; Ferreira, L. Antimicrobial peptide-based materials: opportunities and challenges. *J. Mater. Chem. B* **2022**, *10*, 2384–2429.

(14) Gahane, A. Y.; Ranjan, P.; Singh, V.; Sharma, R. K.; Sinha, N.; Sharma, M.; Chaudhry, R.; Thakur, A. K. Soft matter Fmoc-phenylalanine displays antibacterial activity against Gram-positive bacteria in gel and solution. *Soft Matter* **2018**, *14* (12), 2234–2244.

(15) Irwansyah, I.; Li, Y. Q.; Shi, W.; Qi, D.; Leow, W. R.; Tang, M. B.; Li, S.; Chen, X. Gram-positive antimicrobial activity of amino acid-based hydrogels. *Adv. Mater.* **2015**, *27* (4), 648–654.

(16) Singh, H.; Gahane, A.; Singh, V.; Ghosh, S.; Thakur, A. Antibiofilm activity of Fmoc-phenylalanine against Gram-positive and Gram-negative bacterial biofilms. *J. Antibiot.* **2021**, *74* (6), 407–416.

(17) Gahane, A. Y.; Singh, V.; Kumar, A.; Kumar Thakur, A. Development of mechanism-based antibacterial synergy between Fmoc-phenylalanine hydrogel and aztreonam. *Biomater. Sci.* **2020**, *8* (7), 1996–2006.

(18) Zhao, X. Q.; Wahid, F.; Zhao, X. J.; Wang, F. P.; Wang, T. F.; Xie, Y. Y.; Jia, S. R.; Zhong, C. Fabrication of amino acid-based supramolecular hydrogel with silver ions for improved antibacterial properties. *Mater. Lett.* **2021**, *300*, 130161.

(19) Xie, Y. Y.; Zhang, Y. W.; Liu, X. Z.; Ma, X. F.; Qin, X. T.; Jia, S. R.; Zhong, C. Aggregation-induced emission-active amino acid/berberine hydrogels with enhanced photodynamic antibacterial and anti-biofilm activity. *Chem. Eng. J.* **2021**, *413*, 127542.

(20) Snigdha, K.; Singh, B. K.; Mehta, A. S.; Tewari, R. P.; Dutta, P. K. Self-assembling N-(9-Fluorenylmethoxycarbonyl)-L-Phenylalanine hydrogel as novel drug carrier. *Int. J. Biol. Macromol.* **2016**, *93*, 1639–1646.

(21) Liu, S.; Zeng, T. H.; Hofmann, M.; Burcombe, E.; Wei, J.; Jiang, R.; Kong, J.; Chen, Y. Antibacterial activity of Graphite, Graphite Oxide, Graphene Oxide, and Reduced Graphene Oxide: membrane and oxidative stress. *ACS Nano* **2011**, *5* (9), 6971–6980.

(22) Azizi-Lalabadi, M.; Hashemi, H.; Feng, J.; Jafari, S. M. Carbon nanomaterials against pathogens; the antimicrobial activity of carbon nanotubes, graphene/graphene oxide, fullerenes, and their nanocomposites. *Adv. Colloid Interface Sci.* **2020**, *284*, 102250.

(23) Seabra, A. B.; Paula, A. J.; de Lima, R.; Alves, O. L.; Durán, N. Nanotoxicity of graphene and graphene oxide. *Chem. Res. Toxicol.* **2014**, *27* (2), 159–168.

(24) Krishnamoorthy, K.; Umasuthan, N.; Mohan, R.; Lee, J.; Kim, S. J. Antibacterial activity of graphene oxide nanosheets. *Sci. Adv. Mater.* **2012**, *4* (11), 1111–1117.

(25) Radhi, A.; Mohamad, D.; Abdul Rahman, F. S.; Abdullah, A. M.; Hasan, H. Mechanism and factors influence of graphene-based nanomaterials antimicrobial activities and application in dentistry. *J. Mater. Sci. Technol.* **2021**, *11*, 1290–1307.

(26) Barbolina, I.; Woods, C. R.; Lozano, N.; Kostarelos, K.; Novoselov, K. S.; Roberts, I. S. Purity of graphene oxide determines its antibacterial activity. *2D Mater.* **2016**, *3*, 025025.

(27) Degen, T.; Sadki, M.; Bron, E.; König, U.; Nénert, G. The highScore suite. *Powder Diffr.* **2014**, *29* (S2), S13–S18.

(28) Pawley, G. S. Unit-cell refinement from powder diffraction scans. *J. Appl. Crystallogr.* **1981**, *14* (6), 357–361.

(29) Görbitz, C. H. The development and use of a crystallographic database. *Acta Crystallogr. Sect. B Struct. Sci. Cryst. Eng. Mater.* **2016**, *72*, 167–168.

(30) Draper, E. R.; Morris, K. L.; Little, M. A.; Raeburn, J.; Colquhoun, C.; Cross, E. R.; McDonald, T. O.; Serpell, L. C.; Adams, D. J. Hydrogels formed from Fmoc amino acids. *CrystEngComm* **2015**, *17*, 8047–8057.

(31) Wang, M.; Gao, B.; Tang, D.; Sun, H.; Yin, X.; Yu, C. Effects of temperature on aggregation kinetics of graphene oxide in aqueous solutions. *Colloids Surf. A: Physicochem. Eng. Asp.* **2018**, *538*, 63–72.

(32) Korolkov, V. V.; Allen, S.; Roberts, C. J.; Tandler, S. J. B. Surface mediated L-phenylalanyl-L-phenylalanine assembly into large dendritic structures. *Faraday Discuss.* **2013**, *166*, 257–267.

(33) Bairi, P.; Roy, B.; Routh, P.; Sen, K.; Nandi, A. K. Self-sustaining, fluorescent and semi-conducting co-assembled organogel of Fmoc protected phenylalanine with aromatic amines. *Soft Matter* **2012**, *8*, 7436–7445.

(34) Singh, V.; Snigdha, K.; Singh, C.; Sinha, N.; Thakur, A. K. Understanding the self-assembly of Fmoc-phenylalanine to hydrogel formation. *Soft Matter* **2015**, *11*, 5353–5364.

(35) Pham, V. H.; Cuong, T. V.; Hur, S. H.; Oh, E.; Kim, E. J.; Shin, E. W.; Chung, J. S. Chemical functionalization of graphene sheets by solvothermal reduction of a graphene oxide suspension in *N*-methyl-2-pyrrolidone. *J. Mater. Chem.* **2011**, *21*, 3371–3377.

(36) Marcano, D. C.; Kosynkin, D. V.; Berlin, J. M.; Sinitskii, A.; Sun, Z.; Slesarev, A.; Alemany, L. B.; Lu, W.; Tour, J. M. Improved Synthesis of Graphene Oxide. *ACS Nano* **2010**, *4* (8), 4806–4814.

(37) Yasin, G.; Arif, M.; Shakeel, M.; Dun, Y.; Zuo, Y.; Khan, W. Q.; Tang, Y.; Khan, A.; Nadeem, M. Exploring the Nickel-Graphene nanocomposite coatings for superior corrosion resistance: manipulating the effect of deposition current density on its morphology, mechanical properties, and erosion-corrosion performance. *Adv. Eng. Mater.* **2018**, *20*, 1701166.

(38) Xing, P.; Chu, X.; Li, S.; Ma, M.; Hao, A. Hybrid gels assembled from Fmoc-amino acid and graphene oxide with controllable properties. *Chemphyschem.* **2014**, *15* (11), 2377–2385.

(39) Frenkel, N.; Saar Dover, R.; Titon, E.; Shai, Y.; Rom-Kedar, V. Bistable bacterial growth dynamics in the presence of antimicrobial agents. *Antibiotics (Basel)* **2021**, *10* (1), 87.

DEPARTMENT OF CHEMISTRY, UNIVERSITY OF JYVÄSKYLÄ
RESEARCH REPORT SERIES

1. Vuolle, Mikko: Electron paramagnetic resonance and molecular orbital study of radical ions generated from (2.2)metacyclophane, pyrene and its hydrogenated compounds by alkali metal reduction and by thallium(III)trifluoroacetate oxidation. (99 pp.) 1976
2. Pasanen, Kaija: Electron paramagnetic resonance study of cation radical generated from various chlorinated biphenyls. (66 pp.) 1977
3. Carbon-13 Workshop, September 6-8, 1977. (91 pp.) 1977
4. Laihia, Katri: On the structure determination of norbornane polyols by NMR spectroscopy. (111 pp.) 1979
5. Nyrönen, Timo: On the EPR, ENDOR and visible absorption spectra of some nitrogen containing heterocyclic compounds in liquid ammonia. (76 pp.) 1978
6. Talvitie, Antti: Structure determination of some sesquiterpenoids by shift reagent NMR. (54 pp.) 1979
7. Häkli, Harri: Structure analysis and molecular dynamics of cyclic compounds by shift reagent NMR. (48 pp.) 1979
8. Pitkänen, Ilkka: Thermodynamics of complexation of 1,2,4-triazole with divalent manganese, cobalt, nickel, copper, zinc, cadmium and lead ions in aqueous sodium perchlorate solutions. (89 pp.) 1980
9. Asunta, Tuula: Preparation and characterization of new organometallic compounds synthesized by using metal vapours. (91 pp.) 1980
10. Sattar, Mohammad Abdus: Analyses of MCPA and its metabolites in soil. (57 pp.) 1980
11. Bibliography 1980. (31 pp.) 1981
12. Knuuttila, Pekka: X-Ray structural studies on some divalent 3d metal compounds of picolinic and isonicotinic acid N-oxides. (77 pp.) 1981
13. Bibliography 1981. (33 pp.) 1982
14. 6th National NMR Symposium, September 9-10, 1982, Abstracts. (49 pp.) 1982
15. Bibliography 1982. (38 pp.) 1983
16. Knuuttila, Hilka: X-Ray structural studies on some Cu(II), Co(II) and Ni(II) complexes with nicotinic and isonicotinic acid N-oxides. (54 pp.) 1983
17. Symposium on inorganic and analytical chemistry May 18, 1984, Program and Abstracts. (100 pp.) 1984
18. Knuutinen, Juha: On the synthesis, structure verification and gas chromatographic determination of chlorinated catechols and guaiacols occurring in spent bleach liquors of kraft pulp mill. (30 pp.) 1984
19. Bibliography 1983. (47 pp.) 1984
20. Pitkänen, Maija: Addition of BrCl, B₂ and Cl₂ to methyl esters of propenoic and 2-butenic acid derivatives and ¹³C NMR studies on methyl esters of saturated aliphatic mono- and dichlorocarboxylic acids. (56 pp.) 1985
21. Bibliography 1984. (39 pp.) 1985
22. Salo, Esa: EPR, ENDOR and TRIPLE spectroscopy of some nitrogen heteroaromatics in liquid ammonia. (111 pp.) 1985

DEPARTMENT OF CHEMISTRY, UNIVERSITY OF JYVÄSKYLÄ
RESEARCH REPORT SERIES

23. Humppi, Tarmo: Synthesis, identification and analysis of dimeric impurities of chlorophenols. (39 pp.) 1985
24. Aho, Martti: The ion exchange and adsorption properties of sphagnum peat under acid conditions. (90 pp.) 1985
25. Bibliography 1985 (61 pp.) 1986
26. Bibliography 1986. (23 pp.) 1987
27. Bibliography 1987. (26 pp.) 1988
28. Paasivirta, Jaakko (Ed.): Structures of organic environmental chemicals. (67 pp.) 1988
29. Paasivirta, Jaakko (Ed.): Chemistry and ecology of organo-element compounds. (93 pp.) 1989
30. Sinkkonen, Seija: Determination of crude oil alkylated dibenzothiophenes in environment. (35 pp.) 1989
31. Kolehmainen, Erkki (Ed.): XII National NMR Symposium Program and Abstracts. (75 pp.) 1989
32. Kuokkanen, Tauno: Chlorocymenes and Chlorocymenenes: Persistent chlorocompounds in spent bleach liquors of kraft pulp mills. (40 pp.) 1989
33. Mäkelä, Reijo: ESR, ENDOR and TRIPLE resonance study on substituted 9,10-anthraquinone radicals in solution. (35 pp.) 1990
34. Veijanen, Anja: An integrated sensory and analytical method for identification of off-flavour compounds. (70 pp.) 1990
35. Kasa, Seppo: EPR, ENDOR and TRIPLE resonance and molecular orbital studies on a substitution reaction of anthracene induced by thallium(III) in two fluorinated carboxylic acids. (114 pp.) 1990
36. Herve, Sirpa: Mussel incubation method for monitoring organochlorine compounds in freshwater recipients of pulp and paper industry. (145 pp.) 1991
37. Pohjola, Pekka: The electron paramagnetic resonance method for characterization of Finnish peat types and iron (III) complexes in the process of peat decomposition. (77 pp.) 1991
38. Paasivirta, Jaakko (Ed.): Organochlorines from pulp mills and other sources. Research methodology studies 1988-91. (120 pp.) 1992
39. Veijanen, Anja (Ed.): VI National Symposium on Mass Spectrometry, May 13-15, 1992, Abstracts. (55 pp.) 1992
40. Rissanen, Kari (Ed.): The 7. National Symposium on Inorganic and Analytical Chemistry, May 22, 1992, Abstracts and Program. (153 pp.) 1992
41. Paasivirta, Jaakko (Ed.): CEOEC'92, Second Finnish-Russian Seminar: Chemistry and Ecology of Organo-Element Compounds. (93 pp.) 1992
42. Koistinen, Jaana: Persistent polychloroaromatic compounds in the environment: structure-specific analyses. (50 pp.) 1993
43. Virkki, Liisa: Structural characterization of chlorolignins by spectroscopic and liquid chromatographic methods and a comparison with humic substances. (62 pp.) 1993
44. Helenius, Vesa: Electronic and vibrational excitations in some

DEPARTMENT OF CHEMISTRY, UNIVERSITY OF JYVÄSKYLÄ
RESEARCH REPORT SERIES

- biologically relevant molecules. (30 pp.) 1993
45. Leppä-aho, Jaakko: Thermal behaviour, infrared spectra and x-ray structures of some new rare earth chromates(VI). (64 pp.) 1994
46. Kotila, Sirpa: Synthesis, structure and thermal behavior of solid copper(II) complexes of 2-amino-2-hydroxymethyl-1,3-propanediol. (111 pp.) 1994
47. Mikkonen, Anneli: Retention of molybdenum(VI), vanadium(V) and tungsten(VI) by kaolin and three Finnish mineral soils. (90 pp.) 1995
48. Suontamo, Reijo: Molecular orbital studies of small molecules containing sulfur and selenium. (42 pp.) 1995
49. Hämäläinen, Jouni: Effect of fuel composition on the conversion of fuel-N to nitrogen oxides in the combustion of small single particles. (50 pp.) 1995
50. Nevalainen, Tapio: Polychlorinated diphenyl ethers: synthesis, NMR spectroscopy, structural properties, and estimated toxicity. (76 pp.) 1995
51. Aittola, Jussi-Pekka: Organochloro compounds in the stack emission. (35 pp.) 1995
52. Harju, Timo: Ultrafast polar molecular photophysics of (dibenzylmethine)borondifluoride and 4-aminophthalimide in solution. (61 pp.) 1995
53. Maatela, Paula: Determination of organically bound chlorine in industrial and environmental samples. (83 pp.) 1995
54. Paasivirta, Jaakko (Ed.): CEOEC'95, Third Finnish-Russian Seminar: Chemistry and Ecology of Organo-Element Compounds. (109 pp.) 1995
55. Huuskonen, Juhani: Synthesis and structural studies of some supramolecular compounds. (54 pp.) 1995
56. Palm, Helena: Fate of chlorophenols and their derivatives in sawmill soil and pulp mill recipient environments. (52 pp.) 1995
57. Rantio, Tiina: Chlorohydrocarbons in pulp mill effluents and their fate in the environment. (89 pp.) 1997
58. Ratilainen, Jari: Covalent and non-covalent interactions in molecular recognition. (37 pp.) 1997
59. Kolehmainen, Erkki (Ed.): XIX National NMR Symposium, June 4-6, 1997, Abstracts. (89 pp.) 1997
60. Matilainen, Rose: Development of methods for fertilizer analysis by inductively coupled plasma atomic emission spectrometry. (41 pp.) 1997
61. Koistinen, Jari (Ed.): Spring Meeting on the Division of Synthetic Chemistry, May 15-16, 1997, Program and Abstracts. (36 pp.) 1997
62. Lappalainen, Kari: Monomeric and cyclic bile acid derivatives: syntheses, NMR spectroscopy and molecular recognition properties. (50 pp.) 1997
63. Laitinen, Eira: Molecular dynamics of cyanine dyes and phthalimides in solution: picosecond laser studies. (62 pp.) 1997
64. Eloranta, Jussi: Experimental and theoretical studies on some

DEPARTMENT OF CHEMISTRY, UNIVERSITY OF JYVÄSKYLÄ
RESEARCH REPORT SERIES

- quinone and quinol radicals. (40 pp.) 1997
65. Oksanen, Jari: Spectroscopic characterization of some monomeric and aggregated chlorophylls. (43 pp.) 1998
66. Häkkänen, Heikki: Development of a method based on laser-induced plasma spectrometry for rapid spatial analysis of material distributions in paper coatings. (60 pp.) 1998
67. Virtapohja, Janne: Fate of chelating agents used in the pulp and paper industries. (58 pp.) 1998
68. Airola, Karri: X-ray structural studies of supramolecular and organic compounds. (39 pp.) 1998
69. Hyötyläinen, Juha: Transport of lignin-type compounds in the receiving waters of pulp mills. (40 pp.) 1999
70. Ristolainen, Matti: Analysis of the organic material dissolved during totally chlorine-free bleaching. (40 pp.) 1999
71. Eklin, Tero: Development of analytical procedures with industrial samples for atomic emission and atomic absorption spectrometry. (43 pp.) 1999
72. Väლისаari, Jouni: Hygiene properties of resol-type phenolic resin laminates. (129 pp.) 1999
73. Hu, Jiwei: Persistent polyhalogenated diphenyl ethers: model compounds syntheses, characterization and molecular orbital studies. (59 pp.) 1999
74. Malkavaara, Petteri: Chemometric adaptations in wood processing chemistry. (56 pp.) 2000
75. Kujala Elena, Laihia Katri, Nieminen Kari (Eds.): NBC 2000, Symposium on Nuclear, Biological and Chemical Threats in the 21st Century. (299 pp.) 2000
76. Rantalainen, Anna-Lea: Semipermeable membrane devices in monitoring persistent organic pollutants in the environment. (58 pp.) 2000
77. Lahtinen, Manu: *In situ* X-ray powder diffraction studies of Pt/C, CuCl/C and Cu₂O/C catalysts at elevated temperatures in various reaction conditions. (92 pp.) 2000
78. Tamminen, Jari: Syntheses, empirical and theoretical characterization, and metal cation complexation of bile acid-based monomers and open/closed dimers. (54 pp.) 2000
79. Vatanen, Virpi: Experimental studies by EPR and theoretical studies by DFT calculations of α -amino-9,10-anthraquinone radical anions and cations in solution. (37 pp.) 2000
80. Kotilainen, Risto: Chemical changes in wood during heating at 150-260 °C. (57 pp.) 2000
81. Nissinen, Maija: X-ray structural studies on weak, non-covalent interactions in supramolecular compounds. (69 pp.) 2001
82. Wegelius, Elina: X-ray structural studies on self-assembled hydrogen-bonded networks and metallosupramolecular complexes. (84 pp.) 2001
83. Paasivirta, Jaakko (Ed.): CEOEC'2001, Fifth Finnish-Russian Seminar: Chemistry and Ecology of Organo-Element Compounds. (163 pp.) 2001
84. Kiljunen, Toni: Theoretical studies on spectroscopy and

DEPARTMENT OF CHEMISTRY, UNIVERSITY OF JYVÄSKYLÄ
RESEARCH REPORT SERIES

- atomic dynamics in rare gas solids. (56 pp.) 2001
85. Du, Jin: Derivatives of dextran: synthesis and applications in oncology. (48 pp.) 2001
86. Koivisto, Jari: Structural analysis of selected polychlorinated persistent organic pollutants (POPs) and related compounds. (88 pp.) 2001
87. Feng, Zhinan: Alkaline pulping of non-wood feedstocks and characterization of black liquors. (54 pp.) 2001
88. Halonen, Markku: Lahon havupuun käyttö sulfaattiprosessin raaka-aineena sekä havupuun lahontorjunta. (90 pp.) 2002
89. Falábu, Dezső: Synthesis, conformational analysis and complexation studies of resorcarene derivatives. (212 pp.) 2001
90. Lehtovuori, Pekka: EMR spectroscopic studies on radicals of ubiquinones Q-*n*, vitamin K₃ and vitamine E in liquid solution. (40 pp.) 2002
91. Perkkalainen, Paula: Polymorphism of sugar alcohols and effect of grinding on thermal behavior on binary sugar alcohol mixtures. (53 pp.) 2002
92. Ihalainen, Janne: Spectroscopic studies on light-harvesting complexes of green plants and purple bacteria. (42 pp.) 2002
93. Kunttu, Henrik, Kiljunen, Toni (Eds.): 4th International Conference on Low Temperature Chemistry. (159 pp.) 2002
94. Väisänen, Ari: Development of methods for toxic element analysis in samples with environmental concern by ICP-AES and ETAAS. (54 pp.) 2002
95. Luostarinen, Minna: Synthesis and characterisation of novel resorcarene derivatives. (200 pp.) 2002
96. Louhelainen, Jarmo: Changes in the chemical composition and physical properties of wood and nonwood black liquors during heating. (68 pp.) 2003
97. Lahtinen, Tanja: Concave hydrocarbon cyclophane π -prismans. (65 pp.) 2003
98. Laihia, Katri (Ed.): NBC 2003, Symposium on Nuclear, Biological and Chemical Threats – A Crisis Management Challenge. (245 pp.) 2003
99. Oasmaa, Anja: Fuel oil quality properties of wood-based pyrolysis liquids. (32 pp.) 2003
100. Virtanen, Elina: Syntheses, structural characterisation, and cation/anion recognition properties of nano-sized bile acid-based host molecules and their precursors. (123 pp.) 2003
101. Nättinen, Kalle: Synthesis and X-ray structural studies of organic and metallo-organic supramolecular systems. (79 pp.) 2003
102. Lampiselkä, Jarkko: Demonstraatio lukion kemian opetuksessa. (285 pp.) 2003
103. Kallioinen, Jani: Photoinduced dynamics of Ru(dcbpy)₂(NCS)₂ – in solution and on nanocrystalline titanium dioxide thin films. (47 pp.) 2004
104. Valkonen, Arto (Ed.): VII Synthetic Chemistry Meeting and XXVI Finnish NMR Symposium. (103 pp.) 2004

DEPARTMENT OF CHEMISTRY, UNIVERSITY OF JYVÄSKYLÄ
RESEARCH REPORT SERIES

105. Vaskonen, Kari: Spectroscopic studies on atoms and small molecules isolated in low temperature rare gas matrices. (65 pp.) 2004
106. Lehtovuori, Viivi: Ultrafast light induced dissociation of Ru(dcbpy)(CO)₂I₂ in solution. (49 pp.) 2004
107. Saarenketo, Pauli: Structural studies of metal complexing Schiff bases, Schiff base derived *N*-glycosides and cyclophane π -prismoids. (95 pp.) 2004
108. Paasivirta, Jaakko (Ed.): CEOEC'2004, Sixth Finnish-Russian Seminar: Chemistry and Ecology of Organo-Element Compounds. (147 pp.) 2004
109. Suontamo, Tuula: Development of a test method for evaluating the cleaning efficiency of hard-surface cleaning agents. (96 pp.) 2004
110. Güneş, Minna: Studies of thiocyanates of silver for nonlinear optics. (48 pp.) 2004
111. Ropponen, Jarmo: Aliphatic polyester dendrimers and dendrons. (81 pp.) 2004
112. Vu, Mân Thi Hong: Alkaline pulping and the subsequent elemental chlorine-free bleaching of bamboo (*Bambusa procera*). (69 pp.) 2004
113. Mansikkamäki, Heidi: Self-assembly of resorcinarenes. (77 pp.) 2006
114. Tuononen, Heikki M.: EPR spectroscopic and quantum chemical studies of some inorganic main group radicals. (79 pp.) 2005
115. Kaski, Saara: Development of methods and applications of laser-induced plasma spectroscopy in vacuum ultraviolet. (44 pp.) 2005
116. Mäkinen, Riika-Mari: Synthesis, crystal structure and thermal decomposition of certain metal thiocyanates and organic thiocyanates. (119 pp.) 2006
117. Ahokas, Jussi: Spectroscopic studies of atoms and small molecules isolated in rare gas solids: photodissociation and thermal reactions. (53 pp.) 2006
118. Busi, Sara: Synthesis, characterization and thermal properties of new quaternary ammonium compounds: new materials for electrolytes, ionic liquids and complexation studies. (102 pp.) 2006
119. Mäntykoski, Keijo: PCBs in processes, products and environment of paper mills using wastepaper as their raw material. (73 pp.) 2006
120. Laamanen, Pirkko-Leena: Simultaneous determination of industrially and environmentally relevant aminopolycarboxylic and hydroxycarboxylic acids by capillary zone electrophoresis. (54 pp.) 2007
121. Salmela, Maria: Description of oxygen-alkali delignification of kraft pulp using analysis of dissolved material. (71 pp.) 2007
122. Lehtovaara, Lauri: Theoretical studies of atomic scale impurities in superfluid ⁴He. (87 pp.) 2007
123. Rautiainen, J. Mikko: Quantum chemical calculations of structures, bonding, and spectroscopic properties of some sulphur and selenium iodine cations. (71 pp.) 2007
124. Nummelin, Sami: Synthesis, characterization, structural and

- retrostructural analysis of self-assembling pore forming dendrimers. (286 pp.) 2008
125. Sopo, Harri: Uranyl(VI) ion complexes of some organic aminobisphenolate ligands: syntheses, structures and extraction studies. (57 pp.) 2008
126. Valkonen, Arto: Structural characteristics and properties of substituted cholanoates and *N*-substituted cholanamides. (80 pp.) 2008
127. Lähde, Anna: Production and surface modification of pharmaceutical nano- and microparticles with the aerosol flow reactor. (43 pp.) 2008
128. Beyeh, Ngong Kodiah: Resorcinarenes and their derivatives: synthesis, characterization and complexation in gas phase and in solution. (75 pp.) 2008
129. Väliisaari, Jouni, Lundell, Jan (Eds.): Kemian opetuksen päivät 2008: uusia oppimisympäristöjä ja ongelmalähtöistä opetusta. (118 pp.) 2008
130. Myllyperkiö, Pasi: Ultrafast electron transfer from potential organic and metal containing solar cell sensitizers. (69 pp.) 2009
131. Käkölä, Jaana: Fast chromatographic methods for determining aliphatic carboxylic acids in black liquors. (82 pp.) 2009
132. Koivukorpi, Juha: Bile acid-arene conjugates: from photoswitchability to cancer cell detection. (67 pp.) 2009
133. Tuuttila, Tero: Functional dendritic polyester compounds: synthesis and characterization of small bifunctional dendrimers and dyes. (74 pp.) 2009
134. Salorinne, Kirsi: Tetramethoxy resorcinarene based cation and anion receptors: synthesis, characterization and binding properties. (79 pp.) 2009
135. Rautiainen, Riikka: The use of first-thinning Scots pine (*Pinus sylvestris*) as fiber raw material for the kraft pulp and paper industry. (73 pp.) 2010
136. Ilander, Laura: Uranyl salophens: synthesis and use as ditopic receptors. (199 pp.) 2010
137. Kiviniemi, Tiina: Vibrational dynamics of iodine molecule and its complexes in solid krypton - Towards coherent control of bimolecular reactions? (73 pp.) 2010
138. Ikonen, Satu: Synthesis, characterization and structural properties of various covalent and non-covalent bile acid derivatives of N/O-heterocycles and their precursors. (105 pp.) 2010
139. Siitonen, Anni: Spectroscopic studies of semiconducting single-walled carbon nanotubes. (56 pp.) 2010
140. Raatikainen, Kari: Synthesis and structural studies of piperazine cyclophanes – Supramolecular systems through Halogen and Hydrogen bonding and metal ion coordination. (69 pp.) 2010
141. Leivo, Kimmo: Gelation and gel properties of two- and three-component Pyrene based low molecular weight organogelators. (116 pp.) 2011
142. Martiskainen, Jari: Electronic energy transfer in light-harvesting complexes isolated from *Spinacia oleracea* and from three

- photosynthetic green bacteria *Chloroflexus aurantiacus*, *Chlorobium tepidum*, and *Prosthecochloris aestuarii*. (55 pp.) 2011
143. Wichmann, Oula: Syntheses, characterization and structural properties of [O,N,O,X'] aminobisphenolate metal complexes. (101 pp.) 2011
144. Ilander, Aki: Development of ultrasound-assisted digestion methods for the determination of toxic element concentrations in ash samples by ICP-OES. (58 pp.) 2011
145. The Combined XII Spring Meeting of the Division of Synthetic Chemistry and XXXIII Finnish NMR Symposium. Book of Abstracts. (90 pp.) 2011
146. Valto, Piia: Development of fast analysis methods for extractives in papermaking process waters. (73 pp.) 2011
147. Andersin, Jenni: Catalytic activity of palladium-based nanostructures in the conversion of simple olefinic hydro- and chlorohydrocarbons from first principles. (78 pp.) 2011
148. Aumanen, Jukka: Photophysical properties of dansylated poly(propylene amine) dendrimers. (55 pp.) 2011
149. Kärnä, Minna: Ether-functionalized quaternary ammonium ionic liquids – synthesis, characterization and physicochemical properties. (76 pp.) 2011
150. Jurček, Ondřej: Steroid conjugates for applications in pharmacology and biology. (57 pp.) 2011
151. Nauha, Elisa: Crystalline forms of selected Agrochemical actives: design and synthesis of cocrystals. (77 pp.) 2012
152. Ahkola, Heidi: Passive sampling in monitoring of nonylphenol ethoxylates and nonylphenol in aquatic environments. (92 pp.) 2012
153. Helttunen, Kaisa: Exploring the self-assembly of resorcinarenes: from molecular level interactions to mesoscopic structures. (78 pp.) 2012
154. Linnanto, Juha: Light excitation transfer in photosynthesis revealed by quantum chemical calculations and exciton theory. (179 pp.) 2012
155. Roiko-Jokela, Veikko: Digital imaging and infrared measurements of soil adhesion and cleanability of semihard and hard surfaces. (122 pp.) 2012
156. Noponen, Virpi: Amides of bile acids and biologically important small molecules: properties and applications. (85 pp.) 2012
157. Hulkko, Eero: Spectroscopic signatures as a probe of structure and dynamics in condensed-phase systems – studies of iodine and gold ranging from isolated molecules to nanoclusters. (69 pp.) 2012
158. Lappi, Hanna: Production of Hydrocarbon-rich biofuels from extractives-derived materials. (95 pp.) 2012
159. Nykänen, Lauri: Computational studies of Carbon chemistry on transition metal surfaces. (76 pp.) 2012
160. Ahonen, Kari: Solid state studies of pharmaceutically important molecules and their derivatives. (65 pp.) 2012

DEPARTMENT OF CHEMISTRY, UNIVERSITY OF JYVÄSKYLÄ
RESEARCH REPORT SERIES

161. Pakkanen, Hannu: Characterization of organic material dissolved during alkaline pulping of wood and non-wood feedstocks. (76 pp.) 2012
162. Moilanen, Jani: Theoretical and experimental studies of some main group compounds: from closed shell interactions to singlet diradicals and stable radicals. (80 pp.) 2012
163. Himanen, Jatta: Stereoselective synthesis of Oligosaccharides by *De Novo* Saccharide welding. (133 pp.) 2012
164. Bunzen, Hana: Steroidal derivatives of nitrogen containing compounds as potential gelators. (76 pp.) 2013
165. Seppälä, Petri: Structural diversity of copper(II) amino alcohol complexes. Syntheses, structural and magnetic properties of bidentate amino alcohol copper(II) complexes. (67 pp.) 2013
166. Lindgren, Johan: Computational investigations on rotational and vibrational spectroscopies of some diatomics in solid environment. (77 pp.) 2013
167. Giri, Chandan: Sub-component self-assembly of linear and non-linear diamines and diacylhydrazines, formylpyridine and transition metal cations. (145 pp.) 2013
168. Riisiö, Antti: Synthesis, Characterization and Properties of Cu(II)-, Mo(VI)- and U(VI) Complexes With Diaminotetraphenolate Ligands. (51 pp.) 2013
169. Kiljunen, Toni (Ed.): Chemistry and Physics at Low Temperatures. Book of Abstracts. (103 pp.) 2013
170. Hänninen, Mikko: Experimental and Computational Studies of Transition Metal Complexes with Polydentate Amino- and Aminophenolate Ligands: Synthesis, Structure, Reactivity and Magnetic Properties. (66 pp.) 2013
171. Antila, Liisa: Spectroscopic studies of electron transfer reactions at the photoactive electrode of dye-sensitized solar cells. (53 pp.) 2013
172. Kemppainen, Eeva: Mukaiyama-Michael reactions with α -substituted acroleins – a useful tool for the synthesis of the pectenotoxins and other natural product targets. (190 pp.) 2013
173. Virtanen, Suvi: Structural Studies of Dielectric Polymer Nanocomposites. (49 pp.) 2013
174. Yliniemelä-Sipari, Sanna: Understanding The Structural Requirements for Optimal Hydrogen Bond Catalyzed Enolization – A Biomimetic Approach. (160 pp.) 2013
175. Leskinen, Mikko V: Remote β -functionalization of β' -keto esters. (105 pp.) 2014
176. 12th European Conference on Research in Chemistry Education (ECRICE2014). Book of Abstracts. (166 pp.) 2014
177. Peuronen, Anssi: N-Monoalkylated DABCO-Based N-Donors as Versatile Building Blocks in Crystal Engineering and Supramolecular Chemistry. (54 pp.) 2014
178. Perämäki, Siiri: Method development for determination and recovery of rare earth elements from industrial fly ash. (88 pp.) 2014

DEPARTMENT OF CHEMISTRY, UNIVERSITY OF JYVÄSKYLÄ
RESEARCH REPORT SERIES

179. Chernyshev, Alexander, N.: Nitrogen-containing ligands and their platinum(IV) and gold(III) complexes: investigation and basicity and nucleophilicity, luminescence, and aurophilic interactions. (64 pp.) 2014
180. Lehto, Joni: Advanced Biorefinery Concepts Integrated to Chemical Pulping. (142 pp.) 2015
181. Tero, Tiia-Riikka: Tetramethoxy resorcinarenes as platforms for fluorescent and halogen bonding systems. (61 pp.) 2015
182. Löfman, Miika: Bile acid amides as components of microcrystalline organogels. (62 pp.) 2015
183. Selin, Jukka: Adsorption of softwood-derived organic material onto various fillers during papermaking. (169 pp.) 2015
184. Piisola, Antti: Challenges in the stereoselective synthesis of allylic alcohols. (210 pp.) 2015
185. Bonakdarzadeh, Pia: Supramolecular coordination polyhedra based on achiral and chiral pyridyl ligands: design, preparation, and characterization. (65 pp.) 2015
186. Vasko, Petra: Synthesis, characterization, and reactivity of heavier group 13 and 14 metallylenes and metalloid clusters: small molecule activation and more. (66 pp.) 2015
187. Topić, Filip: Structural Studies of Nano-sized Supramolecular Assemblies. (79 pp.) 2015
188. Mustalahti, Satu: Photodynamics Studies of Ligand-Protected Gold Nanoclusters by using Ultrafast Transient Infrared Spectroscopy. (58 pp.) 2015
189. Koivisto, Jaakko: Electronic and vibrational spectroscopic studies of gold-nanoclusters. (63 pp.) 2015
190. Suhonen, Aku: Solid state conformational behavior and interactions of series of aromatic oligoamide foldamers. (68 pp.) 2016
191. Soikkeli, Ville: Hydrometallurgical recovery and leaching studies for selected valuable metals from fly ash samples by ultrasound-assisted extraction followed by ICP-OES determination. (107 pp.) 2016
192. XXXVIII Finnish NMR Symposium. Book of Abstracts. (51 pp.) 2016
193. Mäkelä, Toni: Ion Pair Recognition by Ditopic Crown Ether Based bis-Urea and Uranyl Salophen Receptors. (75 pp.) 2016
194. Lindholm-Lehto, Petra: Occurrence of pharmaceuticals in municipal wastewater treatment plants and receiving surface waters in Central and Southern Finland. (98 pp.) 2016
195. Härkönen, Ville: Computational and Theoretical studies on Lattice Thermal conductivity and Thermal properties of Silicon Clathrates. (89 pp.) 2016
196. Tuokko, Sakari: Understanding selective reduction reactions with heterogeneous Pd and Pt: climbing out of the black box. (85 pp.) 2016
197. Nuora, Piia: Monitapaustutkimus LUMA-Toimintaan liittyvissä oppimisympäristöissä tapahtuvista kemian oppimiskokemuksista. (171 pp.) 2016

DEPARTMENT OF CHEMISTRY, UNIVERSITY OF JYVÄSKYLÄ
RESEARCH REPORT SERIES

198. Kumar, Hemanathan: Novel Concepts on The Recovery of By-Products from Alkaline Pulping. (61 pp.) 2016
199. Arnedo-Sánchez, Leticia: Lanthanide and Transition Metal Complexes as Building Blocks for Supramolecular Functional Materials. (227 pp.) 2016
200. Gell, Lars: Theoretical Investigations of Ligand Protected Silver Nanoclusters. (134 pp.) 2016
201. Vaskuri, Juhani: Oppiennätyksistä opetussuunnitelman perusteisiin - lukion kemian kansallisen opetussuunnitelman kehittyminen Suomessa vuosina 1918-2016. (314 pp.) 2017
202. Lundell Jan, Kiljunen Toni (Eds.): 22nd Horizons in Hydrogen Bond Research. Book of Abstracts. 2017
203. Turunen, Lotta: Design and construction of halogen-bonded capsules and cages. (61 pp.) 2017
204. Hurmalainen, Juha: Experimental and computational studies of unconventional main group compounds: stable radicals and reactive intermediates. (88 pp.) 2017
205. Koivistoinen Juha: Non-linear interactions of femtosecond laser pulses with graphene: photo-oxidation, imaging and photodynamics. (68 pp.) 2017
206. Chen, Chengcong: Combustion behavior of black liquors: droplet swelling and influence of liquor composition. (39 pp.) 2017
207. Mansikkamäki, Akseli: Theoretical and Computational Studies of Magnetic Anisotropy and Exchange Coupling in Molecular Systems. (190 p. + included articles) 2018.
208. Tatikonda, Rajendhraprasad: Multivalent N-donor ligands for the construction of coordination polymers and coordination polymer gels. (62 pp.) 2018
209. Budhathoki, Roshan: Beneficiation, desilication and selective precipitation techniques for phosphorus refining from biomass derived fly ash. (64 pp.) 2018
210. Siitonen, Juha: Synthetic Studies on 1-azabicyclo[5.3.0]decane Alkaloids. (140 pp.) 2018
211. Ullah, Saleem: Advanced Biorefinery Concepts Related to Non-wood Feedstocks. (57 pp.) 2018
212. Ghalibaf, Maryam: Analytical Pyrolysis of Wood and Non-Wood Materials from Integrated Biorefinery Concepts. (106 pp.) 2018

1. Bulatov, Evgeny: Synthetic and structural studies of covalent and non-covalent interactions of ligands and metal center in platinum(II) complexes containing 2,2'-dipyridylamine or oxime ligands. (58 pp.) 2019. JYU Dissertations 70.
2. Annala, Riia: Conformational Properties and Anion Complexes of Aromatic Oligoamide Foldamers. (80 pp.) 2019. JYU Dissertations 84.
3. Isoaho, Jukka Pekka: Dithionite Bleaching of Thermomechanical Pulp - Chemistry and Optimal Conditions. (73 pp.) 2019. JYU Dissertations 85.
4. Nygrén, Enni: Recovery of rubidium from power plant fly ash. (98 pp.) 2019. JYU Dissertations 136.
5. Kiesilä, Anniina: Supramolecular chemistry of anion-binding receptors based on concave macromolecules. (68 pp.) 2019. JYU Dissertations 137.
6. Sokolowska, Karolina: Study of water-soluble p-MBA-protected gold nanoclusters and their superstructures. (60 pp.) 2019. JYU Dissertations 167.
7. Lahtinen, Elmeri: Chemically Functional 3D Printing: Selective Laser Sintering of Customizable Metal Scavengers. (71 pp.) 2019. JYU Dissertations 175.
8. Larijani, Amir: Oxidative reactions of cellulose under alkaline conditions. (102 pp.) 2020. JYU Dissertations 217.
9. Kolari, Kalle: Metal-metal contacts in late transition metal polymers. (60 pp.) 2020. JYU Dissertations 220.
10. Kauppinen, Minttu: Multiscale computational investigation of catalytic properties of zirconia supported noble metals. (87 pp.) 2020. JYU Dissertations 231.
11. Ding, Xin: Halogen Bond in Crystal Engineering: Structural Studies on Crystals with Ruthenium Centered Complexes and 1-(4-Pyridyl)-4-thiopyridine Zwitterion as Halogen Bond Acceptors. (59 pp.) 2020. JYU Dissertations 323.
12. Neuvonen, Antti: Toward an Understanding of Hydrogen-Bonding Bifunctional Organocatalyst Conformations and Their Activity in Asymmetric Mannich Reactions. (77 pp.) 2020. JYU Dissertations 336.
13. Kortet, Sami: 2,5-Diarylpyrrolidines and Pyroglutamic-Acid-Derived 2-Diarylmethyl-5-Aryl-Pyrrolidines: Their Synthesis and Use in Asymmetric Synthesis. (221 pp.) 2020. JYU Dissertations 337.
14. Saarnio, Ville: Fluorescent probes, noble metal nanoparticles and their nanocomposites: detection of nucleic acids and other biological targets. (80 pp.) 2021. JYU Dissertations 361.
15. Chernysheva, Maria: σ -hole interactions: the effect of the donors and acceptors nature in selenoureas, thioureas, halogenated species, substituted benzenes, and their adducts. (72 pp.) 2021. JYU Dissertations 370.
16. Bulatova, Margarita: Noncovalent interactions as a tool for supramolecular self-assembly of metallopolymers. (62 pp.) 2021. JYU Dissertations 377.

17. Romppanen, Sari: Laser-spectroscopic studies of rare earth element- and lithium-bearing minerals and rocks. (66 pp.) 2021. JYU Dissertations 393.
18. Kukkonen, Esa: Nonlinear optical materials through weak interactions and their application in 3D printing. (58 pp.) 2021. JYU Dissertations 441.
19. Kuosmanen, Riikka: The Effect of Structure on the Gel Formation Ability and the Properties of Bile Acid Based Supramolecular Organogels. (68 pp.) 2021. JYU Dissertations 465.
20. Reuna, Sini: Development of a Method for Phosphorus Recovery from Wastewaters. (67 pp.) 2022. JYU Dissertations 486.
21. Taipale, Essi: Synthetic and Structural Studies on the Effect of Non-Covalent Interactions on N(*sp*²)-Heterocyclic Molecules. (67 pp.) 2022. JYU Dissertations 496.
22. Järvinen, Teemu: Molecular Dynamics View on Matrix Isolation. (143 pp.) 2022. JYU Dissertations 544.
23. Kumar, Parveen: Synthesis and Structural Studies on Halogen(I) Complexes. (160 pp.) 2022. JYU Dissertations 549.
24. Forsblom, Samu: Design and Construction of Metal-Organic Polyhedra. (212 pp.) 2022. JYU Dissertations 569.
25. Korpelin, Ville: Computational Studies of Catalytic Active Site Properties and Reactions at the Metal–Oxide Interface. (78 pp.) 2022. JYU Dissertations 578.
26. Vuori, Hannu: Extending Benson Group Increment Theory to Compounds of Phosphorus, Silicon, and Boron with Computational Chemistry. (59 pp.) 2022. JYU Dissertations 581.
27. Pallerla, Rajanish: Studies Towards Synthesis of Favipiravir & Humilisin E. (139 pp.) 2023. JYU Dissertations 611.
28. Taponen, Anni: Radical-Ion Salts based on Thiazyls and Tetracyanoquinodimethane: Hysteretic Magnetic Bistability in a Multicomponent System. (66 pp.) 2023. JYU Dissertations 613.
29. Aho, Noora: Molecular Dynamics Simulations of Acids and Bases in Biomolecular Environments. (78 pp.) 2023. JYU Dissertations 614.
30. Sabooni Asre Hazer, Maryam: Electronic and Optical Properties of Gold Clusters with Carbene Ligands using Density Functional Theory Calculations. (68 pp.) 2023. JYU Dissertations 650.
31. Kinnunen, Virva-Tuuli: Improving the Accuracy of Single Particle ICP-MS Analyses of Au and Ag Nanoparticles. (67 pp.) 2023. JYU Dissertations 689.
32. Kulomäki, Suvi: Preconcentration, Speciation, and Determination of Mercury in Natural Waters by Inductively Coupled Plasma Mass Spectrometry. (61 pp.) 2023. JYU Dissertations 725.
33. Schirmer, Johanna: Effects of Two-Photon Oxidation for the Development of Graphene-Bio Interfaces. (69 pp.) 2023. JYU Dissertations 726.
34. Halmemies, Eelis: Chemical Changes in the Industrial Extractive-Containing Sidestreams of Norway Spruce (*Picea abies*) during Storage. (84 pp.) 2024. JYU Dissertations 737.

35. Alaranta, Johanna: Synthesis of Monomethine Cyanine Dyes and Gold Nanoclusters and their Applications as Fluorescent Probes. (67 pp.) 2024. JYU Dissertations 766.